

## **General Disclaimer**

### **One or more of the Following Statements may affect this Document**

- This document has been reproduced from the best copy furnished by the organizational source. It is being released in the interest of making available as much information as possible.
- This document may contain data, which exceeds the sheet parameters. It was furnished in this condition by the organizational source and is the best copy available.
- This document may contain tone-on-tone or color graphs, charts and/or pictures, which have been reproduced in black and white.
- This document is paginated as submitted by the original source.
- Portions of this document are not fully legible due to the historical nature of some of the material. However, it is the best reproduction available from the original submission.

(NASA-CR-166447) INTEGRATED TECHNOLOGY  
ROTOR/FLIGHT RESEARCH ROTOR HUB CONCEPT  
DEFINITION (Boeing Vertol Co., Philadelphia,  
Pa.) 219 p HC A10/MF A01 CSCI 01C

N85-18051

Unclas

G3/05 14919

# INTEGRATED TECHNOLOGY ROTOR/FLIGHT RESEARCH ROTOR HUB CONCEPT DEFINITION

Peter G. C. Dixon



Contract DAAK51-81-C-0027  
March 1983

Date for general release March 1985



# INTEGRATED TECHNOLOGY ROTOR/FLIGHT RESEARCH ROTOR HUB CONCEPT DEFINITION

Peter G. C. Dixon  
Boeing Vertol Company  
Philadelphia, Pennsylvania 19142

Prepared for U.S. Army Research and  
Technology Laboratories (AVRADCOM)  
under Contract DAAK51-81-C-0027



March 1985

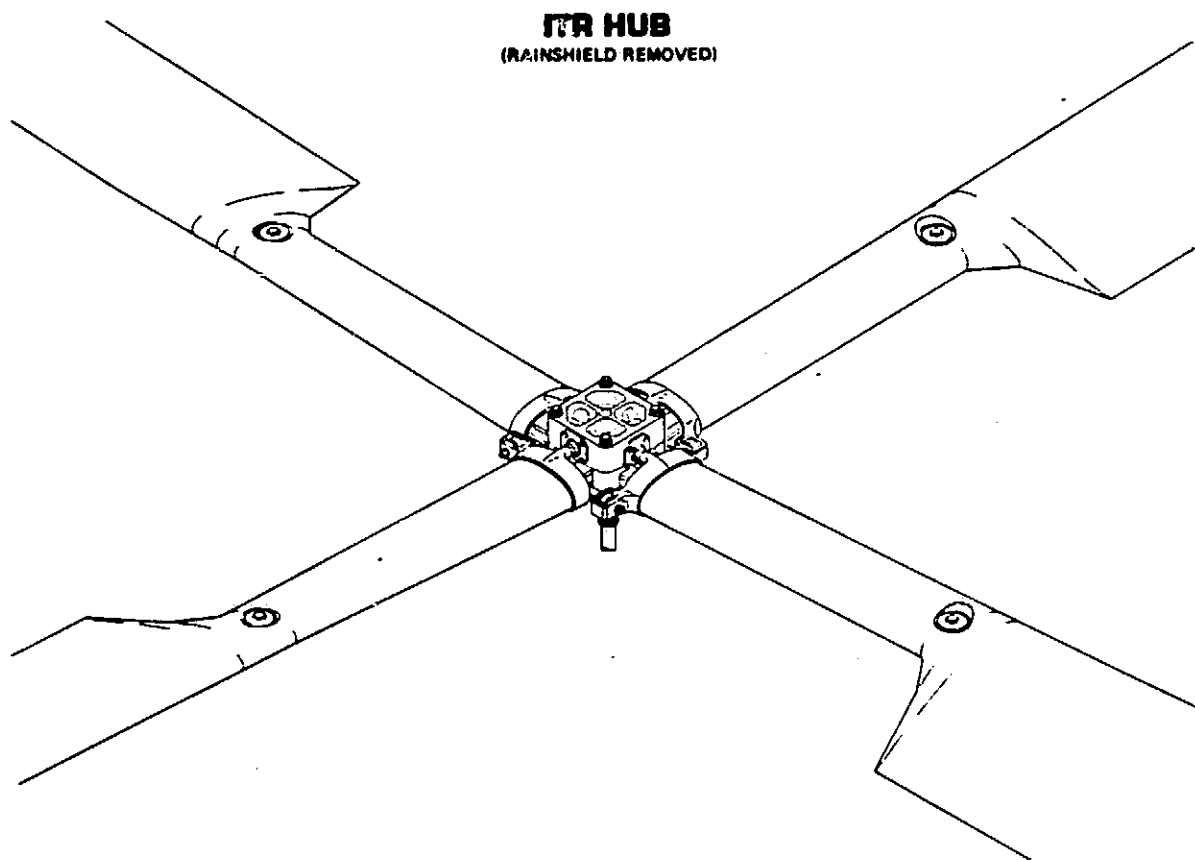
**NASA**  
National Aeronautics and  
Space Administration  
**Ames Research Center**  
Moffett Field, California 94035

United States Army  
Aviation Research and  
Development Command  
Research and Technology  
Laboratory  
Moffett Field, California 94035



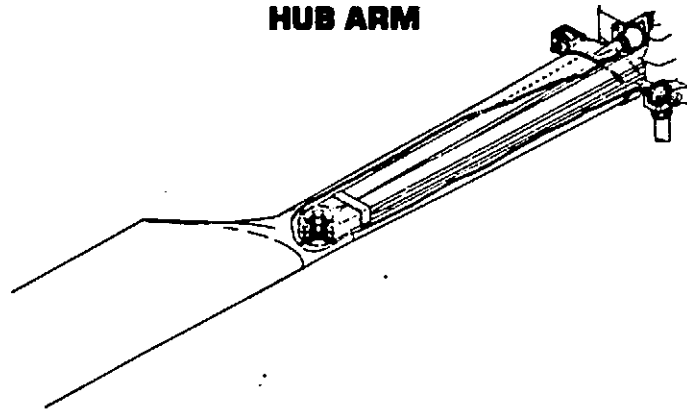
SUMMARY

Two variations of the helicopter bearingless main rotor hub concept shown are candidates for further development in the preliminary design phase of the Integrated Technology Rotor/Flight Research Rotor (ITR/FRR) program. This selection was the result of an evaluation of three bearingless hub concepts and two articulated hub concepts with elastomeric bearings.



The characteristics of each concept were evaluated by means of simplified methodology. These characteristics included the assessment of stability, vulnerability, weight, drag, cost, stiffness, fatigue life, maintainability, and reliability.

## HUB ARM



ORIGINAL PAGE IS  
OF POOR QUALITY

The selected concepts have rotor blade retention at 19-percent radius by a 4-element reinforced-composite flexure which is clamped at the hub and which permits blade flapwise, chordwise, and pitch motions through its flexibility. Blade-feathering torque is reacted by a composite torque sleeve/aerodynamic fairing which is rigidly attached in all modes to the blade root. Control system motions are applied through the fitting at the inboard end of the sleeve.

This fitting is restrained against vertical and lateral translation by a shaft-mounted spherical pivot which reacts only the shear loads applied by the control system and those induced by blade flapwise and lagwise motions. The lagwise shear reaction load, coupled with the vertical offset of the pivot from the flexure axis, produces a feathering motion from lag motion. This motion coupling, made possible by the flexibility of the pitch control system, has been shown to be very effective in enhancing the aeroelastic stability of bearingless rotor systems. This latter is regarded as a major issue to be satisfied since auxiliary dampers have been specified as undesirable.

Survivability to ballistic damage has been enhanced by the extensive use of composites and the redundancy feature of the 4-element flexure. Other characteristics, determined by analysis by simplified methodologies, are tabulated below and compared with the program goals.

CONFORMANCE WITH DESIGN GOALS AND SPECIFICATIONS

Parameter	Units	Goal	Achievement	Remarks
Design Gross Weight	lb	16,000 to 23,000	16,000	-
Design Envelope	g's	+3.5 to -0.5	+3.5 to -0.5	-
Stability	-	Stable	Stable	YUH-61A
No. of Blades	-	4	4	-
Adaptable to Fold	-	Rapid manual	Rapid manual	2-pin removal
Hub Drag	ft <sup>2</sup>	2.8	2.93	-
Hub Weight	% DGW	2.5	1.9	-
Parts Count	-	50	47	-
Hub Moment Stiffness	ft-lb/rad	100,000	150,000	Rigid blades
Min Hub Moment	ft-lb	10,000	11,256	No fatigue damage
Min Hub Tilt (EL)	deg	5	4.3	- Rigid blades
Aux Damping	-	Provisions for	Possible	Elastomeric
Torsional Stiffness	in.-lb/deg	150	108	UH-60 goal
Fatigue Life	hr	10,000	>5,700	>10 <sup>8</sup> cycles endurance
Reliability	hr	3,000	>3,000	-
Mfg Cost	\$	Minimize	85,000	1,000 acft

TABLE OF CONTENTS

	<u>Page</u>
SUMMARY . . . . .	3
LIST OF ILLUSTRATIONS . . . . .	10
LIST OF TABLES . . . . .	15
LIST OF SYMBOLS . . . . .	16
INTRODUCTION . . . . .	19
A REVIEW OF GOALS AND SPECIFICATIONS . . . . .	21
REVIEW OF ITR/FRR SYSTEM DESIGN SPECIFICATIONS . . . . .	21
REVIEW OF ITR/FRR SYSTEM TECHNICAL GOALS . . . . .	26
REVIEW OF HUB DESIGN SPECIFICATIONS . . . . .	41
REVIEW OF HUB TECHNICAL GOALS . . . . .	41
RECOMMENDATIONS FOR CHANGES TO THE GOALS AND SPECIFICATIONS . . . . .	53
ITR SYSTEM DESIGN SPECIFICATIONS - RECOMMENDED CHANGES . . . . .	53
ROTOR SYSTEM STABILITY . . . . .	58
ITR SYSTEM TECHNICAL GOALS - RECOMMENDED CHANGES . . . . .	58
ITR ROTOR HUB SYSTEM DESIGN SPECIFICATIONS - RECOMMENDED CHANGES . . . . .	59
ROTOR HUB TECHNICAL GOALS - RECOMMENDED CHANGES . . . . .	59
REPRESENTATIVE HELICOPTER CHARACTERISTICS . . . . .	61
ITR ROTOR BLADES . . . . .	63
ROTOR SHAFT . . . . .	63
DESIGN CRITERIA FOR DEFINING HUB CONCEPTS . . . . .	67
SELECTION OF CANDIDATE HUB SYSTEMS . . . . .	68
CANDIDATES FOR EVALUATION . . . . .	68
PRELIMINARY STUDIES . . . . .	80
ASSESSMENT OF CONCEPTS . . . . .	139
MERIT FACTORS AND MERIT FUNCTION . . . . .	139
SURVIVABILITY . . . . .	141
STABILITY . . . . .	141
HUB DRAG . . . . .	144
HUB WEIGHT . . . . .	144
NUMBER OF PARTS . . . . .	144
HUB STIFFNESS . . . . .	144
MINIMUM HUB MOMENT . . . . .	144
MINIMUM HUB TILT ANGLE . . . . .	145
RELIABILITY . . . . .	145

	<u>Page</u>
COST . . . . .	145
FATIGUE LIFE . . . . .	146
PROVISIONS FOR AUXILIARY DAMPING . . . . .	146
TORSIONAL STIFFNESS . . . . .	146
SELECTION OF TWO HUB CONCEPTS BY MERIT . . . . .	147
INFLUENCE OF GOALS AND SPECIFICATIONS ON THE DESIGN . . . . .	151
DETERMINATION OF PHYSICAL PROPERTIES . . . . .	154
GEOMETRY . . . . .	154
STIFFNESS . . . . .	154
BLADE PHYSICAL PROPERTIES . . . . .	155
PRELIMINARY STRUCTURAL ANALYSIS . . . . .	159
ALTERNATING FLAP STRAINS . . . . .	159
FLEXURE SYSTEM . . . . .	159
FLEXURE/BLADE ATTACHMENT . . . . .	163
FLEXURE RETENTION AT THE SHAFT . . . . .	163
TORQUE SLEEVE . . . . .	164
PRELIMINARY DYNAMIC ANALYSIS . . . . .	165
NATURAL FREQUENCIES . . . . .	165
PITCH-LAG COUPLING . . . . .	166
PRELIMINARY LIFE ASSESSMENT . . . . .	166
PRELIMINARY FLYING QUALITIES ASSESSMENT . . . . .	166
VIBRATION ASSESSMENT . . . . .	167
VULNERABILITY ASSESSMENT . . . . .	167
CONFORMANCE WITH GOALS AND SPECIFICATIONS . . . . .	168
HUB DRAG . . . . .	168
MANUFACTURING COST . . . . .	168
EVALUATION OF THE CANDIDATE CONFIGURATIONS . . . . .	174
PRODUCIBILITY . . . . .	174
QUALITY CONTROL REQUIREMENTS . . . . .	174
TOOLING CONCEPTS AND COSTS . . . . .	174
INSPECTABILITY . . . . .	179
MAINTAINABILITY AND RELIABILITY . . . . .	179
FRR CONFIGURATION VARIATIONS . . . . .	180
ITR HUB MODIFICATIONS . . . . .	180
DESIGN APPROACH FOR THE ITR HUB MODIFICATIONS . . . . .	192
PRELIMINARY STRUCTURAL ANALYSIS . . . . .	196

	<u>Page</u>
ITR COMPATIBILITY WITH THE RSRA . . . . .	200
FLIGHT CONTROLS MODIFICATIONS . . . . .	200
STABILITY AUGMENTATION/AFCS MODIFICATIONS . . . . .	204
ROTOR SHAFT, TRANSMISSION, AND SUPPORT STRUCTURE MODIFICATIONS . . . . .	205
DRIVE SYSTEM COMPATIBILITY . . . . .	205
LANDING GEAR MODIFICATIONS . . . . .	208
VIBRATION ISOLATION . . . . .	209
RSRA EMERGENCY ESCAPE SYSTEM . . . . .	210
ANALYSIS OF CRITICAL COMPONENTS . . . . .	215
REFERENCES . . . . .	217

## LIST OF ILLUSTRATIONS

<u>Figure</u>		<u>Page</u>
1	The Bearingless Main Rotor System . . . . .	20
2	Maximum Rotor $L/D_E$ . . . . .	27
3	Potential for Achieving the ITR Maximum Figure of Merit Goal . . . . .	29
4	Faired Hub Drag Trends . . . . .	30
5	ITR Speed Capability . . . . .	31
6	Probable Improvements in Noise Reduction . . . . .	32
7	Helicopter External Noise Levels in Level Flight . . . . .	33
8	Effect of Airfoil on Rotor Harmonic Noise . . . . .	34
9	Effect of Airfoil on Sound Pressure Level of a Model Rotor at High Forward Speed . . . . .	34
10	Rotor Blade Weight Trend . . . . .	36
11	Average Rotor Blade Weight Expressed as Percent of Limit Load . . . . .	37
12	Evolution of Rotor System Parts Count . . . . .	37
13	H-46 Fiberglass Rotor Blade Reliability Goals and Status. . . . .	40
14	Derivation of Control Moments . . . . .	43
15	Relative Control Sensitivity of Teetering, Articulated, and Hingeless Rotor Systems . . . . .	46
16	Minimum Allowable Flexure Root Width for $\pm 5$ Degrees of Endurance Limit Flapping; Effect of Hub Stiffness Requirements and Material Types . . . . .	49
17	Hub Stiffness Requirements to Avoid Blade/Boom Contact at 4.67 G's Loading . . . . .	57
18	Overall Dimensions of YUH-61A Helicopter . . . . .	62
19	Advanced Rotor Maneuver Envelope . . . . .	64

<u>Figure</u>		<u>Page</u>
20	Optimum Twist Study With Shank of 2.1 Ellipse . . . . .	65
21	Mass and Stiffness Distributions for Advanced Rotor Blade .	66
22	The Bearingless Main Rotor System . . . . .	69
23	ITR Rotor Blade Concept . . . . .	70
24	ITR Configuration 1A (Modified BMR) . . . . .	71
25	ITR Configuration 1B (Modified BMR) . . . . .	73
26	ITR Configuration 2B (Modified BMR) . . . . .	76
27	ITR Configuration 3 (Flexure/Shoe Rotor) . . . . .	78
28	ITR Configuration 4 (Reversed Starflex Rotor) . . . . .	79
29	ITR Configuration 5 (Lag/Torsion Flexure with Flapping Hinge) . . . . .	81
30	Specific Properties of Composite Materials Compared to Metals . . . . .	85
31	Fatigue Design Allowables for Candidate Materials . . . . .	86
32	Diagram of Clamp Radius and Equivalent Flap Hinge Offset. .	87
33	Effect of Material on Flexure Performance . . . . .	90
34	Interactions of Materials and Interlaminar Shear Strength .	92
35	Blade Root Attachment - Pins Versus Clamping . . . . .	94
36	The Extremes of Hub Clamp Support . . . . .	96
37	Flexure Root Clamp at the Shaft . . . . .	98
38	Flexure Displacement Inside the Clamp . . . . .	98
39	Flexure Shear Loading Inside the Root Clamp . . . . .	98
40	Split Flexure Reduces Interlaminar Shear . . . . .	101
41	Calculation of Endurance Limit Strain . . . . .	102
42	Equations Relating Material Allowable Strain ( $\epsilon$ ) to Flexbeam Root Geometry and Blade Flapping ( $\pm\beta^C$ ) for a Simple Cantilevered Flexure . . . . .	103

<u>Figure</u>		<u>Page</u>
43	Theoretical Flap Flexure . . . . .	106
44	DIFF5 Solution for ITR Theoretical Flexure . . . . .	107
45	BEAMSOL Solution for Optimized Flexure in Kevlar . . . . .	109
46	Endurance Limit Deflection of Optimized 6-Inch-Wide Cantilevered Flexures in Kevlar 49 . . . . .	111
47	Study of Endurance Limit Flapping Versus Flexure Length With Constant 6-Inch-Width . . . . .	112
48	BEAMSOL Solution for Effect of Width on Thickness of Kevlar Flexure . . . . .	113
49	Required Width of Kevlar 49 Constant-Width Flexure Is Proportional to (Endurance Limit Flapping) <sup>3</sup> . . . . .	115
50	Shoe-Restrained Flexure . . . . .	116
51	Limit Bending-Moment Distribution for Shoe-Restrained Flexure . . . . .	118
52	Reversed Starflex Rotor Hub . . . . .	122
53	Additional Flapping From Blade Root of Reversed Starflex Hub . . . . .	128
54	Typical Contributions From Bending and Warping Constraints, Shear Rigidity, and Centrifugal Stiffening to the Torsional Stiffness of a Flexure . . . . .	129
55	Effect of Flexure Geometry on Torsional Stiffness . . . . .	130
56	System for Static Stability Analysis . . . . .	131
57	Shaft Tilt Versus Velocity for Zero Longitudinal Flapping ( $\alpha_F = 0$ ) . . . . .	134
58	Longitudinal Cyclic Flapping Versus True Airspeed . . . . .	135
59	Tail Setting for Fuselage Trim ( $\alpha_F = 0$ ) . . . . .	136
60	Effect of Pitch-Lag Coupling, Predroop, and Sweep on Aeroelastic Stability: Rotor Model . . . . .	137
61	Effect of Pitch-Lag Coupling, Predroop, and Sweep on Aeroelastic Stability: Fuselage Model . . . . .	138

<u>Figure</u>		<u>Page</u>
62	Stability Improvement in Hover Through Pivot Offset . . . . .	138
63	Vulnerability Study of ITR Configuration No. 2B (Modified BMR) . . . . .	142
64	Application of Merit Factors and Merit Function to Selection of ITR Hub Concepts . . . . .	148
65	Studies of Limit Loading on Flexures . . . . .	153
66	Geometry of Flexure Cross Section . . . . .	155
67	Geometry of Sleeve Cross Section . . . . .	156
68	Determination of Steady Flexure Strains Due to Centrifugal Force and Chord Loading . . . . .	157
69	Flap and Torsional Displacement . . . . .	160
70	Loading System for Analysis of Flap Strain by CHORD-Z Program . . . . .	161
71	Fatigue Strains . . . . .	162
72	Fatigue Strength of Torque Sleeve in Chordwise Bending . . . . .	164
73	Determination of Nonrotating Frequency . . . . .	165
74	Drag Estimate for Example ITR Hub Design . . . . .	170
75	ITR Control Positions for Hub Drag Evaluation . . . . .	171
76	Effect of Longitudinal Cyclic Pitch on Shank Drag and Lift. . . . .	172
77	Typical ITR Tooling and Manufacturing Plan . . . . .	176
78	Flexure Tooling Concept . . . . .	176
79	Schematic for Broadgoods Ply Stacking (358 Plies, 113 Patterns per Flexure) . . . . .	177
80	Rotation of Flexure Principal Axis Gives Positive Flap-Lag Coupling . . . . .	181
81	Effect of Beam-to-Hub Pitch Angle on Air Resonance Modal Damping . . . . .	182

<u>Figure</u>		<u>Page</u>
82	Effect of Sweep on Air Resonance Mode Damping . . . . .	183
83	Effect of Sweep Angle on Damping . . . . .	184
84	Effect of Blade and Beam Coning Angles on System Damping. .	186
85	Effect of Predroop Angle on Damping . . . . .	186
86	Effect of Control System Stiffness on Stability of the BMR . . . . .	188
87	Effect of Control System Stiffness on Damping of the BMR II . . . . .	190
88	Effect of Adding Damper Strips to BMR C-Beams . . . . .	191
89	Flap Axis Variation Approach . . . . .	193
90	ITR Hub Fold Configuration - Approach for Blade Sweep Variations . . . . .	194
91	Precone Versus Predroop and Alternate Shear Pivot Locations . . . . .	195
92	Cross Section of ITR Hub Configuration 1B With Chordwise Stiffening of Torque Sleeve . . . . .	195
93	Reduced-Stiffness Pitch Links (BO-105/BMR) . . . . .	197
94	Static Stiffness Determinations for Standard and Soft Pitch Links (BO-105/BMR) . . . . .	198
95	Damper Strip Installation . . . . .	199
96	Attachment of ITR to RSRA . . . . .	201
97	RSRA Controls Modifications . . . . .	202
98	RSRA Main Transmission . . . . .	207
99	Current Blade Severance Position . . . . .	211
100	Alternate Plan for Blade Severance . . . . .	211

LIST OF TABLES

<u>Table</u>		<u>Page</u>
1	Rotor System Stability . . . . .	23
2	Scaled Helicopter Parameters . . . . .	23
3	Maneuver Requirements . . . . .	25
4	Control Power Requirements . . . . .	25
5	Boeing Vertol Rotor System Component reliability . . . . .	39
6	Hub Stiffness Characteristics . . . . .	44
7	A Selection of Material Design Characteristics . . . . .	83
8	Relevant Properties of Materials . . . . .	87
9	Assessment of Five Concepts . . . . .	140
10	Survivability of ITR Concepts . . . . .	143
11	Merit Evaluation . . . . .	150
12	Torque Sleeve Stiffness . . . . .	158
13	Conformance With Design Goals and Specifications . . . . .	169
14	Costs of Manufacturing Hub Flexures . . . . .	173
15	Analysis of Composite Hub Manufacturing Methods . . . . .	175
16	Severance System Qualification Tests . . . . .	214

## LIST OF SYMBOLS

A	cross-sectional area, in. <sup>2</sup> , ft <sup>2</sup>
a	radial length of flexure root clamp from rotor shaft, in.
all.	allowable
B	blade
BRG	bearing
C	chordwise
c	curvature; flexure half thickness, in.; blade chord width, ft
CF	blade centrifugal force, lb
C <sub>T</sub>	rotor thrust coefficient, nondimensional
C <sub>w</sub>	flexure cross section geometric constant for warping constraint, in. <sup>6</sup>
D	drag force, lb
E	material modulus of elasticity, lb/in. <sup>2</sup>
EL	endurance limit for zero fatigue damage up to 10 <sup>8</sup> cycles
E <sub>1</sub>	material tensile endurance limit reduction factor, nondimensional
E <sub>1</sub> /E <sub>2</sub>	material ultimate tensile strength reduction factor, nondimensional
e	equivalent; endurance limit; distance of the equivalent hinge from the rotor shaft center, in.
e'	distance of the equivalent hinge from the clamp
F	flapwise; fuselage
G	material modulus of rigidity, lb/in. <sup>2</sup>
g	gravitational force
H	hub
h	vertical offset of the rotor hub from the aircraft center of gravity, in., ft

I second moment of area about the neutral axis of flexure, in.<sup>4</sup>; second moment of mass (inertia), slugs-in.<sup>2</sup>, slugs-ft<sup>2</sup>  
 K a known mathematical constant; hinge stiffness, in.-lb/rad, ft-lb/rad; geometric constant for section shear rigidity, in.<sup>4</sup>  
 k radius of gyration, in.  
 L length of the flap flexure, in.  
 LLF limit load factor, g  
 l flexure length, in.  
 M moment, in.-lb  
 O station zero  
 P axial load, lb  
 R flexure radius of curvature, in., ft; blade tip radius, in., ft; stress ratio, nondimensional; flexure root  
 r radial distance from the rotor shaft center, in.  
 s shear; static  
 T thrust, lb; horizontal tail  
 TPP tip path plane  
 t flexure thickness, in.; tensile  
 u ultimate  
 V linear velocity, ft/sec, kn, mph; vertical shear load, lb; vulnerability  
 W weight, lb  
 w flexure width, in.  
 x radial distance from the flexure root, in.  
 y vertical linear displacement, in.  
 $\alpha$  angle of inclination, rad, deg  
 $\beta$  blade flapping angle, rad, deg; rotor tilt angle, rad, deg

$\delta$  rotor blade vertical tip deflection, in.  
 $\epsilon$  material tensile strain, in./in.,  $\mu$ in./in.  
 $\zeta$  blade lagging angle, rad, deg  
 $\theta$  pitch angle, rad, deg; twisting angle, rad, deg  
 $\mu$  advance ratio, nondimensional; weight per unit length, lb/in.  
 $\sigma$  material tensile stress, psi; rotor solidity, nondimensional;  
first moment of mass  
 $\tau$  interlaminar shear stress, psi  
 $\Omega$  rotational frequency, rpm, Hz, rad/sec  
 $\omega$  natural frequency, Hz, rad/sec

## INTRODUCTION

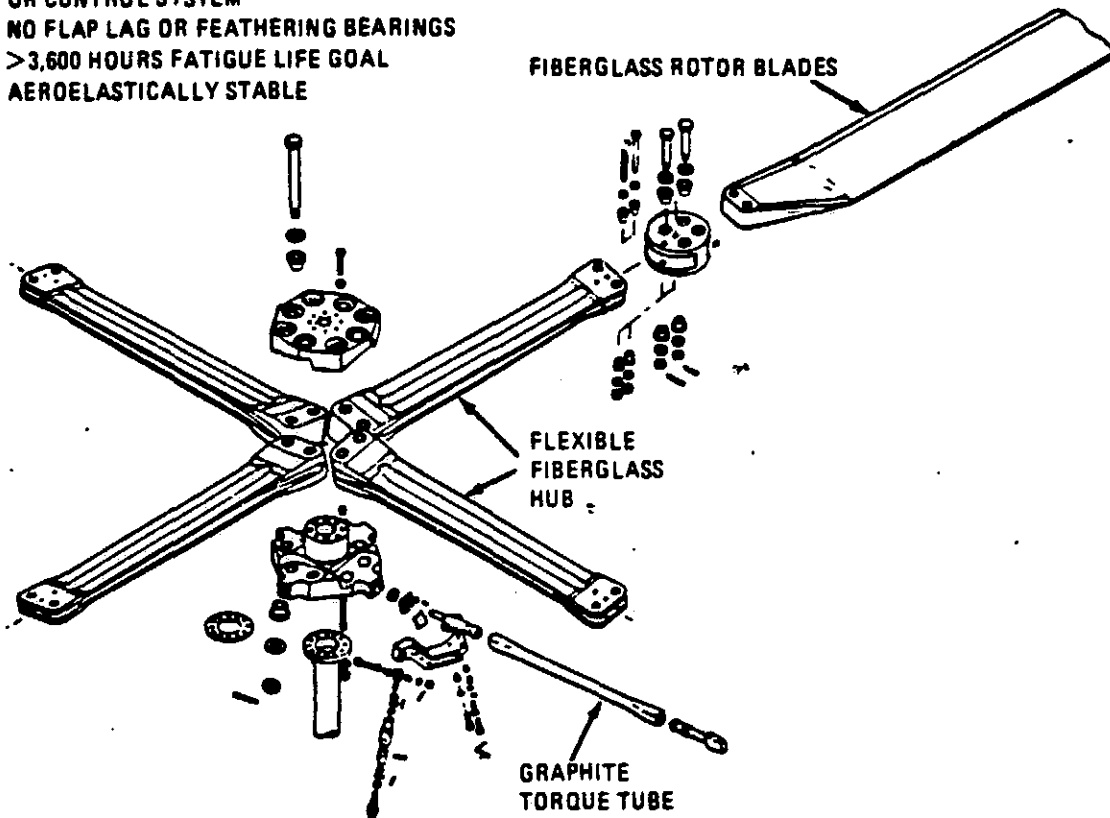
This document is the final report on Phase II, Concept Definition, of a four-phase joint U.S. Army/NASA program to advance rotor technology and to demonstrate these advancements so that a low-risk engineering development effort or a major product improvement program can be initiated. It is also expected that this program will provide the helicopter industry with an advanced engineering data base that can be used in the design and development of future rotary-wing aircraft to satisfy Army and civil requirements. The rotor system technological needs include reduced life-cycle costs; improved reliability, availability, maintainability, durability, survivability, and safety; reduced weight, drag, power, fuel consumption, and noise; improved maneuverability, agility, and air-to-air combat capability; and reduced vibration and gust response. Hingeless or bearingless rotors, coupled with recent developments in blade technology, offer a high potential in meeting these goals. The recent Bearingless Main Rotor (BMR) program (Reference 1), conducted by the Boeing Vertol Company, was highly successful in demonstrating the loads stability and flying qualities characteristics and the feasibility of such a system (Figure 1); however, improvements in all areas are required. The objective of Phase II of this ITR/FRR program was to define a minimum of five hub concepts that address the principal weaknesses of existing bearingless rotor technology and, through simplified methodology, to assess each concept as a prelude to selection of two (of which at least one had to be a bearingless type) for a more detailed estimate of their principal hub characteristics.

- 
- I. Dixon, P. G. C., DESIGN, DEVELOPMENT, AND FLIGHT DEMONSTRATION OF THE LOADS AND STABILITY CHARACTERISTICS OF A BEARINGLESS MAIN ROTOR, USAVRADCOM TR-80-D-3, Applied Technology Laboratory, U.S. Army Research and Technology Laboratories (AVRADCOM), Fort Eustis, VA, 23604, June 1980, AD A086754.

The Integrated Technology Rotor (ITR) is designed to be demonstrated on either the Rotor Systems Research Aircraft (RSRA) alone or on a bailed government or contractor-owned aircraft and on the RSRA. The Flight Research Rotor (FRR) is an ITR modified to facilitate configuration changes for research flight-test evaluations on the RSRA.

**OBJECTIVES**

- SIZE FOR THE B0-105
- NO MODIFICATIONS TO AIRCRAFT OR CONTROL SYSTEM
- NO FLAP LAG OR FEATHERING BEARINGS
- >3,600 HOURS FATIGUE LIFE GOAL
- AEROELASTICALLY STABLE



**ACHIEVEMENTS**

- MET ALL PROGRAM OBJECTIVES
  - STABLE
  - DURABLE
  - FLYING QUALITIES AND VIBRATION SAME AS B0-105
  - BLADE CONTROL LOADS WITHIN SYSTEM CAPABILITY

**FURTHER IMPROVEMENTS PLANNED**

- USE HIGH MODULUS COMPOSITES
- REDUCE NUMBER OF JOINTS
- REPLACE TORQUE TUBE WITH FAIRING
- ADVANCED AIRFOILS AND PLANFORM
- MODAL PLACEMENT
- METHODOLOGY IMPROVEMENT

Figure 1. The Bearingless Main Rotor System

## A REVIEW OF GOALS AND SPECIFICATIONS

The goals and specifications for both the ITR system and the hub components were listed in the appendixes of the RFQ.

A review of these objectives was conducted relative to an independent Boeing Vertol estimate of the potential mission flight envelope and maneuverability requirements. Based on this review, the adequacy and reasonableness of the rotor hub specifications and technical goals with respect to the design loads, stiffness, and moment characteristics of the ITR/FRR hub were determined. For the purpose of independently estimating rotor hub design loads, a representative set of helicopter characteristics and operating conditions was chosen, including, but not limited to, hover, cruise, and maneuvering flight such as nap-of-the-earth operation, and high-speed maneuvers such as rolling pullouts, pushups, and pushovers.

### REVIEW OF ITR/FRR SYSTEM DESIGN SPECIFICATIONS

The following system design specifications, intended to be used as guides for establishing a minimum set of operating conditions and other design constraints, have been reviewed individually. Comments are included in the following paragraphs.

#### Design Gross Weight

The ITR rotor system will be demonstrated on a contractor-owned or government-bailed vehicle and this has an influence upon the selection of the 16,000- to 23,000-pound design gross weight range. A requirement to demonstrate the ITR on the RSRA dictates the upper limit, but a rotor system designed for 16,000 pounds would more directly support YUH-60 product improvement and YAH-64 growth.

For the long-range view, LHX, although not totally defined, at this time appears to be of the 6,000- to 9,000-pound design gross weight class. The small size would have resulted in significant savings in program cost but would not permit significant research testing on the RSRA.

The selected range appears to be a prudent choice that can be met by all participant contractors if they are successful in competing for the follow-on phases of the ITR program.

### Design Envelopes

The structural design envelope is compatible with the design of the UH-60, AH-64, and YUH-61A types of aircraft. If the rotor system is designed for the minimum gross weight, demonstration of the structural envelope extremes on the RSRA would require careful consideration to avoid overloading the rotor due to turbulent conditions. Furthermore, the RSRA will not have enough power to reach 185 knots  $V_{\text{Dash}}$  without the auxiliary propulsion.

The slope landing condition of 12 degrees is a necessary requirement.

### Rotor System Instability

The requirement that the rotor system be free of critical instability, both aeroelastic and mechanical, at all operating conditions and throughout a typical range of gross weights needs to be more definitive. The BMR program demonstrated marginal stability in both autorotation and on the ground, so it would be useful to have an acceptable minimum predicted stability level such as 2-percent critical damping in the fixed system with zero structural damping. This minimum should also apply to future demonstrations through wind tunnel model testing. The specification that "the rotor hub design requirements shall be consistent with fuselage and blade mass and inertia characteristics typical of the design gross weight" is an obvious requirement, but stability demonstration of a 16,000-pound gross

weight rotor design upon the RSRA at an 18,400-pound minimum gross weight may be precluded due to inertial incompatibility.

If the YUH-61A is a typical helicopter of 16,000 pounds design gross weight, then the implication cited above is demonstrated by Table 1.

TABLE 1. ROTOR SYSTEM STABILITY

Aircraft	Design Gross Weight (lb)	Pitch Inertia (lb-in./sec <sup>2</sup> )	Roll Inertia (lb-in./sec <sup>2</sup> )
YUH-61A	15,300	350,500	40,700
UH-60	16,240	480,500	67,545
RSRA	18,400	1,170,000	102,000

Based upon scaling laws where inertia is proportional to the square of design gross weight, typical helicopter parameters scaled up to RSRA gross weight are shown in Table 2.

TABLE 2. SCALED HELICOPTER PARAMETERS

Aircraft	Design Gross Weight (lb)	Pitch Inertia (lb-in./sec <sup>2</sup> )	Roll Inertia (lb-in./sec <sup>2</sup> )
YUH-61A	18,400	507,000	58,863
UH-60	18,400	616,820	86,700
UH-60	23,000	963,800	135,480
RSRA	18,400	1,170,000	102,000

The results show that stability characteristics of a typical ITR/helicopter system cannot be properly simulated on the RSRA unless the ITR is designed to 23,000 pounds gross weight and flown with the RSRA at its minimum gross weight. The only requirement, however, is that the rotor be stable on the RSRA.

## Rotor Configuration

Four-bladed systems are compatible with current state-of-the-art requirements for vibration and, as a practical minimum, for rotor solidity requirements as dictated by hover performance and maneuverability.

The requirement of not precluding the incorporation of simple and quick manual blade folding and removal which does not require rebalancing or re-tracking is necessary for helicopter storage and transportation. Other normal operational requirements are accepted as standard, together with tree and wire strikes, but better definition of vulnerability to combat damage is required. The specification has been interpreted to intend that the concepts should be designed so that survivability against any 23-mm projectile, impacting from any direction, is maximized and that totally vulnerable area of the rotor hub system should be minimized.

## Maneuverability

Accomplishment of the scout, attack, or utility helicopter missions requires a high level of maneuverability for terrain following, obstacle avoidance, evasive action, or nap-of-the-earth (NOE) flight. From a rotor design viewpoint, two particular areas influence the rotor parameters chosen for a vehicle.

One is the ability to generate the thrust necessary for positive load factor in forward flight, and the second is to maintain aircraft control at low or negative load factors.

Since the usable thrust capability of a rotor decreases with increasing speed, the specification of a positive load factor maneuver at given ambients and a high forward speed will establish basic parameters such as radius, tip speed, and solidity. Table 3 compares the ITR specifications to those imposed on the UTTAS and AAH competitions which led to the UH-60A and the AH-64.

TABLE 3. MANEUVER REQUIREMENTS

	UTTAS and AAH	ITR
Positive Load Factor, g's	1.75	1.75
Airspeed, knots	150	170
Ambient Conditions, ft, deg F	4,000, 95	4,000, 95
Maneuver	Symmetrical pullup held for 3 seconds	Constant speed and power turn

While the load factor and the ambient conditions are the same, the increased airspeed presents a more severe lift requirement. In addition, since useful maximum rotor thrust decreases with propulsive force, the steady turn maneuver is more demanding than the symmetrical pullup during which power and propulsive force requirements decrease. The ITR requirements will therefore produce a rotor having significantly better maneuver characteristics than current state-of-the-art aircraft.

Adequate controllability at low load factors is necessary for confident NOE flight and to minimize aircraft exposure to threats while terrain following. Extensive flight evaluations and piloted simulation tests at Boeing Vertol indicate that pilots prefer no more than a one-third change in control sensitivity with maneuver. As shown in Table 4, the ITR design will meet this for a zero-g pushover and will therefore represent an improvement when compared to present service helicopters.

TABLE 4. CONTROL POWER REQUIREMENTS

	YUH-61A	ITR Test Vehicle
Nominal Rotor Thrust (lb)	16,000	16,000
Rotor Height Above CG (ft)	4	Approx 6
Max Steady Flapping (deg)	2.2	4
Hub Moment Endurance Limit (ft-lb)	20,000	16,000
Hub Moment per Unit Flapping (ft-lb/deg)	9,000	4,000
Total Control Moment per Deg (ft-lb/deg)	10,117	5,675
Total Available Control Moment (ft-lb)	22,482	22,700
Control Remaining at 0 g (%)	89	70

## Flight-Test Aircraft

Freedom of choice in the selection of the flight-test aircraft permits the contractor to assess the suitability of its own aircraft against others available, including the RSRA. For ITR concept definition, prior selection of the test demonstration aircraft is not mandatory; however, the definition of representative helicopter characteristics to be conducted under this statement of work is eased if a tentative selection is made. This must include consideration of candidate aircraft capabilities of demonstrating the technical goals, availability of the aircraft in the 1985-87 timeframe, and familiarity with the aircraft characteristics.

## REVIEW OF ITR/FRR SYSTEM TECHNICAL GOALS

The stated purpose of the goals is to stimulate the advance of rotor system technology to the maximum possible extent. A review of the reasonableness of these goals is presented in the following paragraphs and refers to the Boeing Vertol advanced rotor blade as representing current advanced state of the art.

$$\underline{L/D_E \text{ Without Hub Drag at } V_{\text{Cruise}} = 10.5}$$

The blade area requirements associated with meeting the 1.75-g maneuver requirements make it difficult to meet the 10.5 maximum  $L/D_E$  goal. As noted in Figure 2, the advanced rotor that meets the maneuver requirements has a maximum  $L/D_E$  of approximately 9.6 and this occurs at an airspeed of 170 to 180 knots.

In order to meet the  $L/D_E$  goal of 10.5, the solidity would have to be reduced approximately 15 percent, with a corresponding reduction in maneuver capability from 1.75 g's to 1.5 g's. For comparison, the YUH-61A and UH-60  $L/D_E$  characteristics are also presented in Figure 2. As shown, the YUH-61A maximum in  $L/D_E$  is 7.5 and it occurs at an airspeed of 130 knots.

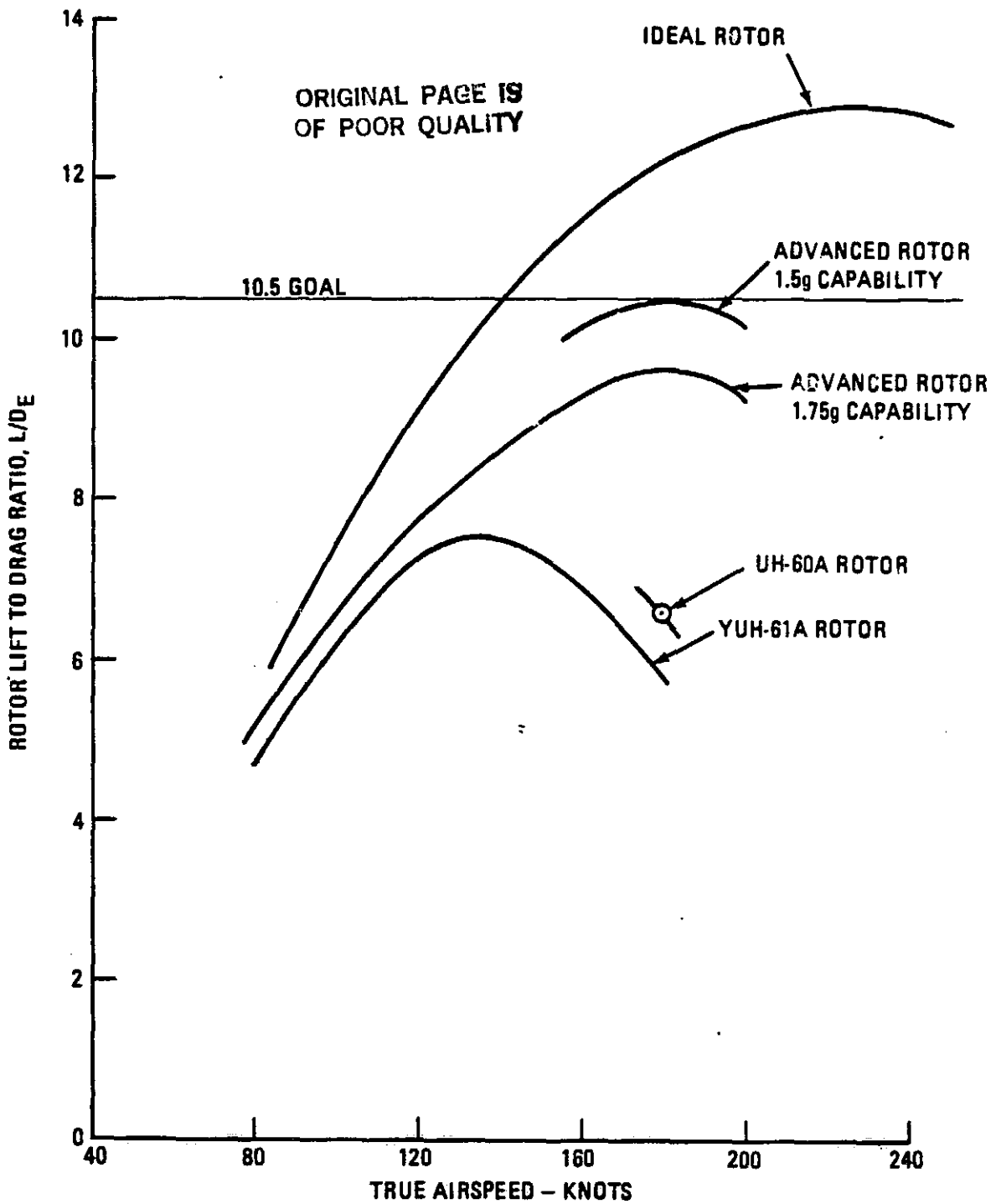


Figure 2. Maximum Rotor  $L/D_E$

The  $L/D_E$  for an ideal rotor based on simplified theory is also shown in Figure 2 to illustrate the potential maximum  $L/D_E$ . The ideal rotor  $L/D_E$  is defined using the classical power equations, assuming  $Cd_0 = 0.0072$  and a torque-adjusted solidity of 0.1. As noted, the maximum  $L/D_E$  for the ideal rotor is 13, indicating that advanced concepts with elastic twist and planform tailoring may be able to close the gap between the ideal and the advanced rotor proposed for the ITR and potentially meet the  $L/D_E$  goal as well as the maneuver requirements. However, such capabilities are in the early development stages and represent a higher risk than is acceptable for the ITR. For this reason, they are being proposed for the FRR. The FRR concepts have the potential of providing a substantial  $L/D_E$  improvement at speeds as high as 225 knots.

Maximum Rotor Figure of Merit, Rotor Alone = 0.80

A preliminary analysis of the 0.8 goal indicates that it cannot be achieved if the rotor is also to meet the 1.75-g maneuver and 170-knot cruise goals. The capability of achieving the hover goal was addressed by computing the maximum figure of merit for a blade with a twist and planform optimized for hover without considering maneuver and forward flight design constraints. The optimum blade geometry was defined with the computer program OPT ROT which selects the twist and chord to achieve uniform downwash with each blade section operating at maximum  $L/D$ . The results of the optimizing program were then input into the B92 vortex theory analysis to obtain a more accurate assessment of performance.

As shown in Figure 3, the resulting maximum figure of merit for the optimum-geometry blade decreases with increasing thrust-weighted solidity. At a solidity of 0.085, the optimum rotor meets the 0.8 goal; however, this solidity is not adequate to satisfy the 1.75-g maneuver requirement. Given a UH-60-size ITR rotor operating at 725 ft/sec tip speed, the solidity required is approximately 0.103. At this solidity the optimum figure of merit is reduced to 0.78. As noted in Figure 3, the advanced blade

figure of merit is 0.75. The figure of merit difference between the optimum and advanced blade geometry is due to the higher cutout and lower twist of the advanced blade. The ideal rotor twist is highly nonlinear and the advanced blade has 12 degrees of linear twist as dictated by cruise performance requirements.

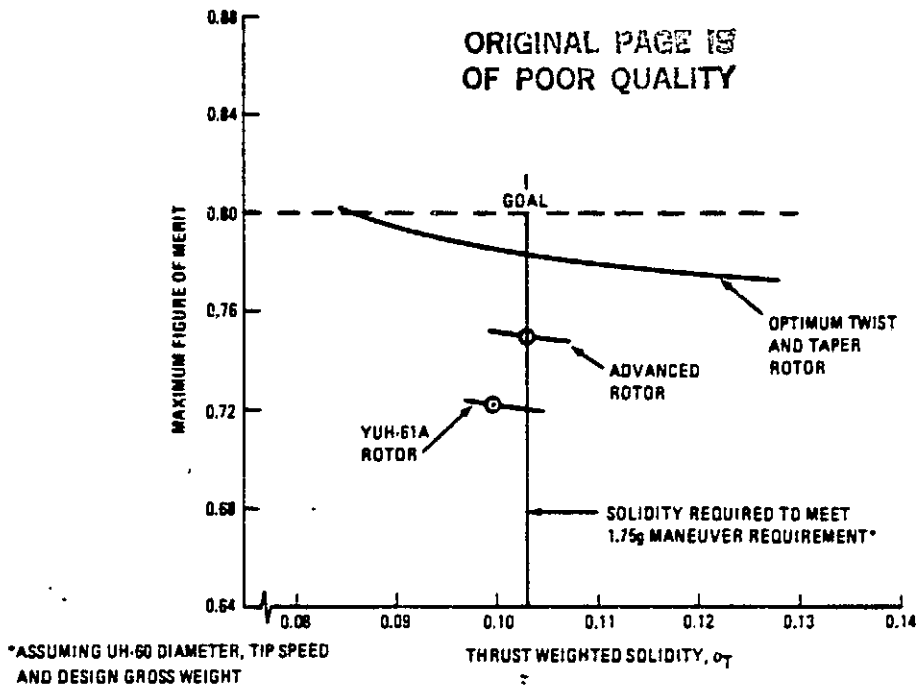


Figure 3. Potential for Achieving the ITR Maximum Figure of Merit Goal

The YUH-61A maximum figure of merit is also presented in Figure 2 to illustrate the improvement of the advanced rotor over the current generation of helicopters. As shown, the YUH-61A peak figure of merit is 0.72, or 3 percent less than that of the advanced rotor.

The trends shown in Figure 3, which have been substantiated by recent test data (Reference 2), indicate that the maximum figure of merit increases as thrust coefficient ( $C_T$ ) decreases. Therefore, the ITR disk loading should be minimized for a given tip speed in order to maximize the figure of merit.

2. McHugh, F. J., and McVeigh, M. A., RECENT ADVANCES IN ROTOR TECHNOLOGY AT BOEING VERTOL, 30th Annual Forum of the American Helicopter Society, Anaheim, California, May 1982.

Rotor Hub Flat-Plate Drag Area at 16,000 Pounds Design Gross Weight = 2.8 Square Feet

A definition of the hub content of the rotor system is a major omission in the attainment of this goal; for the purpose of this program, the hub will be assumed to consist of that portion of the rotor system from the shaft attachment to the start of the main blade airfoil or root cutout.

The ITR hub drag goal of 2.8 ft<sup>2</sup> at 16,000 pounds design gross weight is compared to faired hub drag trends in Figure 4. As noted, the ITR goal is 28 percent below the lowest demonstrated hub drag. However, the drag trends include hub/fuselage interference drag and the goal does not.

Typically, the interference drag is on the order of 25 percent of total hub drag, as defined in Reference 1; this would make the ITR hub drag plus interference drag approximately equal to the minimum demonstrated faired hub drag trend.

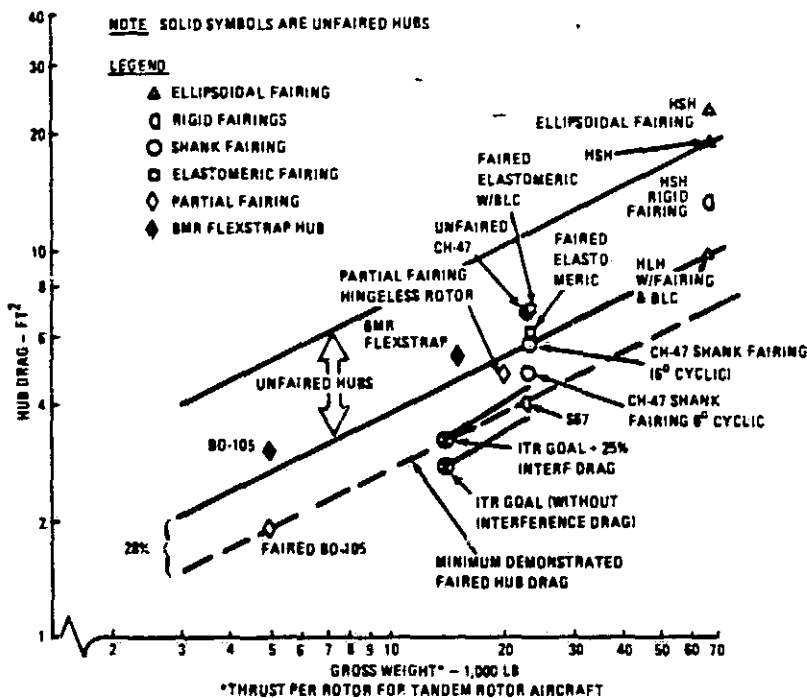


Figure 4. Faired Hub Drag Trends

V<sub>Cruise</sub> Using MCP = 170 KTAS

A preliminary estimate of the advanced rotor speed capability is defined in Figure 5, where the power required is normalized by hover power and is presented as a function of airspeed for 4,000 ft/95°F, 19 ft<sup>2</sup> of drag, and 16,000 pounds gross weight. Performance is shown for tip speeds of 700 ft/sec and 725 ft/sec. As noted, the advanced rotor meets the 170-knot cruise speed goal at 85 percent of hover power required at a tip speed of 700 ft/sec. The cruise and dash speed goals are specified as a function of hover performance, indicating that the rotor should be designed for high disk loading which will increase the hover induced power. It appears that the cruise speed goal can be met.

V<sub>Dash</sub> Using IRP = 185 KTAS

The dash speed goal is compared to the advanced blade dash speed capability in Figure 5. As shown, the advanced blade design meets the 185-knot goal at 100-percent hover power required and 700 ft/sec tip speed.

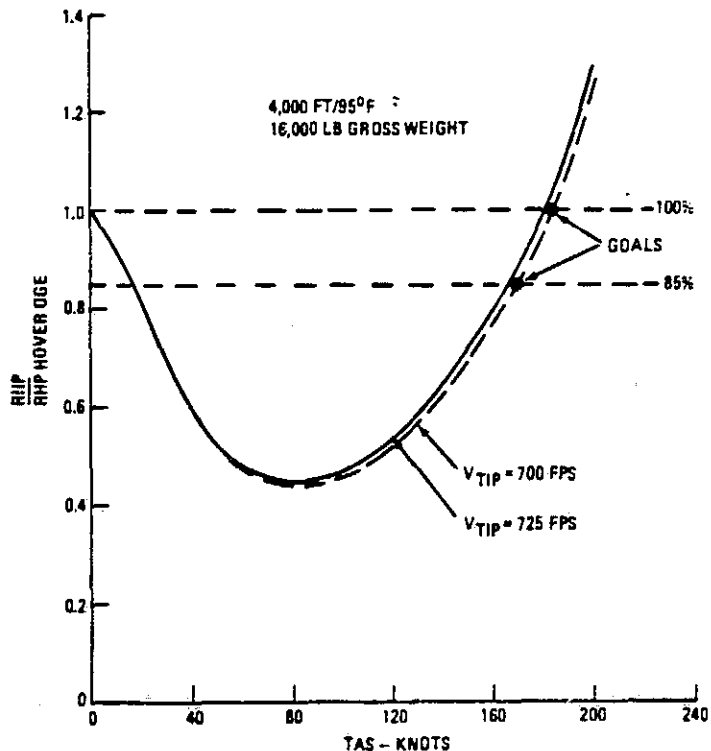


Figure 5. ITR Speed Capability

Reduction in Low-Frequency Impulsive Noise = 6 db

The technical goal for noise is a 6-db reduction based upon the current UH-60 level, which is classified information. In lieu thereof, discussion can center on Figure 6, which is extracted from the U.S. Army Technical Development Plan presented to industry on 9 October 1980.

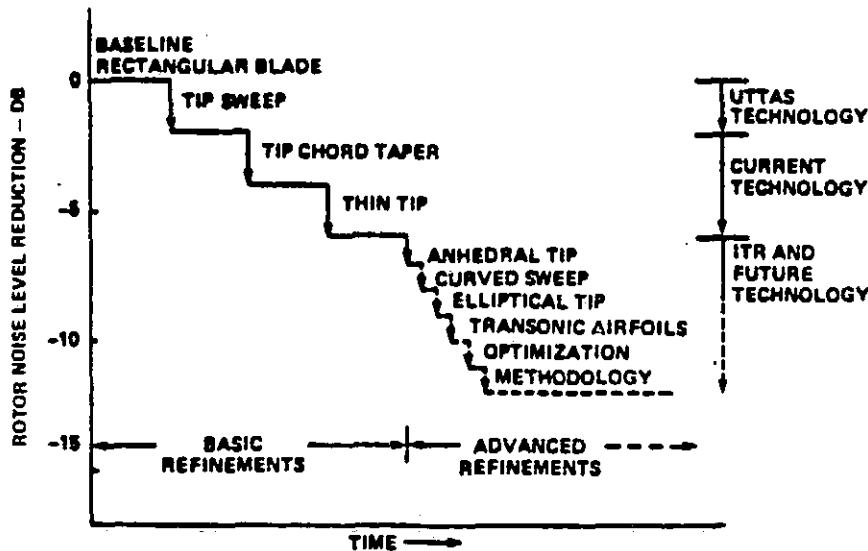


Figure 6. Probable Improvements in Noise Reduction

This rotor acoustics technology chart shows probable improvements in noise generation from the baseline rectangular-tipped blade resulting in 2-db reduction with the UH-60 swept tip. From this new baseline, a further 2-db improvement is promised through tip chord taper; however, Boeing Vertol experiments over the past decade have failed to confirm this potential. A thin tip is shown to result in an additional reduction of 2 db which is generally accepted, unlike the contribution of anhedral which is shown to have a potential of a 1-db reduction.

Future technological advances, as suggested by the figure, of curved sweep, elliptical tip, and transonic airfoils promise to effect additional reductions of 1 db each. However, curved sweep may be a tradeoff with linear sweep, elliptical tips with tip chord taper, and transonic airfoils with thin tips, and thus, the results may not be additive and credit of 1 db can be taken only through optimization, and possibly a further 1 db through methodology improvements.

The Boeing technical staff believes that an overall 6-db reduction is overoptimistic and that a 3-db reduction from the UH-60 noise level is possible, with maybe an additional 2 db through improvements in optimization and methodology.

Boeing Vertol has an ongoing IR&D program directed at improving capability in noise prediction and noise reduction. The success of these efforts is illustrated in Figure 7 which compares noise levels of the Boeing Vertol Model 234 helicopter, which uses an all-fiberglass blade, with most of the rest of the world's fleet. Part of the research background which led to this achievement is presented in Figure 8. The data for each of the rotors were acquired during flights on a CH-47C aircraft and include take-offs, level flyovers, and approaches, with variations in rotor speed and cyclic trim. Despite the fact that the gross weight with the VR7/8 airfoil was slightly greater than that with the 23010 airfoil, the separation of data scatter bands indicates that the reduction in peak chordwise pressure is beneficial in controlling noise and is illustrative of the impact of airfoils on the acoustic signature. Further development of high-speed rotors has included wind tunnel tests of even more advanced transonic airfoils and tips. Figure 9 shows the improvement in suppression of thickness noise at high speeds which has been demonstrated during model development tests of Boeing Vertol's advanced rotor. As illustrated, the new VR12/15 airfoil makes no more noise at 186 knots than did its predecessor, the VR7/8, at 170 knots.

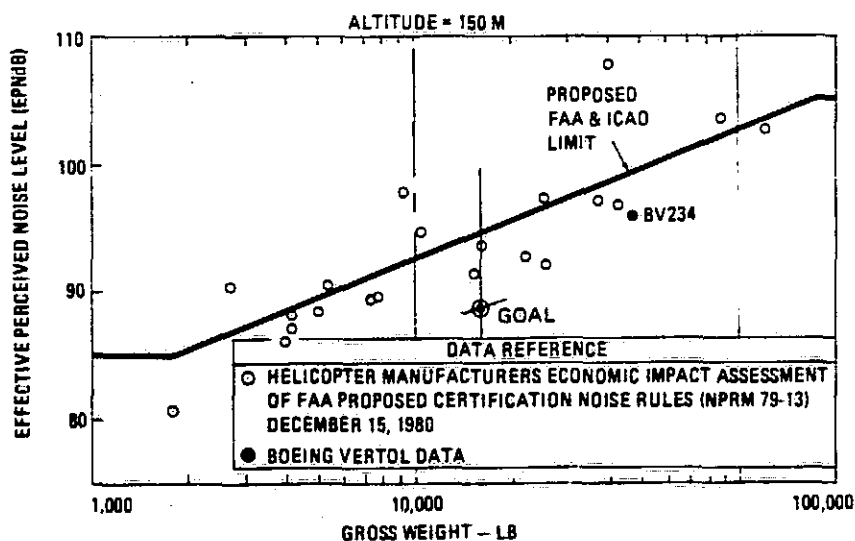


Figure 7. Helicopter External Noise Levels in Level Flight

ORIGINAL PAGE IS  
OF POOR QUALITY

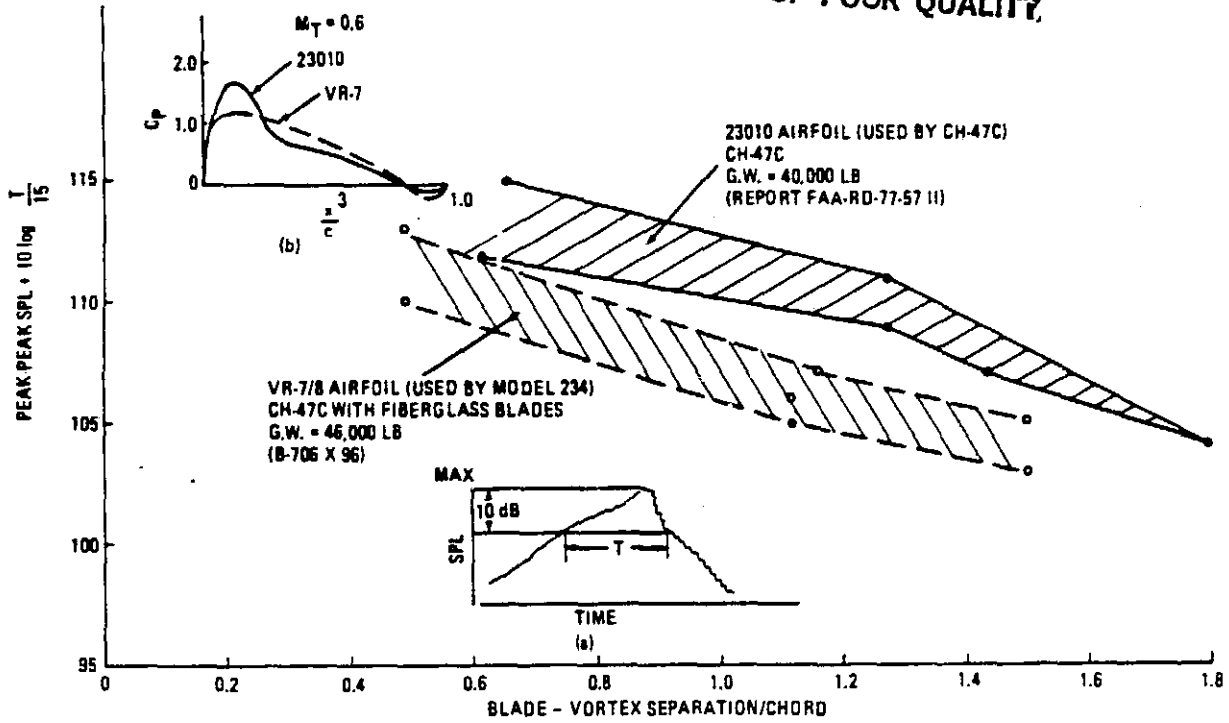


Figure 8. Effect of Airfoil on Rotor Harmonic Noise

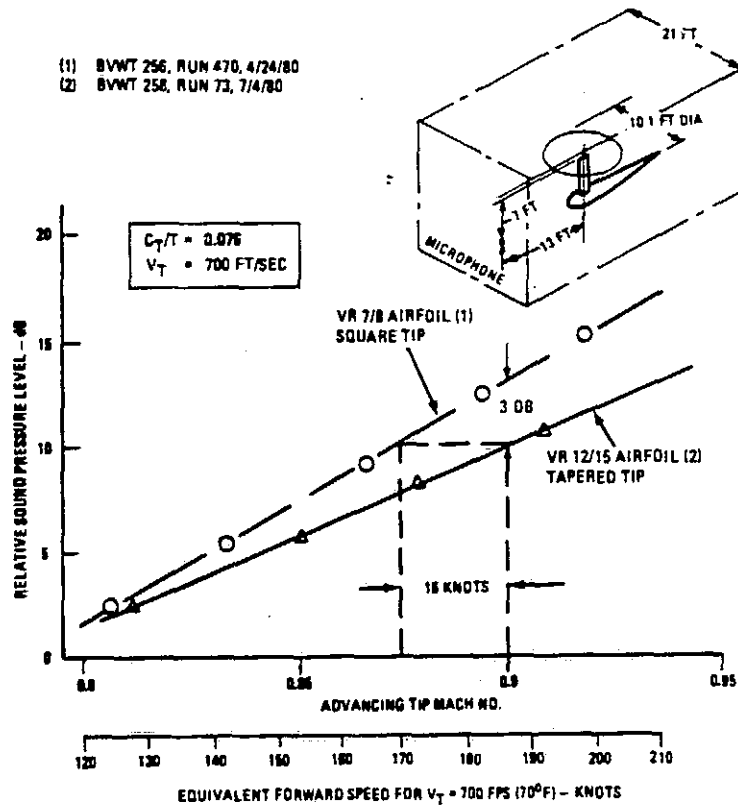


Figure 9. Effect of Airfoil on Sound Pressure Level of a Model Rotor at High Forward Speed

### Rotor Weight as a Percentage of Design Gross Weight = 7.0

Rotor weight is the sum of hub weight and the total weight of the four blades. Minimum allowable blade weight is governed by requirements for safe autorotative landing. From blade weight trend data shown in Figure 10, the probable blade weight contribution to the ITR rotor can be determined. For example, for 16,000 pounds design gross weight, a rotor diameter of 53.7 feet, chord between 26 and 29 inches, and root attachment to the hub at 20-percent radius, a sizing factor ( $K_p$ ) range between 1,653 and 1,843 would be applicable, resulting in a total blade weight ranging from 7.06 to 7.41 percent of design gross weight. These exceed even the goal for the blades and hub together.

Similar trend data for hubs would result in a hub weight range compatible with that obtained for the blade; however, these established trends are for metal configurations and are not appropriate.

Based on the industry survey shown in Figure 10, Figure 11 shows individual blade weight expressed as a ratio of design limit load and number of blades. The Boeing Vertol advanced blade is shown to be 23 percent lighter than the average, but for autorotation it still exceeds the required ratio of KE/HP (1 second). This was achieved through optimization of the radial mass distribution and material selection, to provide maximum inertia with appropriate consideration for the vibration, loads, and strength characteristics.

The lowest weight that the ITR blade can achieve is expected to be 77 percent of the historical trend weight which is 5.44 to 5.71 percent of the design gross weight, which leaves 1.56 percent (not 2.5 percent) for the hub.

It is therefore concluded that this goal will be difficult to achieve and should be more realistically set to 8.0 percent of the design gross weight.

### Rotor System Parts Count = 75

Boeing Vertol believes that to reduce acquisition and life-cycle costs the objective in all design phases must be to reduce the number of nonstandard



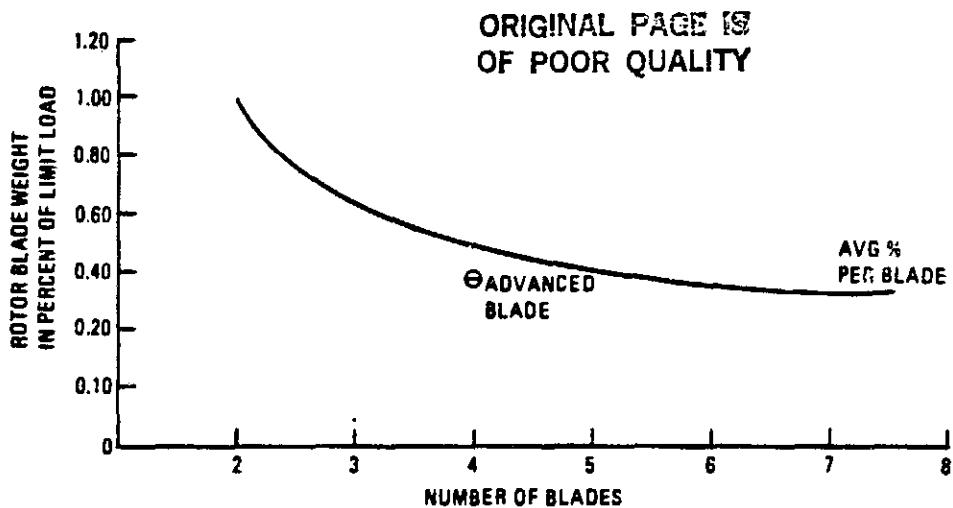


Figure 11. Average Rotor Blade Weight Expressed as Percent of Limit Load

parts. Although individual part cost must be dependent upon size and complexity, such factors are evened out in the overall picture when a large number of parts are to be fabricated, stored, used, and maintained. Figure 12 shows how the evolution of Boeing Vertol rotor hub systems, from articulated with lubricated hinge bearings through hingeless with only lubricated feathering bearings, to bearingless, has reduced parts count. Elastomeric bearings are replacing the lubricated types, but they have a finite fatigue life and attendant frequent inspection interval and do not provide the potential advantages offered by bearingless systems.

The definition of a part must be established. Nonstandard parts or those that cannot be purchased off the shelf could be used. Pitch links should be included, together with the rotor shaft, since it can possibly be integrated as part of the flexure-to-shaft attachment.

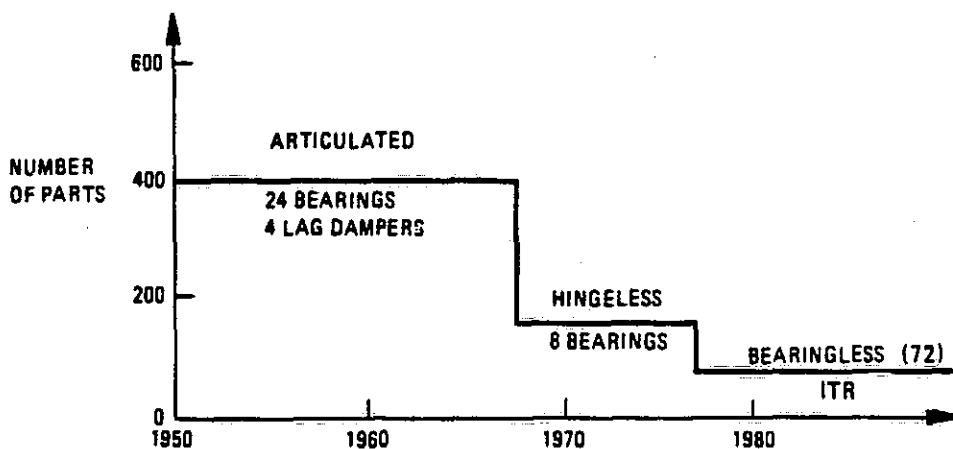


Figure 12. Evolution of Rotor System Parts Count

### Rotor System Fatigue Life = 10,000 Hours

Ten thousand hours of 1-per-rev blade motions in a rotor system of 53.7-foot diameter and 700 ft/sec tip speed are equivalent to  $1.49 \times 10^8$  cycles. The composite material design endurance limit is expressed as  $10^8$  cycles, which is comparable. To meet this ITR goal, "no fatigue damage is acceptable", which may be too conservative.

### Mean Time Between Removals (MTBR) = 1,500 Hours

The ITR technical goal is an MTBR of 1,500 hours for the rotor system, excluding the rotating controls. This MTBR includes scheduled and unscheduled removals for overhaul, repair, and inspection. It does not include removals due to external causes such as accidents, battle damage, operational stresses beyond design limits, crew-induced maintenance actions, cannibalization, or modification.

To meet the technical goal of 1,500 hours for the ITR system MTBR, component goals of 7,500 hours MTBR are necessary for each of the rotor blades and for the hub.

Based on the service performance of our current production rotor systems, including the recently introduced fiberglass-reinforced composite rotor blades (Table 5), this reliability goal is optimistic. If the MTBR for the hub is to be 3,000 hours, then this equates to the rotor blade goal of 12,000 hours MTBR.

Figure 13 gives the reliability growth curve of the CH-46 fiberglass blade, showing a steady rise in MTBF as fleet blade hours are accumulated, malfunctions occur, and design and manufacturing corrective action is introduced. The MTBR achieved a similar growth. It can be seen that the present MTBR of 3,232 hours at 303,800 fleet blade hours projects to an MTBR of over 5,000 hours at 1,000,000 blade hours, based on the growth rate demonstrated by the MTBF history.

TABLE 5. BOEING VERTOL ROTOR SYSTEM COMPONENT RELIABILITY

Component	Model	Component Flight Hour Base	MTBUR (hr)	TBO (hr)	MTBRD (hr)	MTBR (hr)	Note
Rotor Hub (fwd and aft)	234 (Chinook)	10,322	10,322	1,500	-	1,396	1,2,3
Rotor Hub (fwd)	YCH-47D	2,100	-	2,400	2,100	-	3,4
Rotor Hub (aft)	YCH-47D	2,100	-	2,400	700	-	3,5
Rotor Blade (composite)	CH-47C, YCH-47D	24,740	-	None	12,370	-	6
Rotor Blade (composite)	234 (Chinook)	30,966	1,720	None	-	1,720	7
Rotor Blade (composite)	CH-46	303,848	3,232	None	(no depot returns)	3,232	7

NOTES: 1. MTBR computed from MTBUR, TBO; [MTBR = MTBUR (1 - e<sup>-TBO/MTBUR</sup>)]

2. 1,500-hour TBO is TBO sample; TBO to be determined
3. TBO desired for rolling-element bearing replacement
4. 2,100-hour MTBRD was TBO sample.
5. 700-hour MTBRD resulted from rolling-element bearing malfunction.
6. No other reliability data available for this blade
7. MTBR not representative of mature blade; continual improvement in manufacturing processing increases MTBR.

ORIGINAL PAGE IS OF POOR QUALITY



### Vibration Acceleration = 0.1 g

To meet this goal without vibration absorption devices is optimistic. The total understanding of the sources and correction of rotor vibration is not currently available and extensive research and development are required. This target, although only a goal, is beyond the scope of the ITR concept definition program; however, vibration reduction research and development should be a prime objective of the FRR program. Vibration levels should be required at the hub/shaft attachment and exclude shaft effects.

### Cost = Minimum

The lowest possible procurement cost is always the goal of the manufacturer. A specific goal should be set based upon a quantity buy and divided into hub and blade components. The goal should include both recurring and nonrecurring costs.

### REVIEW OF HUB DESIGN SPECIFICATIONS

Hub design specifications stated in Appendix B of the RFQ echo those stated for the ITR system specifications of Appendix A. Comments made on the system specifications are applicable to the hub.

### REVIEW OF HUB TECHNICAL GOALS

The following paragraphs review the goals for this ITR/FRR hub concept definition as specified in Appendix B of the RFQ.

### Rotor Hub Flat-Plate Drag Area = 2.8 Square Feet

This item has been addressed in the ITR system technical goals.

### Rotor Hub Weight as a Percentage of Design Gross Weight = 2.5 Percent

Rotor weight was discussed in the review of the IT<sub>R</sub> system technical goals and a rationale for the breakdown of that 7-percent goal into separate goals for the blades and hub was given. For autorotation characteristics, a first-cut assessment indicates that 5.44 percent should be allotted to the rotor blades which leaves 1.56 percent (assuming 7 percent for the system) for the hub. To meet the overall goal, the hub component should be set at 2 percent. It is important that the hub/blade boundary radial location be defined.

### Rotor Hub System Parts Count = 50

This parts count, exclusive of standard fasteners, appears to be realistic. A part should be defined, for example, as "any component not divisible into subcomponents without causing irreparable damage to the component."

### Rotor Hub Moment Stiffness = 100,000 Foot-Pounds per Radian

The qualification of this goal describes the blades as rigid, implying that the angular measure pertains to the hub/blade attachment.

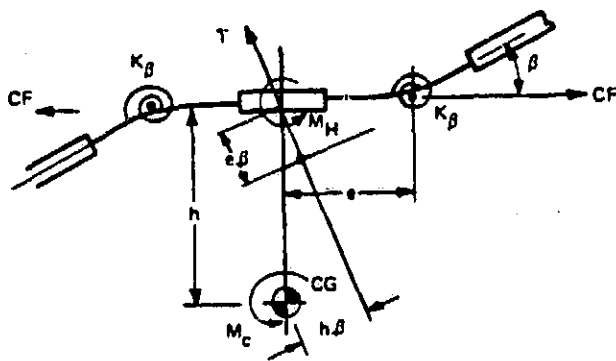
The Blackhawk hub contains a universal elastomeric bearing of low angular stiffness ( $K_{\beta} = 4,167$  ft-lb/rad) and with its rotational center at a distance ( $e$ ) from the hub centerline of approximately 14 inches, or 1.17 feet. In this example, hub stiffness ( $M_H/\beta$ ) of the Blackhawk (for a blade centrifugal force of 70,000 pounds) has been estimated to be 172,134 ft-lb/radian. Even with zero hinge spring, the stiffness of 163,800 ft-lb/radian exceeds the goal of 120,000 ft-lb/radian by 37 percent.

Or, conversely, for 120,000 ft-lb/rad of hub stiffness, each flapping blade must contribute 60,000 ft-lb/rad which would require, with zero hinge stiffness, an equivalent hinge offset ( $e$ ) of 0.86 foot (10.28 inches). For a radius ( $R$ ) of 294 inches (YUH-61A), the percentage is  $3\frac{1}{2}\%R$ .

Adding a hinge spring to the system due to a flexure (as in a bearingless configuration) would miss the goal even more than in the case of the Blackhawk. If the bearingless hub system contains droop restrainers, a hub stiffness goal of 200,000 ft-lb/radian would be reasonable; however, if the hub flexure is designed to react limit flap bending, a further increase up to the order of 300,000 ft-lb/radian is not unexpected.

Hub stiffness provides aircraft pitch and rolling moment at low and negative load factors, a desirable characteristic for improvements in helicopter agility, maneuverability, and control response required for air-to-air combat and nap-of-the-earth missions. Increased hub stiffness, however, increases undesirable system gust response and vibration characteristics. The ITR design process must include steps to minimize these undesirables without deviating from the hub stiffness goal by tailoring the blade so that vibration is minimized. Stability augmentation systems and AFCS have been demonstrated to alleviate the gust response and such systems are now considered to play a necessary role in modern helicopters.

The contribution of hub stiffness to the aircraft control moment is shown in Figure 14, which represents a rotor system situated a distance (h) above the aircraft cg and with blades flapping due to response to control cyclic input and/or gust, through a displacement ( $\beta$ ), about a center a radial distance (e), the effective flap hinge offset, from the shaft centerline.



$$\left. \begin{aligned} \text{If } M_{\text{tilt}} &= T h \beta \\ \text{and } M_{h(\text{offset } e)} &= 2 e CF \beta \\ \text{and } M_{h(\text{spring})} &= 2 K_{\beta} \beta \end{aligned} \right\} = M_H$$

Total Aircraft Control Moment

$$M = \beta (T h + 2 e CF + 2 K_{\beta})$$

Figure 14. Derivation of Control Moments

Hingeless and bearingless rotors have an additional structural spring stiffness ( $K_{\beta}$ ) due to the flexure replacing the flapping hinge arrangement of the articulated rotor. This additional stiffness provides the improvement in control response.

Increase in  $K_{\beta}$  also decreases blade displacement ( $\beta$ ) for both the dynamic and static loading conditions and can, if sufficiently large, preclude the need for blade flap and droop stops which prevent blade tip-to-fuselage contact, at the expense, however, of hub flexure endurance limit flapping capability.

The hub moment ( $M_H$ ) is shown in the figure to be directly proportional to  $\beta$  and consists of the contributions from effective hinge offset and blade CF ( $CF_e$ ) and the spring stiffness ( $K_{\beta}$ ). To reduce the need for droop stops and maintain the goal for total hub stiffness, the spring stiffness must be maximized and the hinge offset minimized.

Table 6 shows the contribution of these parameters to the hub stiffness characteristics of various helicopter systems.

TABLE 6. HUB STIFFNESS CHARACTERISTICS

Hub Type	Helicopter	Radius (ft)	Hinge Offset, C (% radius)	Blade CF (lb)	Hub Stiffness, $M_H/\beta$ (ft-lb/deg)	Hinge Spring, $K_{\beta}$ (ft-lb/deg)
Articulated	UH-60	26.8	4.70	67,798	2,981	0
	CH-46	25.5	1.67	58,887	875	0
	CH-47	30.0	2.22	100,319	1,752	0
Hingeless	YUH-61	24.5	15.	66,175	8,500	515
	BO-105	16.1	13.4	34,750	2,838	144
Bearingless	BMR	16.1	11.38	40,000	2,848	144

Maneuverability and flying qualities characteristics provide the requirement for a high hub moment stiffness. A Boeing Vertol flying qualities criterion is explained in the following discussion on hub overturning moment and concludes that the goal should be 250,000 ft-lb/radian.

Figure 15 shows the relative control sensitivity for teetering, articulated, and hingeless rotor systems.

Control Sensitivity ( $\frac{M}{\beta}$ ) for Figure 15 is written as:

$$\text{Teetering: } \frac{M}{\beta} \sim Th$$

$$\text{Articulated: } \frac{M}{\beta} \sim Th + 2CF_e$$

$$\text{Hingeless: } \frac{M}{\beta} \sim Th + 2CF_e + 2K_\beta$$

A Boeing Vertol flying qualities criterion is that "at least two-thirds of the control moment sensitivity at 1-g level flight must be available at all times."

From inspection of the foregoing equations, minimum control moment sensitivity ( $M/\beta$ ) occurs when the thrust (T) is zero or negative. The ITR criterion specifies the minimum condition to be -0.25 g. Then it follows that,

$$\left(\frac{M}{\beta}\right)_{-0.25g} = \frac{2}{3} \left(\frac{M}{\beta}\right)_{1.0g} \quad (1)$$

Figure 15 presents the relative control moment sensitivity variation with g level for the three rotor types.

It should be noted that the change in sensitivity with thrust ( $\frac{d}{dT} \cdot \frac{M}{\beta}$ ) is constant for all types, and from the above equations is

$$\frac{d}{dT} \left(\frac{M}{\beta}\right) = h \text{ (distance from the hub to the aircraft cg)} \quad (2)$$

or

$$\frac{d}{dT} \cdot \frac{M}{\beta} = \frac{\left(\frac{M}{\beta}\right)_{1.0g} - \left(\frac{M}{\beta}\right)_{-0.25g}}{(1.0 + 0.25)g} \quad (3)$$

ORIGINAL PAGE 19  
OF POOR QUALITY

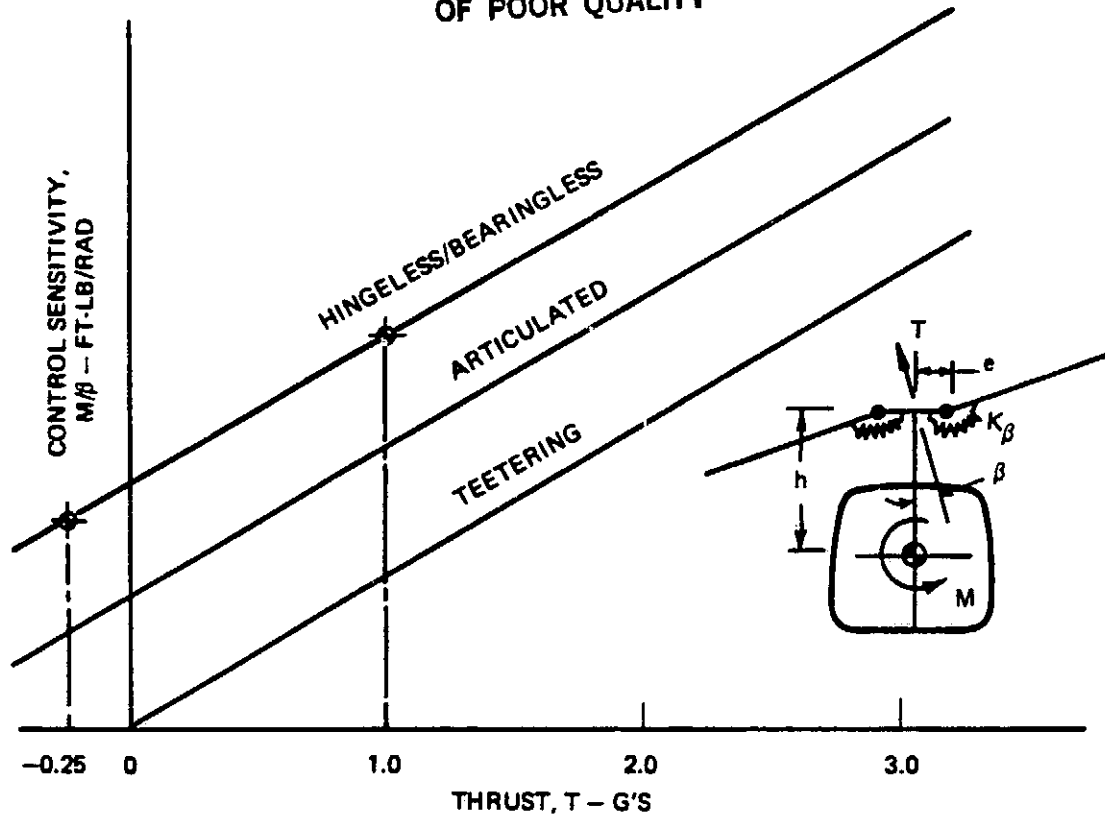


Figure 15. Relative Control Sensitivity of Teetering, Articulated, and Hingeless Rotor Systems

Substituting equations 1 and 2 into 3, we have

$$h = \frac{\left(\frac{M}{\beta}\right)_{1.0g} \times \frac{1}{3}}{1.25g}, \quad \text{or}$$

$$\left(\frac{M}{\beta}\right)_{1.0g} = 3h \times 1.25g \quad (4)$$

For the YUH-61A with the 24-inch shaft extension  $h = (45 + 24) = 69$  inches and 1-g thrust is 16,000 pounds; then from equation 4,

$$\left(\frac{M}{\beta}\right)_{1.0g} = 3 \times \frac{69}{12} \times 1.25 \times 16,000 = 345,000 \text{ ft-lb/radian.}$$

Elimination of thrust component leaves the hub stiffness as follows:

If  $\frac{M}{\beta} = 345,000$  ft-lb/rad, then for the ITR on the YUH-61A ( $h = 69$  inches) for a blade CF of 75,000 pounds,

$$345,000 = 16,000 \times \frac{69}{12} + 2 \times 75,000 \times e + 2k_{\beta}$$

or

$$M_H/\beta = 253,000 \text{ ft-lb/radian } (= 2CF_e + 2K_{\beta}) ,$$

which is higher than the goal of 120,000 ft-lb/rad as an ITR objective.

#### Minimum Rotor Hub Moment = 10,000 Foot-Pounds

The minimum rotor hub moment below which no fatigue damage will occur is the product of the hub stiffness goal ( $M_H/\beta$ ) and the goal for minimum rotor hub tilt angle ( $\beta_{E.L.}$ ) and is therefore redundant.

#### Minimum Rotor Hub Tilt Angle = 5 Degrees

This goal is defined as the minimum rotor disk angle, assuming rigid blades, below which fatigue damage will not be incurred in the hub. It can be redefined as the hub endurance limit flapping ( $\beta_{EL}$ ).

Endurance limit flapping in a hub flexure is constrained by material fatigue design allowable strain level, centrifugal force due to blade weight, the maximum practical flexure width, and maximum allowable flap flexure length, which in turn is constrained by equivalent flap hinge location or hub moment stiffness requirements. Maximum practical width at the flexure root is constrained by the hub drag goal or acceptable hub width.

A simplified methodology for relating root width of a rectangular section flexure to blade CF, endurance limit flapping ( $\beta$ ), flexure material modulus (E), design endurance limit ( $\epsilon$ ), and distance (e) from the flexure root to the effective flap hinge, or flexure length ( $\ell = 2e$ ) is presented below. The methodology assumes (subsequently verified to within  $\pm 5\%$ ) that the most efficient way for the flexure to curve is through an arc of constant radius.

Flexure root width ( $w_0$ ) is defined as:

$$w_0 = \frac{3}{8} \frac{CF}{E.e} \left(\frac{\beta}{\epsilon}\right)^3 .$$

Since width distribution ( $w_x$ ) is defined as:

$$w_x = \frac{3}{4} \frac{CF}{E} \left(\frac{\ell - x}{\ell}\right)^2 \left(\frac{\beta}{\epsilon}\right)^3 ,$$

and thickness ( $t = 2 \times c$ ) is defined as:

$$t = 4e\left(\frac{\epsilon}{\beta}\right) ,$$

constant for constant radius of curvature,

hub moment stiffness ( $M_H/\beta$ ) can be conservatively defined as:

$$\frac{M_H}{\beta} = 2.CF.e .$$

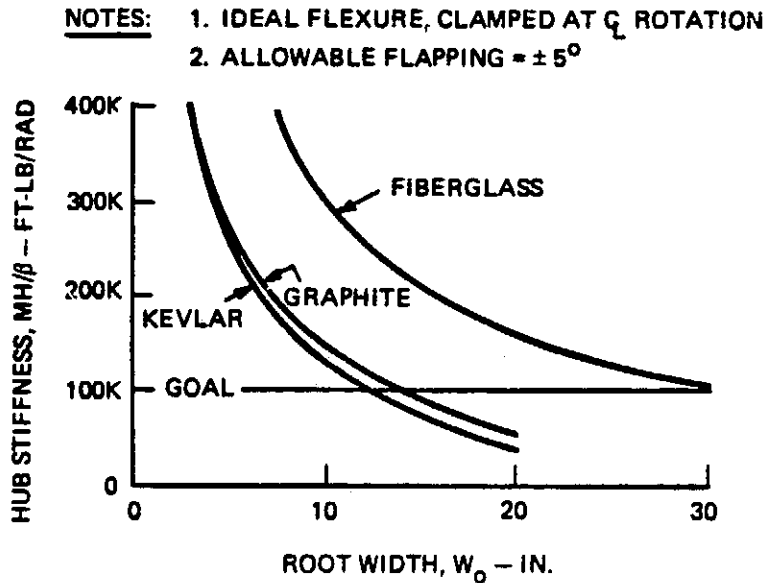
Then maximum endurance limit flapping ( $\beta$ ) becomes

$$\beta_{\max} = \left(\frac{4 E}{3 CF^2}\right)^{1/3} \times (\text{max allowable root width})^{1/3} \\ \times (\text{hub stiffness})^{1/3} \times \epsilon_{\text{allowable}} .$$

Figure 16 shows that the minimum flexure root widths acceptable for meeting the hub stiffness and tilt goals are 12, 14, and 30 inches for Kevlar, graphite, and fiberglass materials, respectively.

The 5-degree hub tilt goal will result in a wide hub with consequent high drag. It should be noted that the example used is an "ideal-unrealistic" flexure, clamped at the centerline of the rotor shaft. Adding a clamp of finite radius will increase the hub stiffness (or equivalent flap hinge offset accordingly), resulting in even higher minimum acceptable flexure root widths.

It is recommended that the hub tilt goal be reduced to 4 degrees.



	TENSILE MODULUS, E (LB/IN. <sup>2</sup> )	END. LIM STRAIN (IN./IN.)
FIBERGLASS	$6.4 \times 10^6$	$2,300 \times 10^{-6}$
KEVLAR	$10.0 \times 10^6$	$2,720 \times 10^{-6}$
GRAPHITE	$20.0 \times 10^6$	$2,100 \times 10^{-6}$

Figure 16. Minimum Allowable Flexure Root Width for  $\pm 5$  Degrees of Endurance Limit Flapping; Effect of Hub Stiffness Requirements and Material Types

### Effect of Limit Loading

Another consideration is limit flap bending caused, for example, by start-up in a 45-knot wind. The YUH-61A structural analysis suggests that an equivalent case would be 4.67 g's static droop.

Without the full effect of CF stiffening, the flexure and blade must be stiff enough to preclude tailboom strikes and strong enough to avoid flexural failure. A classical approach is to include flap restrainers. On low flap stiffness systems, CF retraction mechanisms are required to prevent pounding in flight maneuvers. These devices have maintenance

problems and so flap stops have been regarded as undesirable. With this in mind, the flexure sizing criterion of endurance limit flapping becomes overshadowed by that of limit flap bending.

For this case, the flexure minimum cross section is defined by both the limit bending moment and the material allowable, which results in a structure many times stiffer than when designed for dynamic flapping alone. Endurance limit flapping is consequently reduced and the hub stiffness is approximately doubled.

#### Provisions for Auxiliary Lead-Lag Damping

This provision is necessary as a last resort to enhance the stability characteristics if testing shows undesirable characteristics. Provisions for elastomeric damping only should be specified to preclude the use of expensive, problem-prone hydraulic dampers.

#### Torsional Stiffness = Same as Current Rotor Systems

A definite goal such as 250 in.-lb/degree with blade CF effects included should be specified.

Weight reduction is an important goal; however, high torsional stiffness would require a control system of increased capacity and resultant increased weight.

#### Rotor Hub System Fatigue Life = 10,000 Hours

This has been addressed in rotor system goals.

#### Reliability (MTBR) = 3,000 Hours

MTBR has been addressed in rotor system goals.

### Manufacturing Cost = Minimum

Cost has been addressed in rotor system goals.

### Vulnerability

For this study an HEI projectile of approximately 1 inch in diameter was assumed to remove material completely from an area 1 inch in diameter or larger.

Given a flexure of 1-inch thickness fabricated from composite material with an allowable endurance limit strain of 2,720  $\mu\text{in./in.}$  (Kevlar), let us investigate the endurance limit flapping and hub stiffness resulting from such a structure.

Since  $\frac{M}{I} = \frac{\sigma}{c} = \frac{E}{R}$ , the classical bending theory can be restated,  $\epsilon = \frac{\sigma}{E} = \frac{c}{R}$ ,

where  $\epsilon$  = tensile strain at surface,  
 $c$  = half thickness,  
 $R$  = radius of bending curvature.

Then if  $c = 0.5$  inch (or thickness  $t =$  diameter of the round) and  $\epsilon = 2,720 \times 10^{-6}$  in./in. (Kevlar), the minimum radius of curvature  $R = \frac{0.5}{2,720} \times 10^6 = 184$  inches.

For  $\pm 5$  degrees of flapping, the length of arc required is

$$L = 184 \times 5^\circ / 57.3 = 16.06 \text{ inches.}$$

For a circular arc of deflection, the intersection of the 0 and 5-degree tangents occurs at the midarc location  $e (= L/2)$ . If the flexure is regarded as having negligible stiffness, the resultant hub stiffness (2.CF.e) for a typical CF of 75,000 pounds is 100,000 ft-lb/radian.

It follows, then, that a flexure meeting the flapping and stiffness goals would not survive an edge-on hit with an HEI projectile. The degree of survivability in terms of "Total Vulnerable Area", for example, requires definition.

## RECOMMENDATIONS FOR CHANGES TO THE GOALS AND SPECIFICATIONS

### ITR SYSTEM DESIGN SPECIFICATIONS - RECOMMENDED CHANGES

#### Design Envelopes - Effect of Limit Loading Conditions

Two alternative loading conditions, fatigue or limit, can be chosen to design the hub flexure. If fatigue is used, then it can be shown that flap (or droop) stops will be necessary to prevent blade/boom contact. If limit loads are used so that droop stops are precluded, then the hub flexure will be too stiff to meet the hub stiffness goals and too thick to meet the endurance limit flapping or tilt goals. The specifications should include the requirements to "meet limit loading conditions during startup in a 45-knot wind without incurring blade/boom contact". The following discussion illustrates the possible impact of this requirement upon meeting the objectives of the ITR program and shows that droop stops will be required if the goals are to be met.

#### Rotor Blade Static Droop and Its Effect Upon ITR/FRR Hub Configuration

Past experience on helicopter rotor systems has shown that the inclusion of flap and droop stops to prevent blade/fuselage contact in extreme startup conditions has resulted in compromises in simplicity, drag, weight, reliability, and maintainability characteristics. It is prudent, therefore, to have as a goal for the ITR hub that the system should be devoid of such devices. This section demonstrates how this goal would affect the other objectives listed in the appendixes to the RFQ, i.e.,

hub stiffness = 100,000 to 120,000 ft-lb/radian

and, for zero fatigue damage,  $\beta_{min} = \pm 5^\circ$

and minimum hub moment = 10,000 ft-lb .

Minimum Hub Spring ( $K_{\beta}$ ) to Preclude Droop Stops - To preclude blade/boom contact during startup in a 45-knot wind, the minimum static bending stiffness can be shown to be that which can support a 4.67-g static blade loading condition without tailboom contact.

Tip deflection can be simply regarded to be made up of two components, flexure spring deflection and blade deflection.

The YUH-61A, as a typical hingeless-rotor helicopter, has a virtual flap hinge ( $e'_{old}$ ) at approximately 17 percent of rotor radius and a total undeflected blade tip-to-tailboom clearance of 66 inches. With the experimental 24-inch shaft extension, the arrangement becomes more typical of a single-rotor helicopter and the tip clearance increases to  $24 + 66 = 90$  inches.

A 1-g static droop analysis of the YUH-61A rotor blade results in a static moment of 33,000 in.-lb about the flap hinge and a resultant flap flexure slope at the blade root (25%R) of -1.828 degrees. For the YUH-61A rotor, therefore, the flexure stiffness is

$$K_{\beta_{old}} = \frac{33,000}{1.828^{\circ}} \times \frac{57.3}{12} = 82,600 \text{ ft-lb/radian},$$

which results in a 1-g tip deflection of

$$\delta_{K_{\beta}} = (1 - 0.25) \times 294 \text{ in. radius} \times \frac{1.828}{57.3} = 7.03 \text{ inches}.$$

But, from the static droop analysis, the total 1-g tip deflection is 14.32 inches, of which  $(14.32 - 7.03) = 7.29$  inches must be due to the 1-g blade deflection.

For the YUH-61A with the 24-inch shaft extension, under the 4.67-g case,  $(4.67 \times 7.29) = 34.0$  inches will be from the blade, leaving  $(90.0 - 34.0) = 56.0$  inches for  $\delta_{K_{\beta_{new}}}$ , or 12.00 inches per g allowed for the ITR.

ORIGINAL PAGE IS  
OF POOR QUALITY

For this new system with an equivalent flap hinge at  $e'_{new}$ , the static blade moment about the hinge becomes  $M_o = 33,000 + 200 \text{ lb} \times (e'_{old} - e'_{new})$ , where  $200 \text{ lb} = \text{blade weight}$ . The allowable 1-g slope then becomes

$$\theta_{K_{\beta_{new}}} = \left( \frac{12.00}{294 - e'_{new}} \right) \text{ radians.}$$

For the ITR, therefore,

$$K_{\beta_{new}(\text{min})} \text{ then becomes } \frac{M_o}{\theta_{K_{\beta_{new}}}} = \frac{33,000 + 200 (e'_{old} - e'_{new})}{12.00 / (294 - e'_{new})} \text{ in.-lb/radian.}$$

But  $e'_{old} = 0.17 \times 294 = 50 \text{ inches}$  (i.e., at 17% radius for the YUH-61A);

then

$$K_{\beta_{new}} = (3,583 - 16.67e'_{new}) (294 - e'_{new}) \text{ in.-lb/radian.} \quad (5)$$

Control Moment ( $M_c$ ) and Hub Stiffness - Hub control moment is the resultant of the thrust vector tilt/cg offset effect ( $M_{tilt}$ ), the centrifugal stiffening ( $M_{CF}$ ), and the flexure spring ( $M_{k_{\beta}}$ ).

Since  $M_{tilt} = Th\beta$ , where  $T = \text{rotor thrust}$  and  $h = \text{hub/cg height difference}$ ,

and  $M_{CF} = 2CFe'$ , where  $e' = \text{flap hinge radial offset}$ ,

$M_{k_{\beta}} = 2K_{\beta}\beta$ , where  $K_{\beta} = \text{flap hinge spring stiffness}$ .

Then

$$\begin{aligned} M_c &= M_{tilt} + M_{CF} + M_{k_{\beta}} \\ &= (Th + 2CFe' + 2K_{\beta})\beta. \end{aligned}$$

Control moment sensitivity,  $\frac{M_c}{\beta} = (Th + 2CFe' + 2K_\beta)$

ORIGINAL PAGE IS  
OF POOR QUALITY

and hub stiffness  $\frac{M_H}{\beta} = 2(CFe' + K_\beta)$ . (6)

Effect of Virtual Flap Hinge Offset Upon Hub Stiffness - Substituting equation 5 into 6,

the hub stiffness  $\frac{M_H}{\beta}$  becomes

$$\frac{M_H}{\beta} = 2CFe'_{\text{new}} + 2K_{\beta_{\text{new}}}, \text{ but } CF = 75,000 \text{ lb,}$$

then

$$\frac{M_H}{\beta} = 150,000 e'_{\text{new}} + 2(3,583 - 16.67e'_{\text{new}})(294 - e'_{\text{new}}).$$

Conclusions - Figure 17 presents hub stiffness and flexure spring stiffness about the virtual hinge and shows how their characteristics are affected by virtual flap hinge offset. The ground rules were:

1. No droop stops
2. Blade CF = 75,000 pounds
3. Undelected blade/tailboom clearance = 90 inches
4. Blade weight = 200 pounds
5. The YUH-61A blade flap stiffness is representative.

The ITR/FRR hub stiffness goal is  $100,000 \begin{matrix} +20\% \\ -0 \end{matrix}$  ft-lb/radian, which can only be achieved by a rotor system having a zero virtual flap hinge offset or a rotor which includes a flap hinge no further out than 3.15 percent of radius (and incorporating droop stops).

ORIGINAL PAGE IS  
OF POOR QUALITY

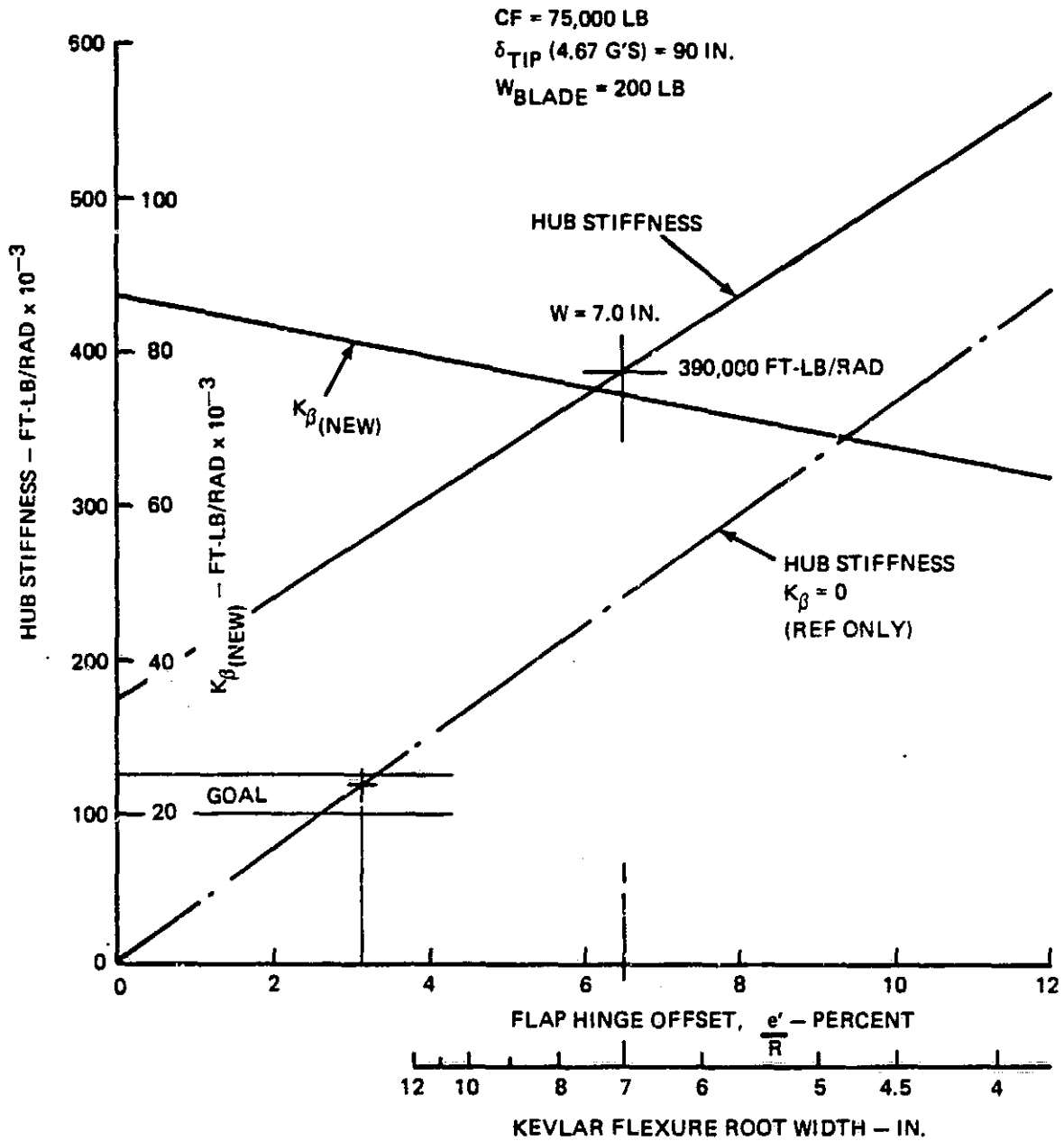


Figure 17. Hub Stiffness Requirements to Avoid Blade/Boom Contact at 4.67 G's Loading

Without droop stops and for a low-drag hub of infinite life ( $\beta = \pm 5^\circ$ ), maximum flexure root width will be on the order of 7.00 inches which, in Kevlar, requires a minimum hinge offset of 6.5-percent radius. A 10.0-inch-wide flexure requires a minimum offset of 4.5-percent radius. A likely minimum hub stiffness ( $W = 7.00$  inches) will be of the order of 390,000 ft-lb/radian and if the flexure is designed for zero fatigue damage at  $\beta = \pm 5^\circ$ , then the minimum hub moment (zero damage) becomes  $M_{H(\min)} = \frac{5}{57.3} \times 390,000 \text{ ft-lb} = 34,000 \text{ ft-lb}$ , which exceeds the technical goal of 10,000 ft-lb by 240 percent.

It should be noted that the merit factors awarded to such a configuration will be a debit of 22.5 points for exceeding the hub stiffness goal, but a credit of 120 points for exceeding the minimum hub moment goal, resulting in a better score than a configuration that met all of the criteria and goals.

#### ROTOR SYSTEM STABILITY

A minimum acceptable level of critical damping in the fixed system, assuming zero structural and/or auxiliary damping, should be specified.

#### ITR SYSTEM TECHNICAL GOALS - RECOMMENDED CHANGES

##### Noise

It is recommended that the noise level goal be reduced to 4 decibels improvement over the UH-60 and that an absolute value be specified, together with frequency content.

##### Rotor System Parts Count

It is recommended that parts count be reduced to 50 to provide a more challenging goal. However, what constitutes a part should be defined.

## Vibration

Due to the importance of vibration reduction the goal should remain at 0.1 g, which may be difficult to meet. The effects of flexible shafts, transmission mountings, etc, and their effectiveness as vibration attenuators should be excluded.

## Cost

A specific goal based on a quantity procurement and including nonrecurring costs should be given in FYXX dollars.

All other system technical goals are realistic and will promote an efficient design for the ITR rotor.

## ITR ROTOR HUB SYSTEM DESIGN SPECIFICATIONS - RECOMMENDED CHANGES

See paragraph entitled ITR SYSTEM DESIGN SPECIFICATIONS - RECOMMENDED CHANGES.

## ROTOR HUB TECHNICAL GOALS - RECOMMENDED CHANGES

### Rotor Hub Weight

This goal could be reduced to 2.0 percent of design gross weight. The geometric extremities of the hub require definition.

### Rotor Hub System Parts Count

This goal could be reduced to 20 nonstandard parts, provided that the definition of a part is given.

### Hub Moment Stiffness and Tilt

Hub tilt and stiffness goals have a major impact on the ITR/FRR hub concepts. Small degrees of flexibility in transmission-to-fuselage mountings and/or main rotor shaft can reduce the challenge in meeting these goals. Hub moment stiffness should be increased to 250,000 ft-lb per radian, hub tilt angle reduced to 4 degrees, and a restriction applied which discounts flexibility of the vehicle drive train system and supporting structure.

### Minimum Hub Moment

This goal is considered to be redundant.

### Torsional Stiffness

A goal should be set at 250 in.-lb per degree of flexure twist at the nominal rpm, assuming a blade weight of 1.25 percent of design gross weight and a center of gravity of 60 percent of the tip radius. Torsional stiffness or torque-to-twist goals should exclude aerodynamic and centripetal moment effects.

### Reliability

It is recommended that the MTBR goal for the rotor system be reduced to 1,000 hours, which, in conjunction with a goal of 5,000 hours for each blade, a goal for the hub of 5,000 hours would be reasonable.

## REPRESENTATIVE HELICOPTER CHARACTERISTICS

The YUH-61A helicopter has a hingeless rotor for which the shaft and transmission attachments are designed to accommodate the loads generated by such a rotor. The ITR is likely to be a hingeless type, but with a lower hub stiffness than the YUH-61A. The characteristics of a UH-60 or AH-64 helicopter designed for an articulated system may be inadequate, since it is reasonable to expect the hub stiffness and resultant shaft moments to be higher for the bearingless ITR system.

The YUH-61A is a Class I, single-main-rotor, twin-engine utility helicopter with General Electric YT-700-GE-700 engines each rated at 1,536 shaft horsepower. In powered flight the engines drive the four-bladed main and tail rotors through the engine, main, intermediate, and tail transmissions and associated shafting. In power-off conditions the engines are protected by automatic decoupling at the engine transmissions and the tail rotor is driven by energy derived from the main rotor. Three hydraulic boost actuators are used to reduce cockpit control forces for cyclic and collective pitch commands to the main rotor, and a fourth hydraulic actuator reduces pedal forces for collective pitch changes to the tail rotor. A variable-incidence horizontal stabilizer is electromechanically positioned to reduce main hub overturning moments for variations in airspeed, altitude, and longitudinal cyclic and collective control positions. The tricycle landing gear is fixed. A damped tail bumper protects the tail rotor and empennage during tail-first landings. Individually operated wheel brakes on the main gear improve ground-handling characteristics.

Folding and securing provisions for the main rotor blades and the tail-boom, combined with main landing gear kneeling capability, reduce the overall dimensions to satisfy air transportability requirements.

The overall dimensions of the YUH-61A are shown in Figure 18.

ORIGINAL PAGE IS  
OF POOR QUALITY

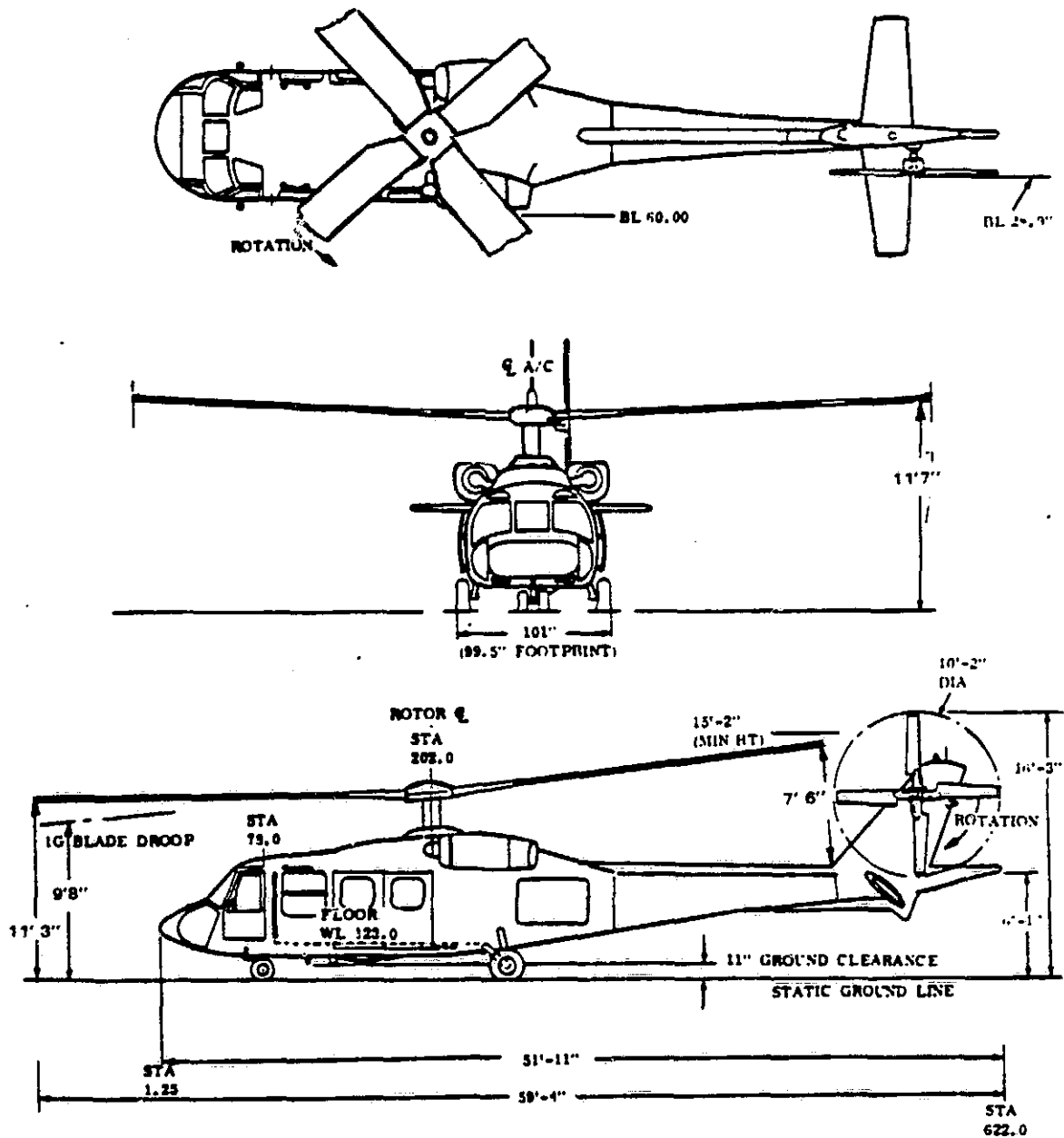


Figure 18. Overall Dimensions of YUH-61A Helicopter

The YUH-61A was chosen as being representative and the characteristics thereof were used in determining loads and stability predictions.

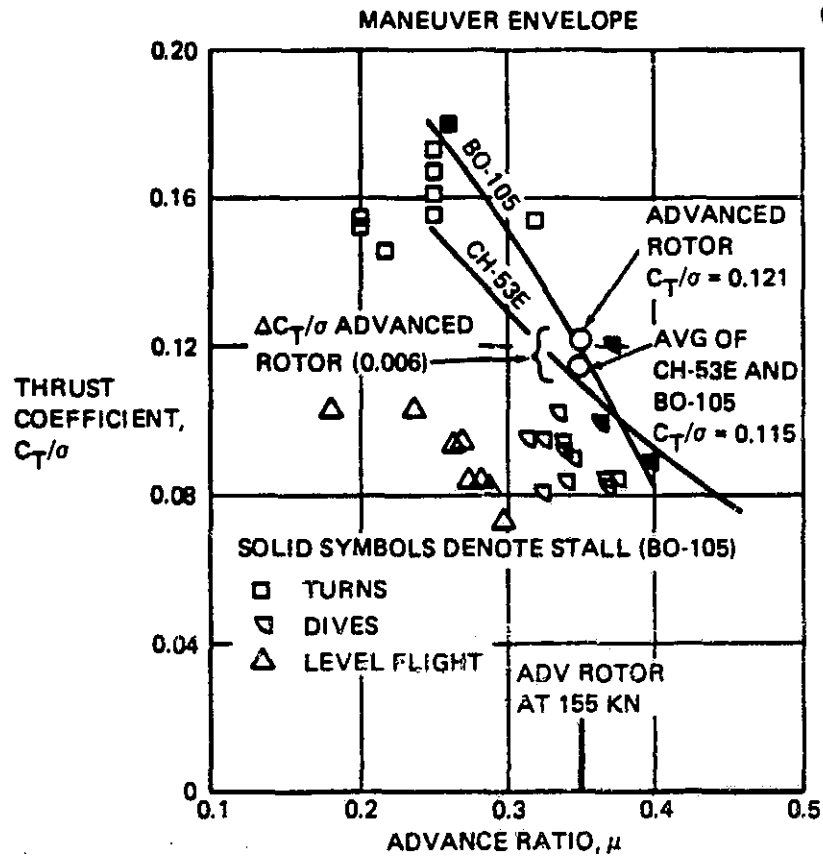
The rotor blades, however, are not those from the prototype aircraft. Boeing Vertol is designing a rotor system for the all-composite Model 360 aircraft in which the utilization of advanced technology is widespread, including the rotor system.

#### ITR ROTOR BLADES

The Model 360 rotor blade considered will be modified in planform and twist to best meet the ITR goals for hover, maneuver, and forward speed with the vehicle drag equivalent ( $15 \text{ ft}^2$ ) and design gross weight (16,000 lb) specified in the RFQ. A basic chord requirement of 26.3 inches was determined as shown in Figure 19; Figure 20 presents the results of an optimization of the twist distribution. Mass and stiffness distributions for the blade are presented in Figure 21.

#### ROTOR SHAFT

For vibration reduction, the YUH-61A flight-test helicopter is currently configured with a 24-inch shaft extension. Limit blade deflection allowances will take credit for this extra tip/tailboom clearance. The fixed forward shaft tilt of 4 degrees has been shown to be acceptable; however, 3.36 degrees is more compatible with the ITR system specifications which include a vehicle drag equivalent to 15 square feet.



CALCULATION OF CHORD REQUIRED TO MEET 1.75-G MANEUVER REQUIREMENT AT 140-170 KNOTS

AVG AIRSPEED = 155 KN  
AVG  $\mu = 0.352$  (744 FT/SEC  $V_{TIP}$ )

THEREFORE:  $\sigma_{ROOT} = \frac{C_T}{C_T \sigma_{ROOT}} = 0.1122$

FROM MANEUVER ENVELOPE:  
 $C_T/\sigma_{ROOT}^*$  (LIMIT) = 0.121

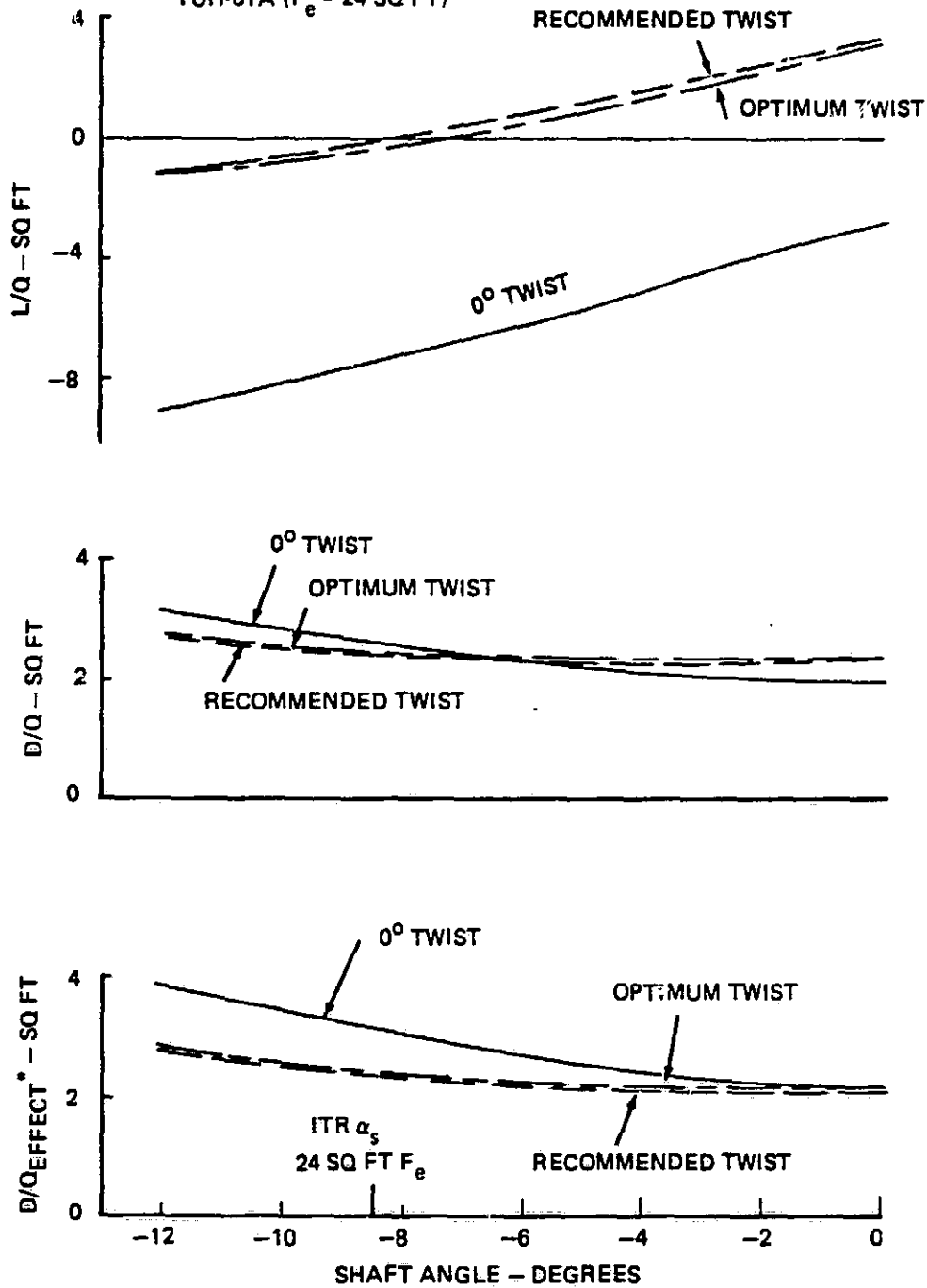
AND  $C_{ROOT} = 26.3$  IN.

AND AT 16,000 LB, 4,000 FT/35°F,  
1.75 G'S, 49.7 FT DIA:  
 $C_T = 0.00776 \times 1.75$   
 $= 0.01358$

\*PLANFORM IS TAPERED WITH  
TIP CHORD = 1/3 ROOT CHORD

Figure 19. Advanced Rotor Maneuver Envelope

V = 170 KN, V<sub>TIP</sub> = 749 FPS, 0° COLLECTIVE,  
4,000 FT/95° F, B/C = 6.6°, A19 ANALYSIS, DOWNWASHED,  
YUH-61A (F<sub>e</sub> = 24 SQ FT)



\*D/Q + ΔD/Q EQUIVALENT TO INDUCED-POWER PENALTY CAUSED BY DOWNLOAD (L/Q)

Figure 20. Optimum Twist Study With Shank of 2.1 Ellipse

ORIGINAL PAGE IS  
OF POOR QUALITY

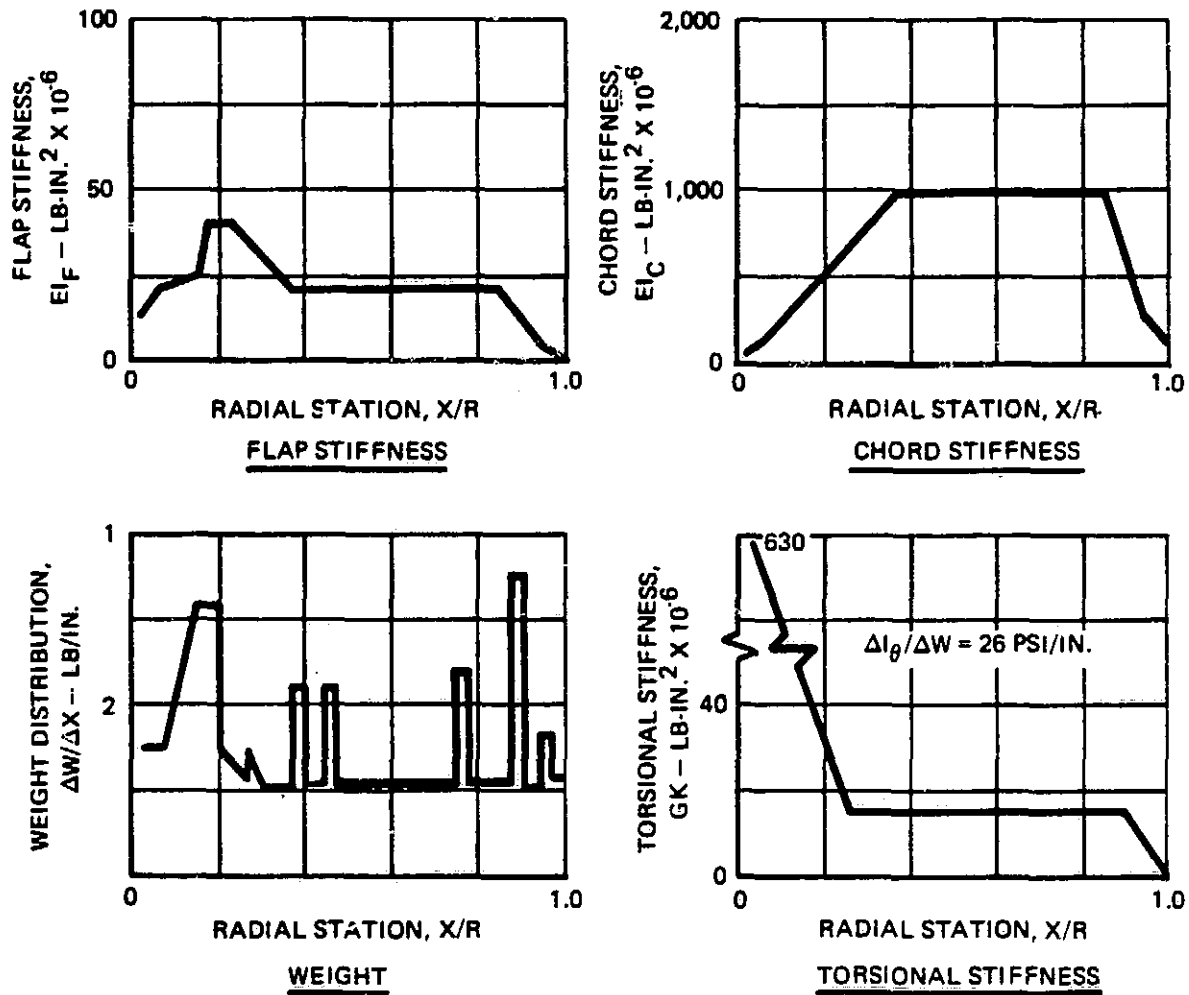


Figure 21. Mass and Stiffness Distributions for Advanced Rotor Blade

## DESIGN CRITERIA FOR DEFINING HUB CONCEPTS

The preliminary investigation into the limitations of bearingless rotor flexures has shown, through the use of simplified methodology, that there is a tradeoff between endurance limit flapping (or hub tilt) and hub stiffness, since both flapping and hinge offset increase with flexure length. Furthermore, it has been demonstrated that the hub stiffness goal is unobtainable with a cantilevered flexure. For defining the hub concepts, the basic design criteria have been established as follows:

Hub definition - blade airfoil root cutout to the rotor shaft

Hub type - bearingless preferred

Hub tilt -  $5^\circ$  ( $\beta^\circ$ ) flapping with zero fatigue damage

Hub stiffness -  $M_H/\beta$ , minimize

Droop stops - undesirable

Torsional stiffness - not more than 1.5 x pitch link of 250 in.-lb/  
degree (excluding aerodynamic and planipetal moments)

Hub weight - minimum

Hub flat-plate drag area - less than 2.8 ft<sup>2</sup>

Design gross weight - 16,000 lb

Ballistic tolerance (any 23-mm) - maximize

Folding - provisions for rapid manual folding

Lag dampers - provisions for elastomeric types only.

## SELECTION OF CANDIDATE HUB SYSTEMS

Based upon simplified methodology for feasibility verification, five hub concepts were defined according to the design criteria, specifications, and goals. First, sketches were made with sufficient characteristic detail to confirm feasibility and, for each, a scheme for manual folding and the application of simple auxiliary lead/lag damping was devised.

For each configuration, the effects of considerations such as material selection and hub shaft attachment were studied, together with the significant influences that the goals and specifications had on the design. It was concluded during this effort that a more vigorously detailed exercise was required to produce truly viable concepts; consequently, the work slated for development of two selected concepts in a succeeding component of the statement of work was preempted and conducted upon all five concepts. Each concept was then assessed for vulnerability, stability, drag, weight, parts count, hub moment stiffness and allowable tilt angle, R&M strength and fatigue life, pitch control system loads, producibility, and fabrication costs. Each concept is described in the subsequent paragraphs.

For reference Figure 22 shows the U.S. Army/Boeing Vertol Bearingless Main Rotor (BMR) system which has been demonstrated through flight test to be an acceptable concept (Reference 1); Figure 23 shows a blade concept applicable to the bearingless concepts discussed herein.

### CANDIDATES FOR EVALUATION

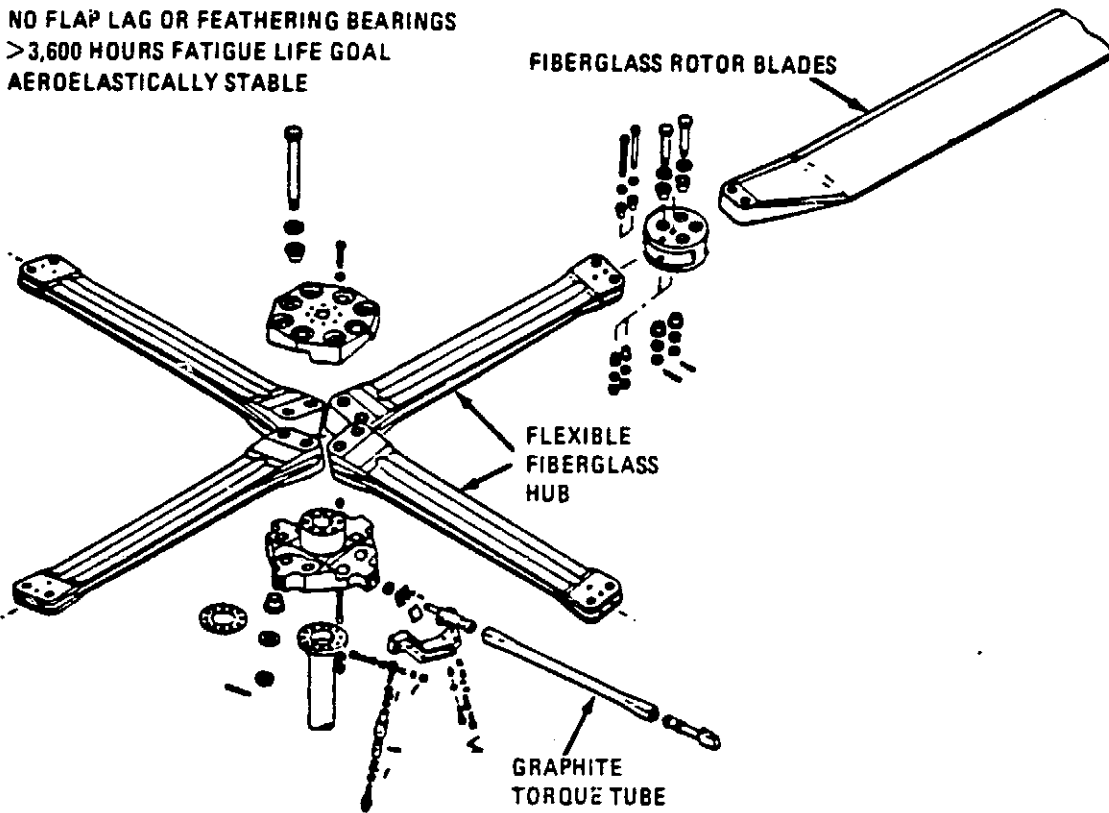
#### Configuration 1A - Modified U.S. Army/Boeing Vertol Bearingless Main Rotor (Baseline)

This configuration, shown in Figure 24, was the BMR reconfigured to reduce hinge offset from 14.5 to 7.0-percent radius. To ensure aeromechanical

### OBJECTIVES

- SIZE FOR THE 80-105
- NO MODIFICATIONS TO AIRCRAFT OR CONTROL SYSTEM
- NO FLAP LAG OR FEATHERING BEARINGS
- >3,600 HOURS FATIGUE LIFE GOAL
- AEROELASTICALLY STABLE

ORIGINAL PAGE IS  
OF POOR QUALITY



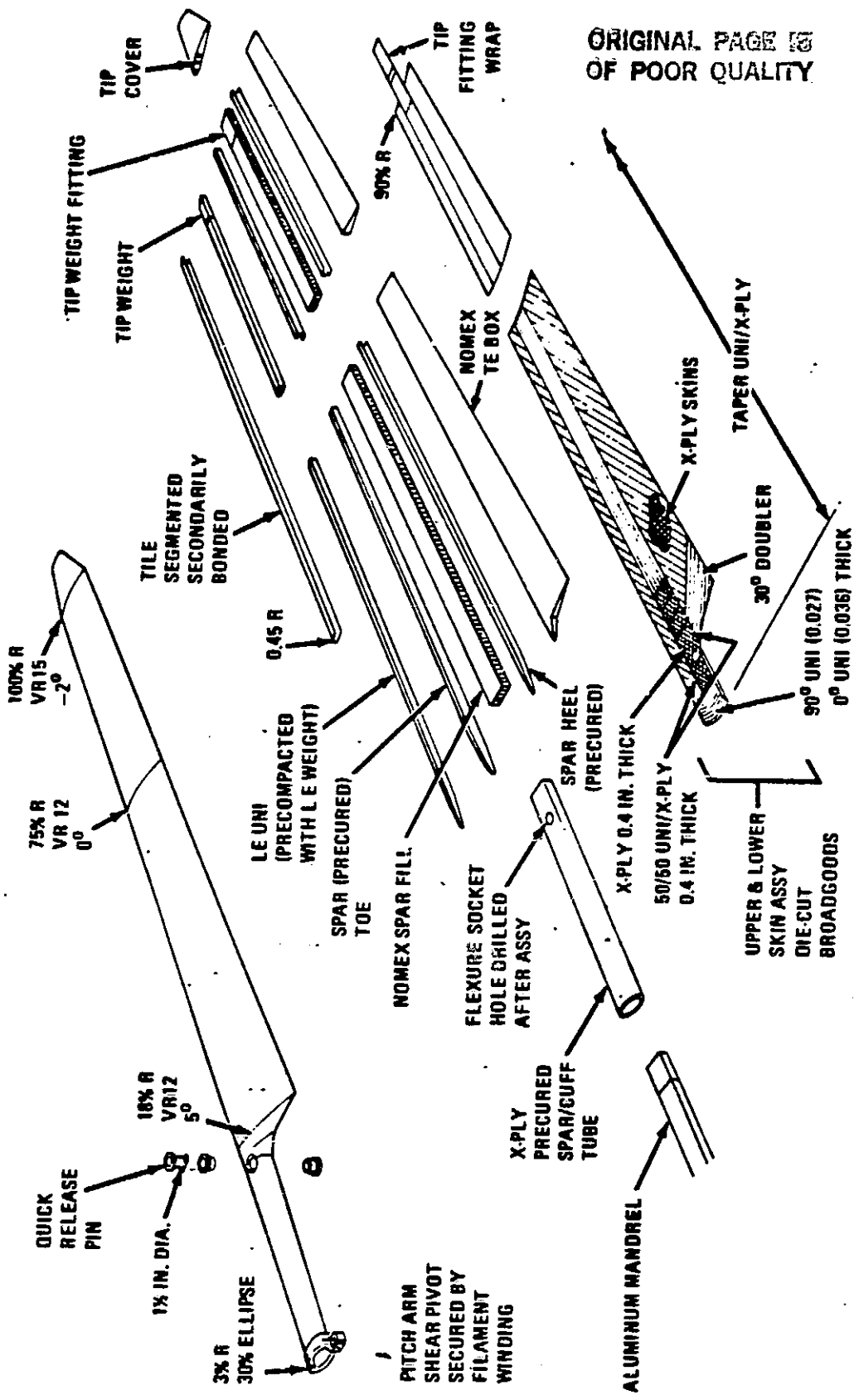
### ACHIEVEMENTS

- MET ALL PROGRAM OBJECTIVES
  - STABLE
  - DURABLE
  - FLYING QUALITIES AND VIBRATION SAME AS 80-105
  - BLADE CONTROL LOADS WITHIN SYSTEM CAPABILITY

### FURTHER IMPROVEMENTS PLANNED

- USE HIGH MODULUS COMPOSITES
- REDUCE NUMBER OF JOINTS
- REPLACE TORQUE TUBE WITH FAIRING
- ADVANCED AIRFOILS AND PLANFORM
- MODAL PLACEMENT
- METHODOLOGY IMPROVEMENT

Figure 22. The Bearingless Main Rotor System



ORIGINAL PAGE 15  
OF POOR QUALITY

Figure 23. ITR Rotor Blade Concept

ORIGINAL PAGE 19  
OF POOR QUALITY

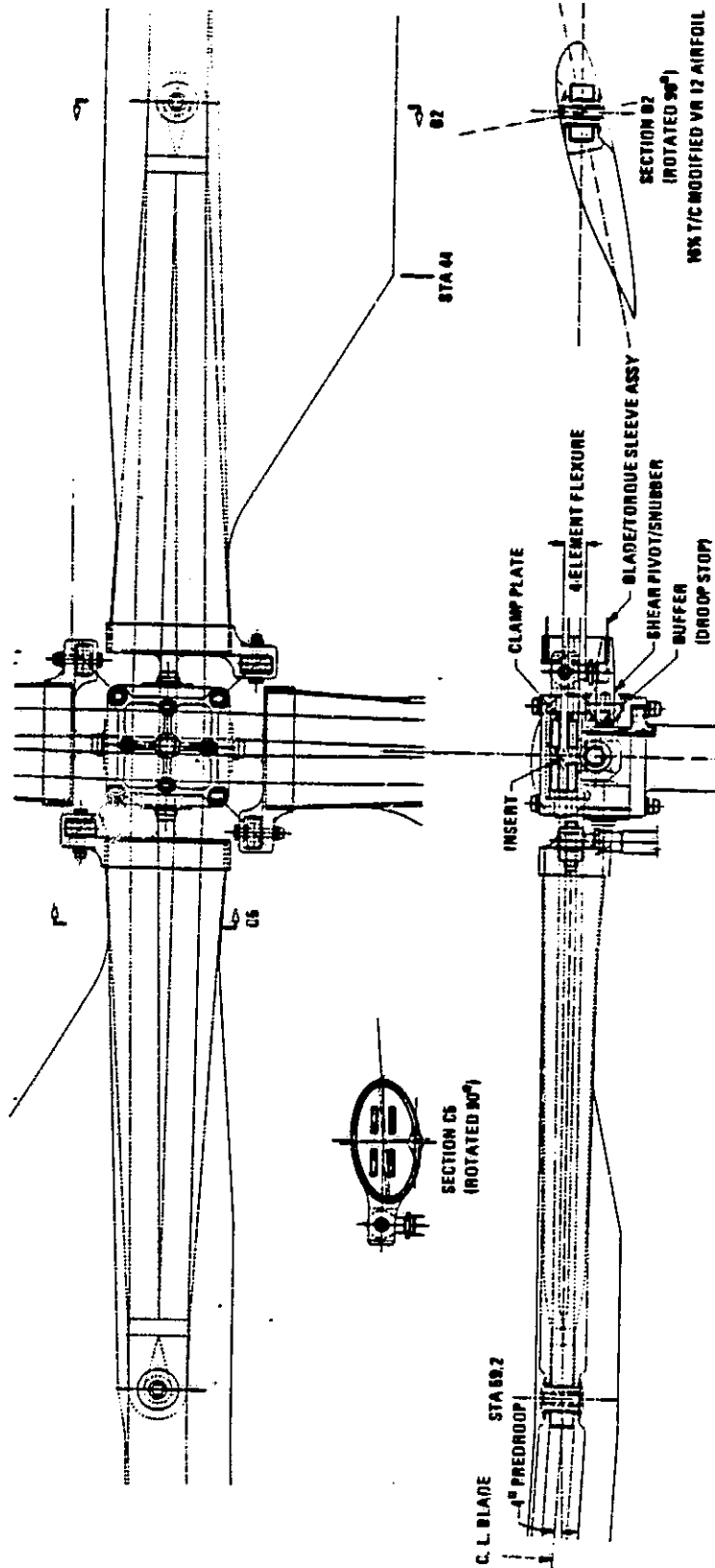


Figure 24. ITR Configuration 1A (Modified BMR)

stability, the BMR features of zero precone coupled with predroop were retained. The predroop was increased from 2-1/2 degrees to 4 degrees to relieve steady root flap bending moments and result in a reduction of the flexure root cross section and the consequent drag.

The BMR flexure pretwist of 12-1/2 degrees, however, was reduced to zero, resulting in reductions in complexity and drag. The reduction in stability from zero lag/flap coupling is expected to be replaced by additional lag/torsion coupling from the 1-1/2 degrees of predroop extra to the BMR.

The torque tube was replaced by an aerodynamic sleeve as an integral part of the rotor blade. Attachment of the blade to the flexure was through a single pin and socket. For blade folding at the flexure/blade attachment, the sleeve and blade become separate components connected by two secondary lag pins and one primary retention pin.

Fore or aft folding is achieved around either of the secondary pins in this adaptation of the concept (see Figure 25).

The BMR back-to-back channel-section dual-beam flexures were modified by removing the web, which allowed the interleaving of orthogonal arms at the shaft attachment which results in a lower hub profile. A study of the BMR two-pin wraparound shaft attachment versus the clamp arrangement shown identified significant peculiarities of each system. The wraparound required a thick (high) structure to prevent load reversal at the pin/bushing fixation due to root flap moment overcoming the steady CF bearing stress. In the chosen clamped arrangement, the flexure root moments result in an interlaminar shear stress within the clamp which is dependent upon clamp rigidity and radial size. An analysis of an initial single, solid flexure configuration showed that these shear stresses would be excessive, so the dual-stacked pair arrangement was devised to react the majority of root flap bending moment in differential tension between the upper and lower flexures. These are restrained laterally in the clamp by

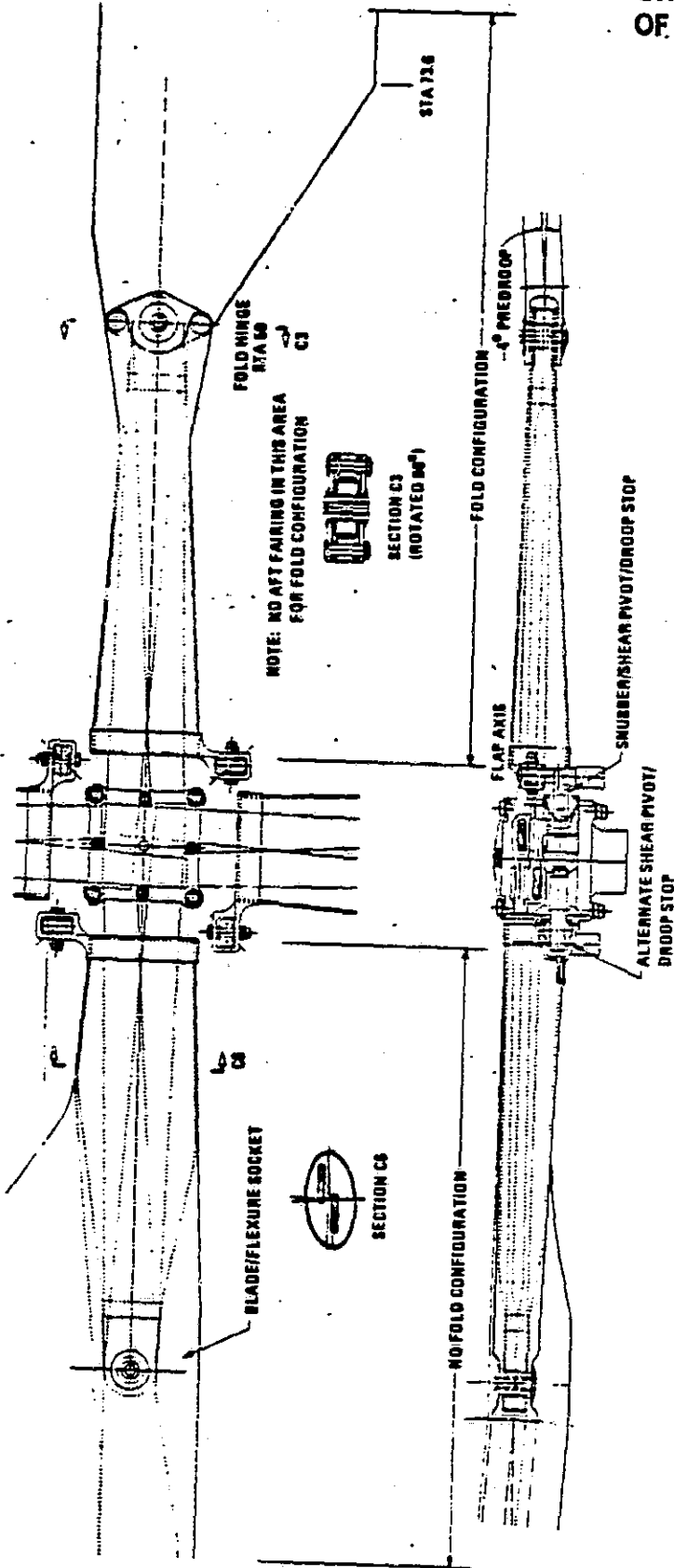


Figure 25. ITR Configuration 1B (Modified BMR)

central buildups in each strap matching with recesses in the hub clamp plates. Thus the root flap bending moment in each of the four flexure straps was greatly reduced which resulted in manageable levels of inter-laminar shear stress within each clamp, together with a hub system of small proportions. This redundant multiflexure arrangement significantly improves the survivability of the system.

Like the BMR, the inboard end of the torque sleeve is restrained in a pivot/snubber bearing, offset from the torsional axis of the flexure. This feature provides a reaction for pitch link shear loads. Due to the rigid attachment of the sleeve to the blade, the blade root shears and moments are shared by both the sleeve and flexures. Blade flap and lag motions therefore result in shear loads at the pivot which can be used to advantage, through the magnitude and direction of the shear pivot offset, to produce mechanical stabilizing flap/pitch/lag coupling as desired.

The configuration is readily adaptable for the inclusion of elastomeric lag dampers similar to that investigated on the BMR in the 40- by 80-foot wind tunnel under contract NAS2-10333.

Configuration 1B - 1A Modified to Include Effective Flexure Root Pretwist  
(Figure 25)

A variation of configuration 1A was studied in which the lower forward and the upper aft of the four flexure elements were excluded. This produces an inclination of the flap and chord neutral axis of 18 degrees (leading edge up), effecting the lag/flap elastic coupling which is believed to augment the stability of the BMR configuration. Structurally, the result was discouraging since the pair of canted rectangular flexures provided a significant decrease in stiffness with an increase in the displacement of the critical fibers at the apexes of the four triangular flexure halves from the respective neutral axes, resulting in a less efficient arrangement. Furthermore, the resultant A-frame with the leading flexure displaced vertically from the trailing results in a large centrifugal pitch-restoring moment.

This configuration became less attractive as its development progressed and was discarded. It is, however, worthy of further study that is beyond the scope of this effort.

Configuration 2A - BMR Without Predroop (Figure 26)

This was the first configuration sketched. A pair of dual flexures, orthogonally stacked and clamped at the shaft, is shown. Elastomeric bushings of high axial shear capability have been added to the root clamp with the intention of possibly alleviating flexure root moments and transmission to the shaft of higher harmonic root shears. Predroop has been deleted and replaced by the conventional precone at the shaft attachment. A torque sleeve rigidly attached to the blade root transmits feathering control torque to the blade. Pitch link shear loads are reacted at the inboard end by a shear pivot which also reacts any shear loading transmitted down the sleeve from the blade root. These additional shears, functions of blade flap and lag motions, have been used to introduce degrees of flap/pitch/lag coupling through the degree and sense of the offset in the sleeve shear pivot.

The torque sleeve appeared disproportionately large and this configuration was modified into 2B.

Configuration 2B - Advanced Bearingless Main Rotor (ABMR) (Figure 26)

Configuration 1A was modified to remove the negative predroop and introduce precone at the shaft attachment. This results in low hub weight, drag, and stiffness. The shear pivot/snubber was moved to its upper central position to provide zero pitch/flap coupling and a pitch/lag coupling to agree in sign with that obtained from the negative predroop of configuration 1A.

ORIGINAL PAGE 18  
OF POOR QUALITY.

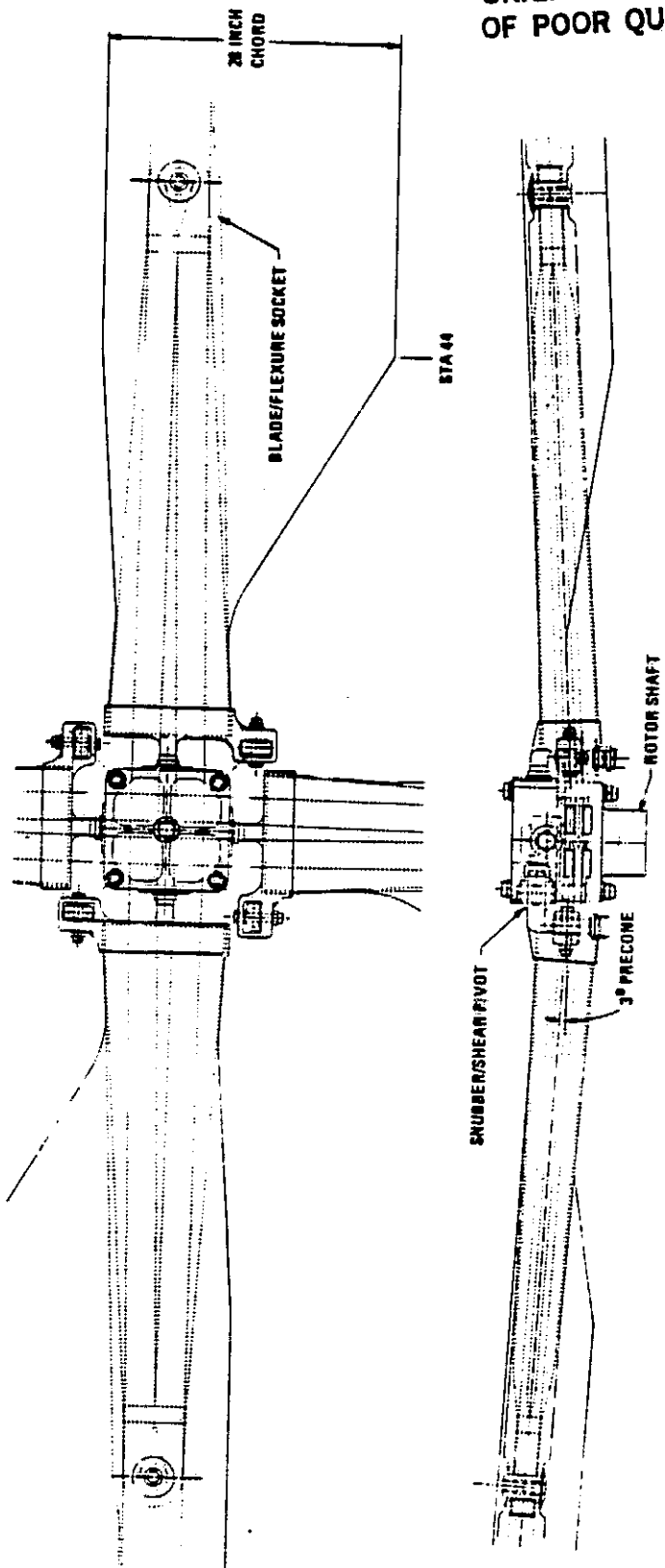


Figure 26. YTR Configuration 2B (Modified BMR)

### Configuration 3 - Shoe-Controlled Flexure (Figure 27)

To increase the allowable flapping and provide a simple flexure, a one-piece, through-the-hub, 4-arm flexure is shown, controlled in flapping by contoured shoes to ensure that the strain-limited radius of curvature was not exceeded. With this technique the virtual flapping hinge offset was minimized, which resulted in a low-stiffness hub. This configuration does not use droop stops, and limit flap bending deflections are controlled by the shoe size and the flap stiffness of the outboard lag/torsion flexure. An integral sleeve/cuff at the blade root transmits feathering control motions to the blade. As in previous configurations, an offset cuff root shear pivot reacts the control shears and provides stabilizing pitch/lag coupling to preclude lag dampers. As for the preceding concepts, without droop stops this arrangement was driven by limit flap bending constraints with the result that the shoes are long, heavy, and high drag. A study of the shoe concept with droop stops would be worthwhile; however, schedule and budget limitations prevented this investigation.

### Configuration 4 - Improved (Reversed) Starflex (Figure 28)

The current Aerospatiale Starflex configuration is an elastomeric bearing type with a flapping/droop stop flexure integrated with the shaft attachment. Simple in concept, it exhibits drag, hub stiffness, and endurance limit flapping characteristics which do not meet the goals of this program.

To reduce drag, the two yoke plates originally attached to the blade root have been reversed and made into flexible composite hub plates (which support universal elastomeric bearings between the extremities of each of the four arms). The droop flexure has likewise been reversed and integrated with the blade root through an elastomeric damper/pitch arm/bearing yoke/fold fitting. The inboard end of the flexure is supported in a Teflon-lined spherical bearing attached to the shaft. Being limit-bending constrained, this flexure is as stiff as the original Starflex with the result that its contribution to hub stiffness is unchanged; however, the

ORIGINAL PAGE IS  
OF POOR QUALITY

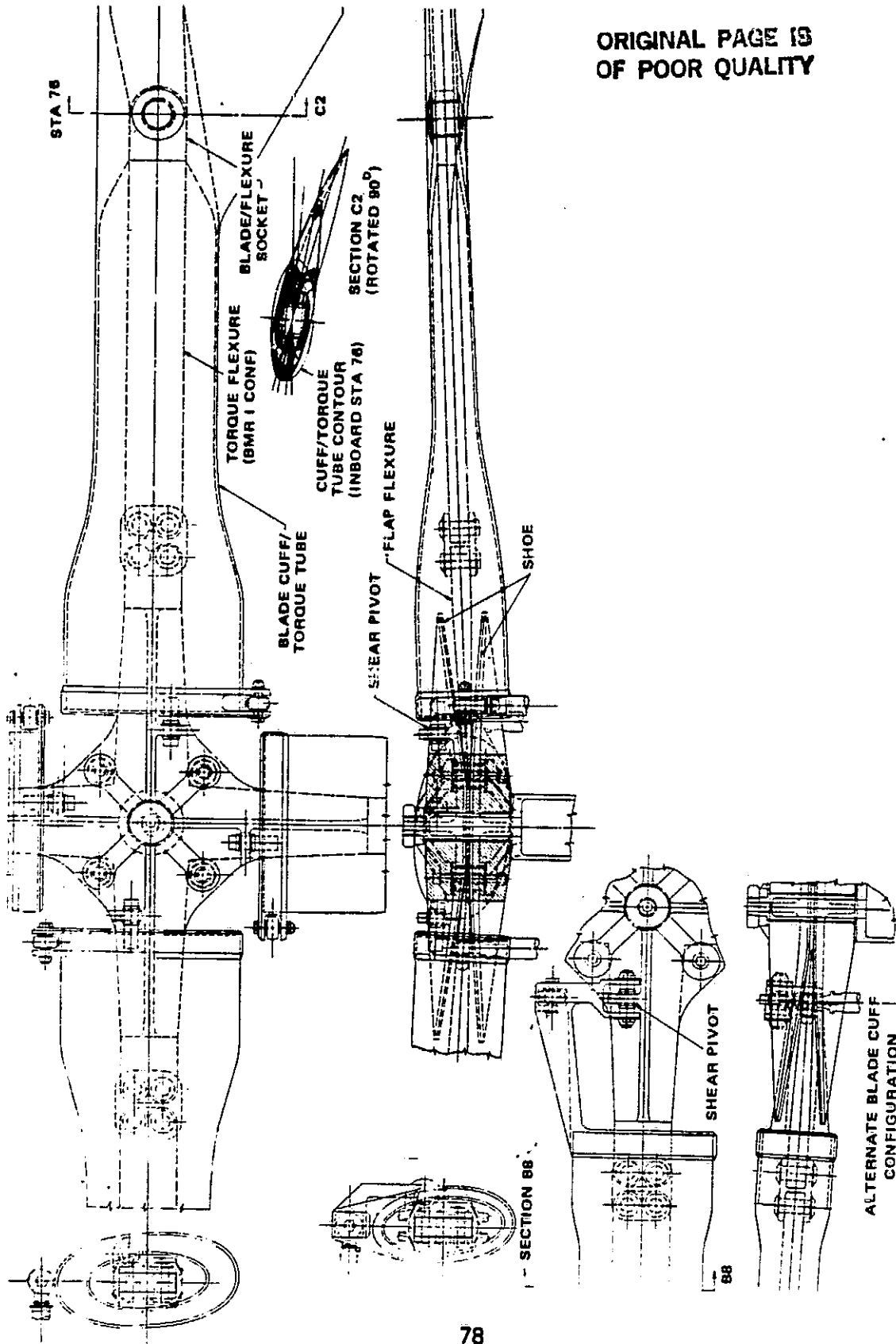


Figure 27. ITR Configuration 3 (Flexure/Shoe Rotor)

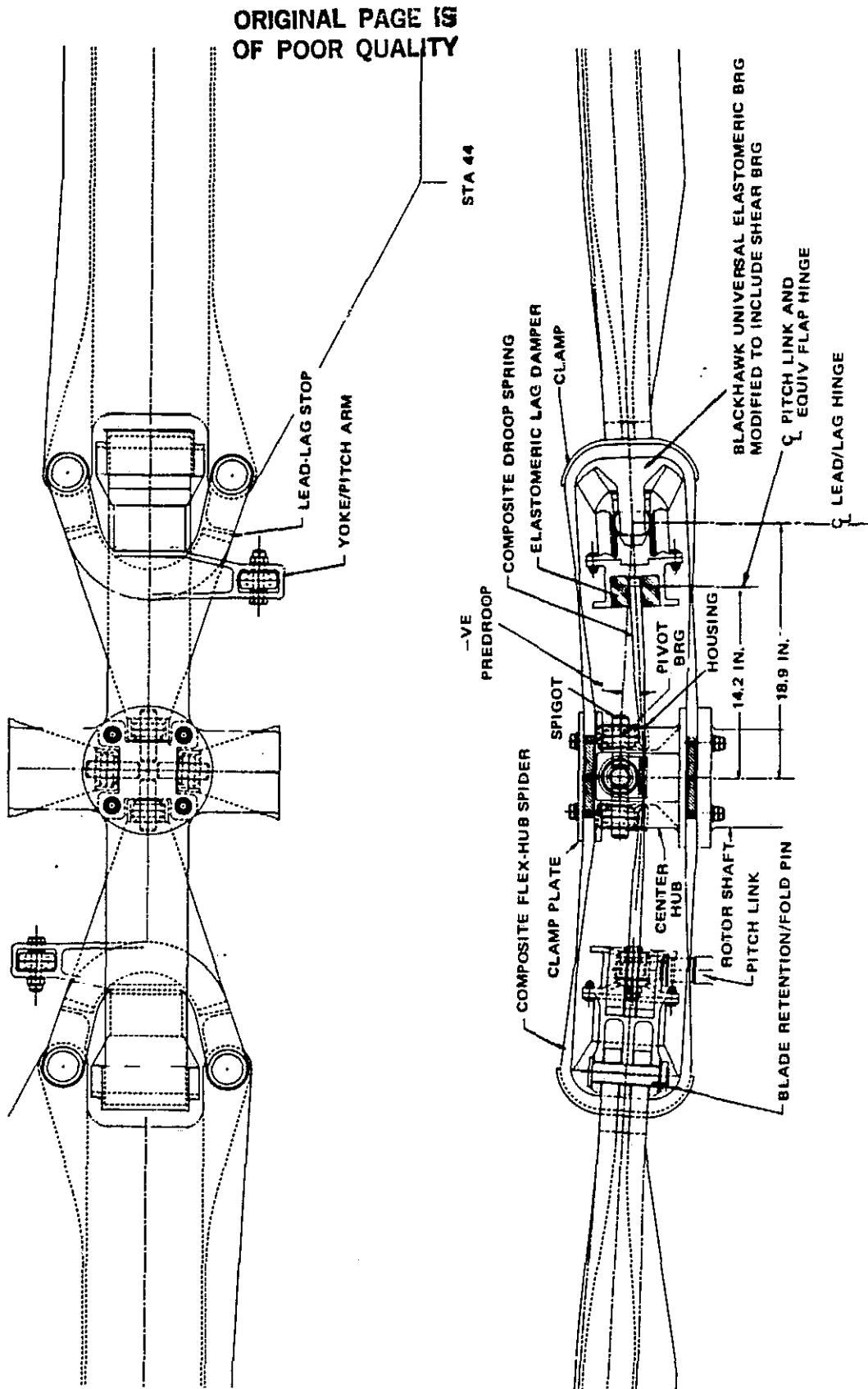


Figure 28. FTR Configuration 4 (Reversed Starflex Rotor)

flexible hub plates allow a small increase in flapping displacement which reduces the overall stiffness but is insufficient to meet the design goals.

The Blackhawk elastomeric bearing, modified to better react normal shear loads, was used in this concept to avoid diverging into the details of elastomeric bearing design.

#### Configuration 5 - Lag/Torsion Flexure With Flapping Hinge (Figure 29)

This configuration has a conventional metal spider for attachment of the rotor to the shaft and which supports the blade through elastomeric bearings sized to permit high-endurance limit flapping. Primary retention against centrifugal loads is with a composite tension/lag/torsion strap wrapped around the flap hinge spindle and outboard, around a vertical blade retention pin which also attaches the separate flexure sleeve to the blade root end. A secondary pin prevents relative lag motions between the blade and sleeve. Folding requires removal of the lag pin. The inboard end of the sleeve is supported by an elastomeric shear pivot attached to the hinge spindle. Due to the negligible static hub stiffness, centrifugally retracted droop stops have been included to limit hinge motions and to permit the high flap stiffness flexure to react limit flap bending loads. Radar-absorbing material has been added to provide aerodynamic fairing to the torque sleeve and blade attachment fold joint.

#### PRELIMINARY STUDIES

In order to result in truly viable concepts, preliminary studies were conducted to investigate proper material selection and optimum flexure geometry (including root attachments) for maximum endurance limit flapping for minimum hub stiffness and torque to twist.

Basic considerations for the material choice are material allowable fatigue strain, flexural stiffness, interlaminar shear strength, ultimate compressive strength, and damage tolerance. A higher allowable fatigue

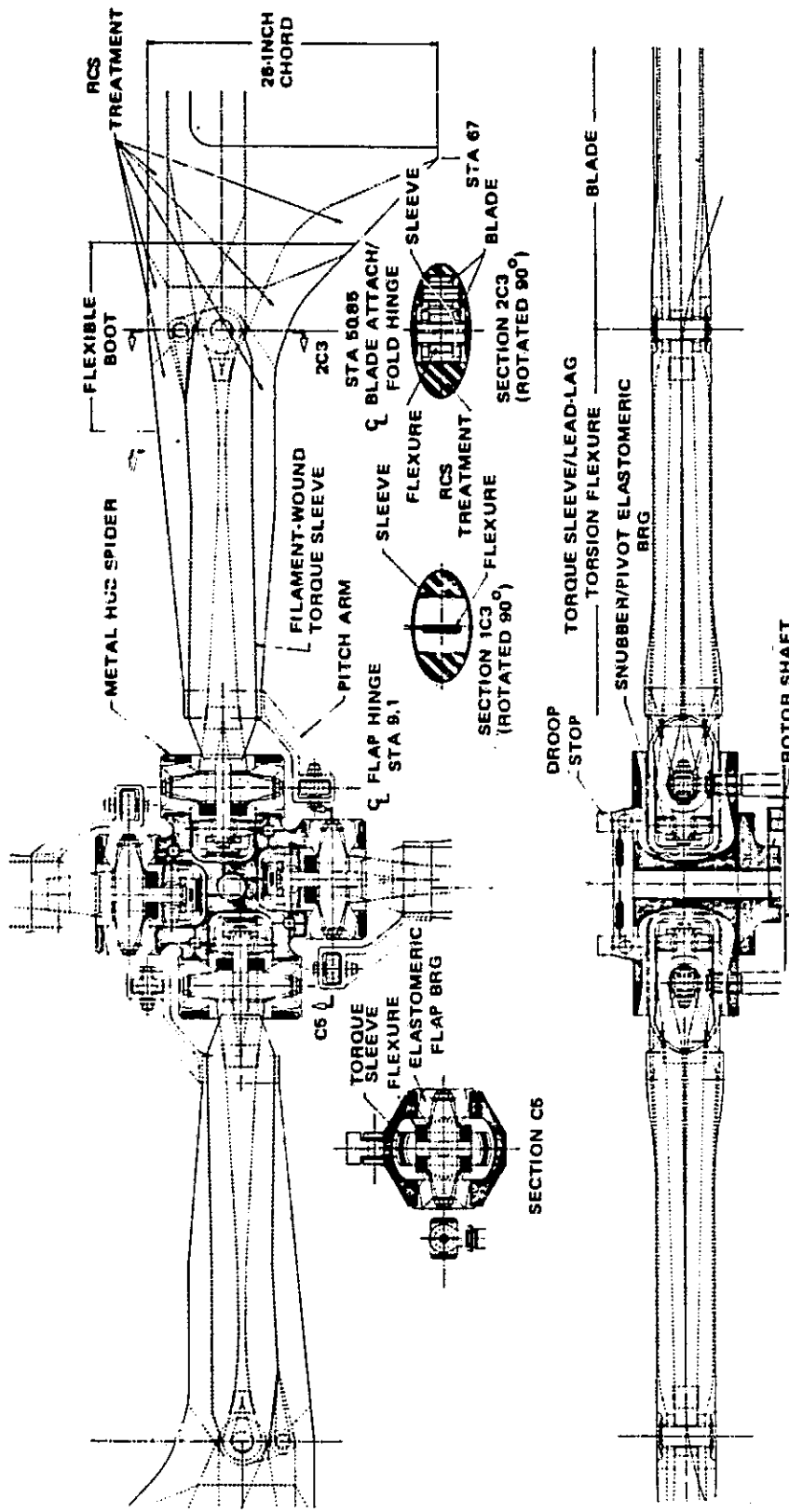


Figure 29. ITR Configuration 5 (Lag/Torsion Flexure With Flapping Hinge)

strain results in a smaller radius of curvature and the attainment of the flapping goal in a shorter flexure length with lower effective flap hinge offset and resultant hub stiffness. A stiffer material of the same strain allowable also results in a smaller radius of curvature and smaller flexure dimensions with lower weight. Interlaminar shear strength governs root clamp radial length, which influences hub stiffness through the effective flap hinge offset location.

For flexure geometry, increased length increases allowable flapping, decreases torque to twist, but increases hub moment. Increased width reduces minimum allowable thickness which permits more flap bending; however, CF torsional stiffening is increased.

### Material Selection

Table 7 lists the properties of the materials under consideration. For maximum flexural stiffness and strength and minimum torsional stiffness, unidirectional reinforcements are considered; however, they are expected to be alternately biased at some small angle to prevent intralaminar splitting. Pros and cons of each material characteristic are included. Recent developments and demonstrations of the application of composite materials to rotor system components indicate that they have potential in providing a solution to many of the ailments of metallic components. Composite materials have been shown to improve life, damage tolerance, and failsafety due to their relative notch insensitivity, slow crack growth, superior fatigue strain endurance, and high energy storage prior to fiber failure. The raw material is basic in that it can be sized and shaped to any proportions with a minimum of trim and scrappage, allowing strength and stiffness to be discretely introduced only where required. Techniques have been developed to reduce damage propagation even further through material hybridization and fiber and layer orientation. Composites are not susceptible to corrosion and are readily inspectable by ultrasonic

TABLE 7. A SELECTION OF MATERIAL DESIGN CHARACTERISTICS

Material	Style	Biax	Density $\rho$ (lb/in. <sup>3</sup> )	Modulus		Static Strength					Fatigue Strength		Impact Notched IZOD ft lb/in.	Fleet. To Temp. Humidity	Remarks
				Tensile $10^6$ lb/in. <sup>2</sup>	Shear $10^6$ lb/in. <sup>2</sup>	u.t.s. $10^3$ lb/in. <sup>2</sup>	u.c.s. $10^3$ lb/in. <sup>2</sup>	I.I.s. $10^3$ lb/in. <sup>2</sup>	Shear Ult $10^3$ lb/in. <sup>2</sup>	Tensile $\mu$ lb/in.	Shear $\mu$ lb/in.				
Glass /Epoxy	Uni	0°	0.067	6.5	0.8	160	125	11	14	2,300	2,900	60	High	(1) Large data bank	
	Uni	± 45°	0.067	1.8	1.8	23	.	11	46	1,400	2,250	-	Medium		
	Woven	0°/90°	0.056	3.1	0.8	45			14	2,540	2,300	11	High/Med		
	Woven	± 45°	0.068	1.8	1.35	27			26	1,600	3,300	-	Medium		
Kevlar /Epoxy	Uni	0°	0.080	11	0.3	145	32	8	8.7	2,720	-	25	Medium	(1) Low fiber/matrix bond strength (2) Low moisture resistance (1) Adequate data bank	
	Uni	± 45°	0.050	1.1	1.8	18		8	27	-	2,900	-	Med/Low		
	Woven	0°/90°	0.048	4	0.3	70	4	4	4	2,670	-	10	Medium		
	Woven	± 45°	0.048	1.1	2.0	20	4	4	26	2,550	2,400	-	Low		
Graphite /Epoxy	Uni	0°	0.056	20	0.8	164	134	9	11.4	2,100	900	8	High	(1) Low damage tolerance (2) Adequate data bank	
	Uni	± 45°	0.056	2.25	4	25		3	45	1,700	1,150	-	Medium		
	Woven	0°/90°	0.056	9	0.6	60	9	9	10	-	-	-	High/Med		
	Woven	± 45°	0.056	2	3.5	20	3	3	36	-	-	-	Medium		
Graphite /PI700	Uni	0°	0.056	16.3	0.56	192	157	14	16	2,782	-	20	High	(1) Toughest matrix (2) High Temp Resistance (3) Small data bank	
	Uni	± 45°	0.056	2.2	4.0	21		11	35	-	-	11	High/Med		
	Woven	0°/90°	0.055	10.2	-	77		9	15	-	-	14	High/Med		
	Woven	± 45°	0.055	-	4.0	-		35	35	-	-	-	High/Med		
Desired Characteristics			Low	High	Low	High	High	High	High	High	High	High	High	High	

ORIGINAL PAGE IS  
OF POOR QUALITY

and/or radiographic techniques to detect flaws in their laminar and fibrous content. Their high specific static strength and stiffness as presented in Figure 30 offer the potential of significant weight and drag reductions.

Specific static tension strengths of unidirectional composite materials are at least 2.4 times that of titanium, which has the highest specific strength of metals used today. Thus, for axially loaded elements, composites result in weight and size reductions. However, for elements under flexural and/or torsional loading, these gains may be reduced due to the necessity to add material to enhance shear strength due to inferior shear capabilities of the matrix of the composite materials, which is down to one-quarter of the strength of the weakest metal.

In addition, the compression strengths of the candidate materials fiberglass, graphite, and Kevlar are less than the tension strength. For Kevlar the reduction is substantial, which may preclude its use as primary flexure material. For fatigue design, Figure 31 presents the Goodman reduction curves for composites reinforced with the three unidirectional fibers under consideration. Mean minus  $3\sigma$  test data are shown which illustrate the nonlinear characteristics of fiberglass and the effect of the compressive strength of graphite and the low compressive strength of Kevlar. For design purposes, the curves have been linearized within the typical range of usage for dynamic applications and additional reductions to the flapping allowables have been taken for chord and torsional strains.

The properties listed in Table 8 size the flapping flexure.

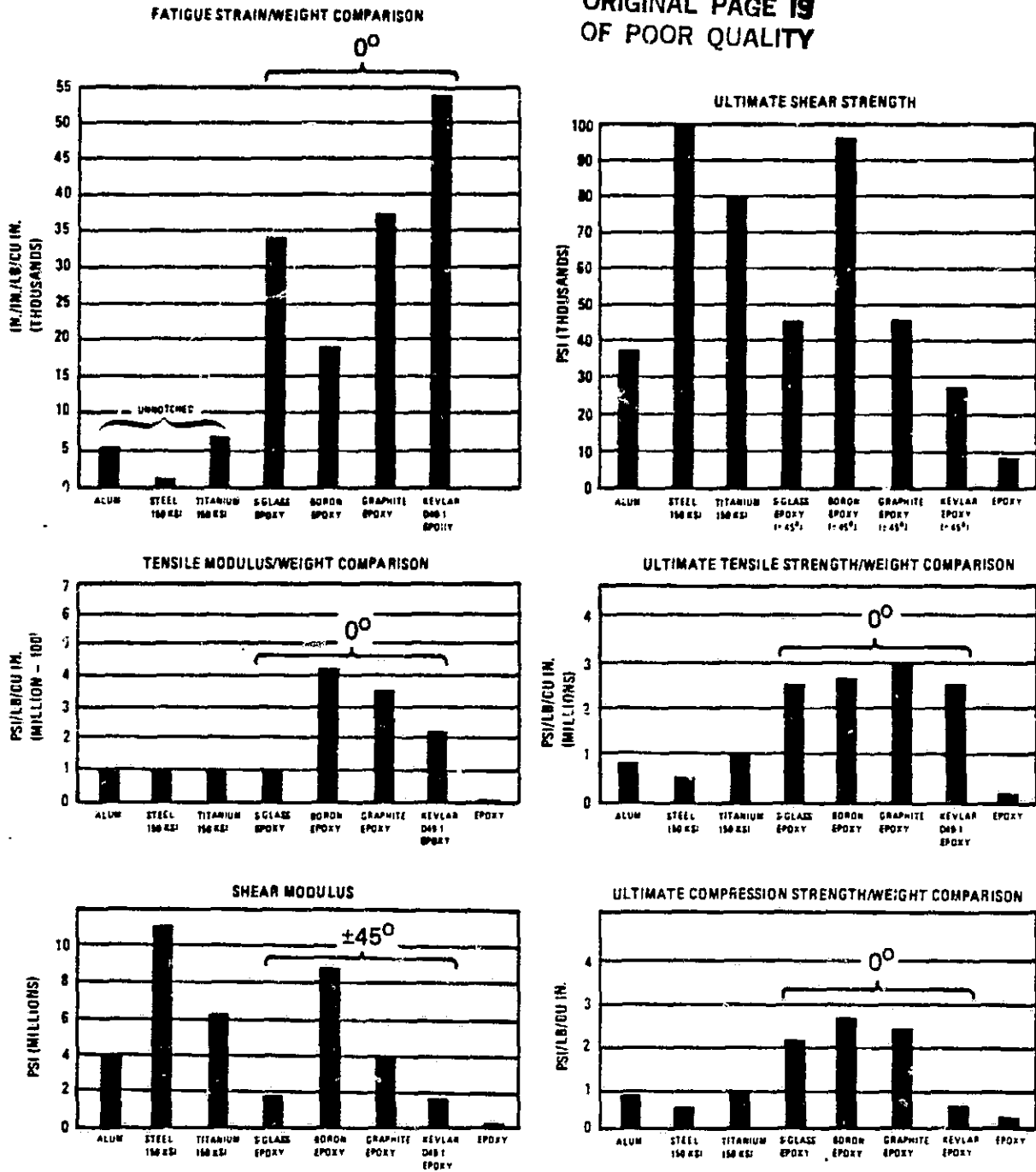


Figure 30. Specific Properties of Composite Materials Compared to Metals

ORIGINAL PAGE IS  
OF POOR QUALITY

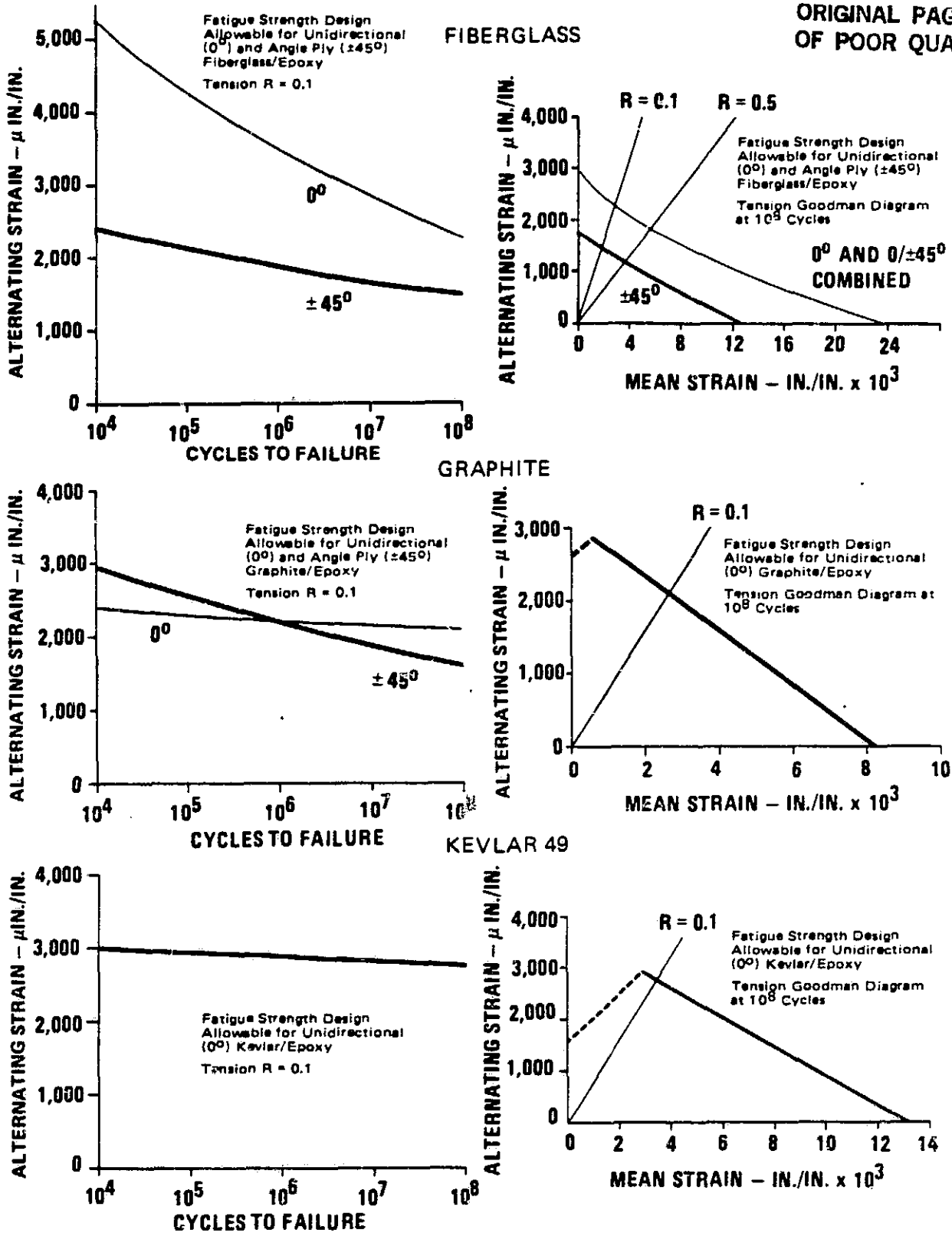


Figure 31. Fatigue Design Allowables for Candidate Materials

TABLE 8. RELEVANT PROPERTIES OF MATERIALS

Unidirectional Composite	Fiberglass	Kevlar	Graphite
$\epsilon$ , allowable tensile fatigue strain ( $\mu\text{in./in.}$ )	$\pm 2,300$	$\pm 2,720$	$\pm 2,100$
$\sigma_t$ , allowable tensile fatigue stress (psi)	$\pm 14,950$	$\pm 29,920$	$\pm 42,000$
E, tensile modulus of elasticity (psi $\times 10^6$ )	6.5	11.0	20.0
$\sigma_s$ , allowable interfiber shear fatigue stress (psi)	$\pm 1,600$	$\pm 1,600$	$\pm 1,600$
Composite density (lb/in. <sup>3</sup> )	0.067	0.050	0.056

Weight

The following simplified methodology shows the likely effect of material choice upon running weight of the flexure.

Clamp Radius (a)/Equivalent Flap Hinge Offset (e') - Figure 32 shows a blade deflected through a flap angle  $\beta$  and supported by a root flap flexure of length  $l (= 2e, \text{ where } e \text{ is the center of flapping})$  and clamped at the root over a distance a.

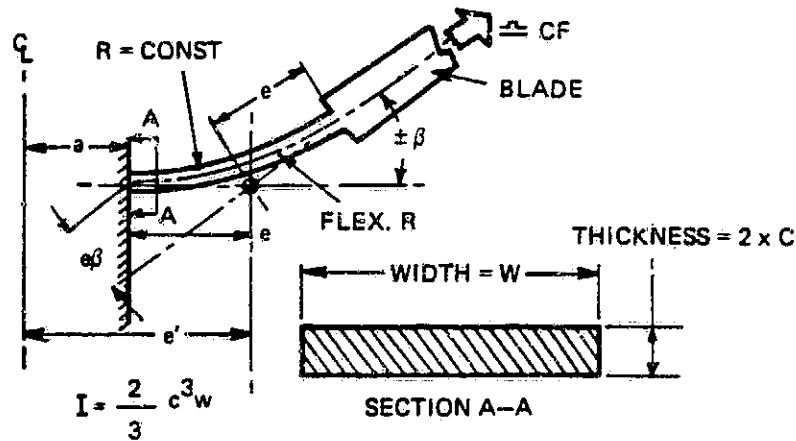


Figure 32. Diagram of Clamp Radius and Equivalent Flap Hinge Offset

Flexure Root Clamp - If it is assumed that a root clamp at the rotor shaft is used, that the clamp area is driven by the flexure root moment, flexure root width and thickness, and that the radial length of clamp required to result in an attenuation of the root moment inside the clamp at such a rate that the interlaminar shear capability of the material is not exceeded, then the interlaminar shear stress ( $\tau_s$ ) within a bending rectangular member of cross-sectional area A is given by the equation

$$\tau_s = \frac{3}{2} \frac{V}{A} ,$$

where V is the rate of change of the bending moment with radial distance (i.e.,  $\frac{dM}{dx}$ ). Given a linear rate of moment decrease from flexure root ( $x = a$ ) to the shaft ( $x = 0$ ), then  $\frac{dM}{dx} = \frac{M_{\text{Root}}}{a}$ , or

$$a = \frac{3M_{\text{Root}}}{4wc} \times \frac{1}{\tau_s} , \quad (7)$$

where  $w$  = flexure root width and  
 $c$  = flexure root semithickness.

The width ( $w$ ) of the flexure root cross section is given by:

$$w = \frac{3}{8} \frac{CF}{Ee} \left(\frac{\beta}{\epsilon}\right)^3 , \quad (8)$$

where  $\epsilon$  is the allowable direct strain in the composite of tensile modulus E.

Since the root bending moment  $M_R = CF \cdot \beta \cdot e$

and the root semithickness  $c = \frac{EI \cdot \epsilon}{M_R}$  ,

and  $I = \frac{2}{3} wc$ ,

then the root semithickness becomes:

$$c = 2 e \left(\frac{\epsilon}{\beta}\right) . \quad (9)$$

But  $e = (e' - a)$  where ( $e'$ ) is the required hinge offset from the center of rotation.

Substituting for  $M_R$ ,  $w$ ,  $c$ , and  $e$  in equation 7 we have

$$\left(\frac{a}{e}\right)_{\text{Min}} = \frac{\left(\frac{\sigma_t}{\tau_s}\right) \frac{\epsilon}{\beta}}{1 + \left(\frac{\sigma_t}{\tau_s}\right) \frac{\epsilon}{\beta}},$$

ORIGINAL PAGE IS  
OF POOR QUALITY

where  $\sigma_t$  is the allowable direct stress ( $E \cdot \epsilon$ ).

For  $\beta = \pm 5^\circ$  or 0.087 radian,

$$\left(\frac{a}{e}\right)_{\text{glass}} = 0.198 \quad \left(\frac{a}{e}\right)_{\text{Kevlar}} = 0.369 \quad \left(\frac{a}{e}\right)_{\text{graphite}} = 0.388,$$

and from  $e = (e' - a)$ ,

$$\left(\frac{e}{e'}\right)_{\text{glass}} = 0.802 \quad \left(\frac{e}{e'}\right)_{\text{Kevlar}} = 0.631 \quad \left(\frac{e}{e'}\right)_{\text{graphite}} = 0.612,$$

and from equation 8, if  $CF = 75,000 \text{ lb}$ ,

$$(w)_{\text{glass}} = \frac{292}{e'} \quad (w)_{\text{Kevlar}} = \frac{133}{e'} \quad (w)_{\text{graphite}} = \frac{258}{e'},$$

and from equation 9,

$$(t = 2c)_{\text{glass}} = 0.084e' \quad (t)_{\text{Kevlar}} = 0.079e' \quad (t)_{\text{graphite}} = 0.059e'.$$

Root cross-sectional area ( $A_R$ ) is ( $w \times t$ )  $\text{in.}^2$ .

$$(A_R)_{\text{glass}} = 24.53 \text{ in.}^2 \quad (A_R)_{\text{Kevlar}} = 10.51 \text{ in.}^2 \quad (A_R)_{\text{graphite}} = 15.22 \text{ in.}^2,$$

and weight per unit length ( $\mu$ ), ( $x = a$ ),

$$(\mu)_{\text{glass}} = 1.64 \text{ lb/in.} \quad (\mu)_{\text{Kevlar}} = 0.53 \text{ lb/in.} \quad (\mu)_{\text{graphite}} = 0.85 \text{ lb/in.}$$

Conclusion - For minimum weight, fiberglass should not be the material choice for the ITR/FRR hub flexbeams.

With the BEAMSOL simplified methodology it can be shown that for a flap flexure of constant width (6 inches) and 24 inches in length, material choice affects deflection, hub stiffness, and allowable flapping. Figure 33 illustrates the effect of material on allowable flapping and shows that the goals have not been reached. Increasing the width to the maximum practical value of 10 inches improves the flapping and stiffness, but the large width results in a high planform area of the system and more than doubles the torque to twist. A material of tensile modulus of  $15 \times 10^6$  psi appears to be the optimum choice.

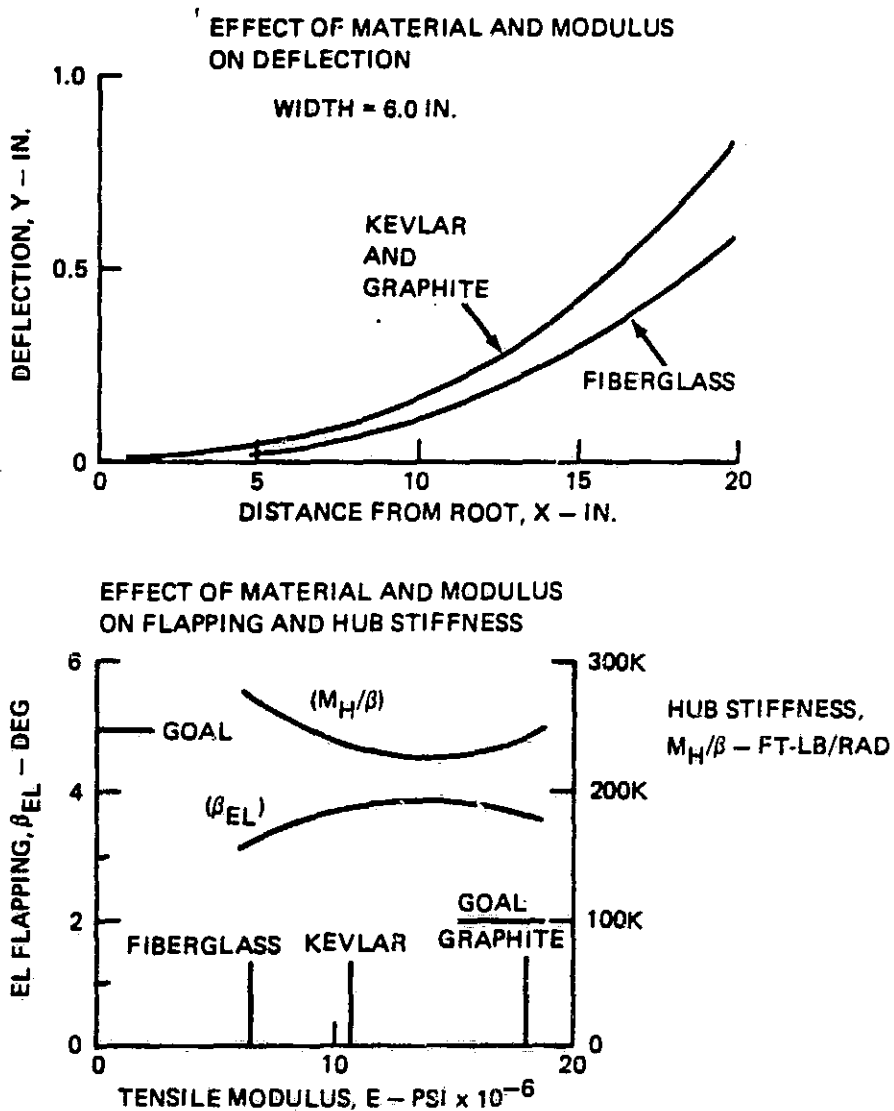


Figure 33. Effect of Material on Flexure Performance

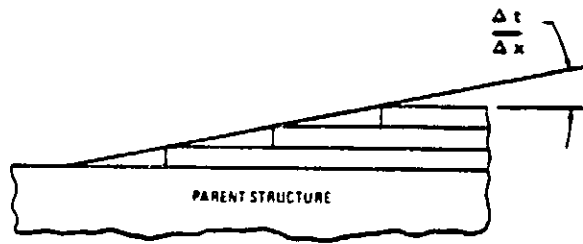
## Width and Thickness Variation - Material Interlaminar Shear Strength Limitations

It has been shown that an increase in width will result in an increase in allowable flapping, but hub planform area and consequently thrust and drag will be compromised. The configuration can be improved, however, by having a maximum width at the flexure root which reduces to a minimum outboard, at the mouth of the enshrouding torque sleeve. Fiber modulus and matrix shear strength limit the rate of change of cross-sectional area, since each additional ply of material has to be strained compatibly with the main flexure without shear failure occurring in the matrix at the end of the additional ply. The interlaminar shear force is proportional to the modulus and thickness of the additional layer as well as the overall strain level. The allowable matrix interlaminar shear stress defines the ply end length over which the shear forces are distributed and thus the maximum allowable rate of change of thickness with length (or material buildup) can be determined.

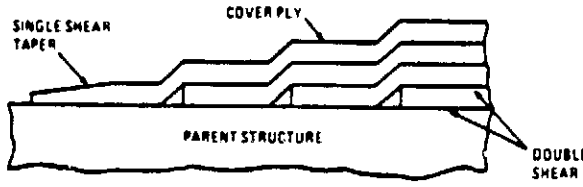
Figure 34 shows the results of such an investigation which compares various types of material and in which each additional ply obtains its loading from one adjacent ply (i.e., by single shear load path).

This structural design criterion for the maximum rate of change of material buildup can be made less restrictive if the plies are laid up so that their end terminations are in double shear. Shorter plies should be on the inside of the buildup and/or a continuous, single, thin, low-modulus cover ply should be added to the outside.

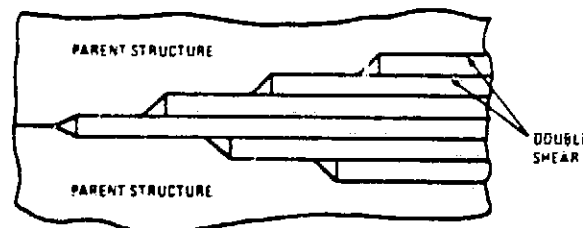
ORIGINAL PAGE IS  
OF POOR QUALITY



SINGLE SHEAR



DOUBLE SHEAR



DOUBLE SHEAR

MATERIAL PROPERTIES

MATERIAL	MODULUS (PSI)		TENSILE STRAIN ALLOWABLE (IN./IN.)		I.L.S. STRESS ALLOWABLE (PSI)	
	E	G	FATIGUE	LIMIT	FATIGUE	LIMIT
100% D <sup>0</sup> UNI						
GRAPHITE/EPOXY	16 X 10 <sup>6</sup>	0.8 X 10 <sup>6</sup>	0.0021	0.005	1600	6000
KEVLAR/EPOXY	10 X 10 <sup>6</sup>	0.36 X 10 <sup>6</sup>	0.0027	0.009	1600	5330
FIBERGLASS/EPOXY	6.5 X 10 <sup>6</sup>	0.8 X 10 <sup>6</sup>	0.0023	0.018	1600	7333

TAPER RATES

MATERIAL	SINGLE SHEAR MAXIMUM TAPER		DOUBLE SHEAR MAXIMUM TAPER	
	FATIGUE	LIMIT	FATIGUE	LIMIT
100% D <sup>0</sup> UNI				
GRAPHITE EPOXY	1 : 20.52	1 : 12.54	1 : 10.26	1 : 6.27
KEVLAR EPOXY	1 : 16.00	1 : 16.02	1 : 8.00	1 : 8.01
FIBERGLASS EPOXY	1 : 8.88	1 : 15.70	1 : 4.44	1 : 7.85

Figure 34. Interactions of Materials and Interlaminar Shear Strength

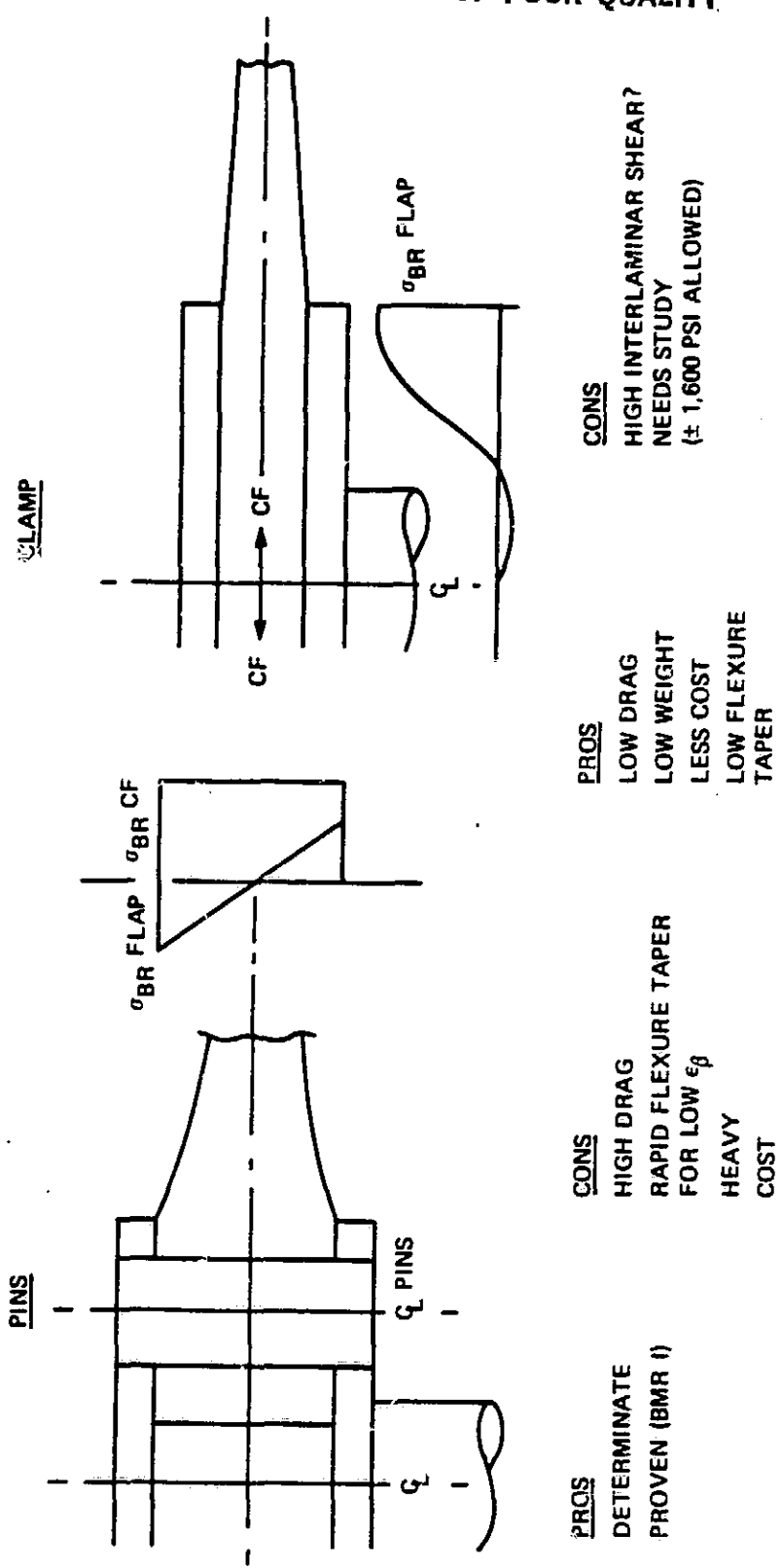
## Flexure Geometry

The general philosophy in the design of bearingless rotor flexures is as follows:

1. To maximize allowable flapping, the flexure is considered as consisting of two discrete regions, a flapping flexure and a lag/torsion flexure. The flapping flexure should be relatively rigid in chord and torsion to permit the majority of strain energy therein to be from flapping alone.
2. To minimize hub stiffness, the flapping flexure must be short and in-board of the lag/torsion flexure.
3. To minimize hub stiffness, the shaft attachment must permit the flexure root to be as close to the centerline of the shaft as possible.

A brief study of the impact of these geometric criteria has been made.

Root Shaft Attachment - Figure 35 shows the attributes and disadvantages of two options for attachment of the flexures to the shaft. The pinned arrangement is typical of the Boeing Vertol Bearingless Main Rotor (BMR) which, by design, had a 14-percent radius effective hinge offset. The design criterion was that CF bearing stress had to overcome the differential bearing stress on the pins throughout the flight spectrum to prevent load reversal and the resultant fretting. An additional feature was the use of bushings to augment the interlaminar shear strength to accommodate the high root bending moments produced by the hinge offset. As a result, a tall buildup was required since bearing stress due to bending reduced faster than that due to CF as the height was increased. The ratio of height to radial length was such that no credit could be taken from clamping between the upper and lower hub plates. Because of the high hinge



CLAMPING IS PREFERRED

Figure 35. Blade Root Attachment - Pins Versus Clamping

offset requirement, sufficient length was available to reduce the flexure cross section outboard within the constraints of the maximum taper rate discussed earlier.

A heavy, high-drag arrangement resulted even though the pins were located at 2.3-percent radius.

In the alternate clamped arrangement, the flexure is clamped between two hub plates and the root moment extracted from the flexure in differential bearing within the clamp. This results in a lower profile hub but the width (i.e., clamp radius) requires increasing to decrease the rate of change of hub moment within the clamp to acceptable limits defined by the material interlaminar shear strength.

Root Clamp Flexibility and Its Effect Upon Flexure Interlaminar Shear Stress - Figure 36 shows the extreme cases for hub clamp support, infinite clamp rigidity and simply supported flexure.

If shear force ( $V$ ) in the flexure having a deflected shape  $y(x)$  is  $EI \frac{d^3y}{dx^3}$ , then the shear force ( $V$ ) is dependent upon the slope of the bending moment within the clamp ( $\frac{dM}{dx}$ ).

At the tip of the infinitely rigid clamp, the rate of change of bending moment ( $V$ ) within the flexure is infinite since the bending moment and deflection of the flexure inside the clamp are zero. The interlaminar shear stress ( $\tau = \frac{3}{2} \frac{V}{A}$ ) at the tip is correspondingly infinite and unacceptable. For the other extreme, the rate of change of bending moment ( $V = M_R/a$ ) within the simply supported clamp is finite and a minimum; however, a true simply supported arrangement would be complex and undesirable. As noted earlier, the simply supported case defines the minimum possible clamp radius ( $a$ ) dependent upon the maximum allowable interlaminar shear strength ( $\tau_s$ ) of the material.

ORIGINAL FIGURE  
OF POOR QUALITY

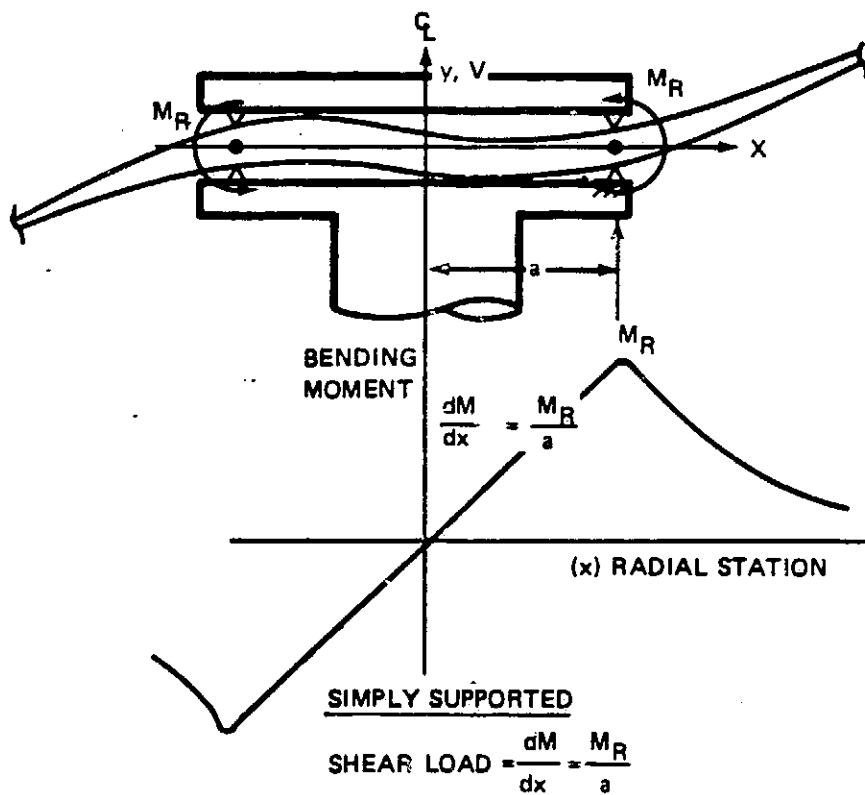
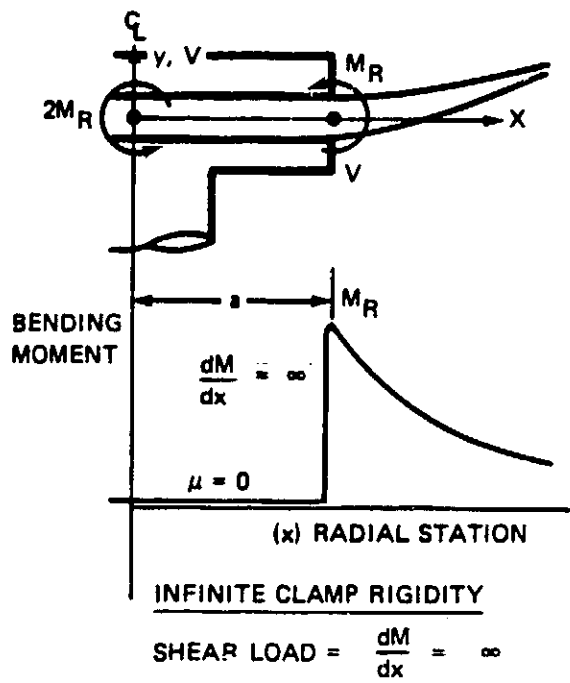


Figure 36. The Extremes of Hub Clamp Support

$$a_{\min} = \frac{3}{2} \frac{M_R}{\tau_s \cdot A} \quad \text{where } A \text{ is the sectional area of the flexure.}$$

It can be remarked that if  $(a \times A) =$  volume of material inside the clamp, then to a first approximation:

The interlaminar shear stress is proportional to the flexure root moment and inversely proportional to the volume of material inside the clamp. It is independent of both width and thickness of the flexure.

A compromise between the infinitely rigid and the simply supported clamp can be achieved by flexibilizing the clamp through the use of elastomeric lining as shown in Figure 37 and analyzing the system according to the CLAMP technique.

A Technique for Reducing the Composite Flexure Shear Stress Inside the Hub Shaft Attachment - CLAMP Program - The CLAMP program is an analysis for the interlaminar shear stress within the composite flexure inside the hub to shaft attachment. These stresses result from the rapid reduction of the flexure root flap bending moment as it is reacted by the upper and lower metal hub clamp plates. For minimum hub drag, the projected frontal area must be minimized and it follows that the flexure root clamp length must be as short as possible. A short clamp length also contributes significantly toward minimizing hub stiffness. Limitations are material interlaminar shear strength, volume of material inside the clamp, and the clamp flexibility, which controls the rate of decrease of flexure root moment and thus the shear stress. The program analyzes the flexure/shaft attachment for the effects of flexibility, resulting, for example, from an elastomeric liner, and helps to minimize the flexure clamp length within the allowable strength of the composite material. Figure 37 shows the flexure root of flap stiffness  $EI$ , clamped between the upper and lower rigid clamp plates lined with elastomer of foundation modulus  $k$ . Figure 38 shows the shear loading ( $ky$ ) as modified by the deflection of the flexure permitted by the elastomeric lining.

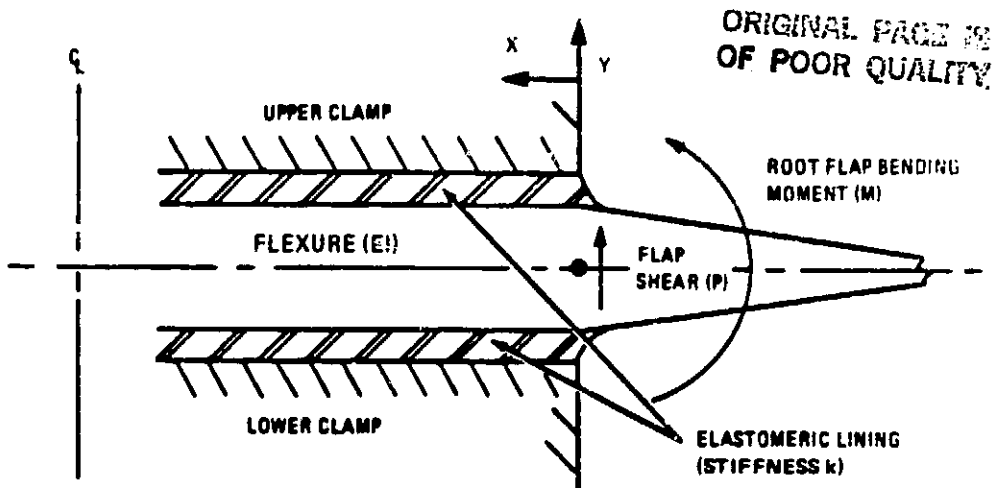


Figure 37. Flexure Root Clamp at the Shaft

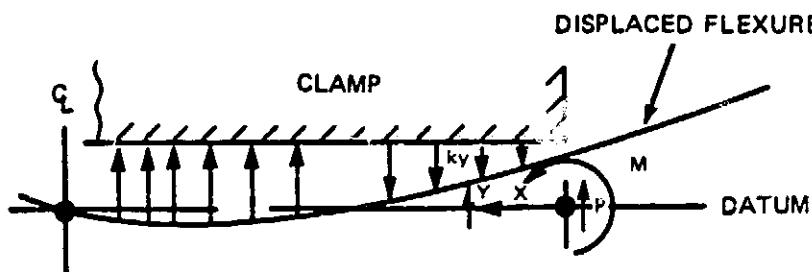


Figure 38. Flexure Displacement Inside the Clamp

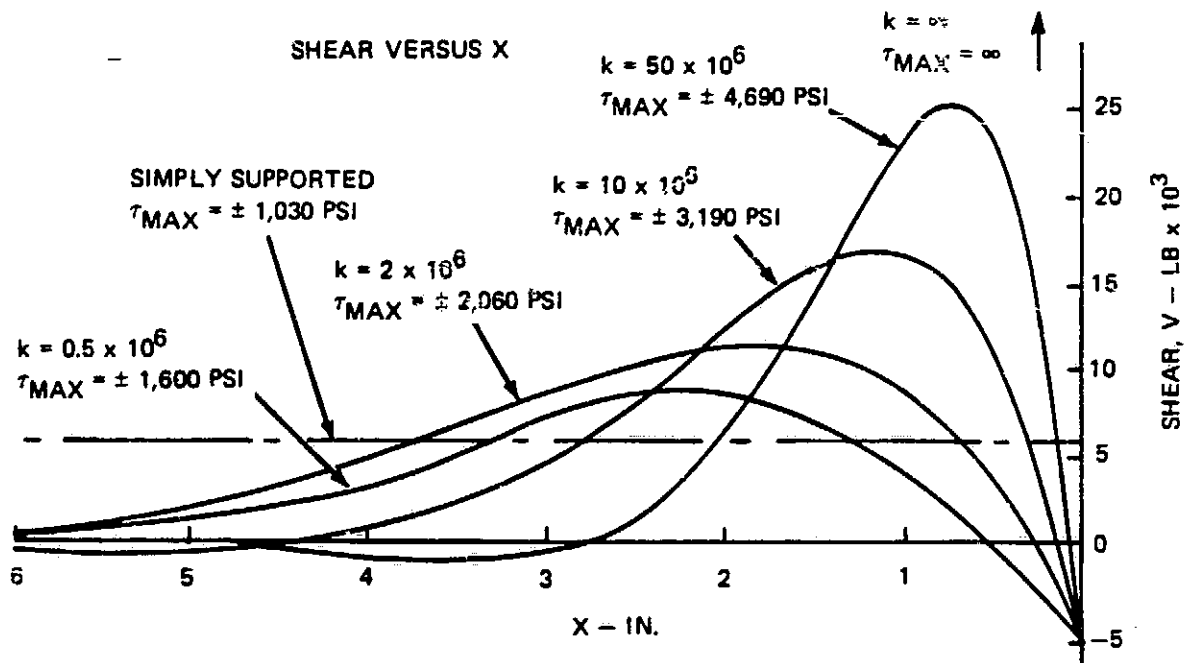


Figure 39. Flexure Shear Loading Inside the Root Clamp

*Handwritten signature or initials*

The shear loading and displacement are related by the equation

$$EI \frac{d^4 y}{dx^4} + ky = 0, \text{ which has a solution of the form}$$

$$y = e^{\beta x} [A \cos \beta x + B \sin \beta x] + e^{-\beta x} [C \cos \beta x + D \sin \beta x],$$

where  $\beta = (k/4EI)^{1/4}$

where A, B, C, D, and  $\beta$  are physical constants of integration as determined by the boundary conditions and material and section properties.

The CLAMP program solves the differential equation and computes the shear distribution ( $V(X)$ ) as defined by

$$V(X) = -EI \frac{d^3 y}{dx^3} = -P e^{-\beta x} (\cos \beta x - \sin \beta x) - 2\beta M (e^{-\beta x} \sin \beta x).$$

$$V_{\max} \text{ occurs at } X = 1/\beta \tan^{-1} \left[ \frac{P}{2M\beta} + 1 \right].$$

The maximum shear stress ( $\tau$ ) found at the neutral axis is

$$\tau_{\max} = \frac{3}{2} \frac{V_{\max}}{A} \text{ where } A \text{ is the flexure cross-sectional area.}$$

Figure 39 shows typical solutions for shear ( $V$ ) and shear stress ( $\tau_{\max}$ ) within the clamp as functions of lining stiffness ( $k$ ) for a graphite flexure of 10-inch root width, 0.8-inch thickness,  $\pm 33,000$  in.-lb of applied bending moment ( $M$ ), and  $\pm 5,790$  pounds of flap root shear load ( $P$ ).

By symmetry, zero deflection (i.e., zero shear) is required at the shaft center. For an allowable shear stress of 2,100 psi within this particular flexure, an elastomeric lining stiffness ( $k$ ) of  $2 \times 10^6$  psi and a minimum clamp length of 6.0 inches must be chosen to preclude interlaminar shear failure.

The technique and rapid execution of the analysis thereof through the CLAMP program will permit rapid iteration of the design of the shaft attachment and minimizing of the hub clamp radius, resultant drag, and hub weight.

Stacked Dual Beams - Another technique for overcoming the high interlaminar shear problem in the flexure root clamp is to divide the flexure into upper and lower stacked beams as shown in Figure 40 and as used in concepts 1 and 2 (Figures 24 and 26).

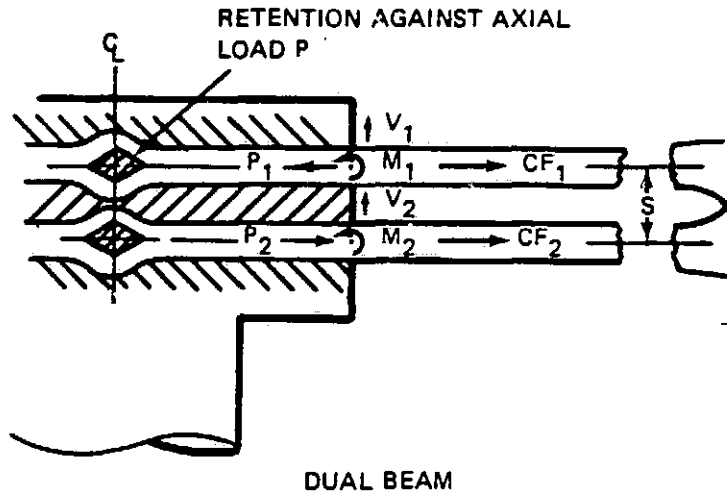
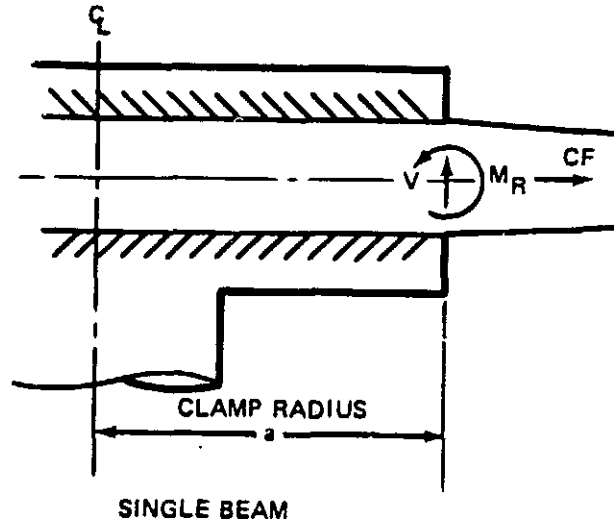
The flexure root moment ( $M_R$ ) is then divided into axial loads ( $P_1$  and  $P_2$ ) which are additional to the centrifugal force components ( $CF_1$  and  $CF_2$ ), and into local beam moments ( $M_1$  and  $M_2$ ) which are many times smaller than  $M_R$ . The CHORD-Z analysis is used to define the magnitude of the component loads in each of the dual beams.

A simple approximation can be made if first-mode bending is considered in which the dual beams act as if they were one. See Figure 41 for the calculation of endurance limit strains ( $\epsilon$ ) in the upper and lower surface extreme fibers.

If the thickness of each beam element is 1/3 that of the single beam, then the volume of material under the clamp for each beam is only 1/3 of that for the single beam; but the local bending moment is reduced to 1/27 of that for the single beam. Interlaminar shear stress within the dual beam clamp is therefore only 1/9 of that for the single beam. An obvious conclusion is that a significant reduction in clamp radius ( $a$ ) can be made.

Another advantage may result from the dual beam configuration which is worthy of investigation. The resulting reduction in flexure shear rigidity may reduce the transmission of blade 4/rev root shears to the airframe, resulting in a significant reduction in cockpit vibration. This

ORIGINAL DESIGN  
OF POOR QUALITY.



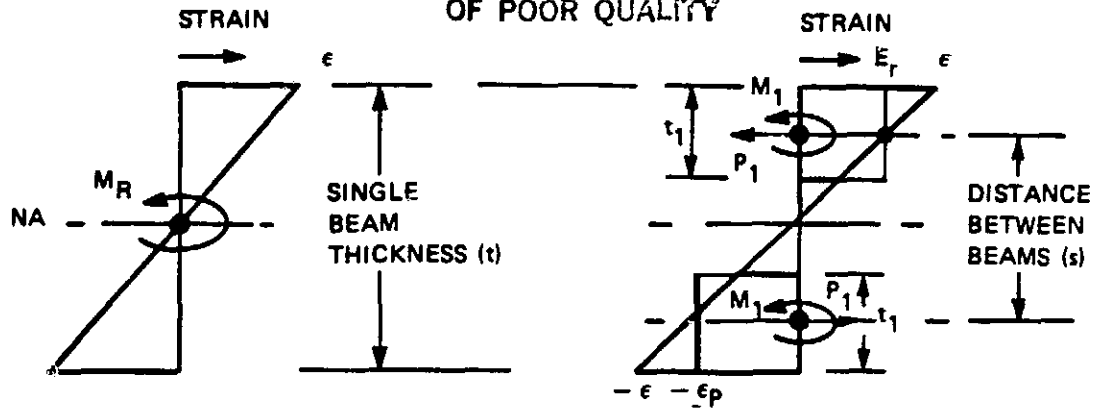
$$M_R = (M_1 + M_2) + (P_1 + P_2) \frac{S}{2}$$

$$V = V_1 + V_2$$

$$CF = (CF_1 - P_1) + (CF_2 + P_2)$$

Figure 40. Split Flexure Reduces Interlaminar Shear

ORIGINAL PAGE IS  
OF POOR QUALITY



STRAIN DISTRIBUTION  
SINGLE BEAM

$$\epsilon = \frac{6 M_R}{E W t^2} \quad \text{or} \quad M_R = \frac{E \epsilon W t^2}{6}$$

STRAIN DISTRIBUTION  
DUAL BEAM

$$(\epsilon - \epsilon_p) = \epsilon (t_1/t)$$

$$M_1 = \frac{E}{6} (\epsilon - \epsilon_p) W t_1^2$$

$$M_1 = \frac{E t_1^3}{6 t} W t_1^2$$

$$\epsilon_p = \epsilon \frac{s}{t} = \epsilon \left( \frac{t - t_1}{t} \right)$$

$$P_1 = \epsilon_p E t_1 W$$

$$P_1 = \epsilon E W (t - t_1) \frac{t_1}{t}$$

If, for example,  $t_1 = t/3$ , then  $E I_{DUAL} = \frac{26}{27} E I_{SINGLE}$

$$\text{and } M_1 = \frac{E}{6 \times 27} \epsilon W t^2 = \frac{1}{27} M_R \quad \text{and} \quad P_1 = \frac{2}{9} E \epsilon W t = \frac{4}{3 t} M_R$$

Figure 41. Calculation of Endurance Limit Strain

should be studied in the next phase of the ITR/FRR program, but it requires refinement of existing mathematical tools for predicting loads and vibration.

Flap Flexure Geometry - Based upon the following simplified methodologies,

1. Equations relating material allowable strain to flexbeam root geometry and blade flapping

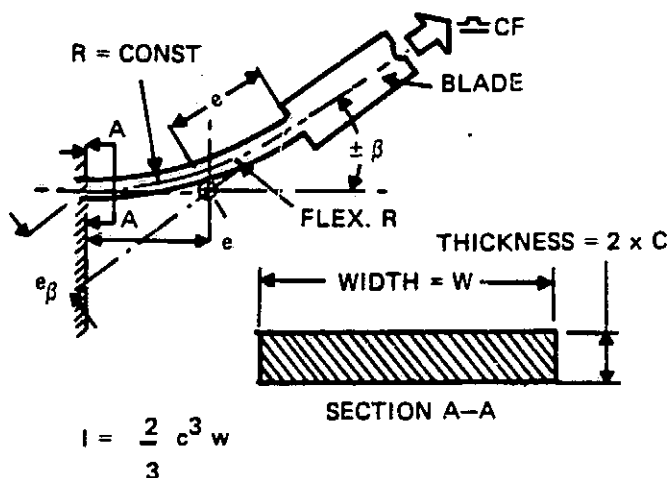
2. Optimization of the geometry of a cantilevered flexure, BEAMSOL solution
3. Analysis for a tension beam cantilever, DIFF5

the significance of flexure width, length, and material allowables upon flexure performance was studied for both the cantilevered and shoe-restrained flexure.

Also included is a preliminary study of the droop spring flexure required for the reversed Starflex configuration.

To Study The Performance of a Flapping Flexure Defined by Simplified Methodology

The methodology is shown in Figure 42.



As shown, this uses the equivalent virtual hinge offset (e) analogy and assumes initially that the most efficient way for the flexure to bend is with a constant radius of curvature (R).

Since  $\frac{M_R}{EI} = \frac{\epsilon}{C} = \frac{1}{R}$ ,  $M_R = CF \beta e$

Root Section A-A

Since  $2e = R\beta$ ,

then flexure root width

$w = \frac{3}{8} \frac{CF}{Ee} \left(\frac{\beta}{\epsilon}\right)^3$

Figure 42. Equations Relating Material Allowable Strain (ε) to Flexbeam Root Geometry and Blade Flapping (±β) for a Simple Cantilevered Flexure

Width Distribution - Since a constant radius of curvature has been assumed, the width distribution over the flexure length (l = 2.e) can be determined since the allowable flapping (β) for a value of strain (ε) is proportional to the flexure length. At a distance (x) from the flexure root,

$$\beta x = \left(\frac{l - x}{l}\right) \beta l \quad (10)$$

The width at  $x$ ,  $W_x$ , is given by the expression

$$W_x = \frac{3}{8} (\ell - x) \frac{CF}{E} \left(\frac{\beta x}{\epsilon}\right)^3 \quad (\text{see methodology above}) . \quad (11)$$

Combining equation 10 with equation 11,

$$W_x = \frac{3}{4} \frac{CF}{E} \left(\frac{\ell - x}{\ell^3}\right)^2 \left(\frac{\beta \ell}{\epsilon}\right)^3 . \quad (12)$$

Thickness Distribution - From the moment distribution  $M_x = CF(\beta e)_{\ell-x}$ , where  $(\ell - x)$  refers to the new flexure length.

$$\text{From equation 10, } M_x = CF \left(\frac{\ell - x}{2\ell}\right)^2 \beta \ell . \quad (13)$$

The strain is given by

$$\epsilon_x = \left(\frac{6M}{EWt^2}\right) x .$$

$$\text{Then } t_x^2 = \left(\frac{6M}{E\epsilon_x}\right) x . \quad (14)$$

Substituting equations 12 and 13 for 14 gives

$$t_x = 4 \left(\frac{e\epsilon}{\beta}\right) \ell . \quad (15)$$

Example: If hinge offset ( $e$ ) = 7%R and  $R = 294$  inches, then  $e = 20.6$  inches and  $\ell = 2e = 41.2$  inches.

For Kevlar, if  $\epsilon = 0.9 \times \epsilon_{EL} = 0.9 \times 2,720 = 2,448$   $\mu\text{in./in.}$  and  $E = 10 \times 10^6$  psi.

If  $CF = 75,000$  lb and  $\beta = 5^\circ = 0.0873$  rad,

$$\text{then } W_x = \frac{75,000}{10 \times 10^6} \left(\frac{41.2 - x}{41.2^3}\right)^2 \left(\frac{0.0873 \times 10^6}{2,448}\right)^3 ,$$

$$W_x = 0.003643 (41.2 - x)^2 ,$$

when  $x = 0$ ,  $W = 6.1835$  inches, and when  $x = \ell$ ,  $W = 0$   
and  $t_x = 2.312$  inches (constant).

Figure 43 shows this theoretical flexure, which, of course, cannot carry an end moment, shear, or even CF since the width at the free end is zero.

A verification of the study so far is demonstrated through DIFF5 nonlinear tension beam analysis for which the output is presented in Figure 44.

Effect of Modifications to the Theoretical Flexure- So far, it has been assumed that the most efficient way to change from zero slope at the root to  $\pm\beta$  at the tip is with a constant radius of curvature.

Since a practical flexure would be of finite width at the end and we can geometrically accommodate a wider flexure outboard at the root, let us modify the root by increasing width and reducing thickness accordingly so that the allowable strain level of 2,448  $\mu\text{in./in.}$  is again met. We may expect a change in end slope (increase) due to the stiffness reduction, but it can be reduced to 5 degrees again by the increase in the outboard width. If the resultant strain level at the root exceeds the allowable, then the constant-radius assumption is valid.

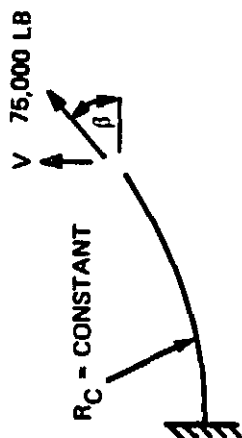
Since strain  $\propto \frac{1}{\text{Width} \times \text{thickness}^2} = \frac{1}{Wt^2}$ ,

then  $(Wt^2)_{\text{new}} = (Wt^2)_{\text{orig}}$ ,

$$t_{\text{new}} = \sqrt{\frac{(Wt^2)_{\text{orig}}}{W_{\text{new}}}}$$

$$= \left( \frac{4.7738 \times 2.312^2}{6.1835} \right)^{\frac{1}{2}}$$

$$t_{\text{new}} = 2.031 \text{ inches.}$$



$\beta = \pm 5^\circ$ ,  $\epsilon_{MAX} = 2,448 \mu \text{ IN./IN.}$ ,  
 $CF = 75,000 \text{ LB}$ ,  $e = 7\% \text{ RAD.}$ ,  
 $R_B = 294 \text{ IN.}$

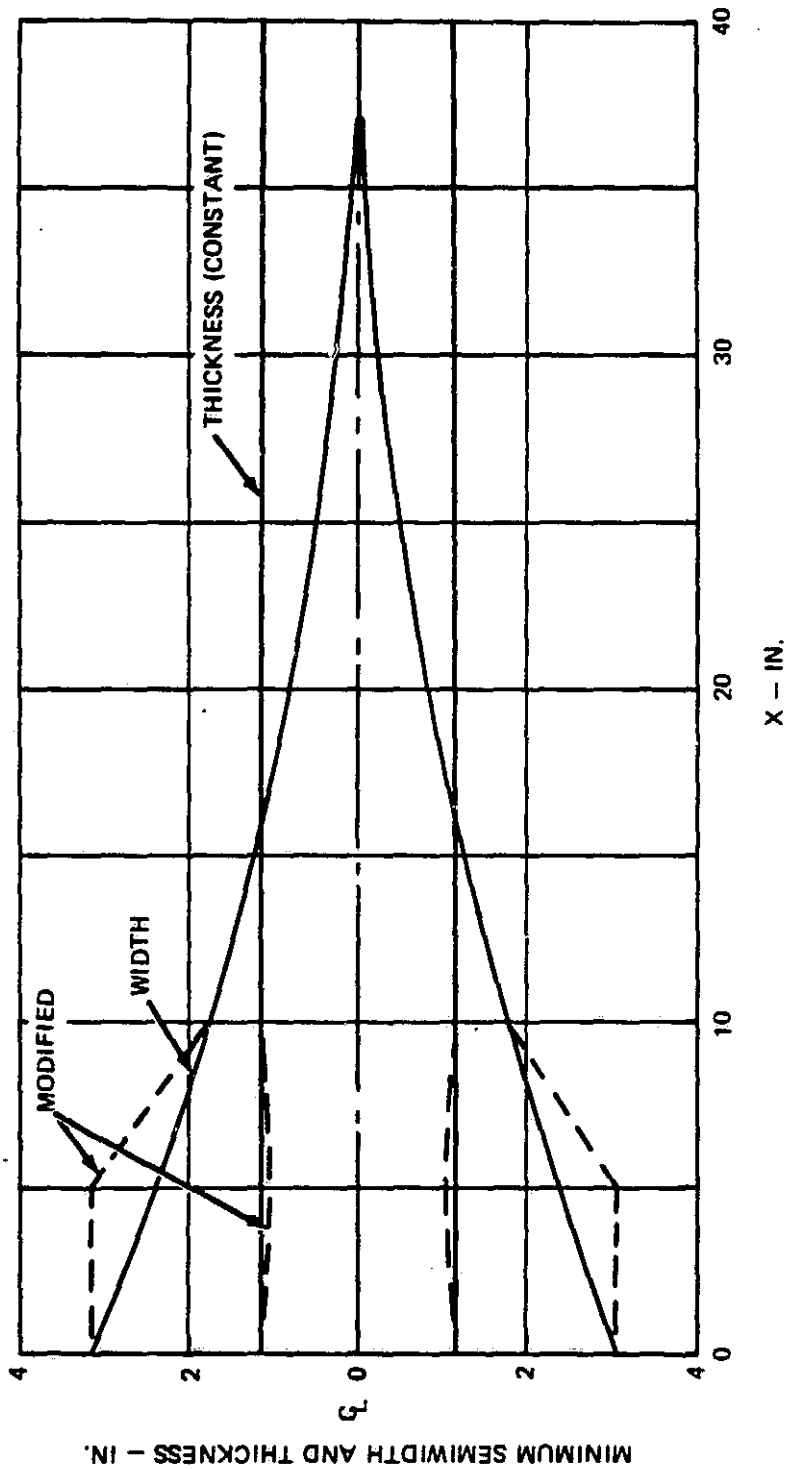


Figure 43. Theoretical Flap Flexure

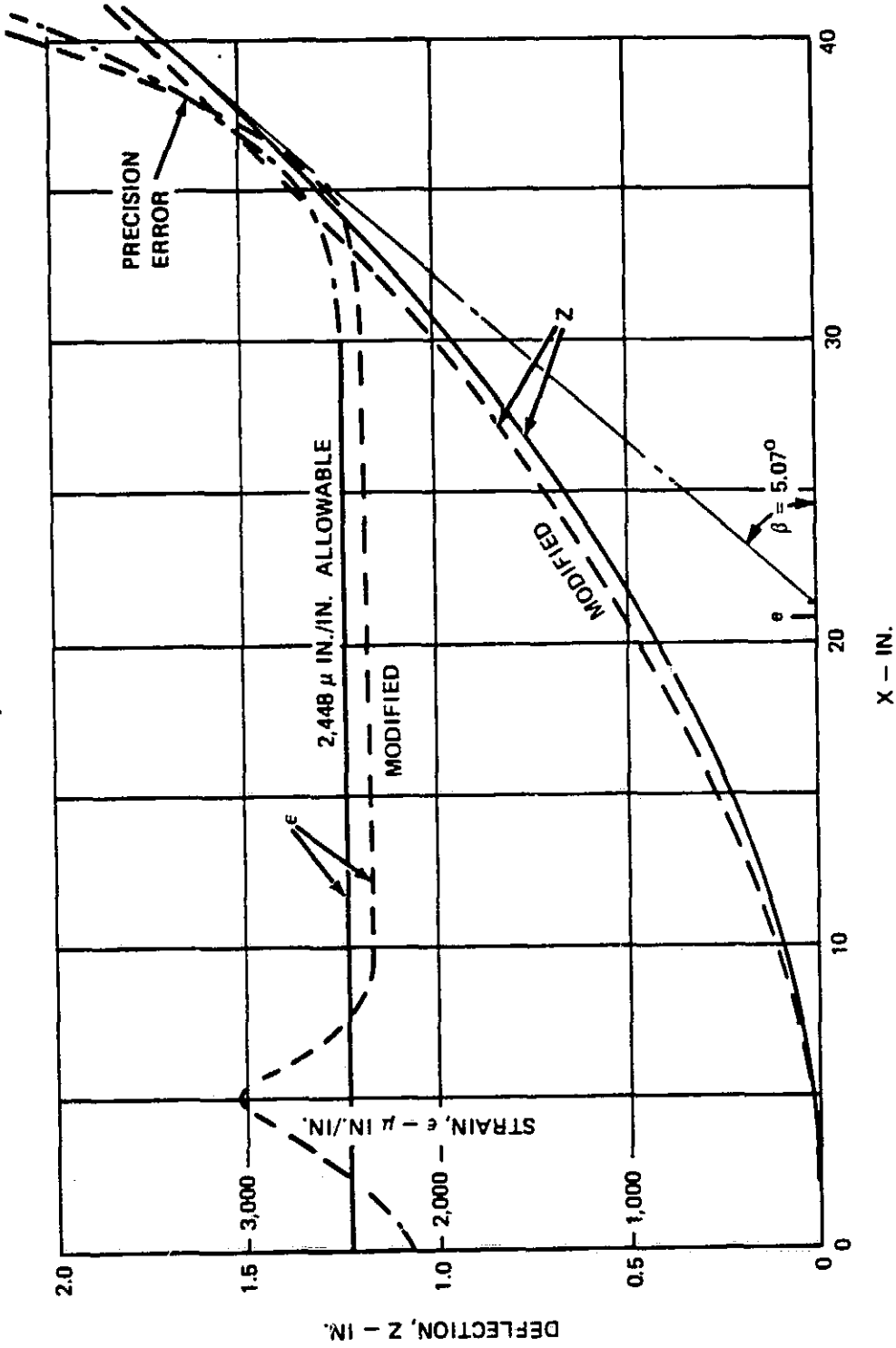


Figure 44. DIFF5 Solution for ITR Theoretical Flexure

Figure 44 shows, by means of the DIFF5 nonlinear tension beam analysis, that the strain level within the modified root exceeds the allowable by 35 percent and that the outboard slope did increase by 0.8 percent, which can be regarded as insignificant. The strain level can only be reduced to within allowable limits by resizing the local flexure modification, which results in the original configuration with constant curvature.

Thus, the constant-curvature assumption for maximum flexure efficiency is valid.

To Find the Relationship Between Flexure Length, Width, Allowable Flapping, and Hub Stiffness

The first approach defines the width distribution of the theoretically ideal flexure. The root width is given by

$$W = \frac{3}{8} \frac{CF}{Ee} \left(\frac{\beta}{\epsilon}\right)^3 .$$

If the length of this flexure  $l = 2e$ , then

$$W = \frac{3}{4} \frac{CF}{El} \left(\frac{\beta}{\epsilon}\right)^3 \quad \text{or, transposing,}$$

$$\beta = \left(\frac{4}{3} \frac{El \cdot W}{CF}\right)^{1/3} \times \epsilon ,$$

which suggests that  $\beta \propto (l)^{1/3}$  for an optimized flexure having a varying width distribution. Since the theoretical flexure cannot sustain CF or end moment due to zero width at the outboard end, and since a finite width only is acceptable, it follows that the cited relationship is not valid for a practical flexure.

The BEAMSOL solution for the optimized thickness distribution gives the thickness as presented in Figure 45. The solution is for a practical constant width of 6.0 inches and includes an endurance limit reduction factor

ORIGINAL PAGE IS  
OF POOR QUALITY

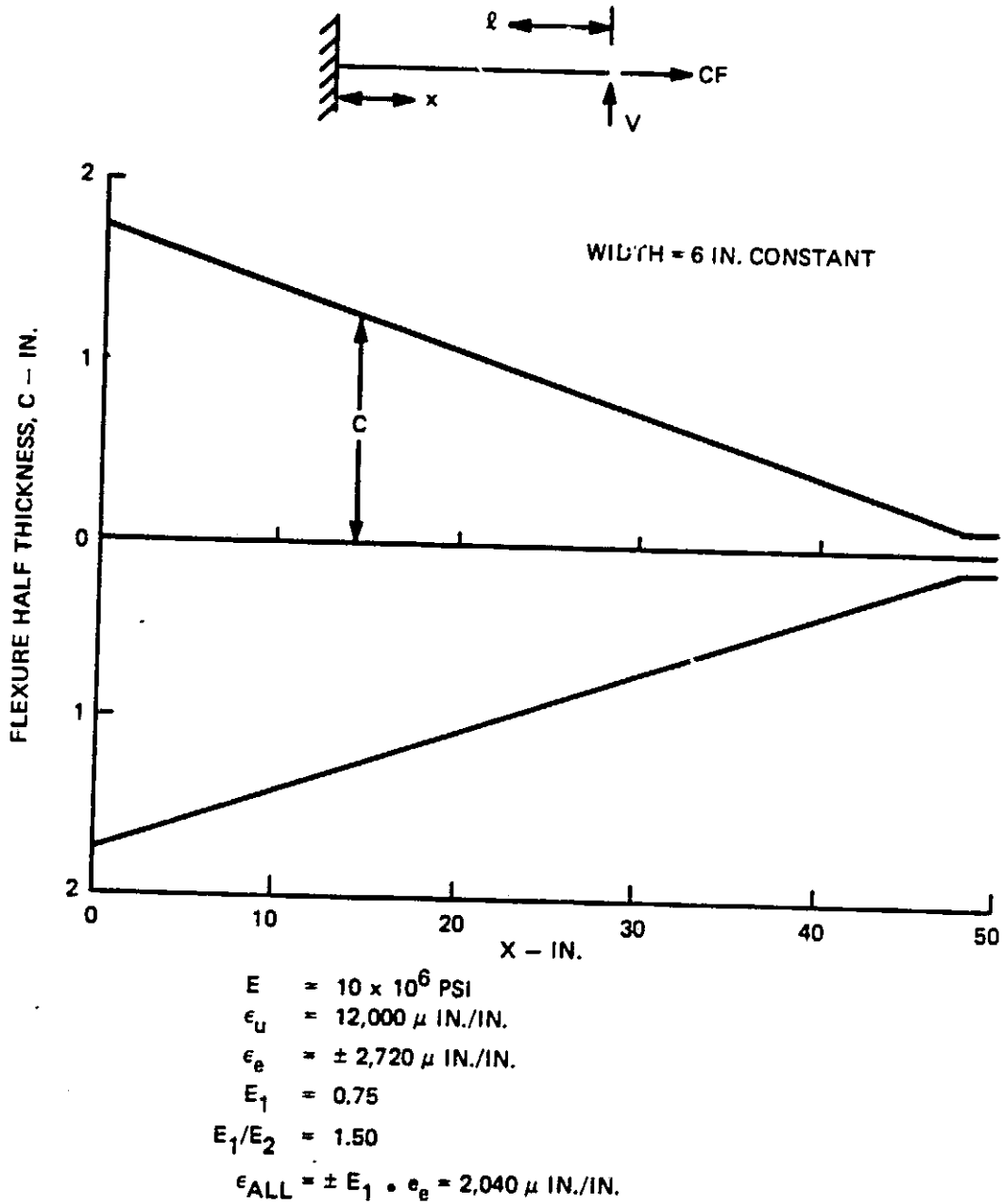


Figure 45. BEAMSOL Solution for Optimized Flexure in Kevlar

of 0.75 to accommodate likely strain levels from chord and torsional oscillations. Only CF and flap shear loadings have been applied.

For flexure lengths ( $\ell$ ) of 48 inches, 36 inches, and 12 inches, the DIFF5 nonlinear tension beam analysis has been applied for each BEAMSOL solution with the shear ( $V$ ) exerted to result in the allowable fatigue strain at the root.

Figure 46 presents the resultant beam deflections and indicates that the endurance limit flapping is not directly proportional to flexure length.

Flapping versus flexure length are plotted in Figure 47 and a fit to the resultant curve shows that for these particular constant-width beams, allowable flapping ( $\beta$ ) is not proportional to  $(\text{length})^{1/3}$  as for the theoretical flexure, but to  $(\text{length})^{2/3}$ .

Hub Stiffness - From the DIFF5 solution for the same cases, the presentation of  $2 \times$  flexure root moment versus flexure length,  $\ell$ , in Figure 47 again illustrates the futility of trying to achieve the ITR goal of 120,000 ft-lb/rad since a flexure length of less than 5 inches would be required, which would result in a maximum endurance limit flapping of  $\beta_{EL} \leq 1.2$  degrees which is far short of the goal of  $\pm 5$  degrees.

Width Versus Flapping - The preceding showed that for the theoretical flexure, the allowable flapping ( $\beta$ )  $\propto$  flexure root width ( $w$ )<sup>1/3</sup>. A question arises whether this relationship holds for a real flexure with, for example, constant width. Figure 48 presents the BEAMSOL solution for flexures of various constant widths and each having the same 24-inch length. From the resultant root semithickness ( $C_0$ ), the allowable root flap moment ( $M_0$ ) for each was calculated using

$$M_{0\text{allow}} = \frac{2}{3} E W C_0^2 \times \epsilon_{\text{allow}}$$

ORIGINAL PAGE IS  
OF POOR QUALITY

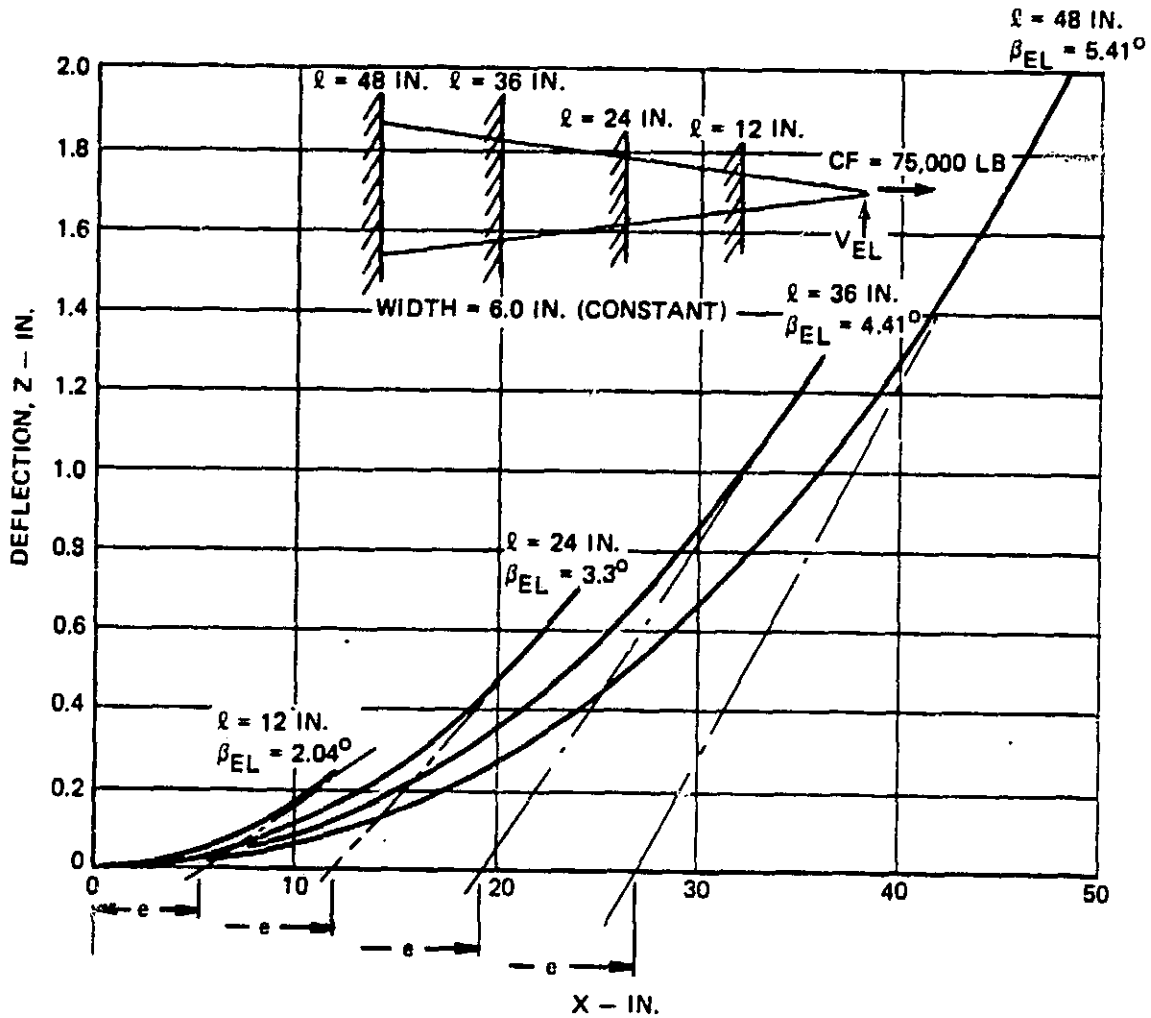


Figure 46. Endurance Limit Deflection of Optimized 6-Inch-Wide Cantilevered Flexures in Kevlar 49

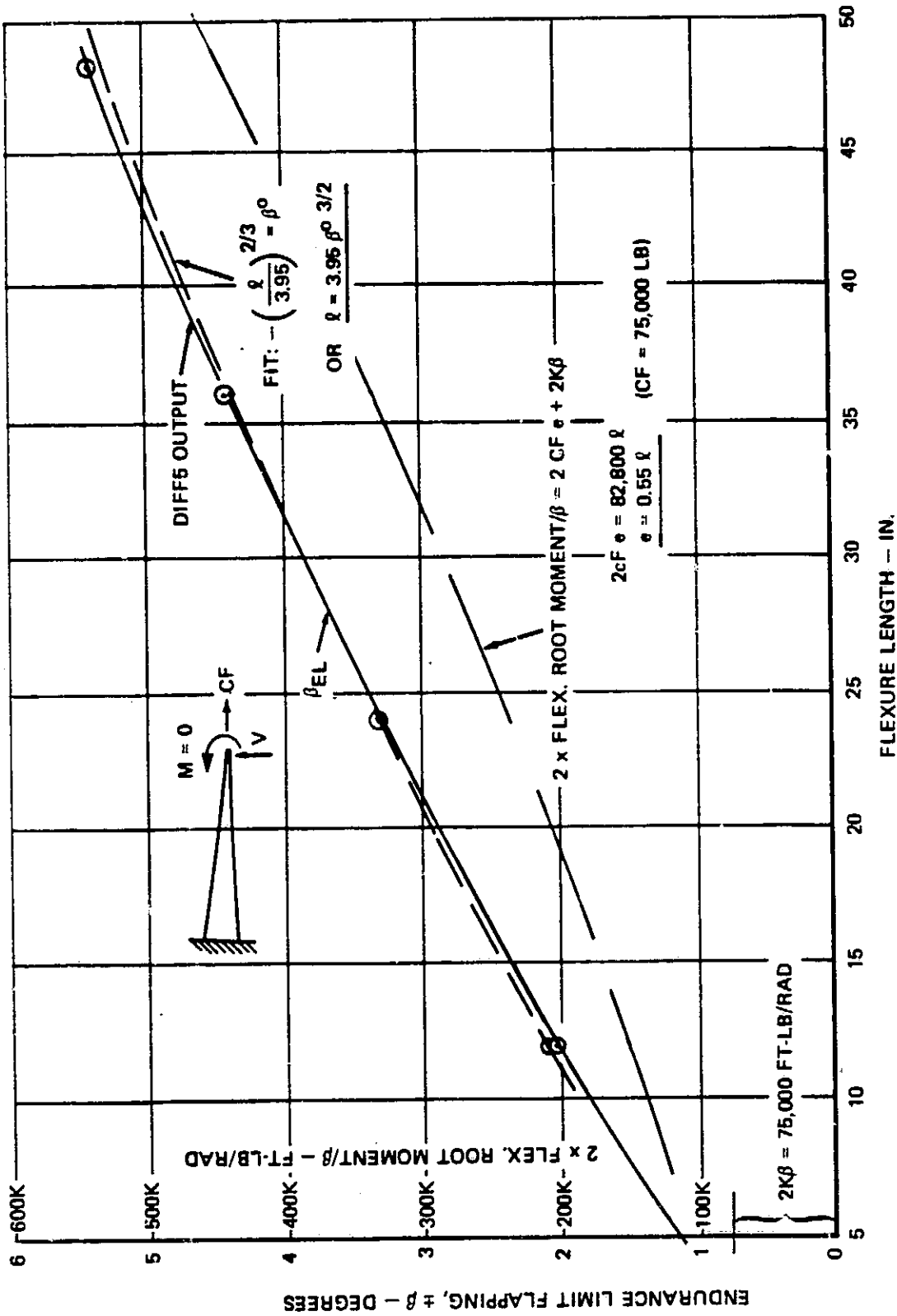


Figure 47. Study of Endurance Limit Flapping Versus Flexure Length  
With Constant 6-Inch Width

ORIGINAL PAGE IS  
OF POOR QUALITY.

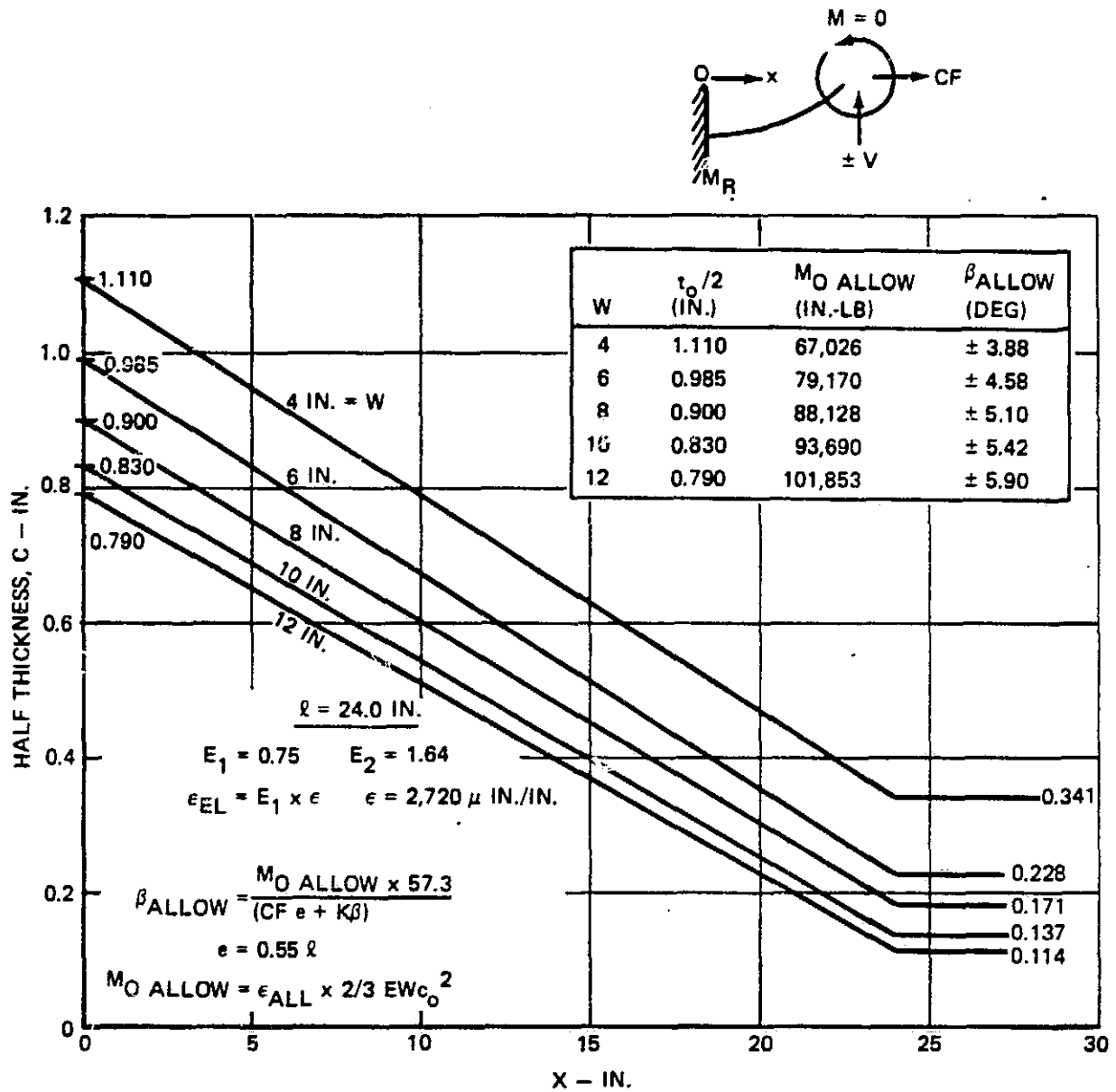


Figure 48. BEAMSOL Solution for Effect of Width on Thickness of Kevlar Flexure

The allowable flapping could then be calculated using

$$\beta_{\text{allow}} = \frac{M_{o\text{allow}}}{(CF \cdot e + K\beta)} \times 57.3 \text{ degrees.}$$

For this simplified methodology  $K\beta$  was ignored as being relatively insignificant and the CF stiffening constant ( $e$ ) was taken as  $0.55\ell$  (see Figure 47). Figure 49 presents a plot of allowable flapping versus flexure width and a curve fit shows that the relationship is, indeed,

$$\beta \propto (W)^{1/3} .$$

CF Stiffening ( $e$ ) - For the theoretical flexure, the coefficient  $e$ , which can be likened to a virtual flap hinge offset, has been fixed at  $e = \frac{1}{2} \times$  length. Using the hub stiffness equation,

$$\frac{M_H}{\beta} = 2 \cdot e \cdot CF + 2K\beta .$$

Figure 47 shows that for a practical flexure of finite width,

$$e \simeq 0.55\ell .$$

Flexure static stiffness constant  $K\beta$  for a 6-inch-wide Kevlar flexure is also shown to be 37,500 ft-lb/rad (min).

Conclusions - It is concluded that:

1. The goal of 120,000 ft-lb/radian for maximum hub stiffness is unobtainable.
2. Flexure length is proportional to required flapping to the 1.5 power, i.e.,  $\ell \propto \beta^{3/2}$ .

ORIGINAL PAGE IS  
OF POOR QUALITY.

$l = 24.0$  IN.

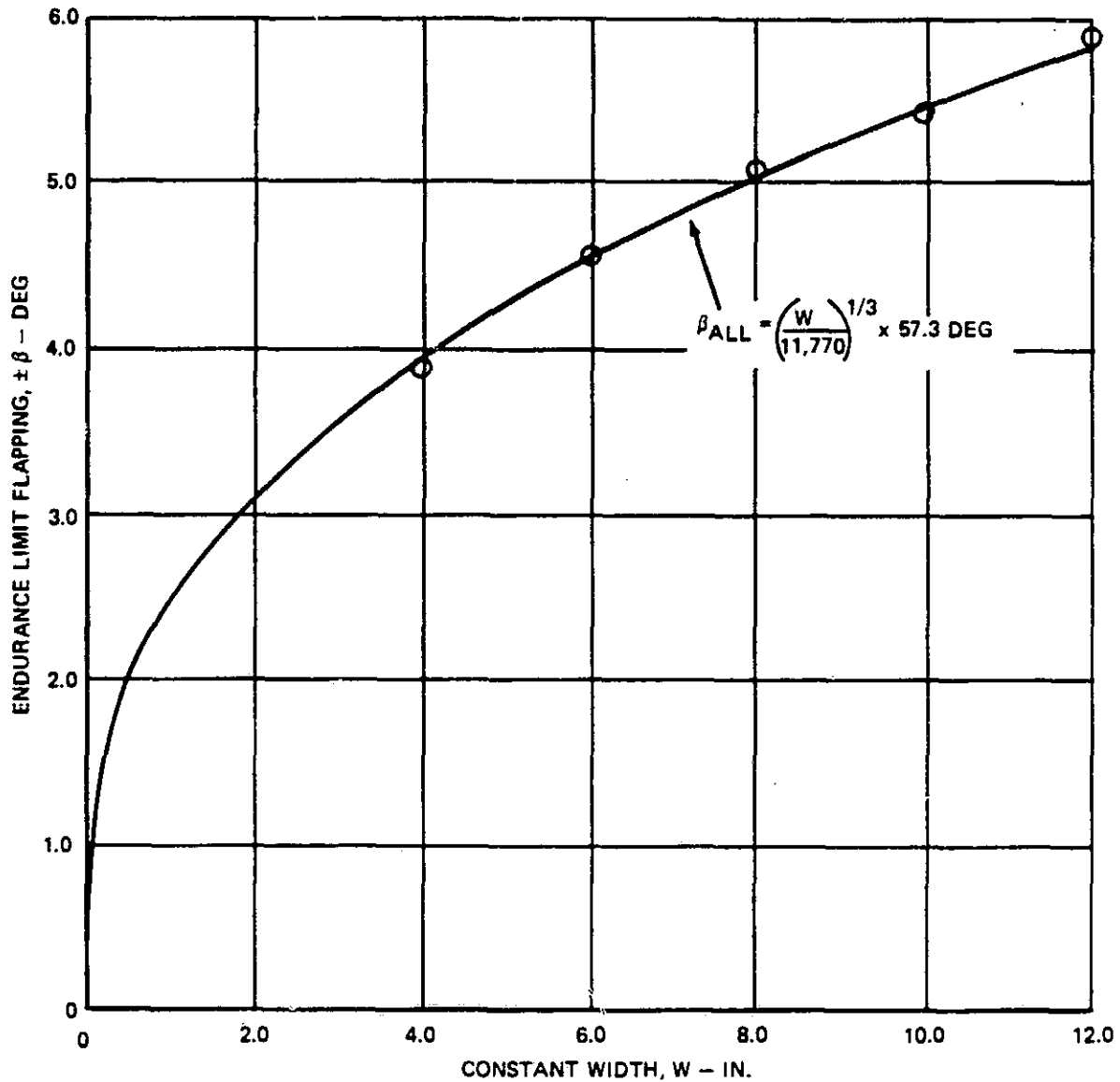


Figure 49. Required Width of Kevlar 49 Constant-Width Flexure Is Proportional to (Endurance Limit Flapping)<sup>3</sup>

3. Flexure width is proportional to required flapping to the 3rd power, i.e.,  $W \propto \beta^3$ .

#### Shoe-Restrained Flexure

Figure 50 illustrates a flapping flexure under CF and shear loading where the flexure radius of curvature and consequently the flexure strain are controlled by a contoured shoe. For a constant-thickness ( $t$ ) flexure, of

material having a fatigue endurance limit strain ( $\epsilon$ ), the shoe radius ( $R$ ) would need to be constant for constant strain by the relationship

$$\frac{Mc}{2EI} = \frac{c}{2} \frac{d^2y}{dx^2} ,$$

or

$$\epsilon = \frac{t}{2} \frac{1}{R} .$$

ORIGINAL PAGE IS  
OF POOR QUALITY

(16)

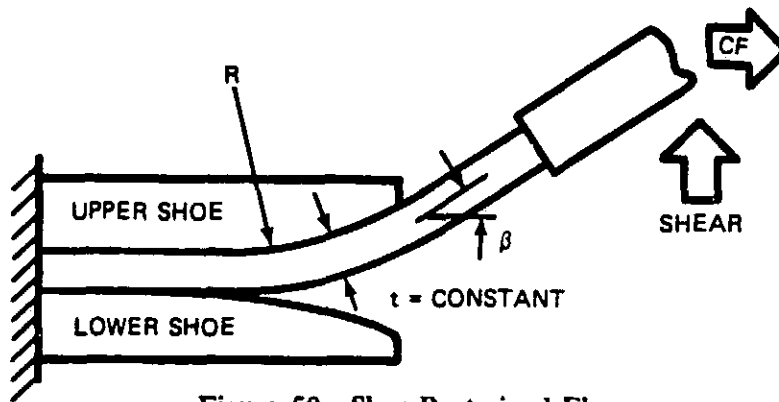


Figure 50. Shoe-Restrained Flexure

For an endurance limit flapping of  $\pm 5^\circ = \beta$ , the flexure length ( $l = 2e$ ) is

$$l = R\beta ,$$

or, by substitution for  $R$  from 16,

$$l = \frac{t}{2} \left( \frac{\beta}{\epsilon} \right) . \quad (17)$$

Since the flexure has to carry the  $CF$  and the allowable  $CF$  stress is

$$\sigma_{ult} \times \left( \frac{1}{1.25} \right)^2 \times \frac{1}{1.5} = 0.43\sigma_{ult} ,$$

then for a flexure width ( $w$ ), the thickness ( $t$ ) is given by

$$0.43 \sigma_{ult} = \frac{CF}{Wt} ,$$

or

$$t = \frac{CF}{0.43\sigma_{ult}W} . \quad (18)$$

The flexure and shoe length then become, as minima,

$$l_{min} = \frac{CF}{0.86\sigma_{ult}W} \left( \frac{\beta}{\epsilon} \right) .$$

Example: If, for Kevlar,  $\sigma_{ult} = 120,000$  psi, a practical width (constant) = 7.0 inches, and  $\epsilon = 2,720$   $\mu\text{in./in.}$ , then for a CF of 75,000 lb and  $\pm 5^\circ$  of flapping,

$$\begin{aligned} \ell &= 3.33 \text{ inches,} \\ t &= 0.208 \text{ inch,} \\ R &= 38.16 \text{ inches.} \end{aligned}$$

ORIGINAL PAGE IS  
OF POOR QUALITY

- Notes: a. This flexure would require droop stops.  
b. A Goodman reduction factor on ( $\epsilon$ ) has not been used.

Shoe and Flexure Sizing to Preclude Droop Stops - If the blade static moment ( $M_s$ ) is 33,000 in.-lb (representing a YUH-61A rotor blade) and the 45-knot-wind startup case is equivalent to 4.67 g's static moment, then, for stress considerations only, where limit allowable stress is

$$\sigma_L = \sigma_{ult} \times \left(\frac{1}{1.5}\right) ,$$

equation 18 can be replaced by

$$t = \sqrt{\frac{6 \times 4.67 \times 1.5 \times M_s}{W \sigma_{ult}}} \quad (19)$$

Substituting for t, as in equation 19, into equation 17,

$$\ell = \frac{1}{2} \sqrt{\frac{6 \times 4.67 \times 1.5 \times M_s}{W \cdot \sigma_{ult}}} \left(\frac{\beta}{\epsilon}\right) \quad (20)$$

Substituting in the values used previously,

$$\begin{aligned} \ell_{\min} &= 0.64 \left(\frac{\beta}{\epsilon}\right) \\ &= 20.5 \text{ inches.} \end{aligned}$$

Note again that no Goodman reduction factor has been applied to the material fatigue allowable ( $\epsilon$ ) and that the hub size (shoe length) is increasing as criteria are being applied. A 20.5-inch-radius hub is excessive and would result in high weight and drag penalties.

Modifications to the Flexure to Reduce Shoe Length - Without auxiliary droop stops, the hub size appears to be dictated by the limit static loading. The system described, however, can be improved by decreasing the flexure thickness from the shoe lip inboard since the full static moment is reacted only by that portion of the flexure outboard of and at the shoe lip.

Figure 51 shows a possible limit bending moment distribution within the flexure.

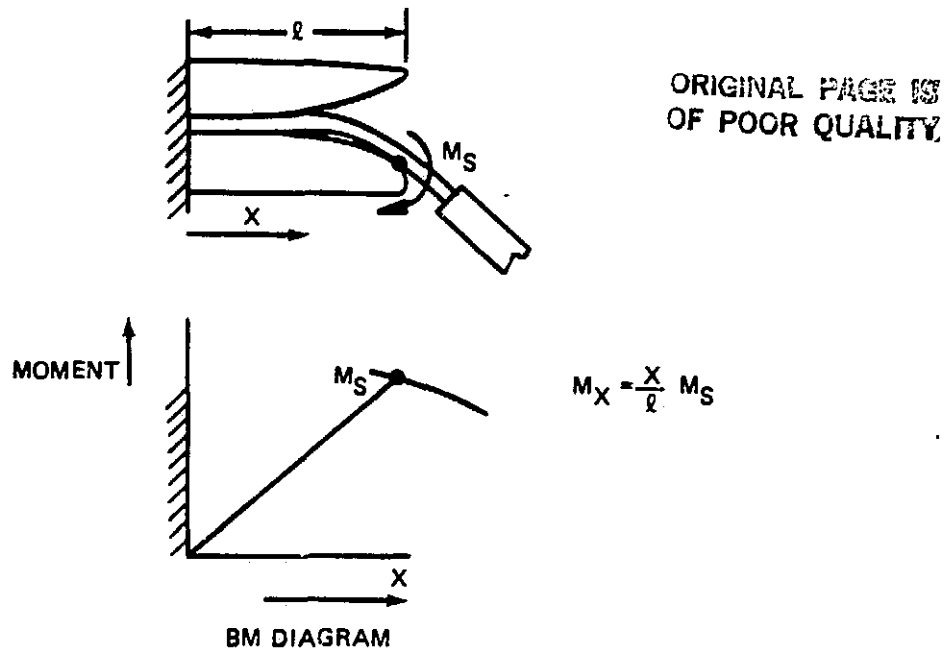


Figure 51. Limit Bending-Moment Distribution for Shoe-Restrained Flexure

The minimum thickness ( $t$ ) defined previously in equation 19 can now be re-defined as

$$t_x = \sqrt{\frac{6 \times 4.67 \times 1.5 \times M_x}{W \sigma_{ult}}} = \sqrt{\frac{6 \times 4.67 \times 1.5 \times x M_s}{W \sigma_{ult} l}} \quad (21)$$

which, if substituted in equation 16, gives

$$\frac{1}{R} = 2\epsilon \left( \frac{W \sigma_{ult} l}{6 \times 4.67 \times 1.5 \times M_s} \right)^{\frac{1}{2}} \left( \frac{1}{x} \right)^{\frac{1}{2}} = \frac{d^2 y}{dx^2}$$

By integration,

$$\left(\frac{dy}{dx}\right)_l = \beta_l = 4e \left(\frac{W\sigma_{ult} l}{6 \times 4.67 \times 1.5 M_s}\right)^{\frac{1}{2}} l^{\frac{1}{2}},$$

or

$$l = \frac{1}{4} \left(\frac{6 \times 4.67 \times 1.5 M_s}{W\sigma_{ult}}\right)^{\frac{1}{2}} \left(\frac{\beta}{\epsilon}\right), \quad (22)$$

which halves the flexure and shoe length given in 20 to 10.25 inches, which is more manageable.

Interlaminar Shear Strength Restriction on Flexure Cross-Sectional Area -

So far, we have shown that a shoe length reduction may be possible if the flexure inside the shoe is tapered according to equation 21. There is, however, another restriction that must be applied, that of material interlaminar shear stress allowable.

Interlaminar shear at the flexure midplane is given by

$$\tau_s = \frac{3}{2} \frac{1}{Wt} \frac{dM}{dx} = \frac{3}{2} \frac{1}{Wt} \frac{M}{l}.$$

By transposing, we find that the minimum flexure cross-sectional area is given by

$$A_{\min} = (Wt)_{\min} = \frac{3}{2} \frac{1}{\tau_{s_{all}}} \frac{M}{l}. \quad (23)$$

Example - For the limit case, moment (M) = 4.67 x 33,000 in.-lb.

For an ultimate shear allowable of 10,000 psi (which is typical for a laminate), then

$$A_{\min} = \frac{3 \times 1.5 \times 4.67 \times 33,000}{2 \times 10,000 \times l} = \frac{34.67 \text{ in.}^2}{l},$$

and if the width = 7 inches, shoe radius = 10.25 inches, then the minimum allowable flexure thickness

$$t_{\min} = \frac{34.67}{10.25 \times 7} = 0.48 \text{ inch.}$$

To carry the CF, equation 18 defines  $t_{\min}$  as

$$t_{\min} = \frac{CF}{0.43 \sigma_{ult} \cdot W}, \text{ which would result in}$$

$$t_{\min} = \frac{75,000}{0.43 \times 120,000 \times 7} = 0.208 \text{ inch.}$$

It appears, therefore, that the minimum thickness will be defined by the material interlaminar shear allowable.

Conclusions - It is concluded that:

1. Flexure root thickness ( $t_0$ ) is defined by the material interlaminar shear allowable and the rate of change of limit bending moment with radial distance,

$$t_{0 \min} = \frac{3}{2} \frac{1}{W} \frac{1}{\ell} M_{LT} \frac{1.5}{\tau_{su}} .$$

2. Flexure thickness ( $t_\ell$ ) under the shoe lip at  $X = \ell$  is defined by the material static tensile strength and the limit bending moment:

$$t_{\ell \min} = \left( 6 \frac{1}{W} M_{LT} \frac{1.5}{\sigma_{tu}} \right)^{\frac{1}{2}} .$$

3. The thickness distribution ( $t_x$ ) is defined by the flexure limit bending moment at the shoe lip ( $M_\ell$ ), shoe radius ( $\ell$ ), material allowable ( $\sigma_{tu}$ ), and flexure width distribution ( $W_x$ ):

$$t_x = \left( \frac{6}{w} \frac{1.5}{\sigma_{tu}} M_l \right)^{1/2} \left( \frac{x}{l} \right)^{1/2} .$$

ORIGINAL PAGE IS  
OF POOR QUALITY

4. The minimum radius of curvature  $(R)_x$  is limited by the material tensile fatigue strain allowable  $(\epsilon)$  and the local flexure thickness  $(t)_x$ :

$$\frac{1}{R} = \frac{d^2y}{dx^2} = \frac{2\epsilon}{t} .$$

5. The allowable flapping  $(\beta)$  is defined by the thickness distribution  $(t)_x$  and the allowable fatigue strain  $(\epsilon)$ :

$$\beta = \left( \frac{dy}{dx} \right)_l = \int_0^l \frac{d^2y}{dx^2} dx = 2\epsilon \int_0^l \frac{1}{t} dx .$$

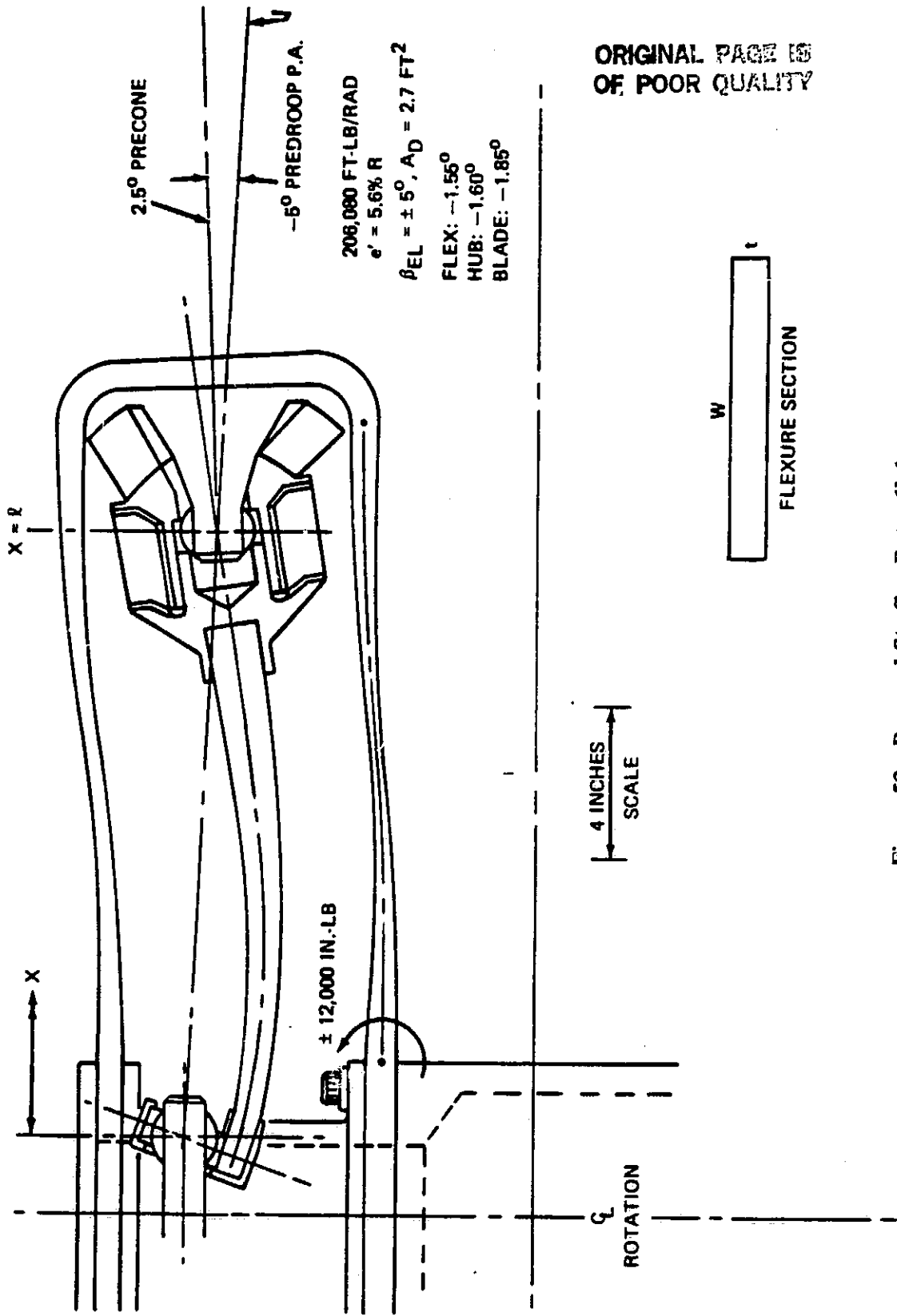
6. For a flexure of constant width, the minimum shoe length  $(l)$  is inversely proportional to the allowable fatigue strain, proportional to required endurance limit flapping, and inversely proportional to the width  $= w^{1/2}$ :

$$l = \frac{3}{4} \left( \frac{M_\beta}{w\sigma_{tu}} \right)^{1/2} \left( \frac{\beta}{\epsilon} \right) \text{ for constant width } (w) .$$

#### Reversed Starflex (Figure 52)

Flexure - The sizing and resultant allowable endurance limit bending of the droop stop flexure are controlled by the limit static bending strength requirement at 4.67 g's.

Thickness Distribution - If the distance between the elastomeric bearing and the reaction pivot is  $l$ , then the reaction at each is



ORIGINAL PAGE IS  
OF POOR QUALITY

Figure 52. Reversed Starflex Rotor Hub

CRITICAL REVIEW  
OF POOR QUALITY

$$V = \frac{M}{\ell} ,$$

where M is the limit flap bending moment (4.67 g's X 33,000 in.-lb). The moment in the flexure at a distance X from the inboard reaction is

$$M_{(x)} = Vx = M \frac{x}{\ell} .$$

The stress in the extreme fibers due to flapping is

$$\sigma_{(x)} = \frac{6M}{W} \left( \frac{1}{t_{(x)}} \right)^2 , \text{ which defines the thickness (t) as}$$

$$t_{(x)} = \left( \frac{6M}{W\sigma} \right)^{\frac{1}{2}}_{LT} \left( \frac{x}{\ell} \right)^{\frac{1}{2}} .$$

Width Distribution - A convenient width must now be chosen. It has been shown that allowable flapping increases as width increases; therefore, the maximum practical flexure width should be chosen. This configuration includes a universal elastomeric bearing which must be capable of withstanding similar loads and motions as that of the UH-60 Blackhawk. Diameter of the bearing is approximately 8 inches. The flexure must separate to pass on either side of a CF bearing ahead of the outboard attachment to the rotor blade.

If a total width of a constant 6 inches is chosen, then the flexure arrangement will not appear to be excessively wide.

The thickness then becomes

$$t_x = \left( \frac{M}{\sigma_{LT}} \right)^{\frac{1}{2}} \left( \frac{x}{\ell} \right)^{\frac{1}{2}} ,$$

if  $\sigma_{LT} = 60,000$  psi and  $M_{LT} = 4.67 \times 33,000$  in.-lb.

Endurance Limit Flapping - The endurance limit strain  $\epsilon_{EL}$  may be factored by  $E_1 = 0.75$  to accommodate chord strains to result in the allowable dynamic strain ( $\epsilon$ ) due to flap bending. If, for Kevlar 49,  $\epsilon_{EL} = 2,720$   $\mu\text{in./in.}$ , then

$$\epsilon = 0.75 \times 2,720 = 2,040 \text{ } \mu\text{in./in.}$$

Since

$$\epsilon = \frac{t}{2} \frac{d^2Z}{dx^2} ,$$

ORIGINAL PAGE IS  
OF POOR QUALITY

then

$$\frac{d^2Z}{dx^2} = \frac{4,080 \times 10^{-6}}{1.6} \left(\frac{\ell}{x}\right)^{\frac{1}{2}} .$$

By integration,

$$\frac{dZ}{dx} = 5,100 \times 10^{-6} (\ell x)^{\frac{1}{2}} + C$$

and

$$Z = 3,400 \times 10^{-6} (\ell x^3)^{\frac{1}{2}} + C X + D .$$

When

$$X = 0 \text{ and } Z = 0, \text{ then } D = 0 .$$

When

$$X = \ell \text{ and } Z = 0, C = -3,400 \times 10^{-6} \ell ,$$

then

$$\frac{dZ}{dx} = 5,100 \times 10^{-6} (\ell x)^{\frac{1}{2}} - 3,400 \times 10^{-6} \ell$$

when

$$x = \ell \frac{dZ}{dx} = \beta_{EL} = (5,100 - 3,400) \times 10^{-6} \times \ell .$$

Therefore, if  $\ell = 16$  inches,

$$\beta_{EL} = \pm 1,700 \times 10^{-6} \times 16 \text{ radians,}$$

$$\beta_{EL} = \pm 1.55 \text{ degrees.}$$

The corresponding  $\beta_{LT} = \frac{6,000}{2,040} \times 1.55 = 4.56^\circ$  (since  $\epsilon_{LT} = 6,000 \text{ } \mu\text{in./in.}$ )  
and at the outboard bearing the endurance limit bending moment

ORIGINAL DRAWING  
OF POOR QUALITY

$$M_L = \frac{2,040}{6,000} \times 154,000 = \pm 52,360 \text{ in.-lb.}$$

Hub Deflection - The flexure capability shown falls far short of the technical goal of  $\beta_{EL} = \pm 5$  degrees; therefore the supporting hub plate system must complement the flexure deflection. For hub plates of a reasonable 6-inch constant width and 17 inches of flexible length, each carrying  $\frac{1}{2} \times 75,000 \text{ lb} = 37,500 \text{ lb}$  of CF, the BEAMSOL solution to the optimum thickness distribution for half the plate flexure length of  $8\frac{1}{2}$  inches follows.

FINAL C-DISTRIBUTION

DISTANCE x(in.)	HALF-THICKNS. c(in.)
0.0	0.1139
0.5000	0.1259
1.0000	0.1372
1.5000	0.1486
2.0000	0.1606
2.5000	0.1731
3.0000	0.1863
3.5000	0.1999
4.0000	0.2139
4.5000	0.2283
5.0000	0.2430
5.5000	0.2579
6.0000	0.2729
6.5000	0.2880
7.0000	0.3032
7.5000	0.3184
8.0000	0.3337
8.5000	0.3489

DIFF 5 INPUT

	l-x(in.)	EI <sub>F</sub> (psi)
00030	0.00	1.715E06
00040	1.00	1.291E06
00050	2.0	9.555E05
00060	3.00	6.861E05
00070	4.00	4.760E05
00080	5.00	3.152E05
00090	6.00	2.074E05
00100	7.00	1.313E05
00110	7.50	1.033E05
00120	8.00	7.980E04
00130	8.50	5.910E04
00140	8.5	l
00150	0.1	M <sub>0</sub>
00160	3000.0	V <sub>0</sub>
00170	37500.0	CF
00180	0.1	1.4 0.01
00190	REV	STARFLEX

The DIFF5 tension beam solution for the 8½-inch hub flexure is given as follows:

I	U	V	ZP	ZDP	W	X	Y
1	0.00000E 00	0.00000E 00	0.00000E 00	0.80800E-02	0.12857E 05	0.30000E 04	
2	0.10000E 01	0.40962E-02	0.82660E-02	0.85289E-02	0.11011E 05	0.26900E 04	
3	0.20000E 01	0.16665E-01	0.16928E-01	0.88772E-02	0.84822E 04	0.23652E 04	
4	0.30000E 01	0.32054E-01	0.25896E-01	0.91594E-02	0.62843E 04	0.20289E 04	
5	0.40000E 01	0.68525E-01	0.35068E-01	0.93003E-02	0.44269E 04	0.16850E 04	
6	0.50000E 01	0.10820E 00	0.44272E-01	0.92474E-02	0.29148E 04	0.13398E 04	
7	0.60000E 01	0.15691E 00	0.53049E-01	0.84004E-02	0.17423E 04	0.10106E 04	
8	0.70000E 01	0.21389E 00	0.60583E-01	0.66885E-02	0.87820E 03	0.72813E 03	
9	0.75000E 01	0.24496E 00	0.63579E-01	0.58598E-02	0.54334E 03	0.61580E 03	
10	0.80000E 01	0.27733E 00	0.65724E-01	0.32224E-02	0.25715E 03	0.53513E 03	
11	0.85000E 01	0.31048E 00	0.66601E-01	0.32510E-02	0.19213E 03	0.50244E 03	

The root bending moment strain for the example shown is  $(\frac{d^2Z}{dx^2} \times \frac{t}{Z})_{x=0} = 0.00808 \times 0.35 \text{ in.} = 2,828 \text{ } \mu\text{in./in.}$ , which exceeds the 2,040  $\mu\text{in./in.}$  allowable; however, this corresponds to a deflection of  $Z = 0.31 \text{ inch.}$

Reducing this to the allowable strain, we have

$$Z = 0.31 \times \frac{2,040}{2,828} = 0.224 \text{ inch.}$$

Since each hub plate is composed of two of these flexures asymmetrically opposed, we have a total deflection of  $2 \times 0.224 \text{ inch} = 0.448 \text{ inch.}$

Since the center flexure is supported by the bearings spaced 16 inches apart, then the contribution of the hub plates to total system allowable flapping is

$$\frac{0.448}{16} \times 57.3 = 1.60 \text{ degrees.}$$

The total hub system endurance limit flapping is therefore  $1.55 + 1.60 = 3.15 \text{ degrees}$ , which still falls short of the goal. The flexure/blade attachment, however, can carry an endurance limit moment of 52,360 in.-lb; therefore, the blade root can possibly be used to complement the hub and provide an additional 1.85 degrees.

Blade Root Flexure - The hub flexure results in a limit bending moment slope of 4.56 degrees, which gives a total of 21.96 inches of tip deflection. However, the blade airfoil can be allowed to increase this by 4.67 g's x 7.29 = 34.04 inches, making a total of 56 inches. Of a total tip clearance of 90 inches, 34 inches remains to accommodate a blade root flexure for which the restricting conditions will be

$$M_{\text{Root}} \leq \pm 52,360 \text{ in.-lb, and the total flexure slope under limit bending moment} \leq \frac{34 \text{ in.}}{(294-20)} \times 57.3 = 7.1^\circ.$$

Since  $(\frac{dZ}{dx}) = \frac{Mx}{EI} \leq \frac{7.1}{57.3}$ , and EI minimum is given by the maximum thickness of the hub flexure (1.60 inches), then for a 6.0-inch width in Kevlar,

$$EI = \frac{10 \times 6.0 \times 1.60^3}{12} \times 10^6 = 20.5 \times 10^6 \text{ psi.}$$

For a similar blade root flexure stiffness under 154,000 in.-lb of limit bending moment, the maximum flexure length is given by

$$l \leq \frac{EI}{M} \times \frac{7.1}{57.3} = \frac{20.5 \times 10^6}{154,000} \times \frac{7.1}{57.3} = 16.5 \text{ inches.}$$

Blade Flexure Slope - From the DIFF5 tension beam analysis of the blade root flexure of 16.5 inches in length of constant EI = 20.5 x 10<sup>6</sup> psi and root bending moment of ±52,360 in.-lb, we can determine the slope of the blade airfoil as shown by Figure 53 to be 0.86 degree. A total of 4.01 degrees of hub flapping is obtained without incurring fatigue damage.

Torsion Flexure Geometry - The equation defining the torque to twist ( $M_\theta$ ) an axially loaded flexure of rectangular cross section is given in Figure 54, together with typical contributions from bending and warping constraints, shear rigidity, and centrifugal stiffening. The example shown is for a varying width and thickness distribution, with minimum thickness occurring at approximately 30 inches outboard of the flexure root. Thickness distribution was optimized with the BEAMSOL technique; however, length and width were chosen by engineering judgment only.

ORIGINAL PAGE IS  
OF POOR QUALITY

TOTAL SYSTEM ENDURANCE LIMIT FLAPPING	
HUB FLEXURE	1.60
DROOP SPRING	1.55
BLADE ROOT	<u>0.86</u>
	4.01 DEGREES

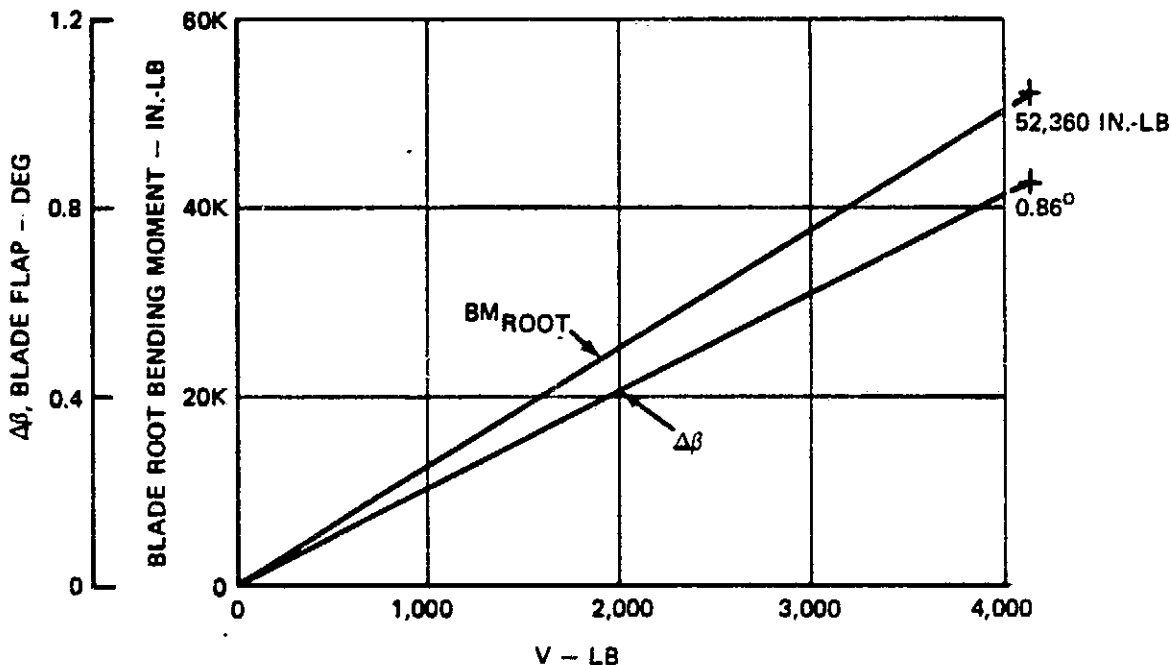


Figure 53. Additional Flapping From Blade Root of Reversed Starflex Hub

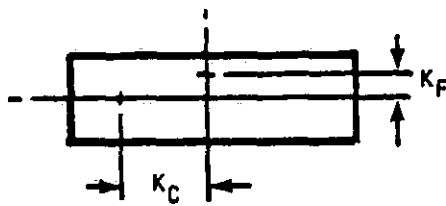
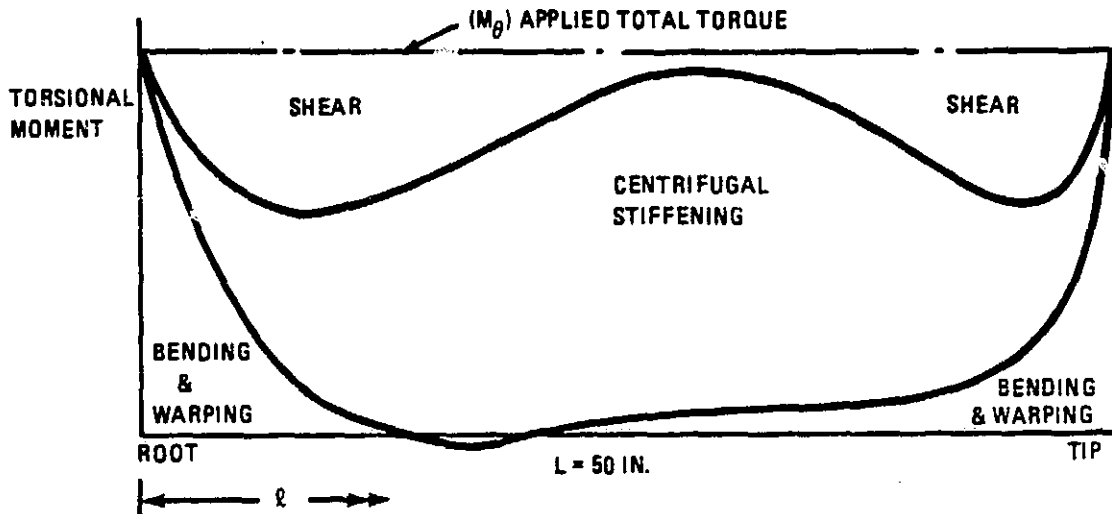
It is useful to study the effect of choice of flexure length and width upon torsional stiffness and Figure 55 was devised for constant-thickness, constant-width flexures as a demonstration.

The conclusions that can be drawn for the ITR are:

1. The classical shear stiffness ( $GK \frac{d\theta}{dx}$ ) accounts for less than 20 percent of the torsional stiffness.
2. The torsion flexure can be no shorter than 30 inches for a 3-inch width.
3. A 1-inch increase in width requires an increase in length of 10 inches.

4. A 30-inch increase in length is required for each inch of increase in thickness.
5. Increasing length over 50 inches produces a diminishing return for reduction of torsional stiffness.

$$M_{\theta} = GK \frac{d\theta}{dx} + CF k^2 \cdot \frac{d\theta}{dx} - EC_W \cdot \frac{d^3\theta}{dx^3}$$



FLEXURE CROSS SECTION

$$k_F^2 = \frac{EI_F}{EA}, k_C^2 = \frac{EI_C}{EA}$$

$$k^2 = \frac{EI_F + EI_C}{EA}$$

$$EC^*W = \frac{EI_F k_C^2 + EI_C k_F^2}{2}$$

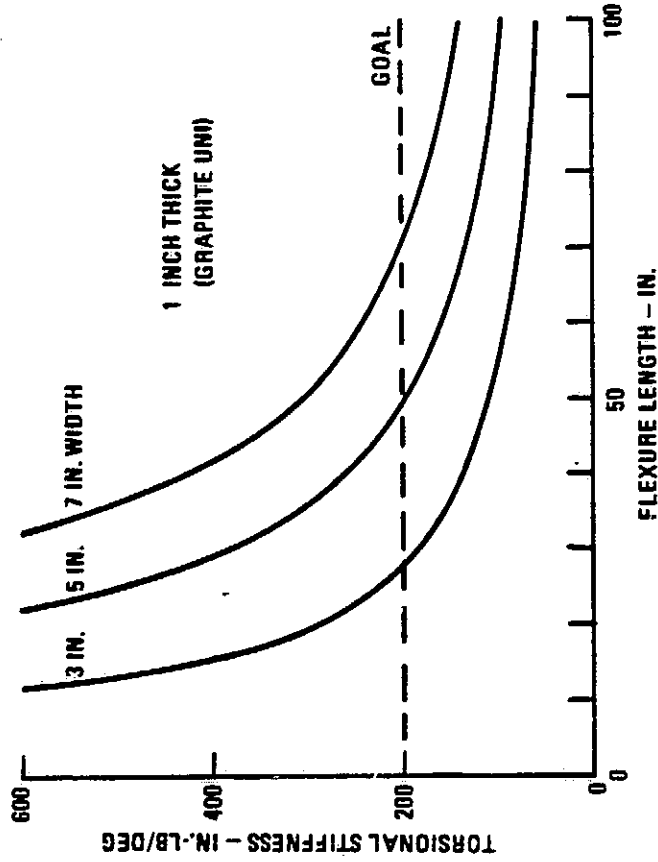
\*FOR A RECTANGLE

Figure 54. Typical Contributions from Bending and Warping Constraints, Shear Rigidity, and Centrifugal Stiffening to the Torsional Stiffness of a Flexure

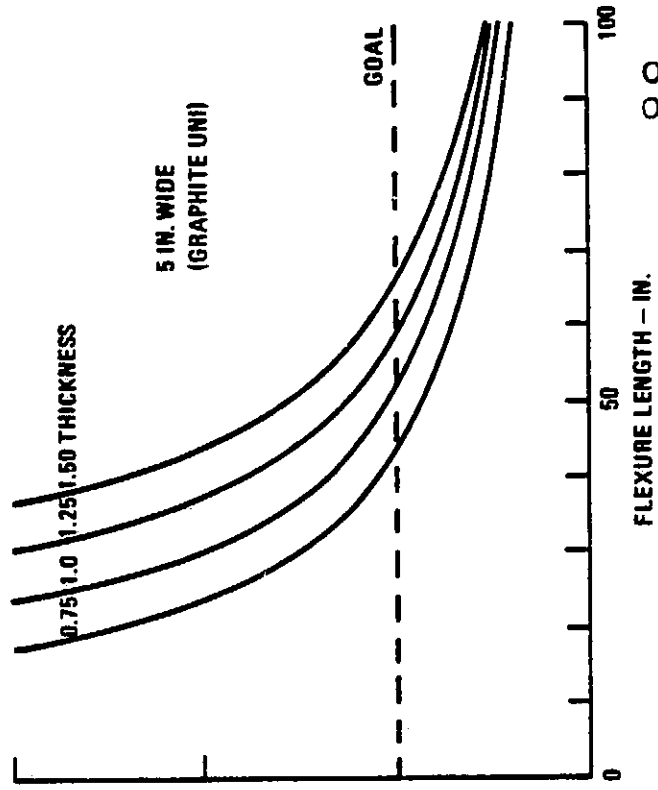
### Dynamic Analyses

Studies were conducted to determine the dynamic characteristics of the concepts. The most important considerations were:

(A) EFFECT OF WIDTH AND LENGTH ON TORSIONAL STIFFNESS



(B) EFFECT OF THICKNESS AND LENGTH ON TORSIONAL STIFFNESS



ORIGINAL PAGE IS OF POOR QUALITY

Figure 55. Effect of Flexure Geometry on Torsional Stiffness



moment, and the moment produced by the horizontal tail force ( $Z_T$ ) acting a distance (a) aft of the vehicle cg.

Aerodynamic forces and moments were assumed to be dependent upon velocity ( $V^2$ ), angle of attack, and coefficients characteristic of the YUH-61A aircraft.

From an existing trim analysis for the YUH-61A, characteristic coefficients for drag ( $K_x$ ), fuselage pitching moment ( $K_m$ ), and tail thrust ( $K_T$ ) were determined for a vehicle drag of 24 square feet.

A minimum-drag fuselage attitude of  $\alpha_F = 0$  was then assumed, and the fixed forward shaft tilt required for zero flapping was determined for trim of the YUH-61A with  $F_e = 24$  and 15 square feet. For 156 knots true airspeed, the prototype YUH-61A was shown to require 4 degrees of forward shaft tilt, but the hypothetical ITR vehicle at 180 knots true airspeed needs only 3.36 degrees of forward shaft tilt for zero longitudinal flapping.

With these values, the effect of forward speed upon flapping ( $\beta_L$ ) was then calculated which demonstrates that the ITR with  $F_e = 15$  square feet will flap as much as 1 degree less than the YUH-61A throughout the velocity envelope; furthermore, the hypothetical ITR will require a lower tail setting range.

These conclusions were obtained as follows:

Static Stability - In. H.S.L.F.

Tractive Force,  $X = -\text{Thrust} \times \alpha_{Tpp}$ .

But

$$\alpha_{Tpp} = \alpha_F + \alpha_S + \beta_L$$

and

$$X \propto V^2 \times \text{equivalent total drag area, } F_e$$

or

$$X = K_x V^2 F_e .$$

Then

$$-\beta_L = \alpha_F + \alpha_S + \frac{K_X V^2 F_e}{T} \quad (24)$$

ORIGINAL PAGE IS  
OF POOR QUALITY

For Pitching Moment Equilibrium,  $\Sigma M_{CG} = 0$

$$\begin{aligned} 0 &= M_{CG} = M_{TILT} + M_{FUS} + M_{TAIL} + M_{HUB} \\ 0 &= -Th\beta_L + K_m V^2 \alpha_F + K_T a V^2 (\alpha_T + \alpha_F) - K_H \beta_L \end{aligned} \quad (25)$$

To determine the force and moment coefficients from trim data for the YUH-61A helicopter at  $V = 170$  knots and  $T = 16,000$  pounds.

$$\begin{aligned} \alpha_S &= -4.0^\circ & M_F &= 20,544 \text{ ft-lb} \\ \alpha_{TTP} &= -4.8^\circ & Z_T &= -596 \text{ lb} \\ \alpha_F &= -4.0^\circ & \theta_T &= 2.5^\circ \\ \beta_L &= 3.3^\circ & h &= 69.0 \text{ in.} = 5.75 \text{ ft} \quad a = 27 \text{ ft} \\ K_H &= 500,000 \text{ ft-lb/rad} & F_e &= 24 \text{ ft}^2 \end{aligned}$$

then

$$\begin{aligned} K_X &= 0.00193 \text{ lb/ft}^2/\text{kn}^2 \\ K_m &= 10,183 \text{ ft-lb/rad/kn}^2 \\ K_T &= -596/\theta_T - \alpha_F = 0.788 \text{ lb/rad/kn}^2 \end{aligned}$$

For Minimum Drag,  $\alpha_F = 0$

Then from equation 25,

if

$$\beta_L = - \frac{K_m V^2 \alpha_F + K_T V^2 a (\alpha_T + \alpha_F)}{Th + K_H} \quad (26)$$

$$\beta_L = - \frac{K_T V^2 \alpha_T}{Th + K_H}$$

and from equation 24,

$$\beta_L = - \left( \alpha_S + \frac{K_X V^2 F_e}{T} \right)$$

Substituting values for the YUH-61A in equation 24,  $\alpha_F = 0$  when  $\beta_L = 0$ ,  $\alpha_S = -29 \times 10^{-7} V^2$  radians.

Figure 57 shows the relation between preset forward tilt angle and the speed at which longitudinal cyclic flapping is reduced to zero if the fuselage attitude ( $\alpha_F$ ) is zero.

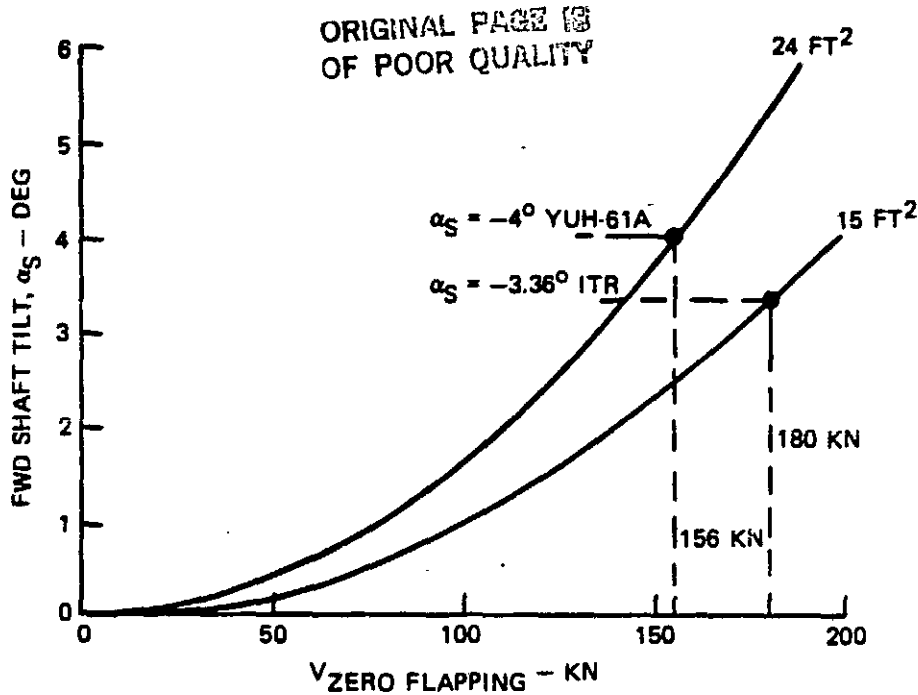


Figure 57. Shaft Tilt Versus Velocity for Zero Longitudinal Flapping ( $\alpha_F = 0$ )

From equation 24, if  $\alpha_S = -4^\circ$ ,  $F_e = 24 \text{ ft}^2$ ; i.e., YUH-61A vehicle  $\beta_L = (-4 + 0.0001659V^2)$  and/or if  $\alpha_S = 3.36^\circ$ ,  $F_e = 15 \text{ ft}^2$ ; i.e., ITR system  $\beta_L = (-3.36 + 0.0001037V^2)$ , then the decrease in longitudinal flapping with forward level flight speed is shown in Figure 58.

But from equations 24 and 26, if  $\alpha_F = 0$ , then

$$\alpha_F = 0 = - \left[ \frac{K_T V^2 a \alpha_T + \left( \alpha_S + \frac{K_X V^2 F_e}{T} \right) (Th + K_h)}{K_m V^2 + K_T V^2 a + Th + K_H} \right]$$

or

$$\alpha_T = - \left( \alpha_S + \frac{K_X V^2 F_e}{T} \right) \frac{(T_h + K_H)}{K_T V^2 a}$$

equals

$$\alpha_T = \beta_L \frac{(T_h + K_H)}{K_T V^2 a}$$

ORIGINAL PAGE IS  
OF POOR QUALITY

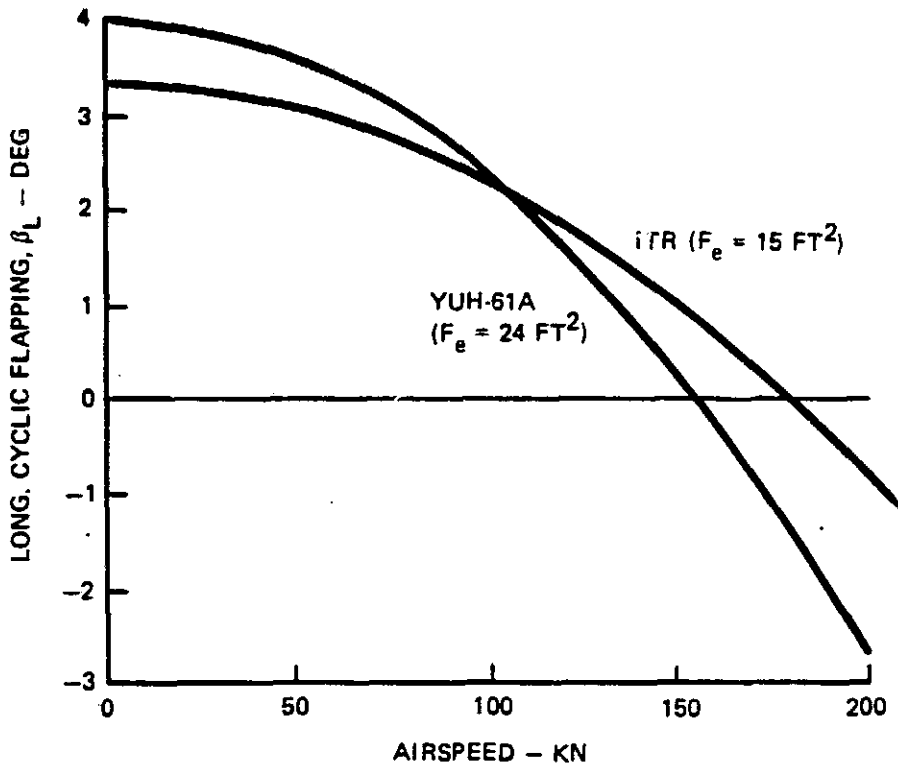


Figure 58. Longitudinal Cyclic Flapping Versus True Airspeed

Figure 59 shows the tail setting schedule required for the YUH-61A as a test vehicle and for the hypothetical aircraft with the same characteristics as the YUH-61A but with drag reduced to  $F_e = 15 \text{ ft}^2$ .

Aeroelastic Stability - The vertically offset torque sleeve inboard shear pivot/snubber of configurations 1 and 2 shown in Figures 24 and 26 is believed to be one of the two major keys to best meeting the technical goals, the other being the use of high-modulus material in the flexure.

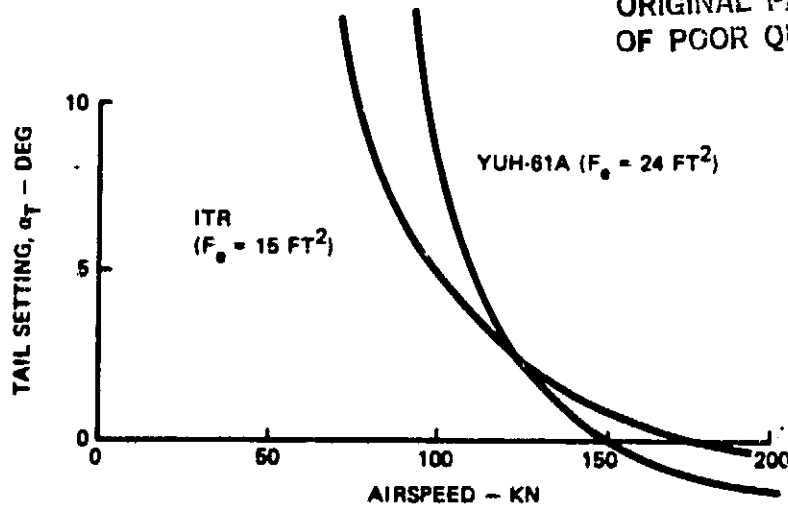


Figure 59. Tail Setting for Fuselage Trim ( $\alpha_F = 0$ )

The offset pivot method of introducing stabilizing pitch-lag coupling is expected to replace the requirement for negative pre-droop and flexure pre-twist which resulted in high weight, drag, and torque-to-twist penalties in the BMR. The effectiveness in hover was studied with the Boeing Vertol C-45 aeroelastic stability analysis. Reference 3 suggests that damping (stability) is not independent of thrust; however, at low and negative thrust conditions the twisted flexure is expected to produce stabilizing lag-flap coupling.

A structural and frequency analysis of the rotor system was made and the characteristics were transformed to suit the rotor mathematical model shown in Figure 60. This model shows a rigid blade set at a prescribed pre-droop and presweep angle and supported by two sets in series of coincident flap and lag hinges with variable spring stiffness. The feathering hinge was located between these hinge systems.

Kinematic coupling could be added through hinge geometric constants.

The configurations were modeled in the form of a rigid blade, flapping and lagging about the inboard hinge set which had finite spring stiffness about each axis. The outboard set of hinges was locked out.

3. Ormiston, R., TECHNIQUES FOR IMPROVING THE STABILITY OF SOFT INPLANE HINGELESS ROTORS, NASA TMX62-390, National Aeronautics and Space Administration, Washington, DC, 1962.

ORIGINAL PAGE  
OF POOR QUALITY

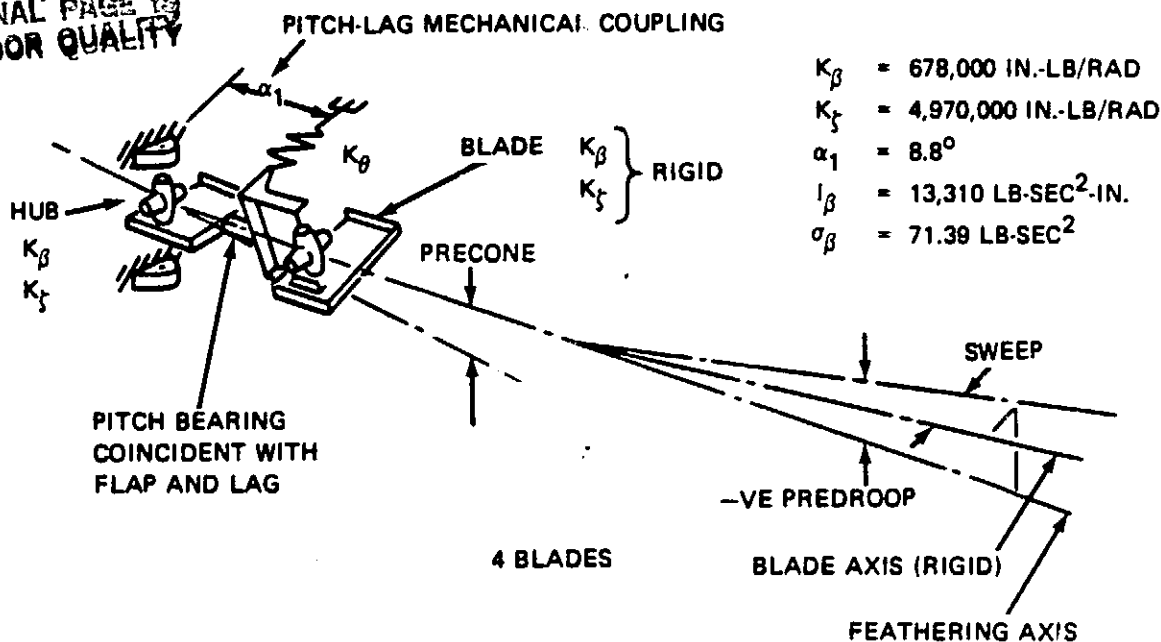


Figure 60. Effect of Pitch-Lag Coupling, Predroop, and Sweep on Aeroelastic Stability: Rotor Model

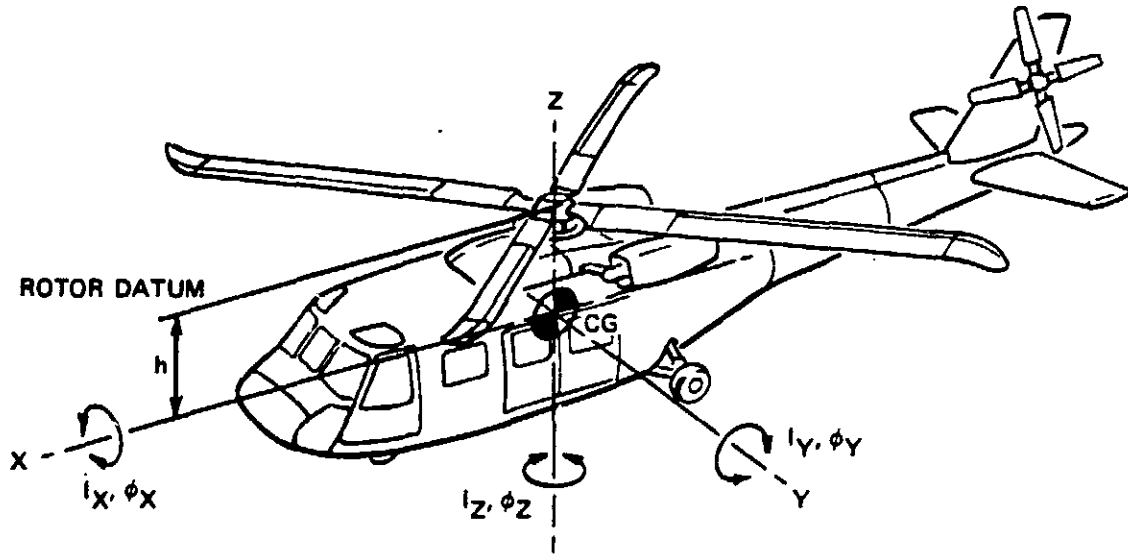
Pitch-lag coupling, in terms of arc tangent of the ratio of degrees of pitch for each degree of lag motion about the hinge, was calculated from the system loads analysis and introduced into the model in terms of  $\alpha_1$  and control system spring stiffness,  $K_\theta$ .

Figure 61 shows the model representing the demonstration test vehicle, together with its physical characteristics.

The study was made in hover at 1-g thrust and normal rpm; 0.5 percent critical structural damping was used.

Figure 62 shows the resultant additional damping that may be expected in hover through the offset pivot without predroop and that the technique is effective.

If predroop effectiveness is retained, however, it appears from this elementary exercise that the offset pivot effects are enhanced. These characteristics will be studied in detail in the next phase of the ITR program.



THRUST = 16,000 LB,  $\theta_{75\%R} = 10^\circ$   
 $I_X = 40,470 \text{ LB-SEC}^2\text{-IN.}$   
 $I_Y = 350,500 \text{ LB-SEC}^2\text{-IN.}$   
 $I_Z = 350,500 \text{ LB-SEC}^2\text{-IN.}$   
 $h = 69 \text{ IN.}$

Figure 61. Effect of Pitch-Lag Coupling, Predroop, and Sweep on Aeroelastic Stability: Fuselage Model

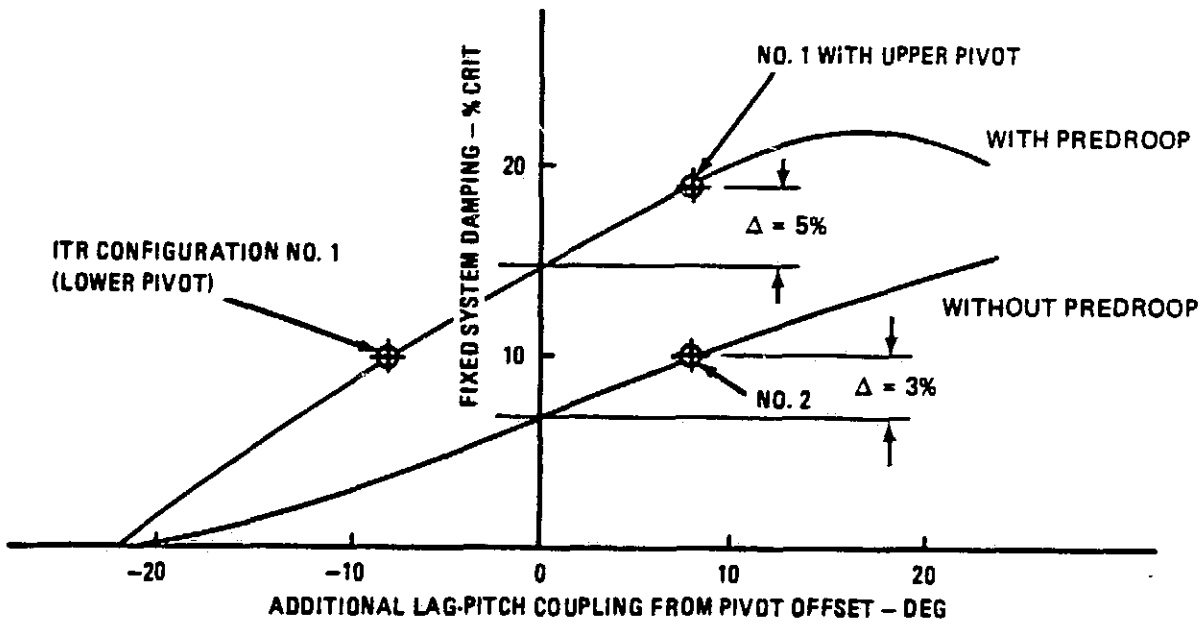


Figure 62. Stability Improvement in Hover Through Pivot Offset

## ASSESSMENT OF CONCEPTS

Each of the five basic concepts was evaluated for each characteristic that contributes to the overall merit function by which each concept could be relatively assessed; Table 9 lists the value of each characteristic. Simplified methodology was to be used; however, bearingless rotors require a certain degree of optimization before they can be regarded as feasible concepts and the methodology becomes less simple than first envisaged. Consequently, the five configurations were conceived with more in-depth techniques to ensure feasibility. The selection of two concepts for further study was to be conducted with the merit system defined in the RFQ. Deficiencies of this system were identified and deserve some discussion.

### MERIT FACTORS AND MERIT FUNCTION

The merit of each concept was to be based upon a score obtained from the product of factors for vulnerability to any HEI projectile, risk of aeromechanical stability, and the sum of the remaining factors for hub drag, weight, parts count, etc.

A location, direction of impact, and type of projectile could be chosen so that, for any of the systems, there is zero probability of surviving a hit, which would reduce all merit scores to zero. As stated, the description of the vulnerability merit factor is inadequate; however, with appreciation of the intent to conduct a relative appraisal, the  $K_V$  factor should be based upon vulnerable area as a percentage of total hub area and the survivability factor ( $1/K_V$ ) should be used for the evaluation.

The factor containing the sum of the merit factors for the first configuration may have a negative value and that for the second an equal but positive value. The merit factor product for survivability and stability may be higher for the first than for the second. This situation could make the total merit function valueless for the purpose intended.

TABLE 9. ASSESSMENT OF FIVE CONCEPTS

Parameter	Units	Goal	Configuration				
			1	2	3	4	5
Survivability	prob, %	100	71	71	69	64	62
Stability	% critical	>2	>2	>2	>2	>2	>2
Hub Drag	ft <sup>2</sup>	<2.8	3.54	3.54	5.04	3.96	5.43
Weight	lb	<400	305	305	473	436	461
No. of Parts	-	<50	47	47	86	67	85
Hub Stiffness	ft-lb/rad	<120,000	240,000	240,000	86,000	333,000	105,000
Min EL M <sub>H</sub>	ft-lb	10,000	13,400	13,400	9,000	18,600	14,700
EL Flapping	deg	<±5	3.4	3.4	5.0	3.2	8.0
MTBR	hr	3,000	2,700	2,700	2,100	1,200	1,500
Cost	\$	100,000	125,500	125,500	193,000	130,500	161,000
Fatigue Life	hr	10,000	8,250	8,250	10,000	8,000	10,000
Damping	Adaptable	Auxiliary	Yes	Yes	Yes	Yes	Yes
Pitch Stiffness	in.-lb/deg	<150	146	146	450	150	300
Folding	Quick manual	Adaptable	Yes	Yes	Yes	Yes	Yes

ORIGINAL PAGE IS  
OF POOR QUALITY

It is recommended that weighting factors for relative importance be applied and that each merit factor be defined so that each is always positive in sign.

### SURVIVABILITY

Figure 63 shows a typical example of how, based upon engineering judgment, the top and side views of each hub were assessed for survivability. In each view, the impacted locations that would result in zero, zero to 50-percent, and 50 to 100-percent probability of survival were mapped and their areas were measured. Only the hub plan view and one side elevation were considered and pitch links and pitch arms were excluded, as shown in Table 10. A mean totally vulnerable area was then calculated. The survivable area was the difference between the exposed and the vulnerable areas of the hub. The probability of the hub surviving a hit was estimated by the percentage of the total hub area that was survivable. Relative hub size was then included by estimating the percentage of exposed aircraft system area that was represented by the hub, which gave the probability of a hit to the aircraft being in the hub.

Survivability rating was estimated by multiplying the probability that the hub will survive a hit by the probability of a hit not being in the hub.

### STABILITY

All configurations are expected to have at least 2-percent critical damping in the fixed system; however, the most stable is expected to be the reversed Starflex (configuration 4) with its built-in elastomeric damper. Less stability may be exhibited by the modified BMR (configuration 1) since it retains most of the stabilizing features of the marginally stable U.S. Army/Boeing Vertol BMR-B0-105; however, it has the additional benefit of the offset shear pivot. The advanced BMR and the shoe-restrained flexure (configurations 2 and 3) rely upon the offset shear pivot technique

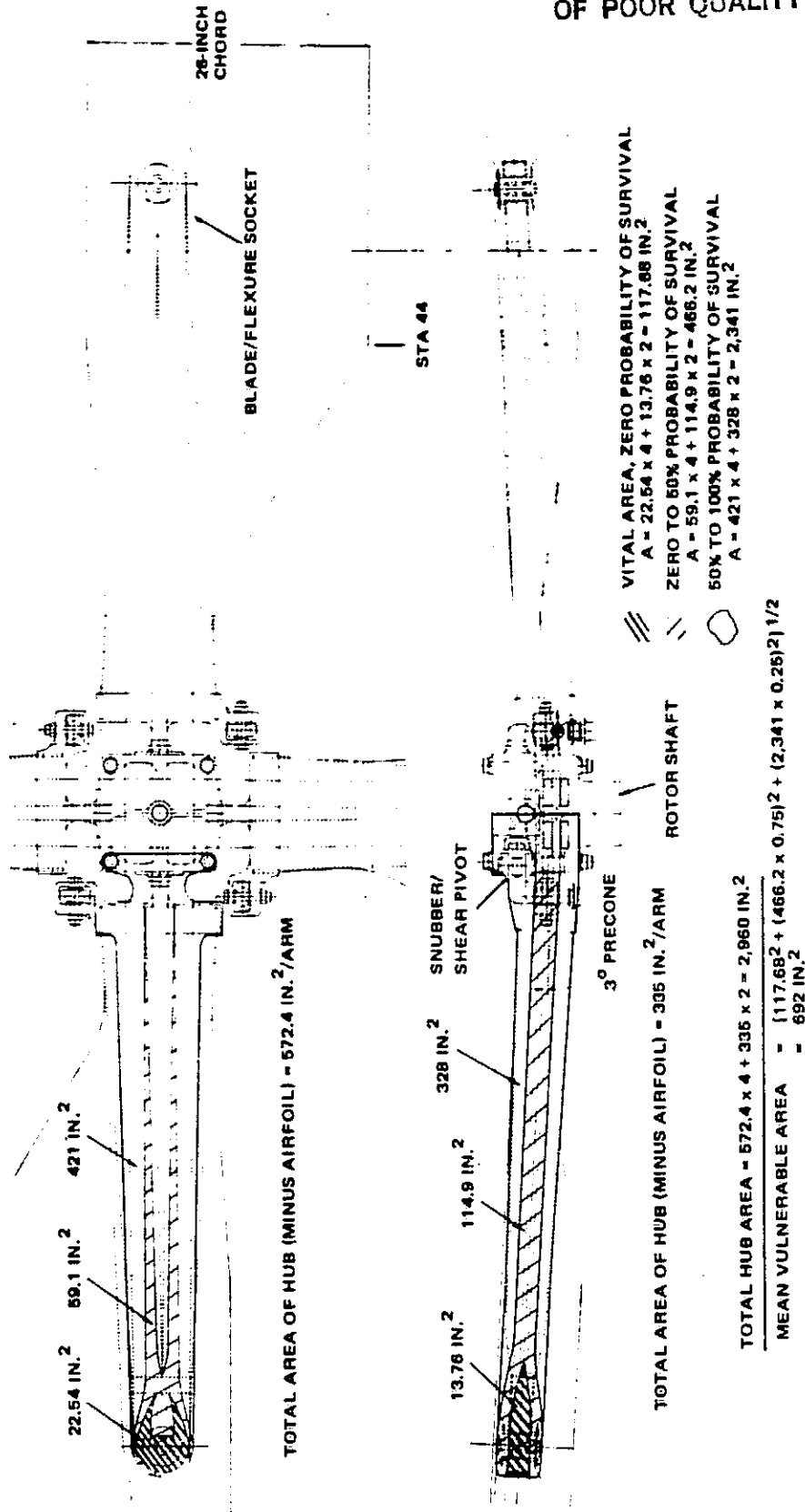


Figure 63. Vulnerability Study of ITR Configuration No. 2B (Modified BMR)

TABLE 10. SURVIVABILITY OF ITR CONCEPTS

Configuration	Area (in. <sup>2</sup> )					Remarks
	1 and 2	3	4	5		
Chance of Zero (A)	Top	22.54	42.80	11.25	10.00	Per arm
	Side	13.76	70.70	31.87	22.91	Per arm
	Total	117.68	312.60	108.74	85.82	(Top x 4 + side x 2)
Surviving 0-50 (B)	Top	59.1	196.5	73.5	162.4	Per arm
	Side	114.9	173.6	20.4	226.4	Per arm
	Total	466.2	1,133.2	333.8	1,102.4	(Top x 4 + side x 2)
a Hit (%) 50-100 (C)	Top	421	200	163	237	Per arm
	Side	328	198	78	92	Per arm
	Total	2,341	1,196	808	1,133	(Top x 4 + side x 2)
Mean Vulnerable Area	692	954	340	878		$[A^2 + (0.75B)^2 + (0.25C)^2]^{\frac{1}{2}}$
Total Hub Area	2,960	5,409	990	2,626		(Top + side) minus airfoil
Probability of Hub Surviving a Hit	77%	82%	66%	67%		$100 (1 - \frac{\text{mean vuln area}}{\text{total}})$
Probability of Hit in Hub	8.2%	15%	2.8%	7.3%		$100 (1 - \frac{\text{hub total area}}{\text{acft area} = 250 \text{ ft}^2})$
Survivability Rating	71	69	64	62		Prob of surv x $(1 - \frac{\text{prob of hub hit}}{100})$

ORIGINAL PAGE IS OF POOR QUALITY.

which requires further evaluation through test. For stability, the least desirable is the flexbeam with flapping hinge (configuration 5) which almost certainly will require auxiliary damping.

#### HUB DRAG

From the rotor shaft center out to the blade airfoil the projected area presented by the hub side elevation was measured. The vertical offset between orthogonal blade arms was ignored for configurations 1 and 2.

#### HUB WEIGHT

The weight of all hub components, including blade attachment hardware, was calculated from configuration geometry and material content.

#### NUMBER OF PARTS

A count of nonstandard parts, defined as "those not available from floor stock and those which, if disassembled, would result in part scrappage," was made for each configuration. Pitch links were excluded. Hub-to-shaft and hub-to-blade attachment hardware was included.

#### HUB STIFFNESS

Each configuration was conceived and its feasibility validated through extensive use of simplified methodology. The objectives were to maximize hub endurance limit flapping and to minimize hub stiffness. The results of each configuration analysis are presented in Table 8.

#### MINIMUM HUB MOMENT

This parameter was calculated as the product of the hub stiffness and the endurance limit flapping or the hub tilt angle.

### MINIMUM HUB TILT ANGLE

During the concept feasibility studies, endurance limit flapping was maximized and the results for each configuration are presented in Table 9.

### RELIABILITY

Six concept layouts of possible ITR hubs were evaluated in an R&M review. A subjective assessment was made of the probability that the rotor would achieve a 3,000-hour mean time between removals in a mature state of development.

Each rotor concept was reviewed to determine the number of significant components; the number of components susceptible to wear; the number and type of bearings (elastomer or Teflon fabric); the number of components requiring adjustment; and the number of components that are loaded principally in fatigue.

The final ranking for each concept is as follows: concept 1A, 9; concept 1B, 8; concept 2, 9; concept 3, 7; concept 4, 4; and concept 5, 5.

MTBR was estimated by assigning the proportion of the 3,000-hour goal according to the rating number as a percentage of 10.

### COST

Cost was estimated based on the summation of the product of the quantity of a particular part times a complexity factor for that part. Complexity factors between 1 and 10 based on engineering judgment were assigned to each part.

For a reference cost, an estimate to fabricate a quantity of 1,000 of the most complex composite part in each configuration was made. These references allowed a total estimated hub cost to be calculated.

### FATIGUE LIFE

Fatigue life was based upon the achievement in meeting the endurance limit flapping goal ( $\beta_{EL}$ ):

$$\text{fatigue life} = \frac{\beta_{EL}}{\beta_{EL \text{ goal}}} \times 10,000 \text{ hours}$$

### PROVISIONS FOR AUXILIARY DAMPING

All concepts could be adapted to include auxiliary damping and therefore were assessed equally, with the exception of the reversed Starflex which should require no additional damping.

### TORSIONAL STIFFNESS

With the methodology available, the true torsional stiffness was calculated for each configuration based upon flexure geometry and material content. Centrifugal, shear, and warping constraint stiffening effects were included but aerodynamic pitching and planipetal moments were excluded.

## SELECTION OF TWO HUB CONCEPTS BY MERIT

Figure 64 describes the application of the merit function to each concept. Table 11 presents the goals as well as the merit factor for each parameter assigned to each configuration.

Inadequacies in the determination of the merit function for each hub were discussed previously.

The product  $(K_V \times K_a) \times \Sigma[ ]$  has not been calculated; selection of two candidate configurations was made by appraising the components  $(K_V \times K_a)$  and  $\Sigma[ ]$  separately and by exercising engineering judgment on the final product.

Configurations 1A and 2B were selected for further development and for subsequent consideration as baselines for the preliminary design phase of the ITR/FRR program.

CONTINUATION SHEET		REP NO OF DOCUMENT BEING CONTINUED	PAGE	OF
		RFQ DAAK51-81-Q-0054	18	55
NAME OF OFFICE OR CONTRACTOR				
<u>SECTION C - Continued</u>				
APPENDIX C MERIT FACTORS/MERIT FUNCTION				
<u>Parameter</u>	<u>Merit Factor</u>			
a. Vulnerability to 23mm HEI projectile	$K_v$ - probability of surviving hit			
b. Risk of aeromechanical instability	$K_a$ - probability that rotor system will be free from air/ground resonance instability			
c. Hub drag area	$K_d$ - % reduction from technical goal			
d. Hub weight	$K_w$ - % reduction from technical goal			
e. Part counts	$K_p$ - % reduction from technical goal			
f. Rotor hub moment stiffness	$K_e$ - equal to 5 if rotor hub moment stiffness is within $\pm 20\%$ of the technical goal. $K_e$ is reduced from 5 by one-tenth of the percentage that the parameter exceeds a $\pm 20\%$ margin from the goal			
g. Minimum rotor hub moment	$K_m$ - one half of the percentage by which the parameter exceeds the technical goal			
h. Minimum rotor hub tilt angle	$K_\theta$ - one half of the percentage by which the parameter exceeds the technical goal			
i. Reliability	$K_r$ - ten times the probability of meeting or exceeding technical goal* for MTBR			
j. Manufacturing cost	$K_c$ - qualitative estimate from 1 to 10, varying inversely with expected cost			
k. Fatigue life	$K_f$ - ten times the probability of meeting or exceeding the technical goal*			
l. Auxiliary lead-lag damping	$K_z$ - 0 to 2, qualitative estimate of practicality of incorporating auxiliary damping			

DRSTSP Form 6554 (J)  
1 Apr 79

Edition of 1 Aug 77, may be used.

Figure 64. Application of Merit Factors and Merit Function to Selection of ITR Hub Concepts (Sheet 1 of 2)

CONTINUATION SHEET	REF NO OF DOCUMENT BEING CONTINUED	PAGE	OF
NAME OF OFFICER OR CONTRACTOR		19	55
<u>SECTION C - Continued</u>			
m. Torsional stiffness	$K_s$ - if pitch control system forces exceeds of 1.5 times typical pitch bearing hub $K_s = -2$ ; if forces less than this level, $K_s = 0$		
Merit Function = $K_v \times K_a \times (K_d + K_w + K_p + K_e + K_m + K_b + K_r + K_c + K_f + K_z + K_s)$			
Note: Technical goals refer to values given in Appendix B, Rotor Hub Technical Goals.			

Figure 64. Application of Merit Factors and Merit Function to Selection of ITR Hub Concepts (Sheet 2 of 2)

TABLE 11. MERIT EVALUATION

Merit Function = $K_v \times K_a [K_d + K_w + K_p + K_e + K_m + K_b + K_r + K_c + K_f + K_z + K_s]$						
Parameter	Symbol	Configuration				
		1	2	3	4	5
Survivability	$1/K_v$	72.7	72.7	47.2	117	56
Stability	$K_a$	8	6	6	10	9
Hub Drag	$K_d$	-26	-26	-56	-41	-94
Weight	$K_w$	24	24	-18	-9	-15
No. of Parts	$K_p$	6	6	-72	-34	-70
Hub Stiffness	$K_e$	-5	-5	-1.6	-12.8	6.3
Min EL $M_H$	$K_m$	17	17	-2.5	43	24
EL Flapping	$K_b$	-16	-16	0	-18	30
MTBR	$K_r$	9	9	7	4	5
Cost	$K_c$	8	8	5.2	7.7	6.2
Fatigue Life	$K_f$	8	8	10	8	10
Adaptable for Damping	$K_z$	1.5	1.5	1.5	2	1.5
Pitch Stiffness	$K_s$	0	0	-2.0	0	0
	$\Sigma [ ]$	26.5	26.5	-128.4	-50.1	-96
	$K_v \times K_a$	582	437	283	1,170	504
	Rating	1st	2nd	5th	3rd	4th

ORIGINAL PAGE IS  
OF POOR QUALITY

## INFLUENCE OF GOALS AND SPECIFICATIONS ON THE DESIGN

As explained earlier, the hub moment stiffness goal is unreachable by means of a simple cantilevered flexure and the hub tilt goal is obtainable but only at the expense of significantly increased hub stiffness. To minimize hub stiffness and maximize hub tilt require minimizing of the flexure thickness at the root radial station and maximizing of flexure width. Both these criteria result in a hub shaft attachment of minimum proportions which is conducive to minimum hub weight and minimum drag. Optimizing hub stiffness tilt and weight goals also required the use of higher modulus materials for the flexure such as Kevlar or graphite since, for a required stiffness, cross-sectional geometry is reduced, thus allowing a smaller radius of flexure curvature for the same allowable strain.

Higher modulus materials have lower damage tolerance which may require inherent redundancy to be included in the flexure system, such as multiplicity of flexures.

The torsional stiffness goals require a flexure of at least 50 inches in length for a 16,000-pound design gross weight aircraft hub.

Stability requirements without the help of auxiliary dampers have a major influence on the hub configuration geometry. For low in-plane stiffness aeroelastic stability has to be achieved, in lieu of auxiliary dampers, through various means of kinematic coupling such as pitch from lag and/or lag from flap. In the U.S. Army/Boeing Vertol BMR-80-105, pitch/lag coupling was achieved by a negative predrump angle between the flexure torsional and blade radial axes, which resulted in the strengthening of the inboard end of the flexure in order to accommodate the blade steady vertical shear loads. This resulted in high weight and drag penalties. In addition, lag-flap coupling was achieved by a flexure leading-edge-up pre-twist of  $12\frac{1}{2}$  degrees, which further increased the hub frontal area. To

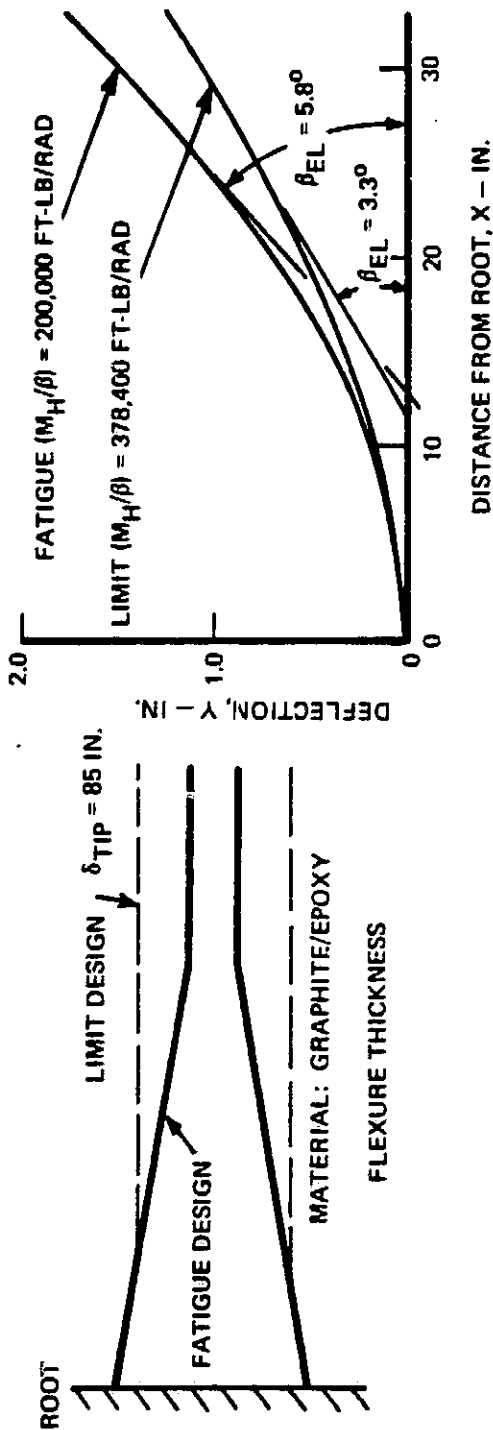
reduce these penalties, the offset shear pivot technique has been devised; however, its effectiveness should be further evaluated in the next phase of the ITR/FRR program.

The requirement to incorporate provisions for rapid manual folding also has a major influence on the configurations. For an adequately compact folding envelope, the fold point must be at a significant radial location to accommodate the wide-chord blades required to meet the performance goals. Hub stiffness and endurance limit flapping goals dictate that this joint be outboard of the flapping flexure, so the most convenient location is at the flexure/torque sleeve/blade joint, resulting in a compromise in parts count and drag.

Another unspecified requirement of structural adequacy to withstand limit static loading conditions has a major influence on the configuration. Figure 65 again shows that the flexure that is designed to withstand these loads and deflections without hub failure or blade/boom contact is compromised with regard to endurance limit flapping and hub stiffness. Auxiliary droop stops and their attendant reliability problems should be weighed along with the other specified goals.

FLEXURES DESIGNED FOR FATIGUE ONLY  
WILL NOT CARRY LIMIT STATIC LOADING.

- STATIC LIMIT FLAP LOADING = 154,000 IN.-LB
- MODIFICATIONS REQUIRED TO A SIMPLE CANTILEVERED FLEXURE DESIGNED FOR FATIGUE



CONCLUSION: SIMPLE CANTILEVER WILL NOT  
MEET THE GOALS!!

Figure 65. Studies of Limit Loading on Flexures

## DETERMINATION OF PHYSICAL PROPERTIES

### GEOMETRY

#### Flexures

Figure 66 provides the geometric characteristics of the flexures.

#### Torque Tube/Sleeve

Figure 67 provides the geometric characteristics of the torque tube.

### STIFFNESS

#### Flexure

The stiffness distribution of the 4-element flexure can be calculated from the geometry and material properties; however, they are meaningless to the reader without familiarity with the CHORD-Z dual-element flexure-bending procedure. A detailed explanation is beyond the scope of this work; however, the resulting force moment distribution, together with deflections and strains, are presented in the structural analysis.

#### Torque Sleeve

For a thin-walled shell, as shown in Figure 68, flapwise second moment of area of the modified ellipse is approximated by

$$I_F \approx \frac{\pi}{4} W t_1 h^2 ,$$

where  $W$ ,  $t$ , and  $h$  are median width, wall thickness, and height, respectively, and for chord,

$$I_C \approx W^2 \left( \frac{1}{2} a t_2 + \frac{\pi}{4} h t_1 \right)$$

ORIGINAL FACE IS  
OF POOR QUALITY

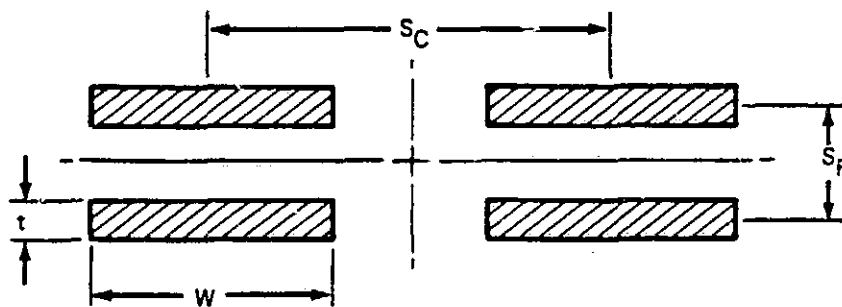
where  $a$  is the end radius center distance and  $t_1$  and  $t_2$  are upper and lower wall thickness, respectively.

Table 12 presents the sleeve material content as a ratio of  $0^\circ/\pm 45^\circ/90^\circ$  bias ply in fiberglass/graphite/graphite together with equivalent composite bending moduli.

Stiffness to bending at the blade attachment of the torque sleeve was calculated to be  $2 \times 10^6$  in.-lb/radian in flap,  $18 \times 10^6$  in.-lb/radian in chord, and in torsion 60,000 in.-lb/degree.

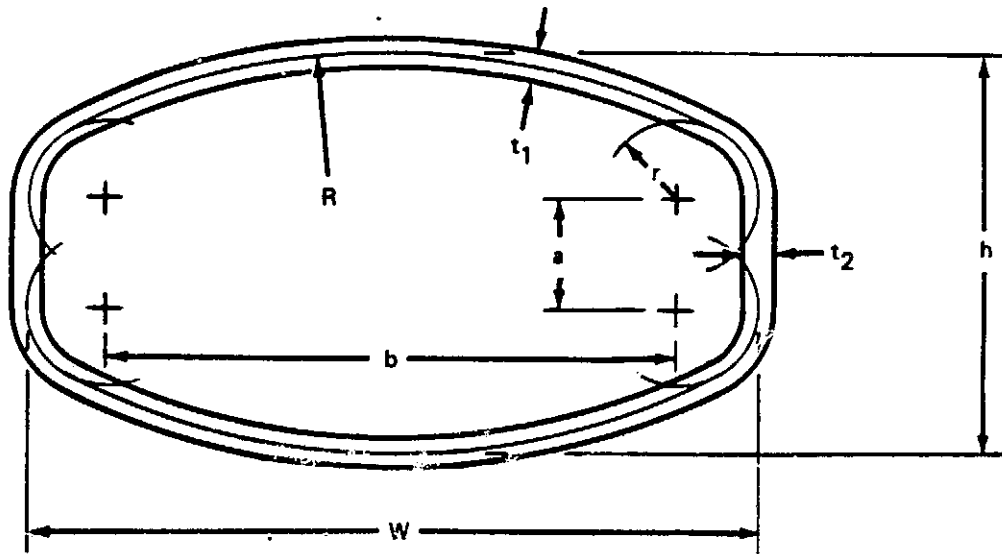
### BLADE PHYSICAL PROPERTIES

For this concept study, the blade has been assumed to be rigid. Rotor length has been chosen at 294 inches and the weight has been assumed to be on the order of 200 pounds acting at 60 percent of the radius.



RADIAL STATION, X (IN.)	t (IN.)	W (IN.)	S <sub>F</sub> (IN.)	S <sub>C</sub> (IN.)	
0	0.661	2.50	1.722	4.50	☐ SHAFT HUB EDGE
5	0.661	2.50	1.722	4.50	
10	0.180	2.50	1.590	4.30	
15	0.112	2.50	1.457	4.10	
20	0.330	2.50	1.325	3.90	
25	0.330	2.50	1.192	3.70	
30	0.330	2.50	1.061	3.50	
35	0.330	2.50	0.928	3.30	
40	0.330	2.50	0.796	3.10	
45	0.110	2.50	0.664	2.90	
50	0.145	2.00	0.531	3.20	
55	0.399	1.50	0.399	3.50	

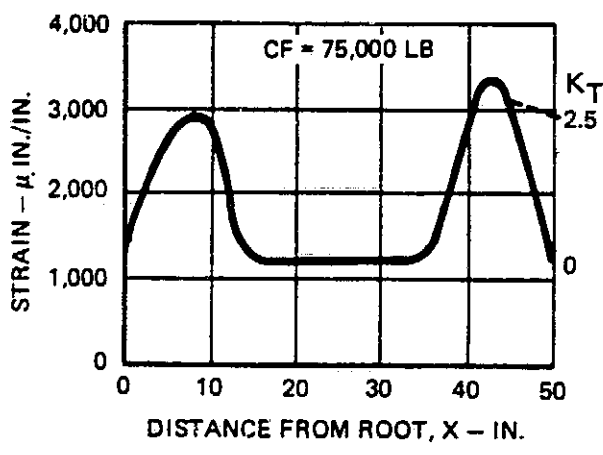
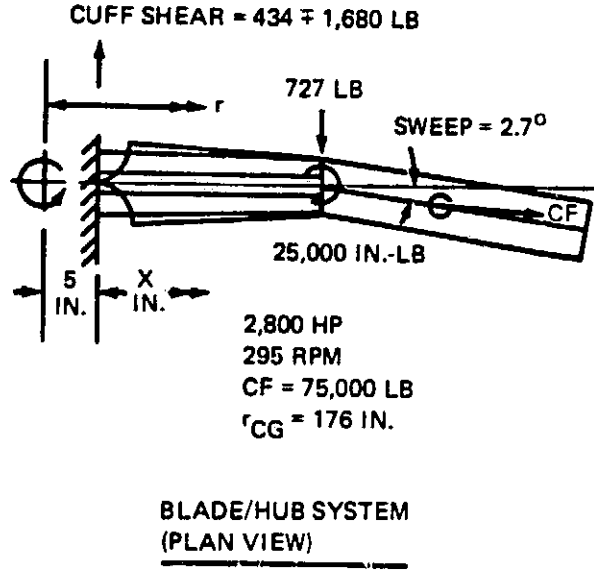
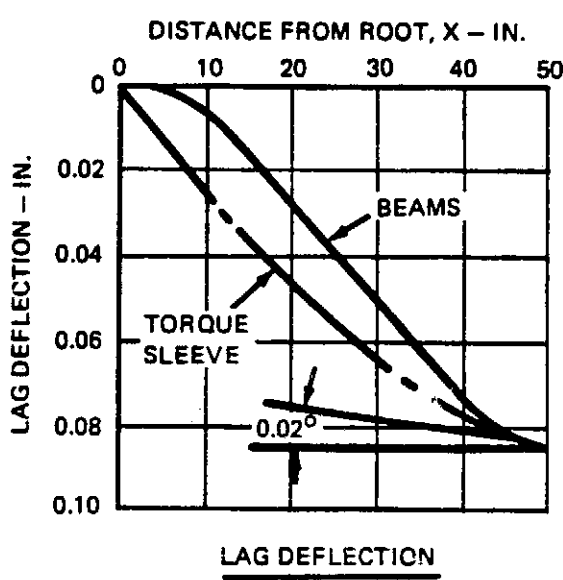
Figure 66. Geometry of Flexure Cross Section



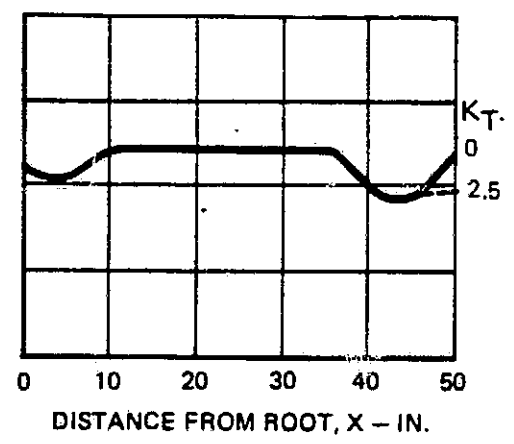
RADIAL STATION, X (IN.)	$t_1$ (IN.)	$t_2$ (IN.)	a (IN.)	b (IN.)	r (IN.)	R (IN.)	h (IN.)	W (IN.)	
0	—	—	—	—	—	—	—	—	CL SHAFT
5	—	—	—	—	—	—	—	—	HUB EDGE
10	0.20	0.20	0	5.50	2.20	7.80	6.80	9.90	PITCH ARM
15	0.10	0.20	0	5.64	1.99	7.80	6.26	9.62	
20	0.10	0.20	0	5.79	1.77	7.80	5.71	9.33	
25	0.12	0.20	0	5.93	1.56	7.80	5.17	9.05	
30	0.14	0.20	0	6.07	1.34	7.80	4.63	8.75	
35	0.16	0.20	0	6.21	1.13	7.80	4.09	8.47	
40	0.18	0.20	0	6.36	0.91	7.80	3.54	8.18	
45	0.20	0.20	0	6.50	0.70	7.80	3.0	7.90	
50	0.28	0.35	0.40	6.00	0.35	—	2.50	6.70	
55	0.35	0.50	0.80	5.50	0	$\infty$	2.00	5.50	
59	0.35	0.50	0.80	5.50	0	$\infty$	2.00	5.50	CL HOLES

Figure 67. Geometry of Sleeve Cross Section

ORIGINAL FAILURE OF POOR QUALITY



CRITICAL FIBER STEADY STRAIN (LAG + CF)



ALLOWABLE CRITICAL FIBER FATIGUE STRAIN - FLAP OR CHORD AND TWIST

Figure 68. Determination of Steady Flexure Strains Due to Centrifugal Force and Chord Loading

TABLE 12. TORQUE SLEEVE STIFFNESS

Radial Station, X(in.)	Fg/Gr/Gr 0°/±45°/90°	$E_B$ (lb/in. <sup>2</sup> x 10 <sup>-6</sup> )	$I_F$ (in. <sup>4</sup> )	$I_C$ (in. <sup>4</sup> )	$E I_F$ (lb x in. <sup>2</sup> x 10 <sup>-6</sup> )	$E I_C$ (lb x in. <sup>2</sup> x 10 <sup>-6</sup> )	G (lb/in. <sup>2</sup> x 10 <sup>-6</sup> )	GK (lb x in. <sup>2</sup> x 10 <sup>-6</sup> )
0	-	-	-	-	-	-	-	-
5	-	-	-	-	-	-	-	-
10	5/89/6	3.9	72	104	280	406	3.6	630
15	8/85/5	3.9	59	91	230	355	3.5	530
20	15/81/5	4.2	48	78	202	328	3.4	430
25	19/76/5	4.2	38	67	160	281	3.2	340
30	24/71/5	4.3	29	56	125	241	3.1	270
35	29/67/4	4.5	22	46	99	207	2.9	200
40	34/62/4	4.6	16	37	74	170	2.8	150
45	38/57/4	4.6	11	29	51	133	2.6	105
50	43/53/4	4.7	7.0	27	33	127	2.5	85
55	48/48/4	4.8	3.1	25	15	120	2.3	65
59	48/48/4	4.8	3.1	25	15	120	2.3	65

## PRELIMINARY STRUCTURAL ANALYSIS

Flap and chord bending and twist mode shapes are presented in Figures 68 and 69 for the flexure together with force and moment distributions and resultant critical fiber fatigue strains. First-harmonic chordwise bending and cyclic twist from control input have been assumed to occur 90 degrees out of phase with flapwise bending; however, a moderate strain margin has been allowed for higher harmonic loadings.

The structural analysis of the hub system to determine strain distributions, critical locations, deflections, and stiffnesses was based upon the assumption, verified by examination of flight-test measurements on existing rotor systems, that the first-mode chordwise and torsional displacements are 90 degrees out of phase with the flapwise displacements.

The methodology used for the analysis was the CHORD-Z program for both flap and chord and the DIFF.Q program for torsion.

### ALTERNATING FLAP STRAINS

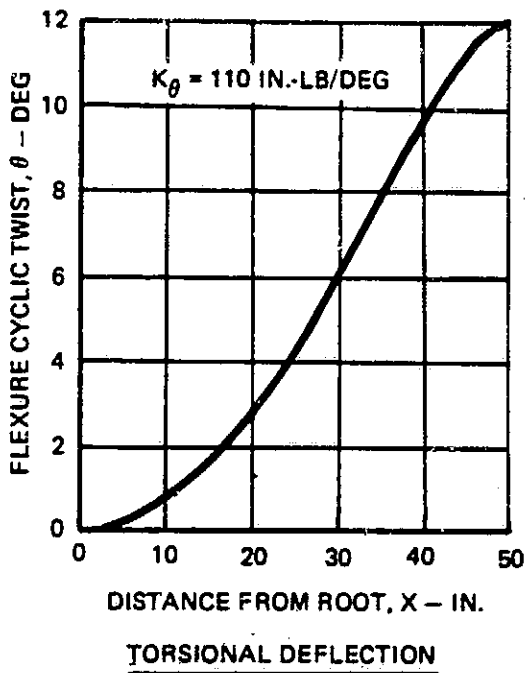
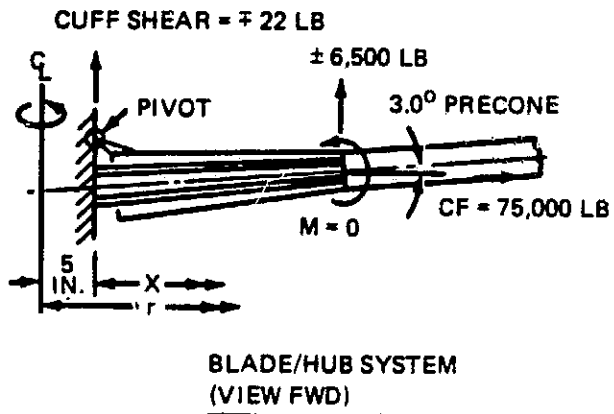
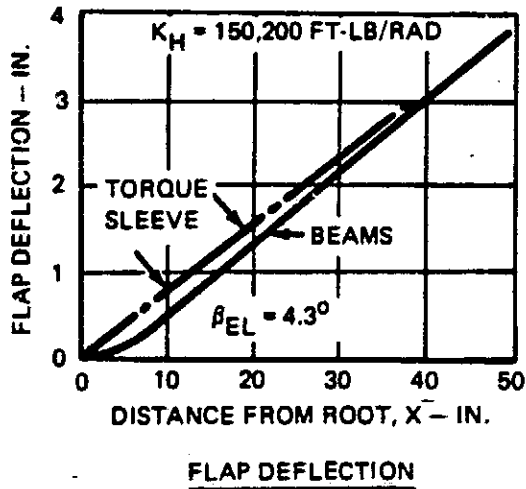
The flexbeam dimensions presented in the physical properties were input to the CHORD-Z analysis together with an applied axial load (P), end shear (V), and end moment (M) for the flexure/torque sleeve system shown diagrammatically in Figure 70. Other inputs required were flexure material flexural modulus (E), length (L), torque sleeve stiffness to end moment (CK), root spacing (SS), and outboard end spacing (S).

### FLEXURE SYSTEM

Steady chordwise strains together with steady centrifugal strains were minimized by introducing 2.7 degrees of blade sweep at the blade/flexure attachment. Due to the stress concentrations in the wraparound fibers at the single-pin attachment, a factor of  $K_T = 2.5$  was applied:

$$(K_T \sim \frac{\text{outside radius}}{\text{inside radius}}).$$

ORIGINAL FIGURE  
OF POOR QUALITY



$$M_\theta = \underbrace{GK \left( \frac{d\theta}{dx} \right)}_{\text{SHEAR}} + \underbrace{CF \left( \frac{EI_F + EI_c}{EA} \right) \left( \frac{d\theta}{dx} \right)}_{\text{CF}} + \underbrace{EC_W \left( \frac{d^3\theta}{dx^3} \right)}_{\text{DB AND W}}$$

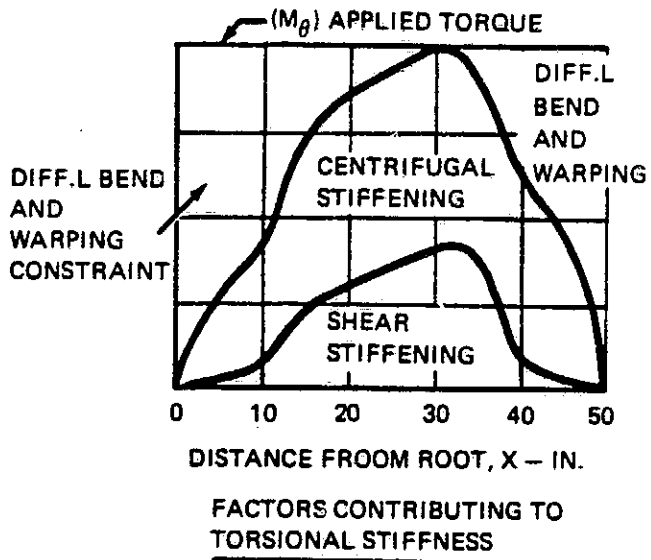


Figure 69. Flap and Torsional Displacement

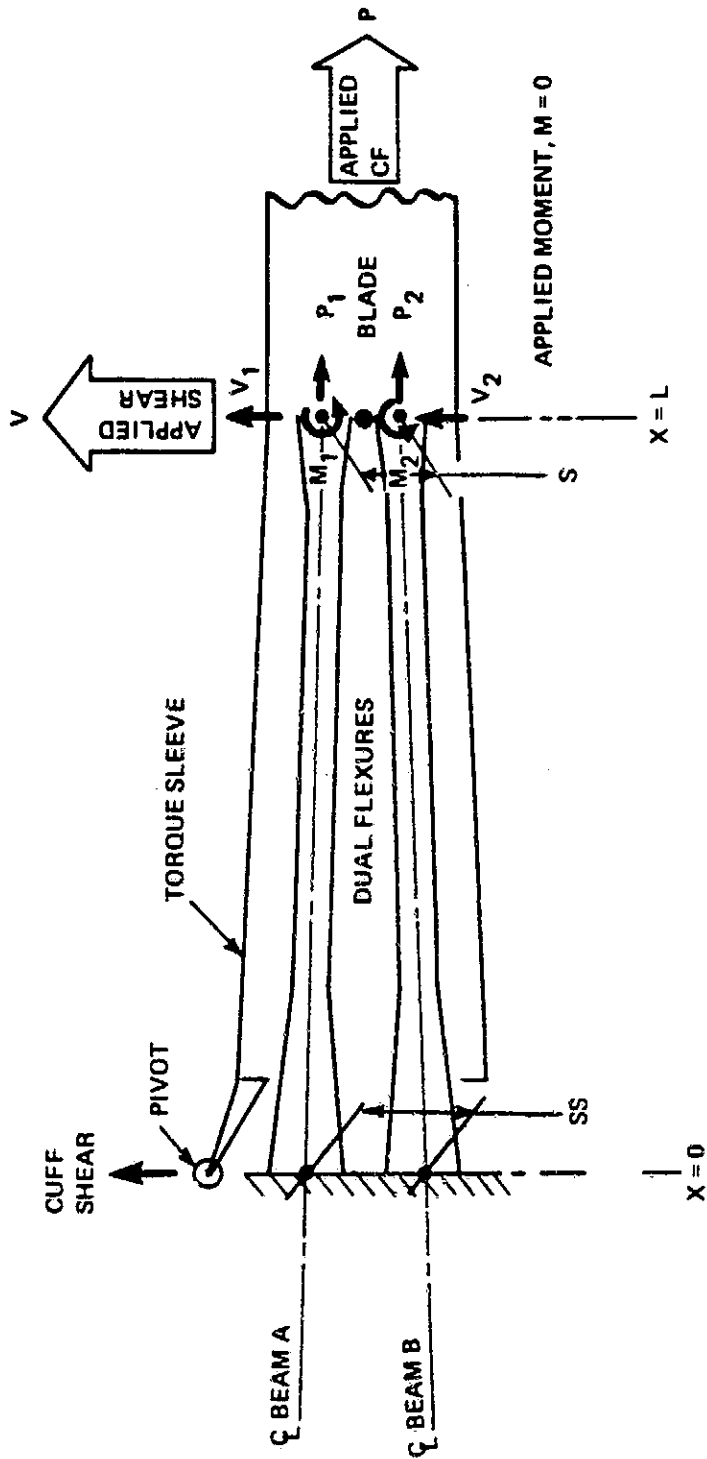


Figure 70. Loading System for Analysis of Flap Strain by CHORD-Z Program

From the Goodman curve for graphite unidirectional composite, the allowable fatigue strains for  $10^8$  cycles of endurance were calculated. Figure 68 shows the loading system, the steady lag deflection, and resultant critical fiber strains together with the distribution of alternating strains allowed from either cyclic flapping or the total of lag and torsional cyclic displacements. Figure 69 presents the cyclic loading system for flapping and the calculated displacements of the flexure beams. The figure also shows the twisted shape and the relative contributions to the overall torsional stiffness of the hub from the classical shear rigidity, centrifugal stiffening, and differential bending and warping constraints due to the fixed ends of each beam. The alternating direct strain distributions are given in Figure 71. A station five inches outboard from the flexure root appears to be the critical point, but further optimization could improve this condition. It should be noted that the flexures have been enlarged between stations  $X = 15$  and  $X = 40$  inches to enhance ballistic tolerance, and consequently an abundance of fatigue margin is available. Bending moment distributions are not presented since the CHORD-Z dual-beam analysis used for both flap and chord computes critical fiber strains directly.

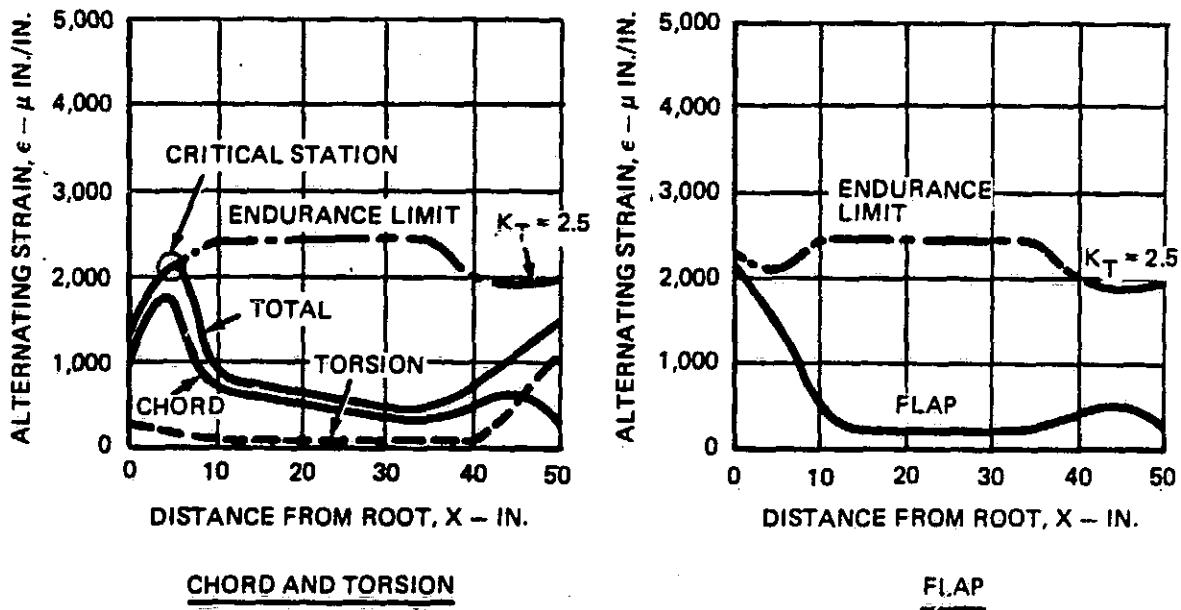


Figure 71. Fatigue Strains

Twelve degrees of cyclic twist was used as a maximum requirement for torsion based upon that used in the MBB BO-105 and the YUH-61A helicopters.

For chord, cyclic strains were based upon a requirement for the chordwise lagging to be one-quarter of the cyclic flapping angle, according to the law of conservation of angular momentum.

#### FLEXURE/BLADE ATTACHMENT

For a limit overspeed case of 125-percent overspeed, the attachment has to withstand 117,200 pounds of centrifugal force without exceeding the allowable limit tensile stress ( $\frac{2}{3} \times 164,000 = 109,300$  psi) of the material. A stress concentration of 2.5 is present in the flexure loop which dictates a requirement for 2.68 square inches of material at the pin. For an outside radius of 2.5 inches and an inside radius of 1.0 inch, the total required thickness of material is 0.89 inch or 0.445 inch for both upper and lower beam pairs.

Figure 66 shows that 0.798 inch is available at the pin station and only 0.09 inch of reinforcement is required, which is easily accommodated.

The bushing in the flexure loop is required to provide a shear connection between the upper and lower flexure pairs. The magnitude of the shear, given by the CHORD-Z analysis, is  $\pm 5,485$  pounds which requires a wall thickness for the 2.0-inch-outside-diameter steel bushing of only 0.0625 inch, leaving 1.875 inches diameter for the retention pin. This provides an ultimate strength margin of 3.0 for this solid pin, allowing for a weight reduction when it is hollowed out for the emergency blade release charge during testing on the RSRA.

#### FLEXURE RETENTION AT THE SHAFT

The alternating differential tension load between the upper and lower beam pairs is reacted by the flexure enlargements provided by the inserts at the shaft centerline shown in configuration 1A, Figure 24. As in the blade attachment, this load is  $\pm 5,485$  pounds (due to flapping). Due to cyclic chord, however, the equivalent load is higher at  $\pm 10,815$  pounds and is reacted by the enlargements in the fore and aft pairs of beams. For

each of the four 2.5-inch-wide beams, the required projection area, based on an allowable of 11,000 psi, is 0.5 square inch. An insert of only 0.2 inch in height is required.

Interlaminar shear stress within the clamp caused by the root cyclic moment of  $\pm 6,724$  in.-lb in each of the four flexures is  $\pm 1,220$  psi. This calculation is based upon a linear reduction of moment within the clamp, which is very optimistic. Detail design will require the use of an elastomer in the hub clamp as described in Figure 37.

### TORQUE SLEEVE

The alternating flap shear of  $\pm 22$  pounds introduced into the cuff shear pivot is many orders of magnitude within the capability of the sleeve and requires no further consideration. For the design condition, the chord shear of  $434 \pm 1,680$  pounds is sizable and merits a chordwise strength analysis.

Figure 72 shows the chord moment distribution and the resultant dynamic chordwise strains compared with the endurance limits. A substantial strength margin is evident since the cuff is stiffness-designed to result in a chord shear to provide substantial pitch/lag coupling through the shear pivot offset and to maximize torsional stiffness. Consequently, a substantial strength margin is also available in torsion.

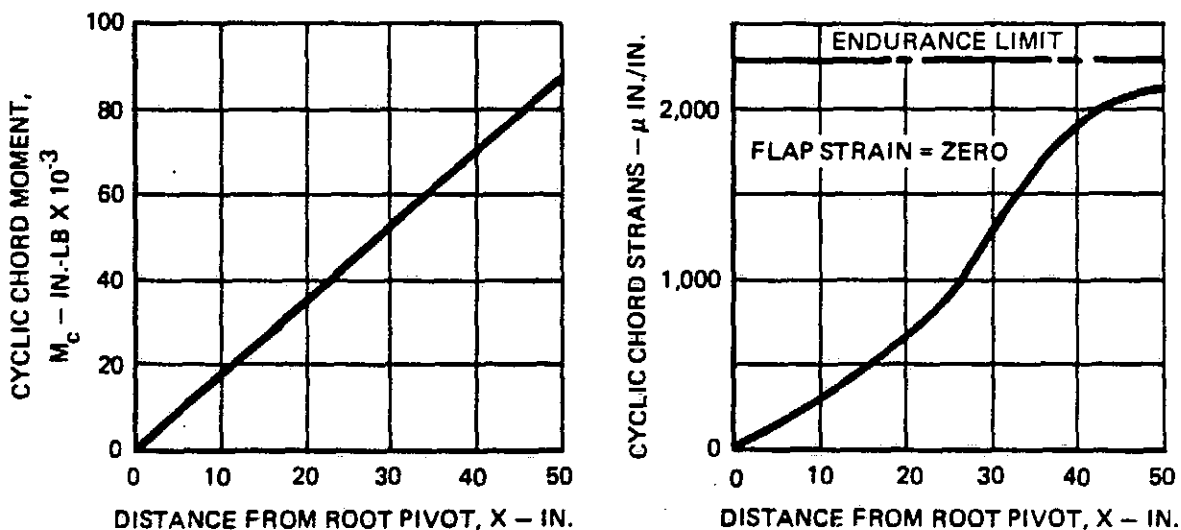


Figure 72. Fatigue Strength of Torque Sleeve in Chordwise Bending

NATURAL FREQUENCIES

First flapwise and chordwise frequency were calculated with the equations,

$$(\omega_{\beta})^2 = (\omega_{\beta_0})^2 + (1 + \frac{e_{\beta} \sigma_{\beta}}{I_{\beta}}) \Omega^2 ,$$

$$(\omega_{\zeta})^2 = (\omega_{\zeta_0})^2 + (\frac{e_{\zeta} \sigma_{\zeta}}{I_{\zeta}}) \Omega^2 .$$

Nonrotating frequencies were determined simply from the static droop in flap and chord with the system shown in Figure 73.

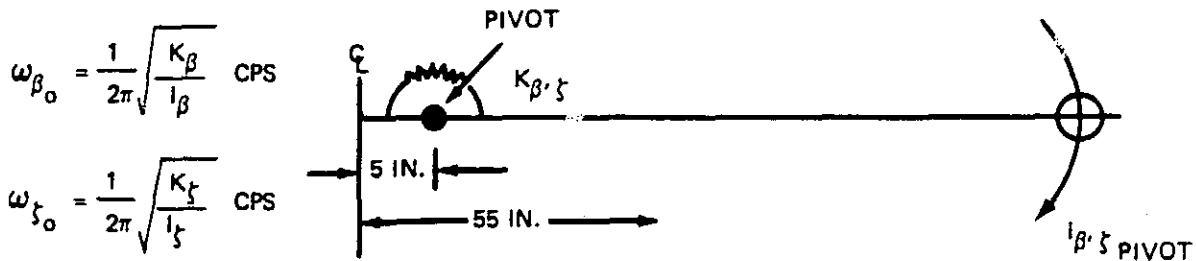


Figure 73. Determination of Nonrotating Frequency

From the hub tilt stiffness of 150,000 ft-lb/radian, from the equation  $\frac{MH}{\beta} = 2(CF.e + K_{\beta})$  where  $e = 5$  inches,  $K_{\beta}$  can be deduced to be equivalent to 9,162 in.-lb/radian. From a static chord moment stiffness analysis,  $K_{\zeta}$  has been estimated at  $4.1 \times 10^6$  in.-lb/radian.

From the rotor blade properties shown in Figure 21, a first mass moment ( $\sigma$ ) about the pivot of 71.394 lb sec<sup>2</sup> and a second mass moment ( $I$ ) about the hinge of 13,308 lb-in. sec<sup>2</sup> have been calculated.

From the equations above, first-mode flapwise and chordwise frequencies at  $\Omega = 295$  rpm of  $1.015\Omega$  and  $0.59\Omega$  have been calculated.

## PITCH-LAG COUPLING

From the structural analysis for the hub flexures, a shear pivot load of  $434 \pm 1,680$  pounds for  $\pm 4.3$  degrees of flapping is available for mechanical pitch-lag coupling. With a vertical pivot offset of 3 inches, a cyclic pitching moment of 1,172 in.-lb per degree of flapping is available. Acting against the control system stiffness of 500,000 in.-lb/radian, 0.13 degree of pitch per degree of flapping is available as an equivalent pitch-lag coupling of 7.7 degrees; this is shown in Figure 62 to match the coupling produced by the zero precon/negative predroop combination used to provide adequate hover stability in the BMR B0-105 configuration. The coupling provided by the offset shear pivot, unlike the BMR, is independent of collective and thrust and should not exhibit the degraded stability of the BMR B0-105 shown in autorotation and on the ground.

## PRELIMINARY LIFE ASSESSMENT

The structural analysis has demonstrated that all hub components considered have infinite life provided that the endurance limit flapping of 4.3 degrees is not exceeded. A complete life assessment requires the definition of a mission flight profile and fuselage characteristics (such as shaft tilt) optimized to suit the flight profile. This is beyond the scope of this study.

## PRELIMINARY FLYING QUALITIES ASSESSMENT

The development of the selected configurations has resulted in a hub moment stiffness of 150,000 ft-lb/radian, primarily due to striving to better meet the goals set by the government. According to the Boeing Vertol criterion that "at least two-thirds of the control moment sensitivity at 1-g level flight must be available at all times," a hub stiffness of the order of 250,000 ft-lb/radian is required for the YUH-61A aircraft. Accordingly, hub stiffness may require increasing; however, a compromise in endurance limit flapping will result. For maneuverability, the product of hub stiffness and endurance limit flapping may be the proper criterion.

The YUH-61A rotor shaft has an endurance limit bending of  $\pm 20,000$  ft-lb, at which the aircraft demonstrates excellent maneuverability characteristics. The hub stiffness of the YUH-61A was 487,000 ft-lb/radian and endurance limit flapping 2.35 degrees. The ITR/FRR goals of 120,000 ft-lb/radian (max) and  $\beta_{EL}$  of 5 degrees results in an endurance limit hub moment of 10,500 ft-lb, only one-half of that available for the YUH-61A; however, the characteristics for the ITR hubs exceed this value by 7 percent.

### VIBRATION ASSESSMENT

Vibration is believed to be the result of blade root loads, hinge offset, hub transmissibility, and fuselage dynamic structural response. Blade-induced loads and fuselage dynamic response are a function of their dynamic characteristics, for which definition is beyond the scope of this effort. Discussion is therefore restricted to a qualitative assessment of hinge offset and hub transmissibility.

The ITR/FRR concept hub stiffness characteristics define an equivalent flap hinge offset for an articulated rotor of 12 inches or 4 percent of the radius. This is compared to 4.7 percent for the Blackhawk as shown in Table 6.

The hub concepts with stacked dual beams exhibit lower shear stiffness characteristics than the single cantilever types. Hub impedance to shear loads may be expected to increase, thus decreasing vibration caused by vibratory blade root shears. This characteristic should be investigated.

### VULNERABILITY ASSESSMENT

Graphite has been used as a primary reinforcement to the composite matrix to best meet the hub stiffness, endurance limit flapping, and torsional stiffness goals. Ballistic and damage tolerance has therefore been compromised due to the brittleness of the fiber. Structural redundancy through the 4-beam concept is relied upon for ballistic tolerance. The vulnerability assessment conducted earlier and shown in Figure 63 still

applies to the developed concept, resulting in a total mean vulnerable area for the hub of 692 square inches.

The next phase of the ITR/FRR program should evaluate through newly developed optimization techniques the effects of changing to fiberglass as the prime reinforcing fiber to achieve the benefits of its superior ballistic and damage tolerance.

### CONFORMANCE WITH GOALS AND SPECIFICATIONS

Resulting conformance with hub goals and specifications for the selected developed concepts is summarized in Table 13.

A reevaluation of hub drag and fabrication cost is included as follows.

#### HUB DRAG

An evaluation of the actual hub drag of the concept was made after optimizing the torque sleeve geometry. As shown in Figure 74, the total estimated drag is 2.93 square feet, assuming an unfaired center section and optimized blade shank twist. This low drag was achieved primarily by minimizing the frontal area, with the result that the shanks account for 40 percent and the center section, pitch links, and shaft account for the remaining 60 percent. Refinement of the design by fairing and cleaning up the center section should achieve the 2.8-square-foot goal. Control positions for hub drag evaluation are presented in Figure 75 and show a drag at 9 degrees of collective pitch required at 170 knots true airspeed. Cyclic pitch trim setting, however, must be considered in the preliminary design phase of the ITR/FRR since it is demonstrated by the test data for elliptical shanks (Figure 76) to be significant.

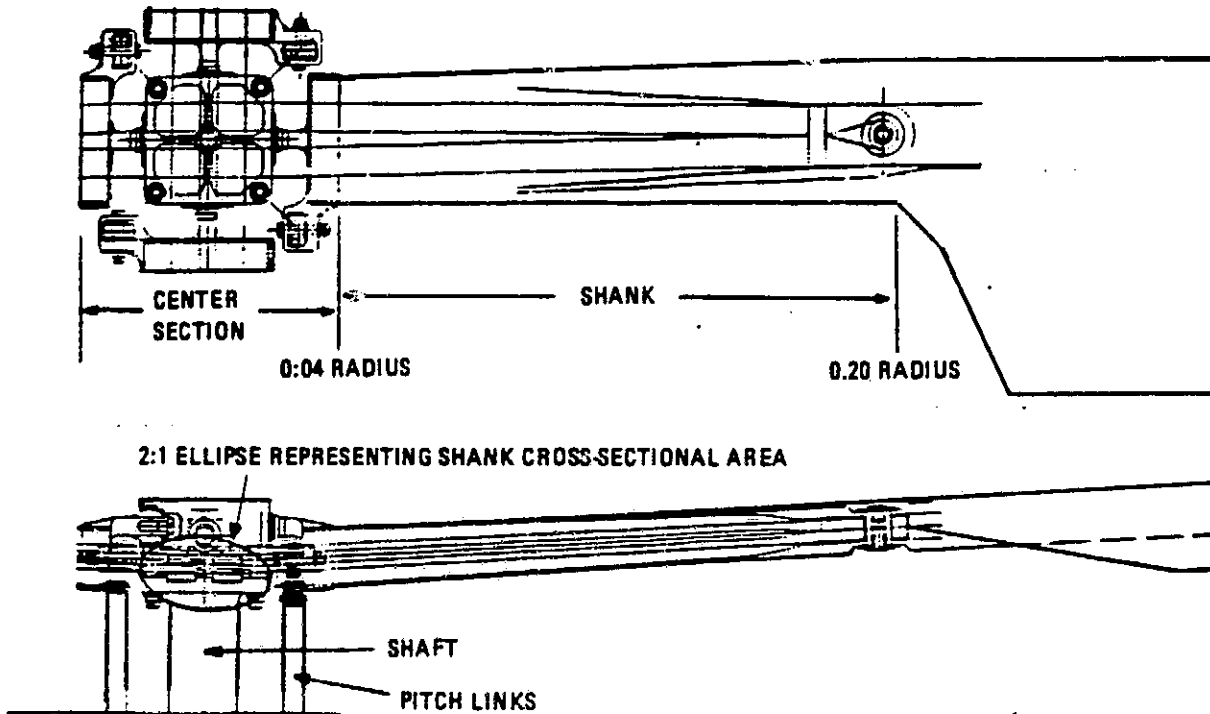
#### MANUFACTURING COST

An estimate to fabricate quantities of the hub flexures with filament-winding techniques was obtained from a subcontractor.

TABLE 13. CONFORMANCE WITH DESIGN GOALS AND SPECIFICATIONS

Parameter	Units	Goal	Achievement	Remarks
Design Gross Weight	lb	16,000 to 23,000	16,000	-
Design Envelope	g's	+3.5 to -0.5	+3.5 to -0.5	-
Stability	-	Stable	Stable	YUH-61A
No. of Blades	-	4	4	-
Adaptable to Fold	-	Rapid manual	Rapid manual	2-pin removal
Hub Drag	ft <sup>2</sup>	2.8	2.93	-
Hub Weight	% DGW	2.5	1.9	-
Parts Count	-	50	47	-
Hub Moment Stiffness	ft-lb/rad	100,000	150,000	Rigid blades
Min Hub Moment	ft-lb	10,000	11,256	No fatigue damage
Min Hub Tilt (EL)	deg	5	4.3	Rigid blades
Aux Damping	-	Provisions for	Possible	Elastomeric
Torsional Stiffness	in.-lb/deg	150	108	UH-60 goal
Fatigue Life	hr	10,000	>5,700	>10 <sup>8</sup> cycles endurance
Reliability	hr	3,000	>3,000	-
Mfg Cost	\$	Minimize	85,000	1,000 acft

ORIGINAL PAGE IS  
OF POOR QUALITY



DRAG BREAKDOWN

ITEM	$C_D$	A (ft <sup>2</sup> )	$K_{ROT}$	$F_g$ (ft <sup>2</sup> )	COMMENTS
CENTER SECTION	0.88	1.47	-	1.29	UNFAIRED
SHAFT	0.40	0.43	-	0.17	
PITCH LINKS	1.17	0.11	1.01	0.26*	
SHANK	0.3	1.84	1.1	1.21*	OPTIMUM SHANK TWIST
TOTAL				2.93 FT <sup>2</sup>	

$$*F_g = 2 C_D \times A \times K_{ROT}$$

(1) A. = FRONTAL AREA

(2)  $K_{ROT}$  = FACTOR ACCOUNTING FOR ROTATIONAL EFFECTS

Figure 74. Drag Estimate for Example ITR Hub Design

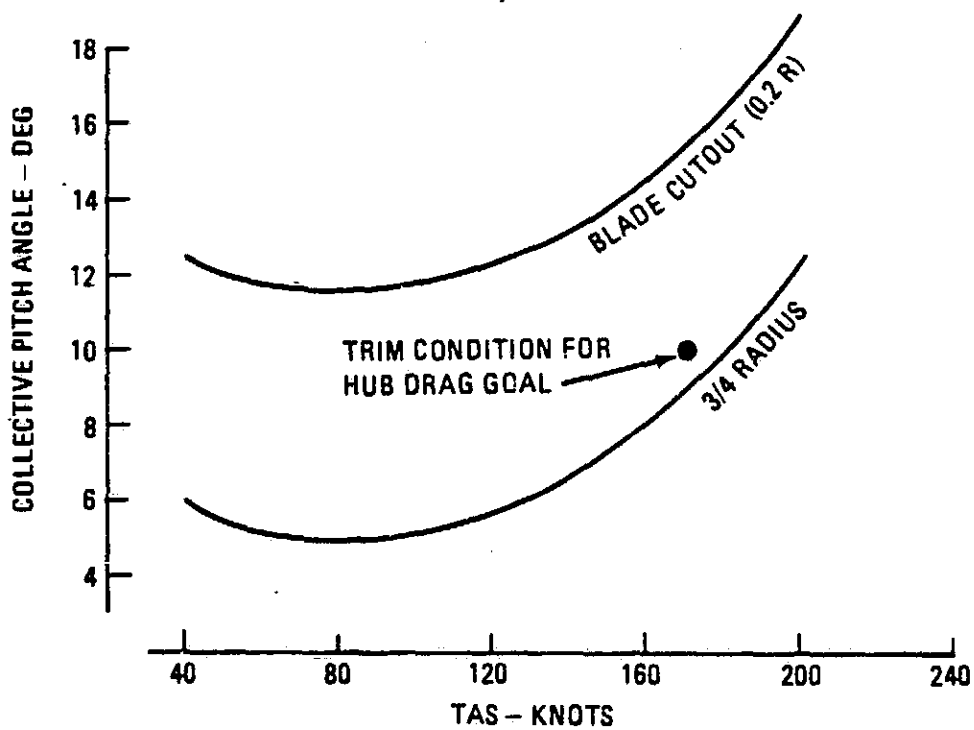
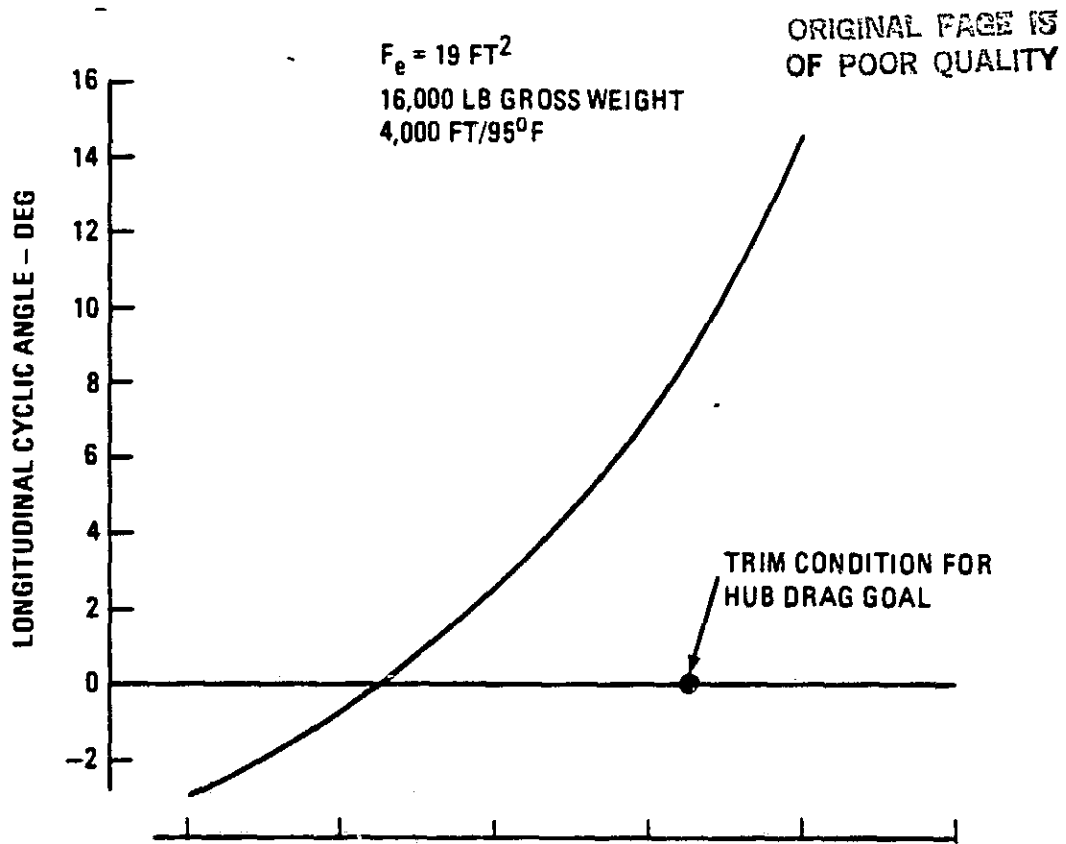


Figure 75. ITR Control Positions for Hub Drag Evaluation

7/10 SCALE MODEL HUB  
ELLIPTICAL OUTBOARD SHANKS

ORIGINAL PAGE IS  
OF POOR QUALITY

BVWT 261  
180 KT  
0° SHANK COLLECTIVE  
10° LATERAL CYCLIC

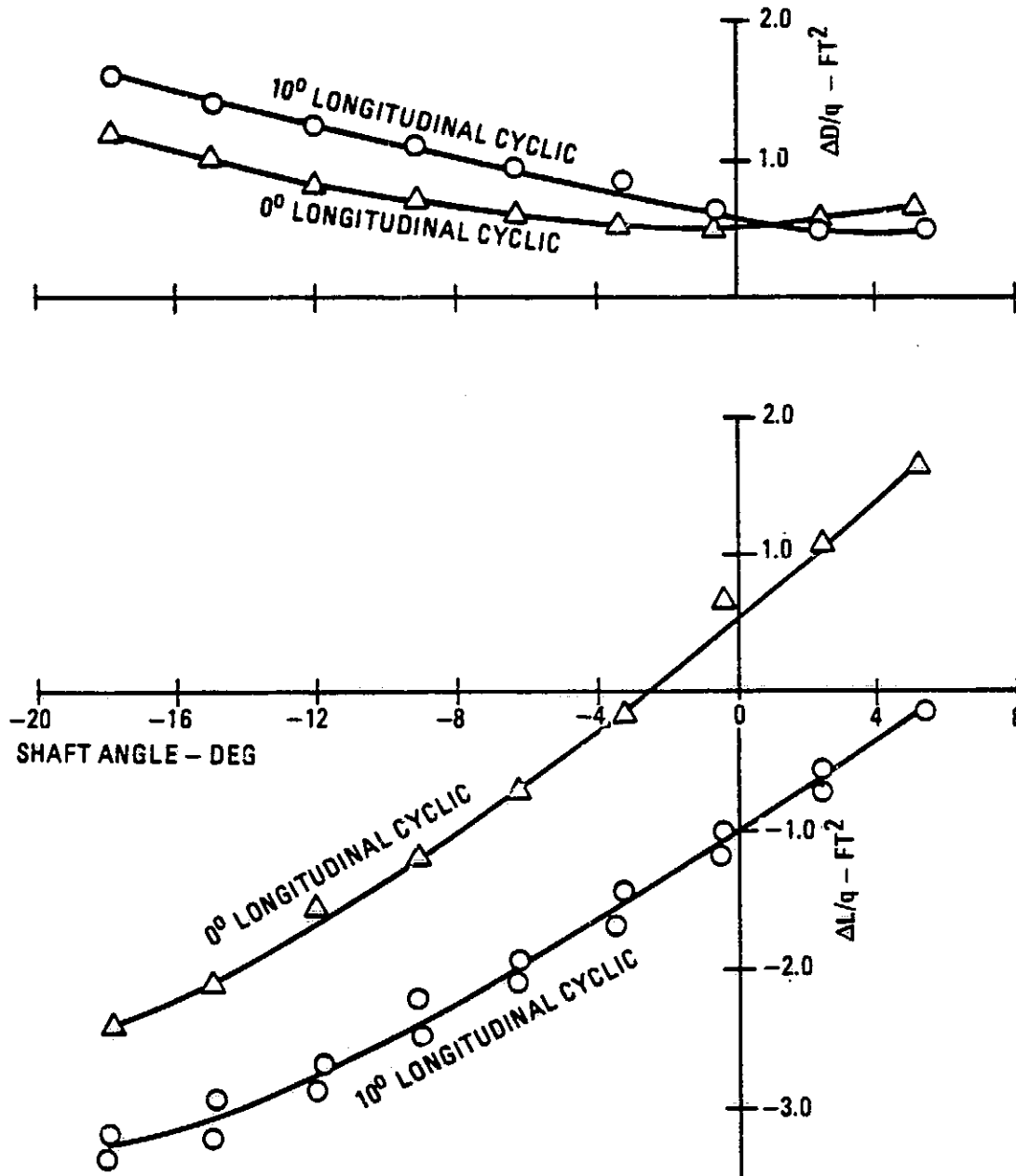


Figure 76. Effect of Longitudinal Cyclic Pitch on Shank Drag and Lift

ORIGINAL PAGE IS  
OF POOR QUALITY

One thousand aircraft sets were considered over the 4-year period 1985 through 1988. Estimates were made from the assembly drawings presented in this report and do not include the cost of assembling the straps into the hub.

Fabrication in either graphite or Kevlar was considered.

TABLE 14. COSTS OF MANUFACTURING HUB FLEXURES

	Graphite	Kevlar
1985	\$ 5,234,000	\$ 5,789,000
1986	4,637,000	5,105,000
1987	4,602,000	5,064,000
1988	<u>4,717,000</u>	<u>5,186,000</u>
Total	<u>\$20,216,000</u>	<u>\$22,208,000</u>
Average per Hub	<u>\$20,216</u>	<u>\$22,028</u>

The current design requires 16 subcomponents for each strap assembly and it is believed by the potential subcontractor that design improvements conducted in the preliminary design phase will result in a reduction in the number of composite parts.

An estimate of the metallic hub components results in \$27,500 per set, with hub assembly and checkout an additional \$15,000. The torque sleeves are expected to add \$22,250 per aircraft set, resulting in a total of \$85,000 for the completed hub system.

## EVALUATION OF THE CANDIDATE CONFIGURATIONS

An evaluation of the candidate configurations was made by the Boeing Vertol Manufacturing Technology Organization and Project Engineering.

### PRODUCIBILITY

The design of the composite flexures is such that filament-winding, automatic tape layup, braided fiber, and die-cut broadgoods techniques are applicable. Table 15 presents an assessment which shows that filament-winding or die-cut broadgoods are the preferred methods of fabrication. Die-cut broadgoods, however, would require minor changes to the concepts to replace the filament wraparound at the blade attachment by an interleaved bias-ply  $\pm 5$ -degree unidirectional arrangement with a punched hole. Both the selected methods have been widely demonstrated in the fabrication of rotor blades.

Die-cut broadgoods would allow the use of fiber-reinforced thermoplastic composites if required to enhance damage tolerance through additional matrix toughness.

### QUALITY CONTROL REQUIREMENTS

Standard material quality control and storage requirements would be necessary. In-process evaluation would include both the usual ultrasonic and x-ray techniques.

### TOOLING CONCEPTS AND COSTS

#### Flexures

Figure 77 presents a typical tooling and manufacturing plan for the filament-winding process. A 4-axis winder would be required with significant

TABLE 15. ANALYSIS OF COMPOSITE HUB MANUFACTURING METHODS

Technique	Equipment	Material Forms	Special Tooling	Curing Process	Machining	Dimensional Control	Inspectability	Risks	Cost
Filament Winding	Winder 4-axis NC controlled	Prepreg roving (0° and ±10°)	Wind fixt Cure fixt	Rubber exp Thermoset	Resin flash removal	Critical	X-ray tracer Ultrasonic	Concept demonstrated	Nonrec high Recurring low
Automated Tape Layup	Tape winder 4-axis NC controlled	Prepreg Tape (0°) Tension strap Net width Secondary cloth wrap	Wind fixt Cure fixt	Rubber exp Thermoset	Resin flash removal	Critical	X-ray tracer Ultrasonic	Not demo Variable strand length may cause fiber distortion	Nonrec high Recurring low
Braided Fiber Preform		Dex fiber preform Liquid resins	Cure fixture	Closed die	Hone	Critical	Ultrasonic	Not demo Vendor dependent	Nonrec low Recurring high
Broadgoods	Rule Die-cutter Robot for ply stacking	Prepreg ±5° uni + bias plies at ends	Cure fixture	Rubber exp Thermoset	Resin flash removal	Critical	X-ray tracer Ultrasonic	Concept demonstrated	Nonrec med Recurring low

FLEXURE FABRICATION  
BY FILAMENT WINDING

ORIGINAL PAGE IS  
OF POOR QUALITY

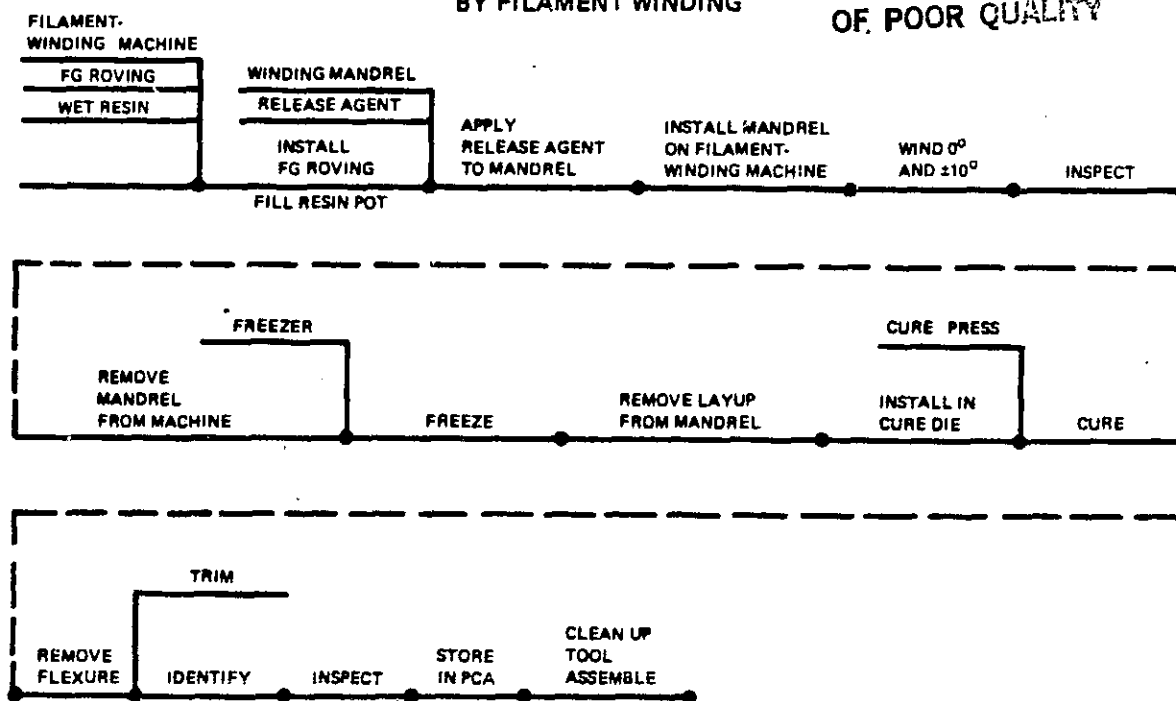


Figure 77. Typical ITR Tooling and Manufacturing Plan

nonrecurring costs. Winding mandrels would be metallic for stiffness and durability and to facilitate the installation of heaters for improving the tack of prepreg rovings.

The cure die would be a steel mold for durability and cure pressure would be applied by internal silicone rubber through metal cauls contoured to suit augmented by the press (Figure 78).

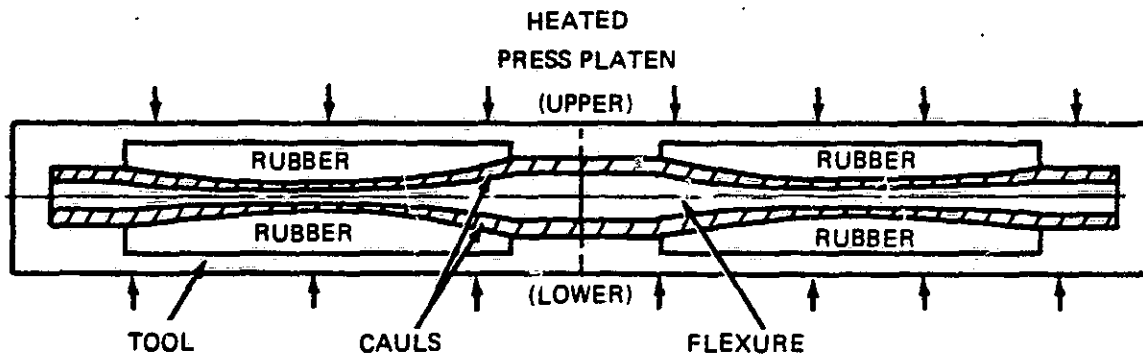


Figure 78. Flexure Tooling Concept

For the die-cut prepreg broadgoods concept, at each end the wraparound filament concept is replaced by drilled-through  $\pm 10^\circ/\pm 45^\circ$  interleaved broadgoods. Each flexure requires two sets of 113 different ply shapes. Each half-set is robot-stacked starting with the continuous plies on the outside with  $\pm 45$ -degree interleaved at each blade attachment end. The center buildup together with the midspan and the remainder of the interleaved  $\pm 10^\circ/\pm 45^\circ$  at the ends are then added as illustrated in Figure 79.

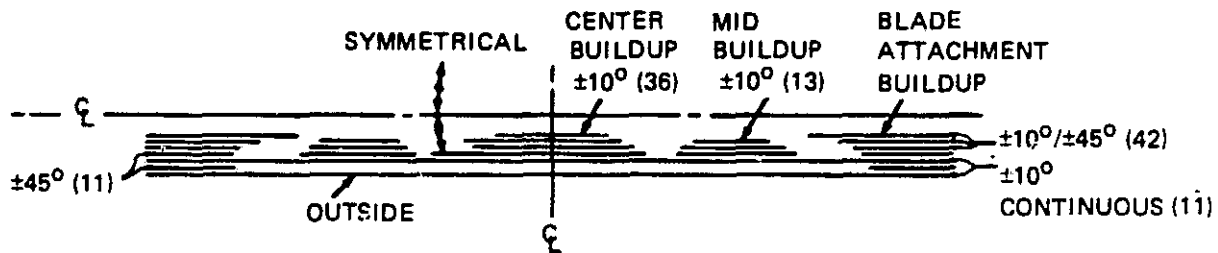


Figure 79. Schematic for Broadgoods Ply Stacking (358 Plies, 113 Patterns per Flexure)

The robot-assembled stack of plies is then precompacted at  $200^\circ \pm 10^\circ\text{F}$ , frozen, and removed from the compaction die and stored. The assembly is cured in the tool shown in Figure 78 at  $350^\circ\text{F}$ .

Cost of the flexure tooling hardware would be moderate since dimensions are critical,  $\pm 0.015$  inch in minimum thickness, necessitating contoured metal tooling.

For the filament-winding process a 4-axis machine would be designed and programmed for this operation. This cost may be high. For the die-cut broadgoods concept, rule dies are inexpensive and durable (500 sets between sharpening); however, with extensive use of IDS and CAD/CAM a Gerber-type cutting machine may be used. Robots for ply transfer and positioning are already becoming state of the art.

### Hardware

Upper and lower hub plates and pitch arms would be precision-forged from titanium, together with the contoured inserts. For quantity production this would be cost-effective; however, the first test and development articles would be machined from solid billets.

### Torque Sleeves

Conventional filament-winding techniques would be used for the torque sleeves. Machines would be off-the-shelf commercial types. Tooling would be heated metal dies and internal expanded-rubber pressure techniques would be used.

### Material Costs

Each flexure weighs approximately 10 pounds and two are required for each hub assembly. At \$90.89 per pound for graphite prepreg, the cost per rotor for flexures would be \$1,800.

The torque tubes would weigh approximately 25 pounds each if fabricated from fiberglass and 18 pounds if made from Kevlar. At four per rotor set, the material cost would be \$1,500 or \$3,400 for fiberglass or Kevlar, respectively.

Exclusive of forging cost, hub hardware material would amount to \$2,600 per aircraft.

Material costs would total approximately \$7,800 per aircraft.

### Fabrication and Assembly Costs

These costs were addressed in the paragraph entitled Conformance With Goals and Specifications.

### INSPECTABILITY

In-service visual and ultrasonic nondestructive inspections require removal of the blade and torque sleeve. Visual and ultrasonic pulse-echo inspection of the torque sleeve could be conducted in situ.

For the metal components of the shaft attachment, only removal of a hub cover would permit dye check of the upper and lower hub plates. Hub retention bolts would have visual crack-detection indicators currently used on such critical items; blade attachment bolts would be similarly treated. Inspection of the blade flexure socket and main retention bushings would be conducted after removal of the blade and torque sleeve.

### MAINTAINABILITY AND RELIABILITY

Maintainability and reliability have been addressed earlier during the evaluation of the five concepts.

## FRR CONFIGURATION VARIATIONS

FRR hub configurations which have potentially high research payoff have been established. These consist of investigations into rotor stability and the effect of changes in hub dynamic characteristics.

### ITR HUB MODIFICATIONS

#### Variations in Lag-Flap and Pitch-Flap Coupling

The coupling of flap bending with lag and pitch motion can be altered in two ways. The built-in flexure pitch angle and the blade sweep angle can both be varied to change the couplings which affect aeroelastic stability.

The effect of propitch angle on stability has been investigated analytically, References 4 and 5, and experimentally, References 6 and 7. In 1973 Huber of MBB found from a computer simulation study that rotation of the blade principal axes relative to the fixed root end, which gives lag-flap and to a lesser extent pitch-flap coupling, can be used to modify the rotor system stability characteristics. This investigation (Reference 4) was conducted with the B0-105 hingeless rotor. Staley and Miao (Reference 5) looked at the effect of lag-flap coupling on the BMR with the C-45 stability analysis program. They found that increasing lag-flap coupling (defined as blade lag due to flap up) was stabilizing for all cases considered. This effect is achieved on the BMR by installing the flexures at a built-in pitch angle at the hub (Figure 80); thus, when the blade flaps up it also lags back due to the inclination of the principal axes.

4. Huber, H.B., EFFECT OF TORSION-FLAP-LAG COUPLING ON HINGELESS ROTOR STABILITY, Preprint 731, 29th Annual Forum of the American Helicopter Society, Inc., 1325 18th Street, N.W., Suite 103, Washington, DC 20036, May 1973.
5. FLIGHT EVALUATION OF LOADS AND STABILITY CHARACTERISTICS OF A BEARINGLESS MAIN ROTOR, PRELIMINARY DESIGN, VOLUME A, Boeing Document D210-11129-1, Boeing Vertol Company, P. O. Box 16858, Philadelphia, Pennsylvania 19142, September 1976.

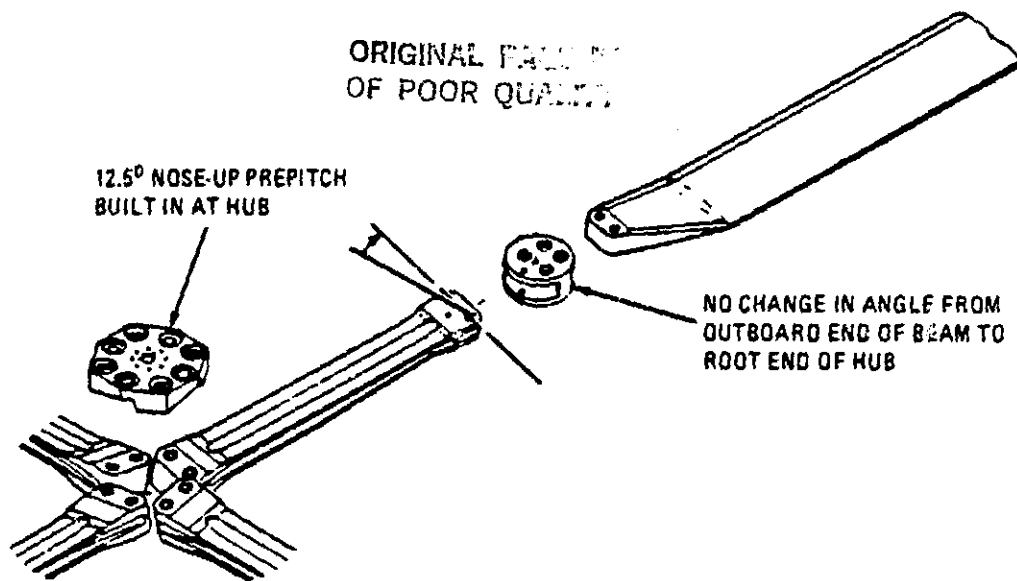


**Figure 80. Rotation of Flexure Principal Axis Gives Positive Flap-Lag Coupling**

The same effect was determined in several test cell and wind tunnel investigations. A 1/5.86 Froude-scale model of the BMR was tested in the wind tunnel, Reference 6, with and without a built-in hub prepitch angle. The results, Figure 81, confirm that the positive flap-lag coupling which results from the nose-up built-in prepitch angle is stabilizing. This result was duplicated for a low-hinge-offset bearingless rotor, BMR II, Reference 7, in a hover test cell.

The analytical and test results presented indicate that for the FRR the effect on stability of relative prepitch angle between the hub, flexures, and blade would be an interesting parametric variation. ITR predesign configuration 1B has prepitch while the other predesign concepts do not.

6. Chen, C., and Staley, J.A., FLIGHT EVALUATION OF LOADS AND STABILITY CHARACTERISTICS OF A BEARINGLESS MAIN ROTOR, 1/5.86 Froude Scale Model Test Results, Boeing Document D210-11245-1, Boeing Vertol Company, P. O. Box 16858, Philadelphia, Pennsylvania 19142, June 1977.
7. Gardner, B., and Sheffler, M., BMR-II WIND TUNNEL MODEL TEST: STABILITY DATA ANALYSIS, Boeing Document D210-11488-1, Boeing Vertol Company, P. O. Box 16858, Philadelphia, Pennsylvania 19142, November 1979.

For the FRR, the prepitch could be added or removed depending on the final ITR configuration selected. Since prepitch involves a potential tradeoff between aerelastic stability and hub weight, drag, and complexity, this could be an important parametric variation.

BMR I - 1/5.86 FROUDE SCALE MODEL TESTS

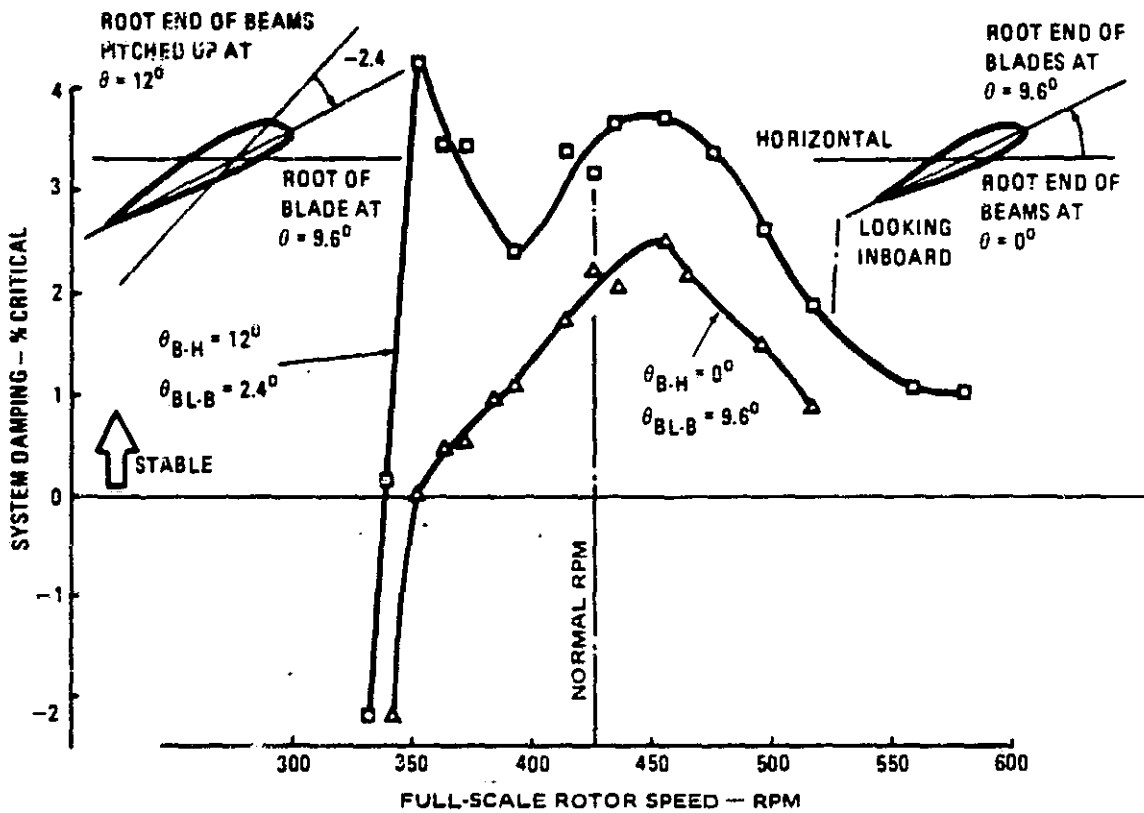


Figure 81. Effect of Beam-to-Hub Pitch Angle on Air Resonance Modal Damping

Blade sweep results in pitch-flap coupling. The effect on stability of sweeping the blade at the blade/flexure attachment point has been reported extensively in the literature. Reference 4 shows that analytically the BO-105 at 100 knots can go from 2.5-percent unstable to 0.5-percent stable damping with the addition of 2 degrees aft sweep. On the other hand, Figures 82 and 83 from References 6 and 7, respectively, show that aft blade sweep is destabilizing in hover. Since aft sweep is similar to  $\delta_3$  in that

ORIGINAL PAGE IS  
OF POOR QUALITY

BMR I - 1/5.86 FROUDE SCALE TESTING

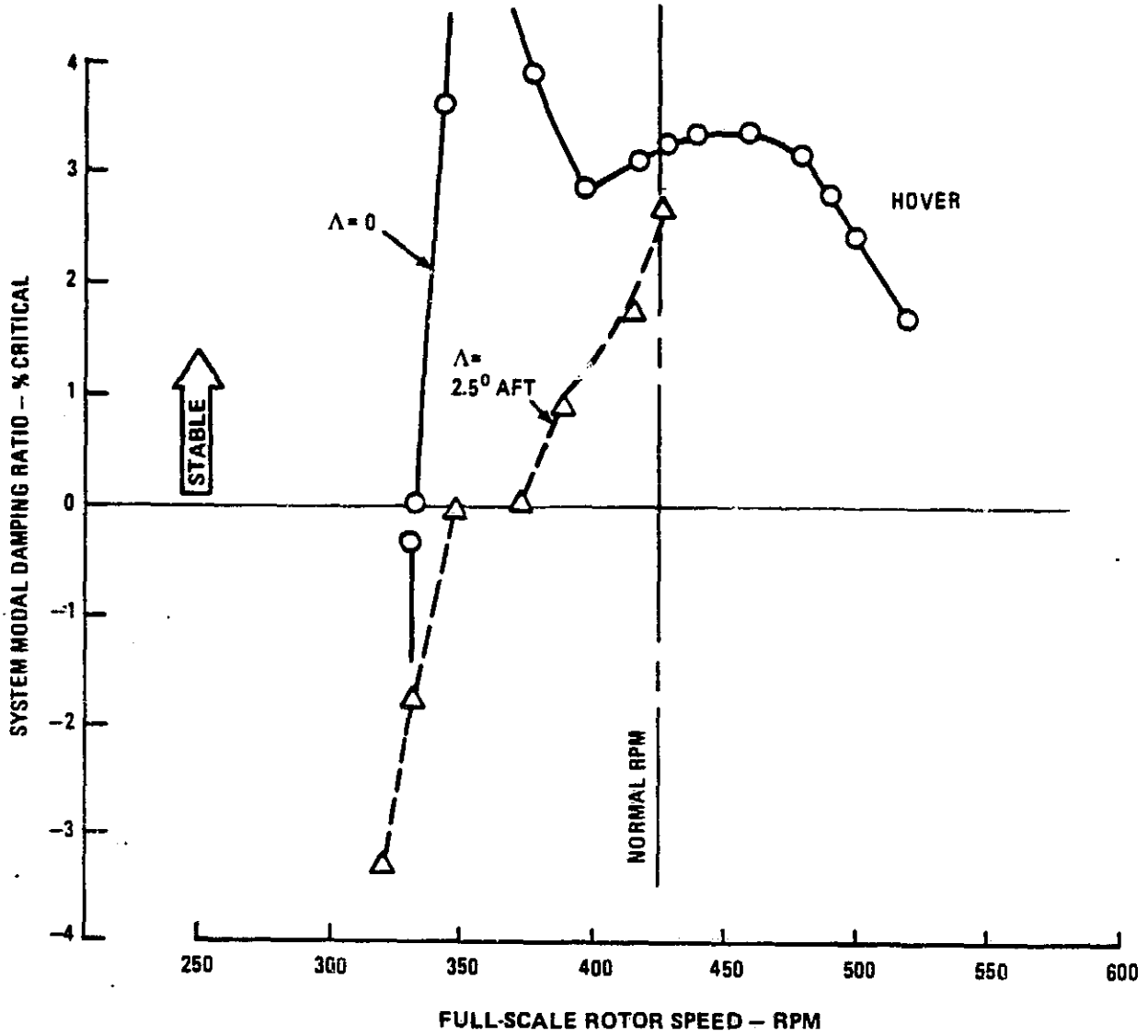


Figure 82. Effect of Sweep on Air Resonance Mode Damping

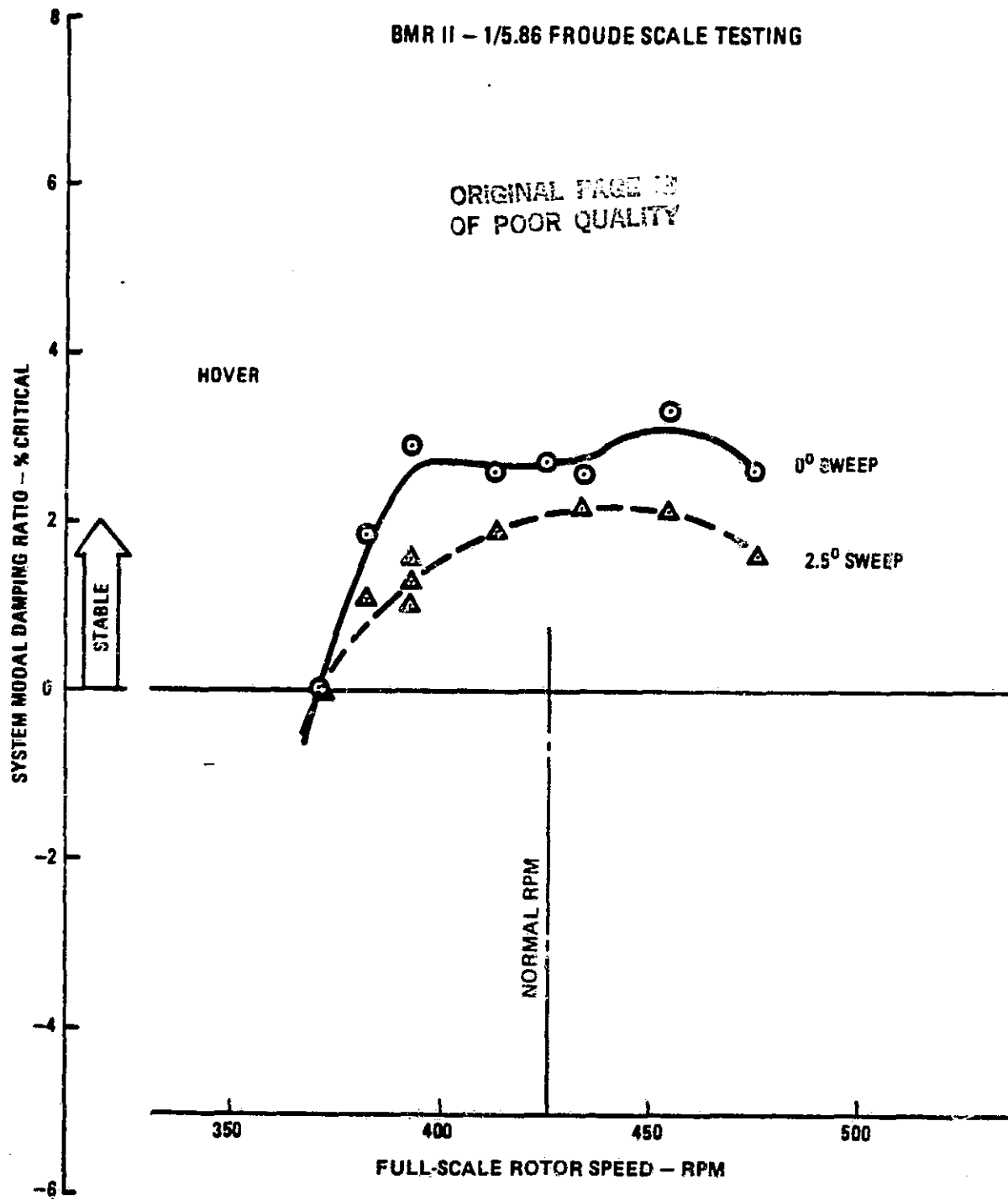


Figure 83. Effect of Sweep Angle on Damping

up flap causes nose-down pitch, this result is contrary to what would be expected. Since sweeping the blade is a relatively simple addition to a production rotor design, its effect on stability should be investigated further.

### Variations in Pitch-Lag Coupling

For the FRR program, three means of altering pitch-lag coupling are envisioned. These are precone/predroop variations, torque sleeve chord stiffness variations, and shear pivot offset variations.

Of these parameters, predroop/precone angle variations have been reported the most in the literature. The results show that precone, a built-in upward slope of the blade pitch axis, is not interchangeable with predroop, which is a bend in the neutral axis of the blade outboard of the pitch bearings or torque tube input. Many combinations of precone and predroop have been analyzed or tested, but not all in the same investigation. Reference 4 analyzed the B0-105 with various precone angles at zero predroop and found that increasing precone angle gave a destabilizing trend. In Reference 5, positive pitch-lag coupling was analyzed as predroop and was found to be stabilizing on the BMR.

Model scale testing also showed mixed results for the effect of precone/predroop variations. Figure 84 from Reference 6 shows that interchanging predroop for precone is highly stabilizing. On the other hand, Figure 85 from Reference 7 shows that changing predroop with precone fixed at zero has little or no impact on stability. Thus, despite a considerable amount of analysis and testing on the effects of predroop and precone angles on stability, it appears that more work is required to understand the optimum combination of these two angles for maximum stability.

Altering the torque sleeve chord stiffness and the shear pivot offset location will change the amount of pitch-lag coupling present. Since this

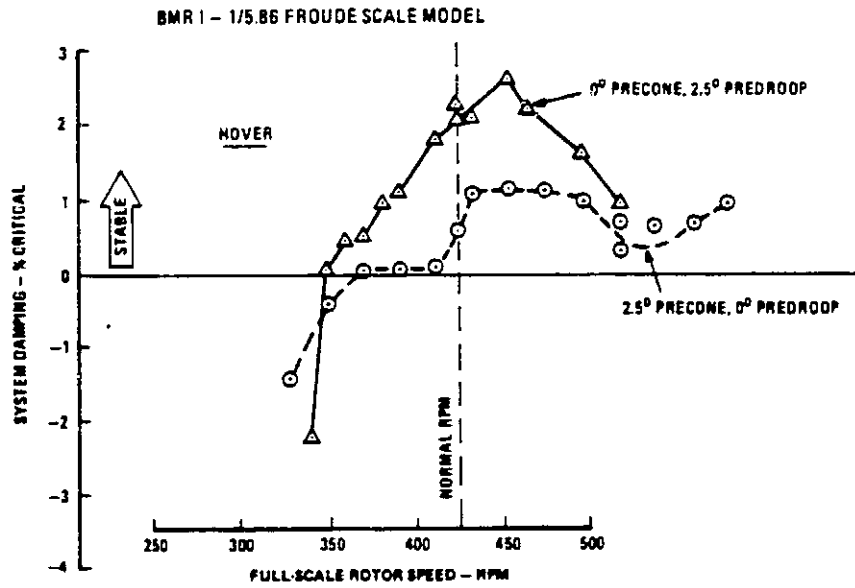


Figure 84. Effect of Blade and Beam Coning Angles on System Damping

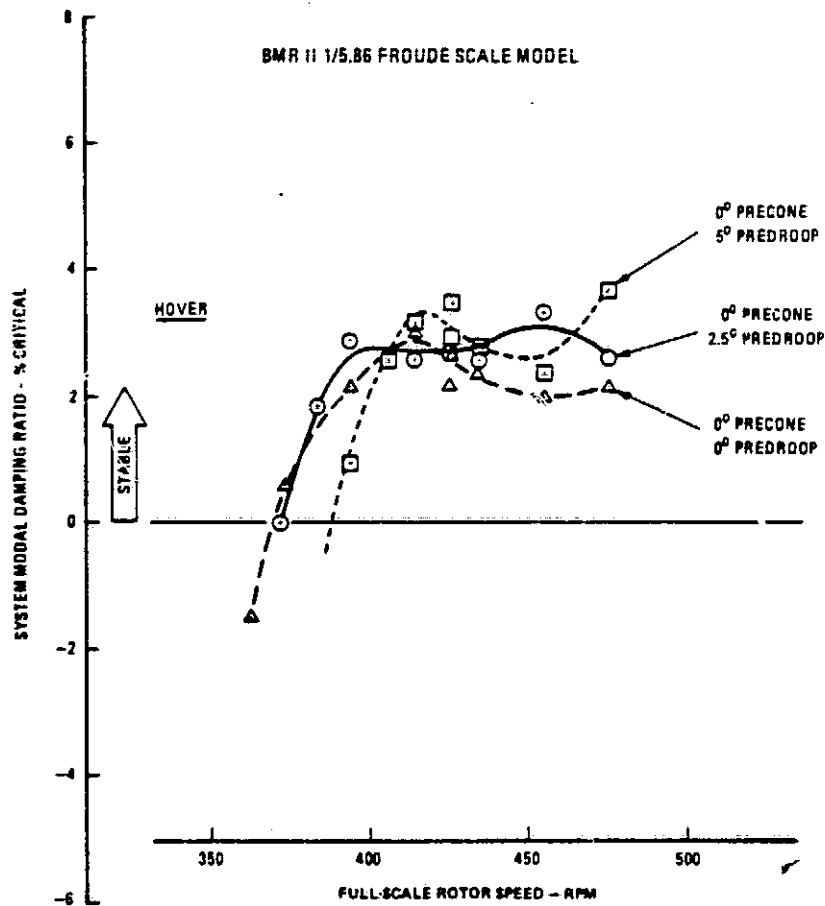


Figure 85. Effect of Predroop Angle on Damping

is a new design concept, the effect of adding pitch-lag coupling to the rotor system in this manner has not previously been analyzed or tested. Since positive pitch-lag coupling has been shown to be stabilizing, increasing the coupling through either of these two parameters should be beneficial. The cost benefit ratio of these parametric variations will be examined during the FRR preliminary design.

### Control System Stiffness Variations

The importance of control system stiffness to aeroelastic stability has been investigated for both hingeless and bearingless rotors, but the results to date have not proven conclusive. It appears that the results may be sensitive to other aeroelastic coupling parameters. Further testing of the effects of control system stiffness seem to be warranted.

In Reference 4 Huber looked at the change in modal damping due to control system stiffness variations. His analysis indicated that a softer control system was beneficial for certain configurations (5-degree precone B0-105), but destabilizing for other configurations (0-degree precone B0-105). Full-scale BMR wind tunnel test results, Reference 8, showed mixed results as well. Figure 86 indicates that a softer control system, achieved with an axially flexible pitch link, did not have a significant effect in hover at normal rotor speed but was destabilizing in forward flight. Model testing at 1/5.86 scale of a low-effective-hinge bearingless rotor, Reference 7, demonstrated a significant improvement in stability when the control system stiffness was reduced by 20 percent with a

8. Sheffler, M., Staley, J., Hoover, J., Sovjak, C., and White, F., FULL SCALE WIND TUNNEL INVESTIGATION OF A BEARINGLESS MAIN HELICOPTER ROTOR: FINAL REPORT, NASA CR152373, National Aeronautics and Space Administration, Washington, DC, October 1980.

BMR ROTOR IN AMES 40-BY-80-FOOT WIND TUNNEL  
425 RPM - NORMAL ROTOR SPEED

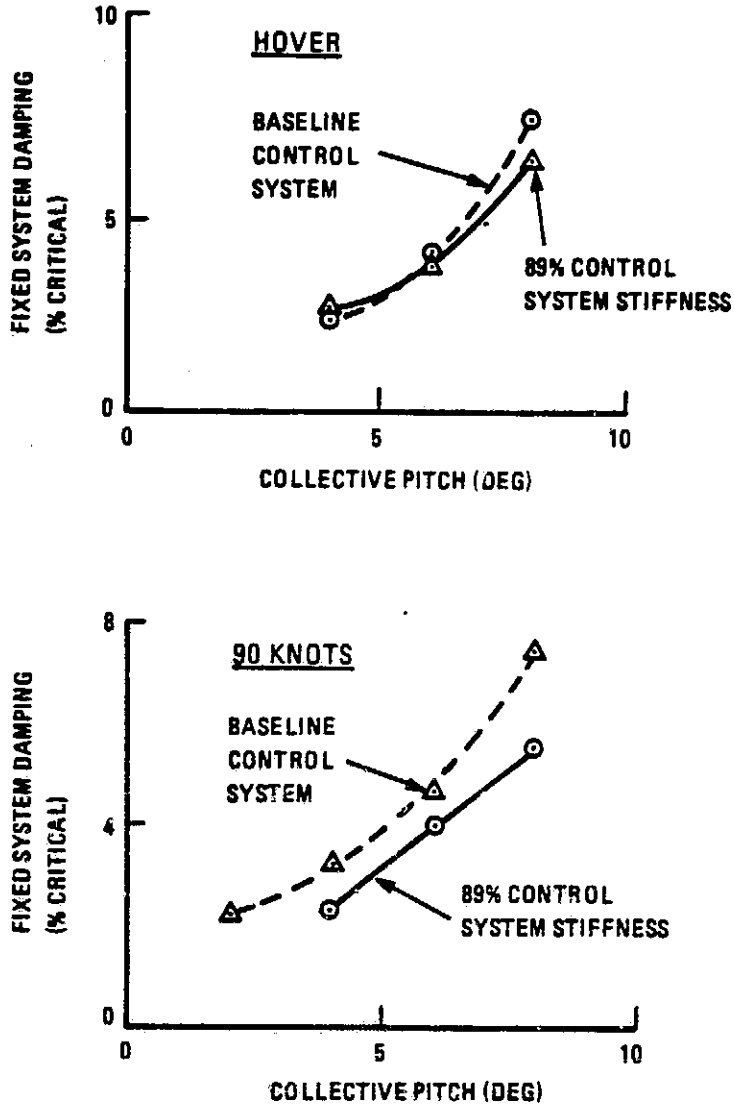


Figure 86. Effect of Control System Stiffness on Stability of the BMR

softer torque rod (Figure 87). The next test of the BMR in the 40- by 80-foot wind tunnel will specifically evaluate the effect of control stiffness. It is evident that this parameter requires additional testing to understand its effect on aeroelastic stability, and this will be considered for the FRR program.

### Auxiliary Damping

A simple means of adding damping to the rotor system was investigated during the first full-scale wind tunnel test of the BMR (Reference 9). As seen in Figure 88, when constrained-layer elastomeric material was added to the inner contours of the BMR flexures, the modal damping was substantially increased; however, this process was never tested in an extended-service-type environment. Because of the high potential cost benefit advantage of this procedure, this variation is considered for the FRR program.

### Natural Frequency Variations

Variations in natural frequencies of the rotor system can affect both aeroelastic stability and vibratory loads. When the first fundamental in-plane frequency is changed, the frequency where the lead-lag regressing mode intersects the airframe natural modes is moved. This alters the stability characteristics of the coupled rotor/airframe modes.

9. Sheffler, M., Warmbrodt, W., and Staley, J., EVALUATION OF THE EFFECT OF ELASTOMERIC DAMPING MATERIAL ON THE STABILITY OF A BEARINGLESS MAIN ROTOR SYSTEM, Preprint I-2, National Specialists Meeting on Rotor System Design, American Helicopter Society, Inc., 1325 18th Street, N.W., Suite 103, Washington, DC, October 1980.

ORIGINAL PAGE IS  
OF POOR QUALITY

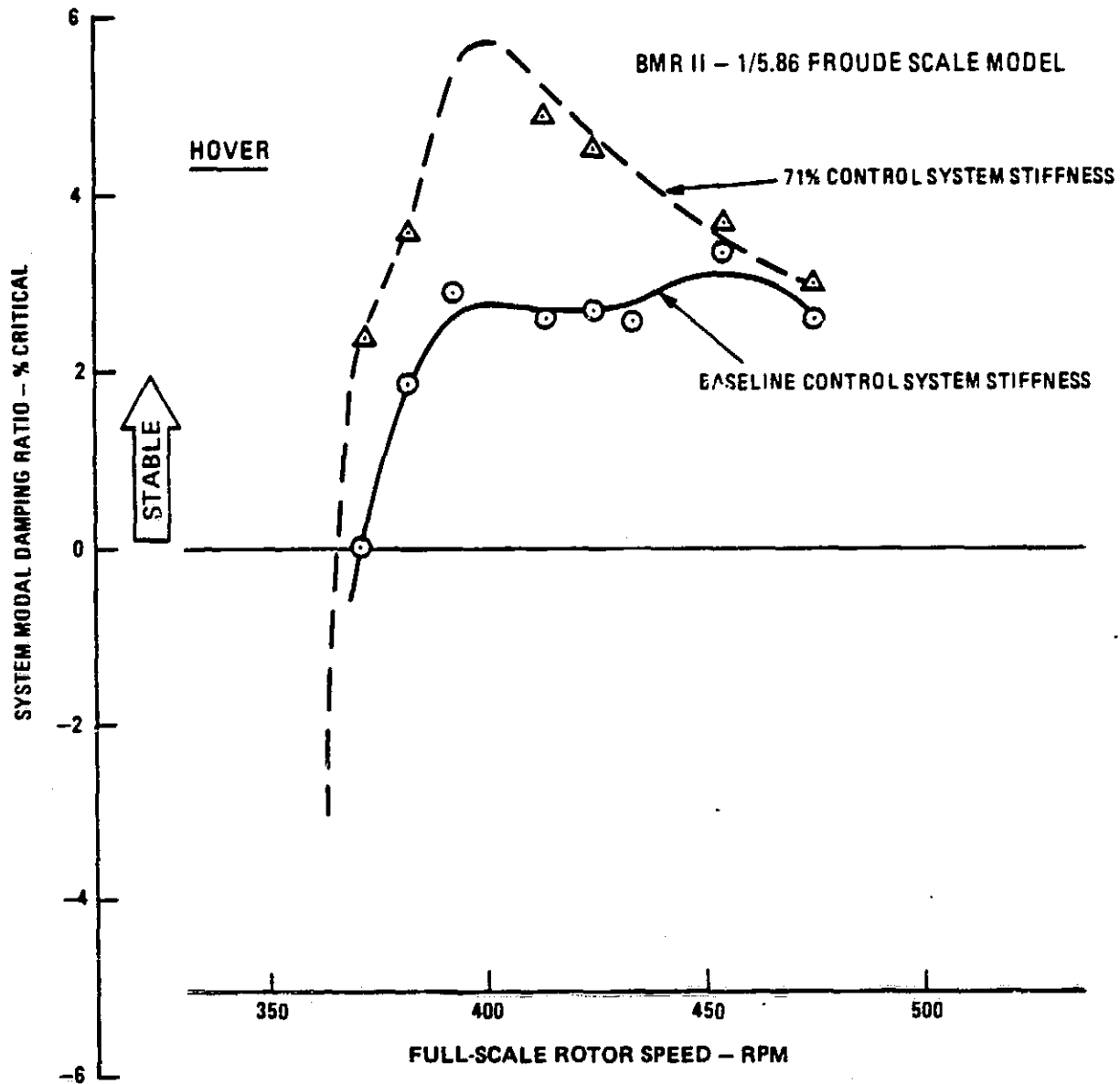


Figure 87. Effect of Control System Stiffness on Damping of the BMR II

ORIGINAL PAGE IS  
OF POOR QUALITY

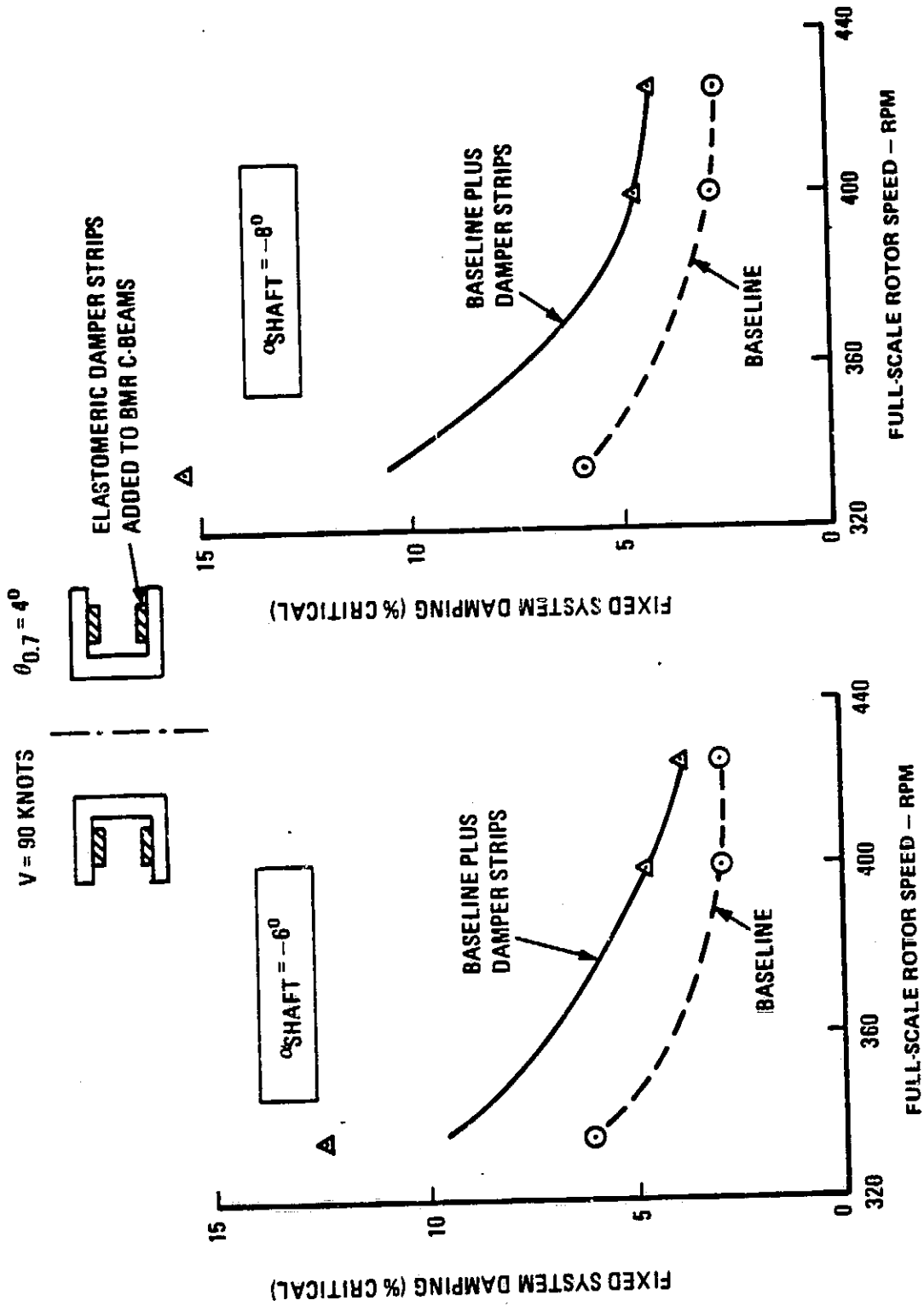


Figure 88. Effect of Adding Damper Strips to BMR C-Beams

## DESIGN APPROACH FOR THE ITR HUB MODIFICATIONS

As in the case of the FRR blade, the FRR hub preliminary design will identify the modifications to the ITR hub which will provide the selected parametric variations for Phase 4 FRR testing.

### Rotor Hub Variable Features

The key hub parametric variations considered are as follows:

- Lag-flap coupling
- Pitch-flap coupling
- Pitch-lag coupling
- Flexure stiffness
- Control system stiffness
- Damping.

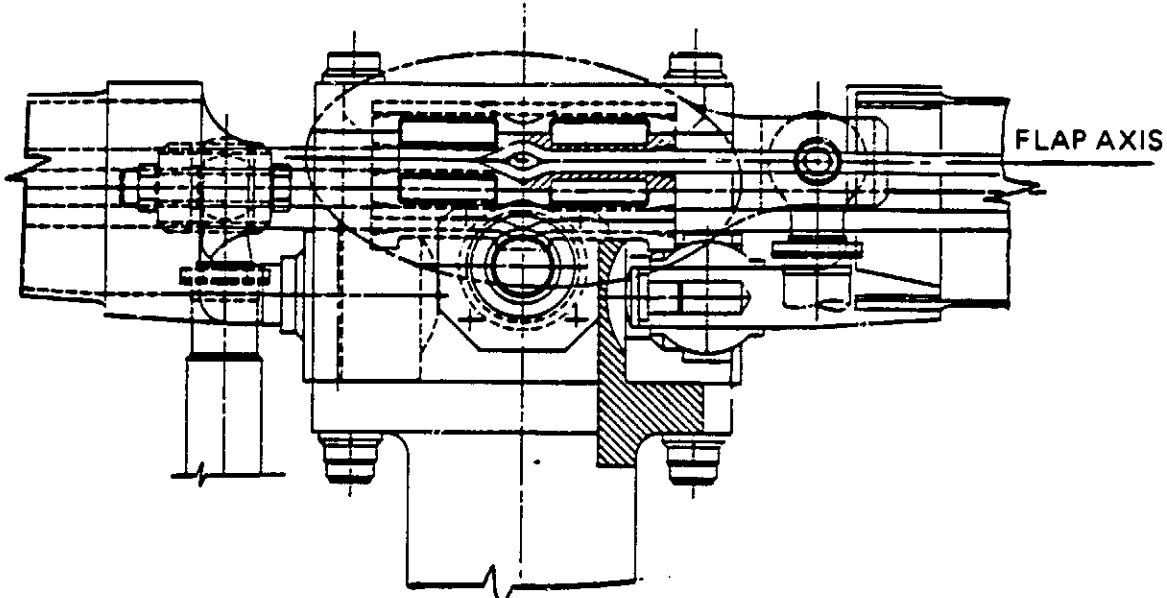
The following discussion offers one or more techniques considered and evaluated for achieving the selected parametric variations.

Lag-Flap Coupling - Lag-flap coupling variations may be accomplished through variations in the flap axis angle (i.e., prepitch of the flexure). Flap axis angle variation testing would be accomplished through comparative testing of ITR hub configurations 1A and 1B as illustrated in Figure 89.

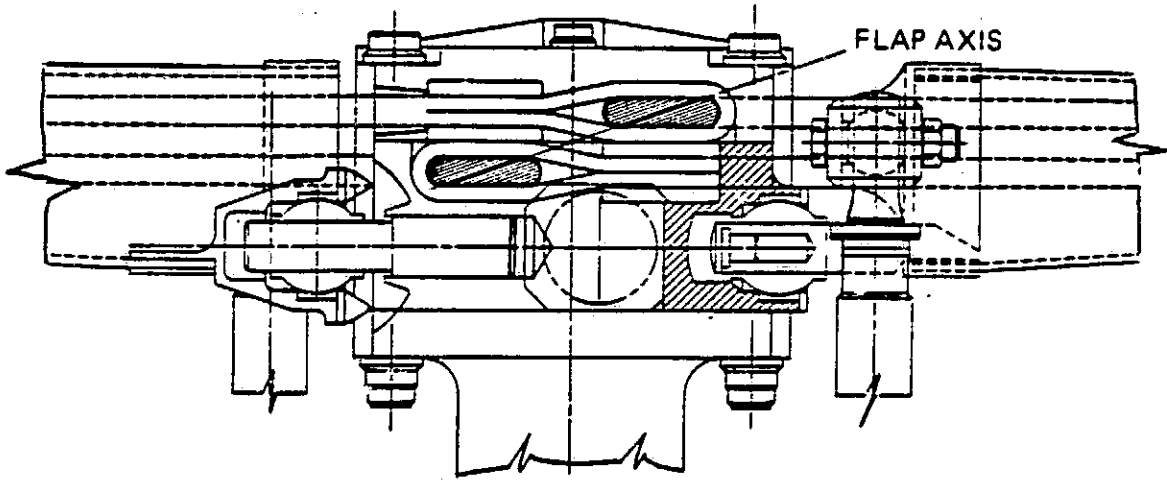
Pitch-Flap Coupling - The ITR hub configuration folding arrangement as shown in Figure 90 would permit blade sweep variations to be tested by rotating and locking eccentric forward and aft folding pins.

Pitch-Lag Coupling - Pitch-lag coupling variations may be accomplished by varying the following hub features:

ORIGINAL PAGE 13  
OF POOR QUALITY



ITR HUB CONFIGURATION 1A



ITR HUB CONFIGURATION 1B

Figure 89. Flap Axis Variation Approach

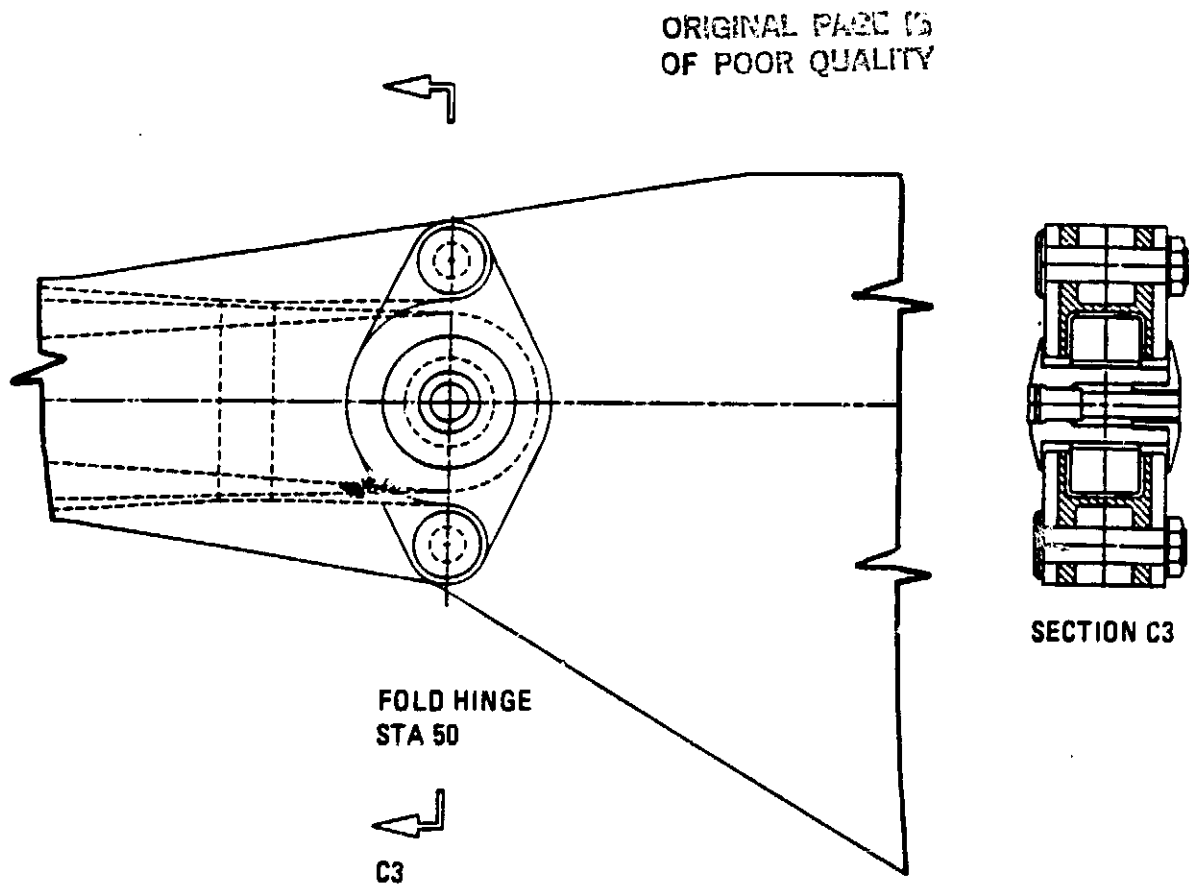


**Figure 90. ITR Hub Fold Configuration – Approach for Blade Sweep Variations**

- a. Predroop versus precone
- b. Torque sleeve chordwise stiffness
- c. Shear pivot location.

As shown in Figure 91, precone is a built-in upward slope of the blade pitch axis, whereas droop is a cant in the blade axis outboard of the torsionally soft hub flexure. Therefore, precone and predroop variation effects on pitch-lag coupling can be tested by comparing ITR hub configurations 1A and 2B.

Torque sleeve chordwise stiffness variations may be accomplished by bonding spanwise unidirectional graphite stiffeners to the leading and trailing surfaces of the sleeve as shown in Figure 92.

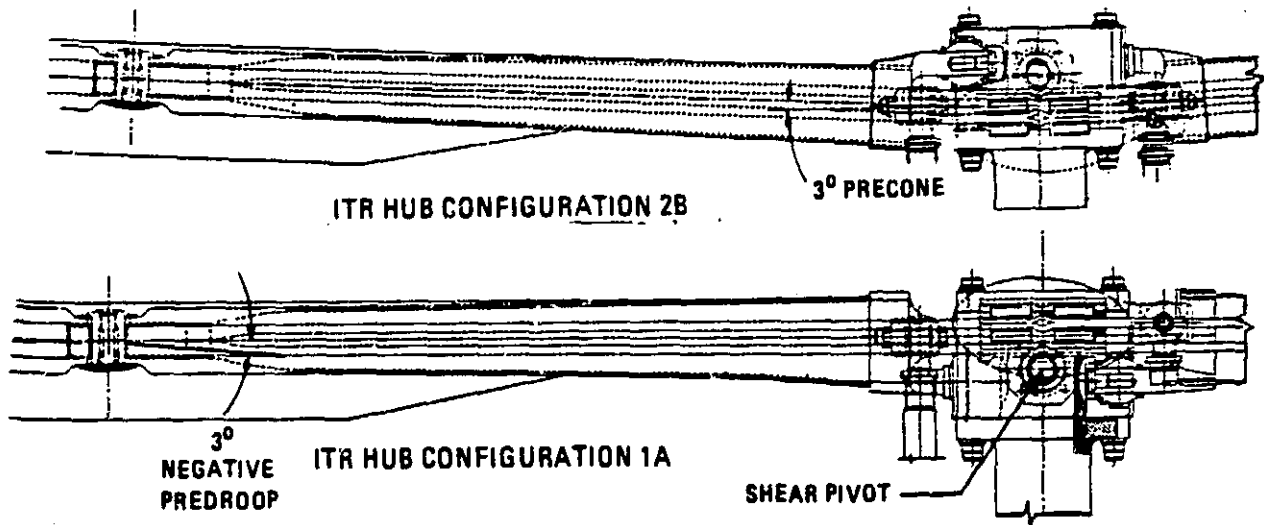


Figure 91. Precone Versus Predroop and Alternate Shear Pivot Locations

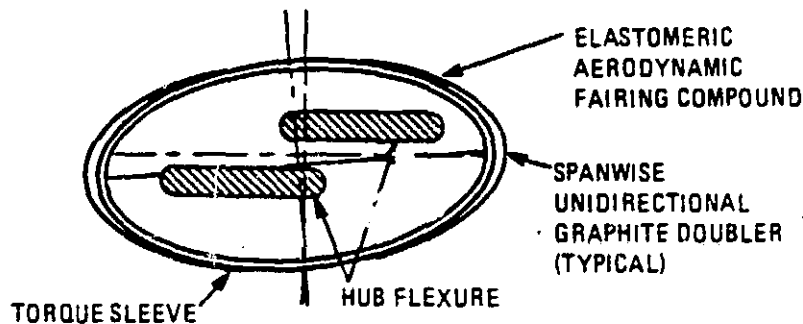


Figure 92. Cross Section of ITR Hub Configuration 1B With Chordwise Stiffening of Torque Sleeve

Shear pivot location variations may be evaluated through comparative testing of ITR hub configurations 1A and 2B as illustrated in Figure 91.

Flexure Stiffness (Frequency Variations) - Flexure stiffness may be varied by designing and fabricating flexures with material variations and/or fiber orientation variations. The flexure material may vary from low-modulus fiberglass in the flexible matrix through hybridized fiberglass/graphite laminates to all-high-modulus graphite/epoxy structures. Fiber orientation may be varied from primarily spanwise unidirectional through a balanced mix of spanwise unidirectional and bias-ply ( $\pm 45$ -degree) material to a mix of unidirectional fibers and plies at any predetermined angle.

Another approach to vary flexure stiffness is to bond secondary stiffeners (flap, chord, and/or torsional) to the ITR/FRR hub flexure. Flexure stiffness variations should be defined in conjunction with FRR blade stiffness and mass variations.

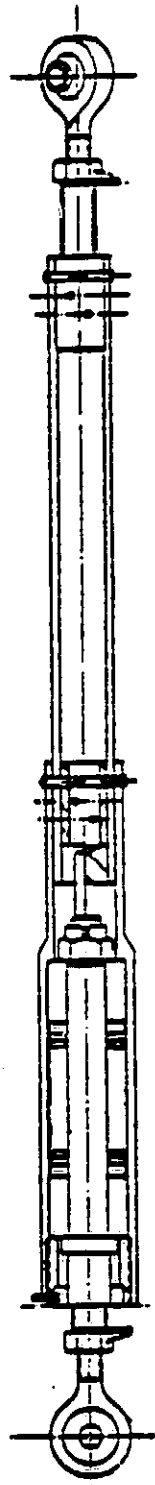
Control System Stiffness - The simplest method to vary control system stiffness is by replacing the rigid pitch links with soft pitch links with an adjustable spring rate. This approach would employ a flexible pitch link similar to the one tested on the BO-105/BMR rotor system in the NASA Ames wind tunnel as shown in Figure 93. Figure 94 illustrates the difference in stiffness between the BO-105/BMR rigid pitch links and the flexible pitch links. The spring assembly is composed primarily of Belleville spring washers stacked in series. The spring rate is varied by adding or subtracting washers or by stacking washers in parallel.

Damping - Chordwise damping of the flexure may be accomplished following the same concepts as applied to the BMR I system tested in the NASA Ames wind tunnel. Figure 95 presents the details of the constrained-layer elastomeric damper strip installation. The damper strips consisted of an outer constraining layer of graphite/epoxy, an elastomeric damping material, and a fiberglass bonding strip.

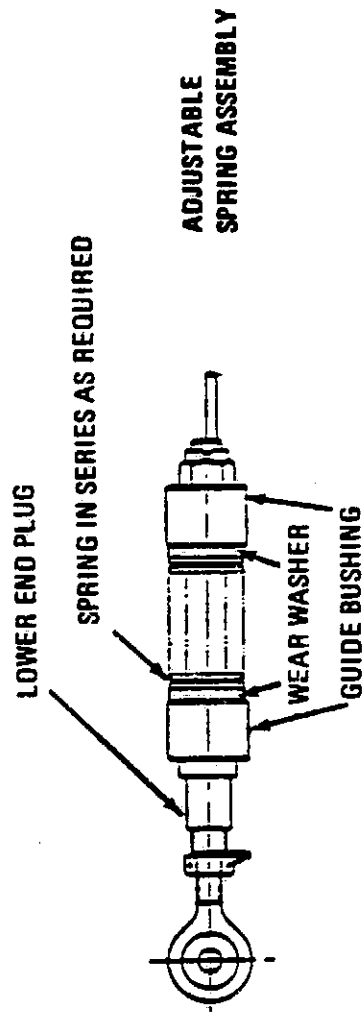
#### PRELIMINARY STRUCTURAL ANALYSIS

The FRR configurations will probably use the erector-set approach by which the selected variations can be made by changing rotor system elements. This means attachments which are additional to the basic ITR system, and will result in structural and dynamic characteristic differences between configurations and from the ITR. The loads, fatigue, static, limit, and ultimate characteristics will be determined for each research configuration and, to the extent of the differences between the ITR and the FRR, structural analyses will be conducted to size and substantiate each variation.

ORIGINAL PAGE IS  
OF POOR QUALITY



ASSEMBLY VIEW



LOWER END PLUG

SPRING IN SERIES AS REQUIRED

ADJUSTABLE  
SPRING ASSEMBLY

WEAR WASHER

GUIDE BUSHING

Figure 93. Reduced-Stiffness Pitch Links (BO-105/BMR)

ORIGINAL PAGE IS  
OF POOR QUALITY

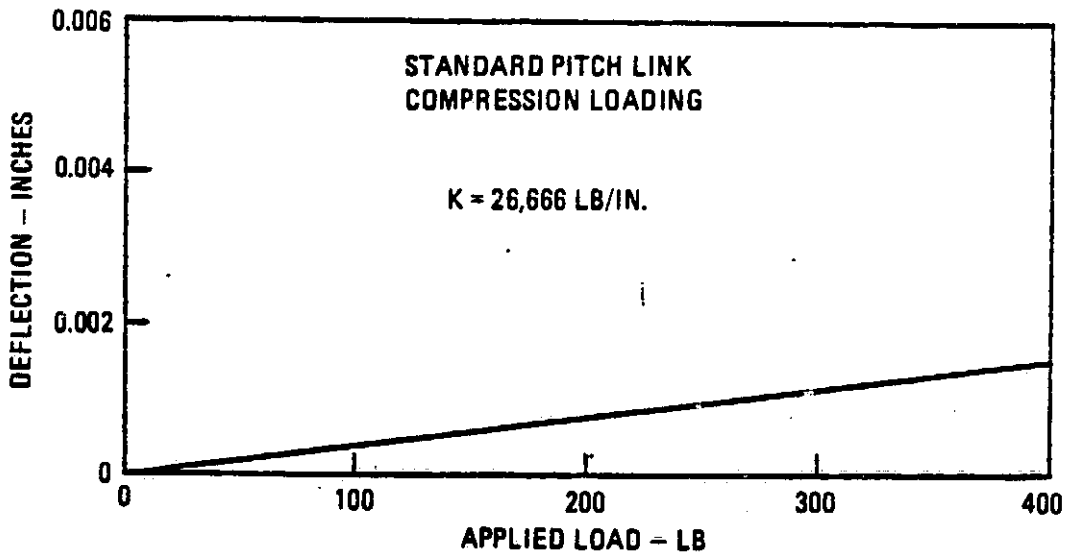
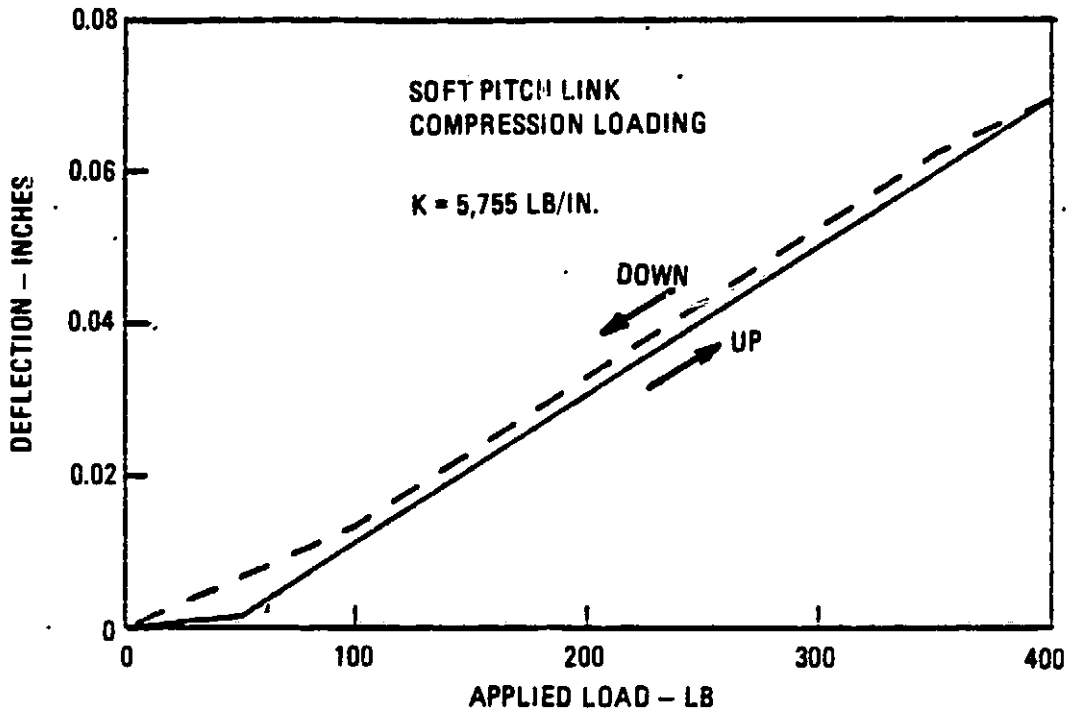


Figure 94. Static Stiffness Determination for Standard and Soft Pitch Links (BO-105/BMR)

ORIGINAL PAGE IS  
OF POOR QUALITY

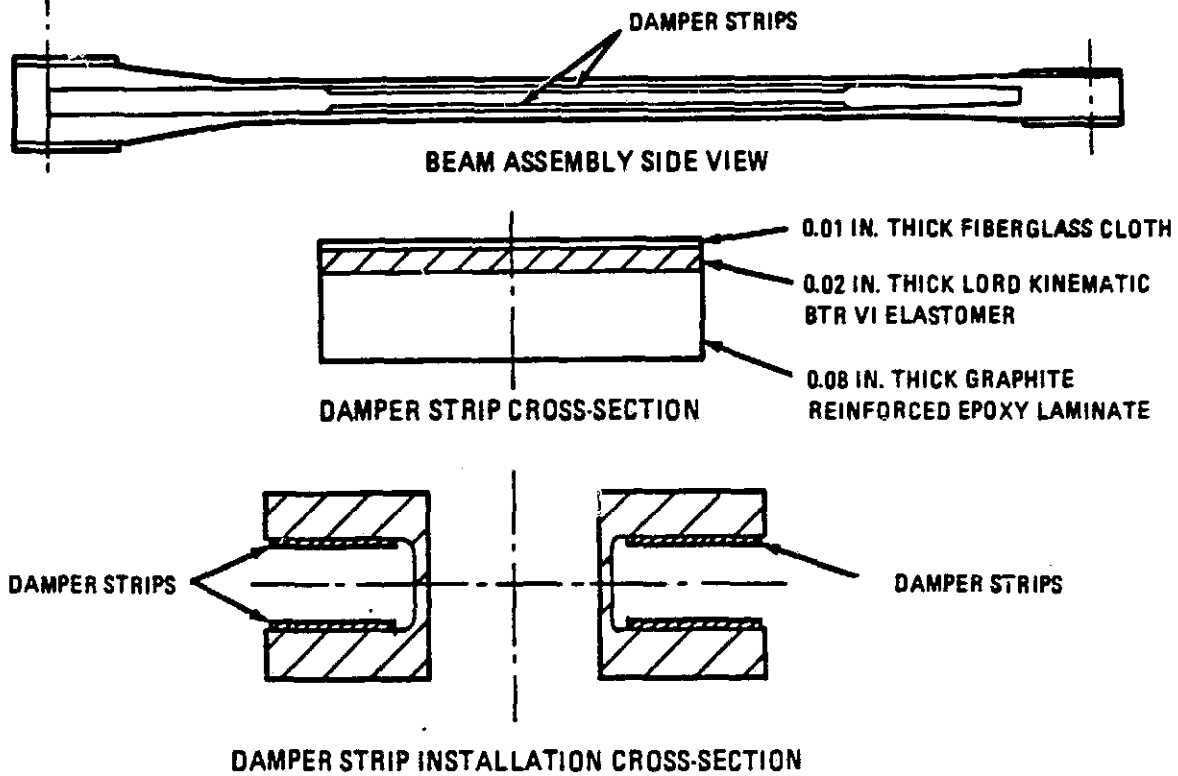


Figure 95. Damper Strip Installation

## ITR COMPATIBILITY WITH THE RSRA

Boeing Vertol's experience in conversion of existing aircraft with incorporation of advanced rotor systems includes the following:

- a. Integration of Bearingless Main Rotor (BMR) on the MBB 80-105 helicopter.
- b. CH-47 conversion into the Model 347 (a tandem-rotor aircraft with three-bladed rotor systems replaced with four-bladed rotor systems, along with other major conversion changes).
- c. Design study to install a four-bladed composite structures rotor on the RSRA (Reference 10).
- d. Design study to install an existing modern four-bladed rotor on the RSRA (Reference 11).

Of particular importance is the rotor installation preliminary design under the design study referenced in item d above. Initially, the same approach will be considered for the preliminary design to be performed for the integration of the ITR/FRR on the demonstration test aircraft and the RSRA. For example, this approach will install the ITR/FRR hub on the RSRA by means of shaft adapters which provide an interface between the splined and coned rotor shaft and the hub as shown in Figure 96. Rotor thrust and control forces are transmitted to the aircraft and shaft torque is transmitted to the rotor system through this adapter.

## FLIGHT CONTROLS MODIFICATIONS

The ITR/FRR aircraft systems will require flight control system modifications to compensate for the following differences from the baseline demonstration test aircraft/RSRA systems:

10. ADVANCED SYSTEM DESIGN STUDY OF A COMPOSITE STRUCTURES ROTOR, NASA Report No. NASA CR-145092, Boeing Vertol Document D210-11092-1.
11. Bishop, H. E., FINAL REPORT - PREDESIGN STUDY FOR A MODERN 4-BLADED ROTOR FOR THE NASA ROTOR SYSTEMS RESEARCH AIRCRAFT, NASA Report No. CR-166153, Boeing Vertol Document D210-11723-3.

ORIGINAL PAGE IS  
OF POOR QUALITY

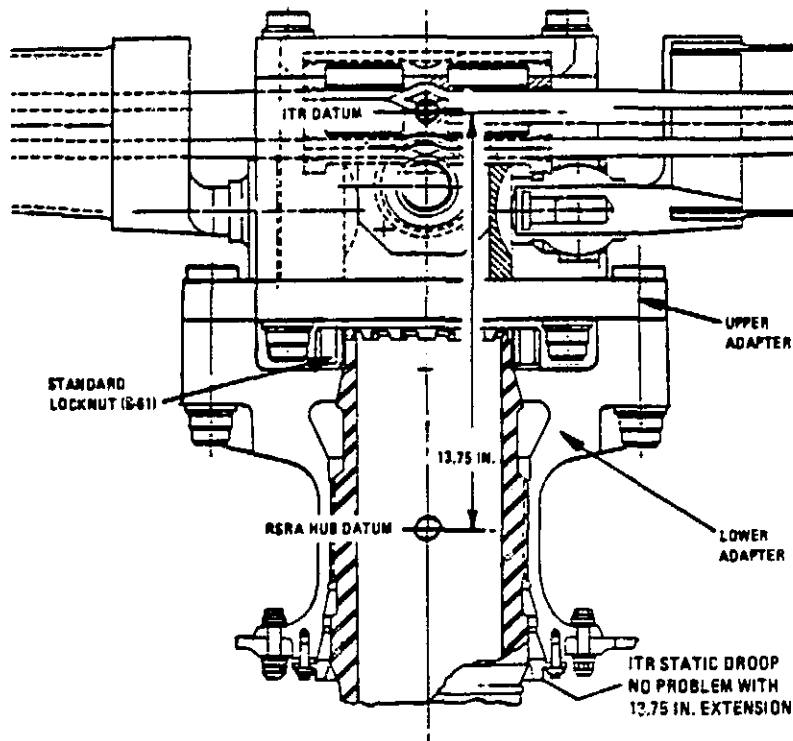


Figure 96. Attachment of ITR to RSRA

- a. Number of blades - The original five-bladed RSRA articulated system is changed to a four-bladed hingeless system.
- b. Pitch arm radius - The ITR/FRR systems will have different pitch link attachment points.
- c. Control phase angle - The ITR/FRR systems will have a different blade flap response to pitch inputs.

Two objectives will be established for flight control system interface evaluations and modification preliminary design: (1) To retain the existing control system components to the maximum extent feasible in order to minimize program costs, and (2) to accommodate the changes cited above.

Consider the RSRA installation, for example. To satisfy the first objective, it will be assumed that the existing control system from the swash-plate bearing down will be retained. This includes the bearing itself,

the stationary ring, stationary scissors, ball slider, and control actuators. Figure 97 illustrates the RSRA control system modifications identified under the design study referenced in item c previously. Kinematic and installation layouts will be prepared to fully define the modification required to the demonstration test aircraft and the RSRA control systems for the ITR/FRR, which will guarantee the required capability and travels.

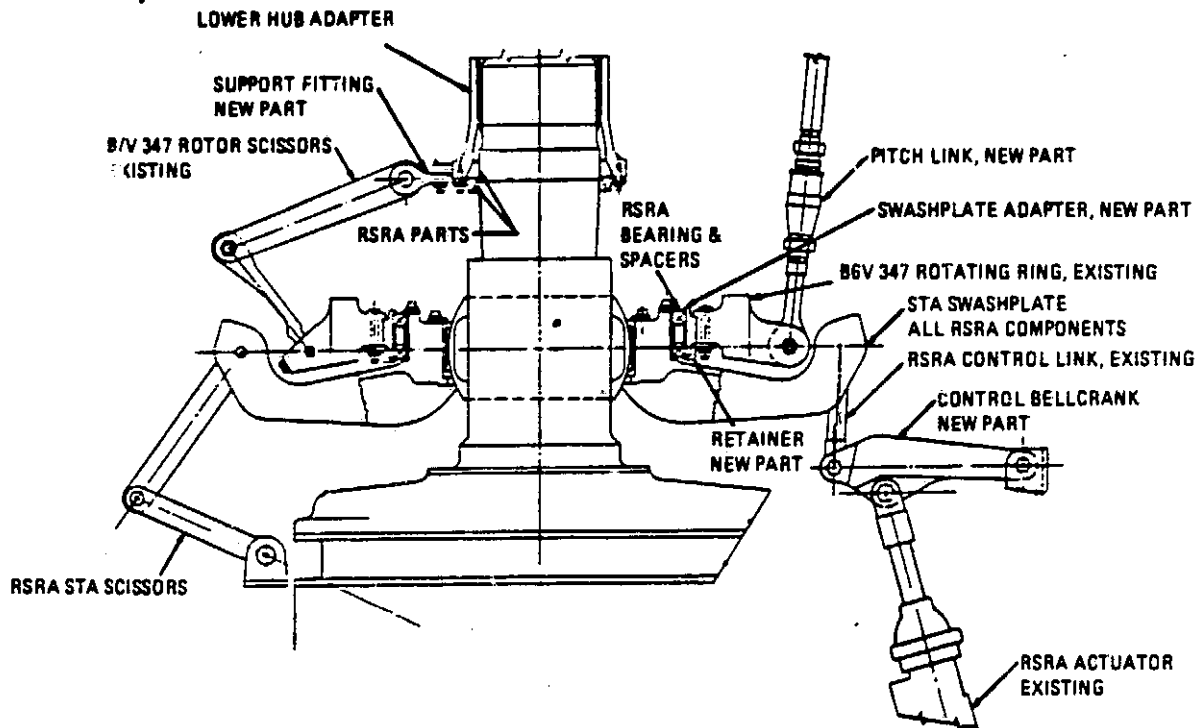


Figure 97. RSRA Controls Modifications

Different rotors require different phasing of swashplate tilt to obtain pure longitudinal response to longitudinal stick motion. This depends upon hub stiffness and the kinematics of the rotor system as defined by azimuthal location of the pitch arm/pitch link attachment. As an example, the RSRA control axes are at 29 degrees from the centerline of the blade pitch axis. That is, when the articulated S-61 blade is at zero azimuth, the pure lateral cyclic input is at 29 degrees azimuth and pure longitudinal cyclic input is at 119 degrees azimuth. The swashplate actuators are not on the control axes for the articulated rotor. Drawing number

72400-00400, "Servo Actuator Installation, Main Rotor Flight Controls" shows that they are located at 45 degrees, 135 degrees, and 225 degrees azimuth. The stationary scissors is at 315 degrees azimuth. This indicates that the lower controls are providing the required mixing to move all three actuators simultaneously for pure pitch and roll control inputs. With the four-bladed hingeless ITR/FRR, the control lead angle may be 80 degrees. To change the lead angle from the baseline 72.5 degrees to 80 degrees for the ITR/FRR will require mixing modifications in the lower controls.

The RSRA rotating swashplate will be replaced by a new or existing component with four lugs for pitch link attachment and one for interface with the rotating drive scissors.

The structural adequacy of the retained rotor flight control system components will be analyzed and assessed. If there are any structural inadequacies that jeopardize flight safety or significantly impact the primary objective of achieving the technical goals, the preliminary design will include the necessary modifications.

The RSRA hydraulic flight control system contains three actuators per swashplate. Each actuator is capable of 9,600 pounds (4,800 pounds single stage) stall load with some reduction as the boost rate is increased. For example, consider the four-bladed hingeless YUH-61A rotor system installed on the RSRA. Maximum actuator loads during YUH-61A 2-g maneuver testing were measured at approximately  $3,000 \pm 3,000$  pounds. During 1-g flight, actuator loads were  $600 \pm 500$  pounds. The actuator arrangement on the YUH-61A is similar to that of the RSRA. Therefore, the RSRA secondary power system would be satisfactory in this case, even up to a 2-g maneuver, if both actuator stages are in operation. However, if one stage of the hydraulic system becomes inoperative, maneuver capability may be restricted.

## STABILITY AUGMENTATION/AFCS MODIFICATIONS

The flying qualities of the ITR/FRR/test aircraft combinations will be analytically compared to the flying quality requirements of MIL-H-8501A and the flying qualities of the baseline aircraft for the helicopter mode of operation to ensure that no degradation has occurred.

The general evaluation of trim data and the formulation of design requirements will be based in part on the following:

- a. Static longitudinal and directional stability
- b. Control travels and margins
- c. Requirements for tail incidences, programed or fixed
- d. Tail rotor considerations
- e. Hinge offset effects.

The ITR/FRR systems will be analyzed in all axes for SAS-off damping levels and dynamic stabilities. This would include a complete tabulation of stability derivatives. Any impact of the rotor design on the flight envelopes will be identified and assessed and modifications will be defined under the preliminary design.

Control travel requirements will be reviewed and integrated into the hardware design. The impact of hinge offset on stability and control will be compared to the baseline aircraft with their offsets. This typically will impact trim position, control power, and damping.

The trim analysis will be conducted following the same format of analysis as the RSRA 4-bladed rotor predesign study (Reference 11). This analysis

made use of the Boeing Vertol computer program Y-92 which contains a strip integration analysis of the rotor with airfoil tables complete with Mach and stall effects. The program was completely specified for the RSRA configuration including the fuselage aerodynamic forces based on data from References 12 and 13.

### ROTOR SHAFT, TRANSMISSION, AND SUPPORT STRUCTURE MODIFICATIONS

Structural analyses will be conducted to ensure that the rotor shaft, transmission, and all rotor and controls support structure have adequate margin when subjected to design fatigue and ultimate loading. Any structural inadequacies will be identified and assessed and the required modifications will be included under the preliminary design. For example, under the RSRA 4-bladed rotor predesign study, the aforementioned structural analyses were performed. It was revealed that rotor shaft bending limitations restricted blade flapping due to the hinge offset change coupled with the rotor height change, but this restriction did not represent an important rotor limitation. Therefore, no rotor shaft changes were proposed. However, the analysis may define the need for modifications due to the increased hub stiffness goal of the ITR/FRR.

### DRIVE SYSTEM COMPATIBILITY

#### Transmission Modifications (RSRA Only)

The ITR/FRR system design rpm will be based upon maximizing the rotor merit function with additional consideration of the RPM range of the Demonstration Test Aircraft drive system. The RSRA systems handbook (Reference 13) defines the transmission gear mesh changes to be made for a rotor

12. Rorke, J., PERFORMANCE, STABILITY AND CONTROL REPORT, Sikorsky Report No. SER-72006, 21 June 1974.
13. Monteleone, R., SYSTEM REQUIREMENTS HANDBOOK FOR THE ROTOR SYSTEMS RESEARCH AIRCRAFT, Sikorsky Document No. SER-72039, 15 May 1977.

system design speed different from the basic RSRA speed of 203 rpm. For example, with a rotor design speed of 285 rpm, the following gears of the RSRA must be changed:

- a. Input spur mesh (from 2.34 to 1.854 reduction ratio)
- b. Main bevel mesh (from 3.40 to 3.05 reduction ratio).

To modify the main bevel mesh would require removing and replacing the main bevel gear and its driving pinion cartridge, part numbers S6137-23053-1 and S6137-23054-1, items 10 and 20 illustrated in Figure 98. The tail rotor speed and the speeds of accessory equipment may be maintained, if required, by changing the gear ratio at the bevel mesh takeoff for the tail rotor shaft. This mesh change would require a change in the mesh between items 10 and 14 (part number S6135-20871-1). If the accessory and tail rotor speed increase is acceptable, then the tail rotor collective pitch control gain may need reduction.

#### Drive System Analyses

If it is assumed that the strength and speed capabilities of the aircraft drive systems are adequate, resonant dynamic coupling between blade chord modes and drive system torsional modes must be avoided to prevent drive system-induced vibration and stresses from increasing to unacceptable levels. In addition, the torsional stability of the aircraft/rotor system, including the fuel control, must be assessed. In order to accomplish the rotor/ drive analyses, the following drive system data are required:

- a. Torsional stiffness of main rotor shaft, engine shaft, and tail rotor shaft
- b. Torsional inertia of power turbine, tail rotor, and all transmissions
- c. Transmission gear ratios (or shaft speeds).

ORIGINAL PAGE IS  
OF POOR QUALITY

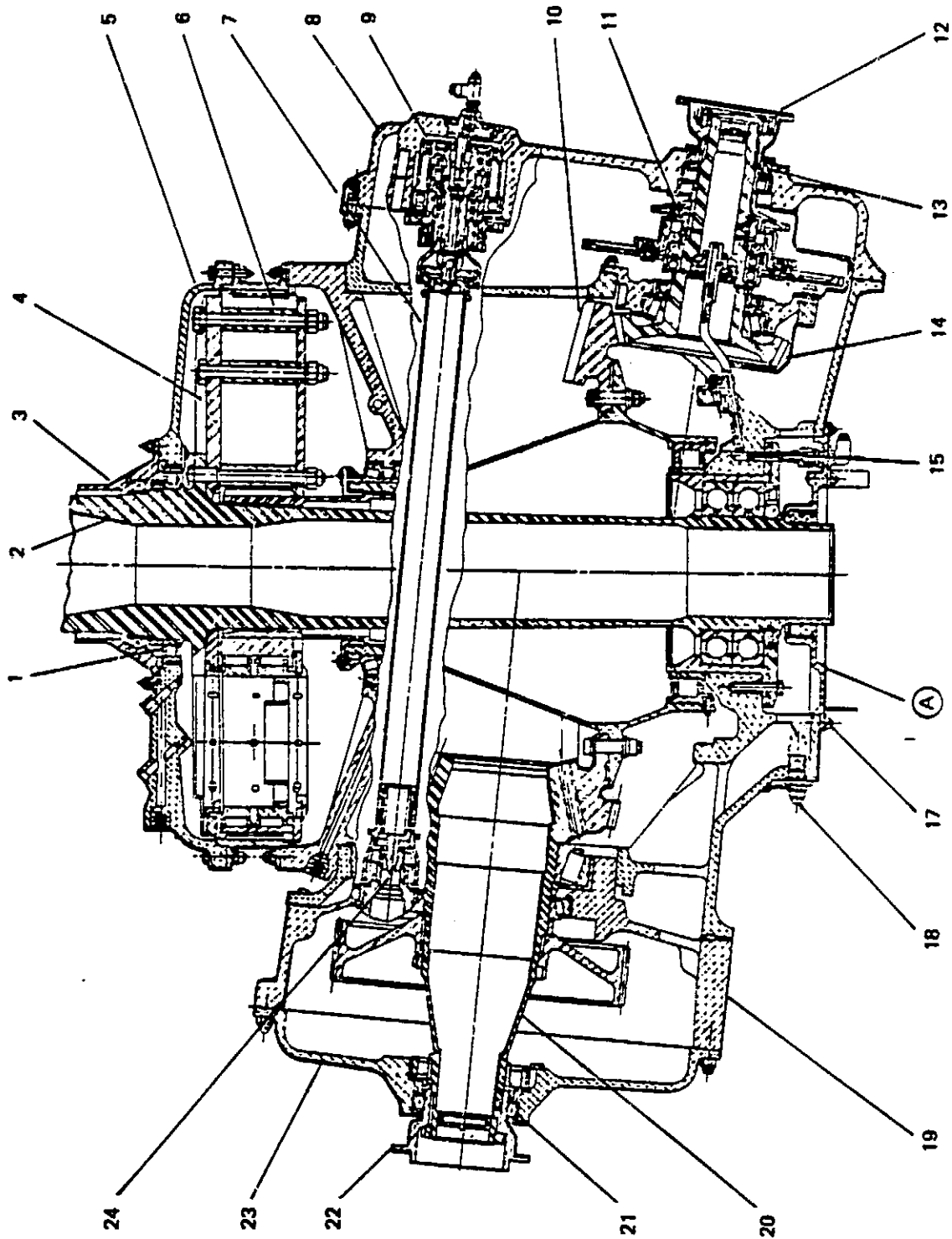


Figure 98. RSRA Main Transmission

Any drive system compatibility problems must be identified and assessed and the required modifications defined and preliminarily designed.

### LANDING GEAR MODIFICATIONS

For the ITR/FRR/test demonstration aircraft/RSRA system combinations, the coupling of blade lead-lag dynamics with airframe and landing gear dynamics will be studied to ensure the avoidance of ground resonance on the aircraft at full and intermediate ground contact conditions. Boeing Vertol capability exists at several levels of complexity for ground resonance analysis:

1. Program D-22: Simple Coleman analysis with body lead-lag and aircraft roll.
2. Program C-45: Equivalent-hinge sequence rotor with landing gear represented by ground springs, flexible pylons, and coupled flap, lag, and torsional blade motion with arbitrary equivalent-hinge sequence.
3. Program C-90: Ground resonance and hover and forward flight air resonance capability; up to 15 fuselage modes; a modal blade representation.

In the preliminary design effort, Program D-22 will be used to evaluate the adequacy of overall damping for the complete aircraft; the more sophisticated C-45 or C-90 program will be used for final assessments of the installation of the ITR/FRR on the aircraft.

To complete the ground resonance analyses, landing gear stiffness and damping characteristics as a function of landing load are needed for the test demonstration aircraft and RSRA. If required by the results of the ground resonance analyses, landing gear modifications will be identified and preliminarily designed.

## VIBRATION ISOLATION

The following dynamic areas will be considered for their effects on integration of the ITR on the demonstration test aircraft and RSRA and the FRR on the RSRA:

- a. Rotor blade hub and control system vibratory loads
- b. Coupled rotor/drive system torsional mode natural frequencies
- c. Single rotor blade stability.

Boeing Vertol's C-60 rotor loads analysis computer program will be used to determine rotor blade bending and torsional vibratory loads for design point flight conditions for the ITR/FRR. Rotor blade natural frequencies versus rotor speed will be computed with computer program D-01. Blade frequencies will be compared with integer multiples of the rotor rotational frequency at normal rotor speed to assure that rotor blade flap, chord, and pitch frequencies are not adversely located.

Coupled rotor and drive system natural frequencies will be determined to assure avoiding resonances of drive system modes at multiples of  $N/\text{rev}$  ( $N = 4$ ).

Stability of an individual blade (blade flutter and divergence boundaries) can be predicted by computer program L-01.

Based on the results of these analyses, any adverse system vibration condition will be identified and assessed. Required modifications to the aircraft vibration isolation systems (active or passive) will be preliminarily designed.

## RSRA EMERGENCY ESCAPE SYSTEM

The emergency escape system provided in the basic helicopter will remain essentially intact. Canopy removal, control lever disconnect, and crew ejection system will be maintained. However, changes will be required to the blade severance system. These changes are necessitated by the fact that the five-bladed rotor system is being replaced by a four-bladed rotor system. Replacement of the S-61 metal blades with the composite ITR/FRR will require further changes. The principal changes anticipated will be in the method of severance and the sequencing of blade severance. Several approaches for severance may be considered.

The RSRA modern four-bladed rotor predesign study (Reference 14) included a proposal and quotation offered by Teledyne McCormick Selph (TMC/S), the supplier of the RSRA emergency escape system. The following preliminary design technical approach based on the referenced proposal is offered.

### Blade Severance Sequencing

The proposed task requires the preliminary design of the modification of the existing Rotor Systems Research Aircraft (RSRA) escape system to convert the current five-bladed rotor system to a four-bladed configuration.

Blade severance angle will be dictated by the necessity to ensure that the aft blade clears the tail assembly of the aircraft. Figure 99 defines the angular severance position for the aft rotor blade as currently established for the five-bladed RSRA configuration. This configuration presents a problem in that the ITR/FRR severance charge may contain slightly more explosive than the current RSRA blade severance assembly. It is

14. Bishop, H. E., et al, FINAL REPORT - PREDESIGN STUDY FOR A MODERN 4-BLADED ROTOR FOR THE NASA ROTOR SYSTEMS RESEARCH AIRCRAFT, NASA CR-166153, January 1981.

ORIGINAL PAGE IS  
OF POOR QUALITY.

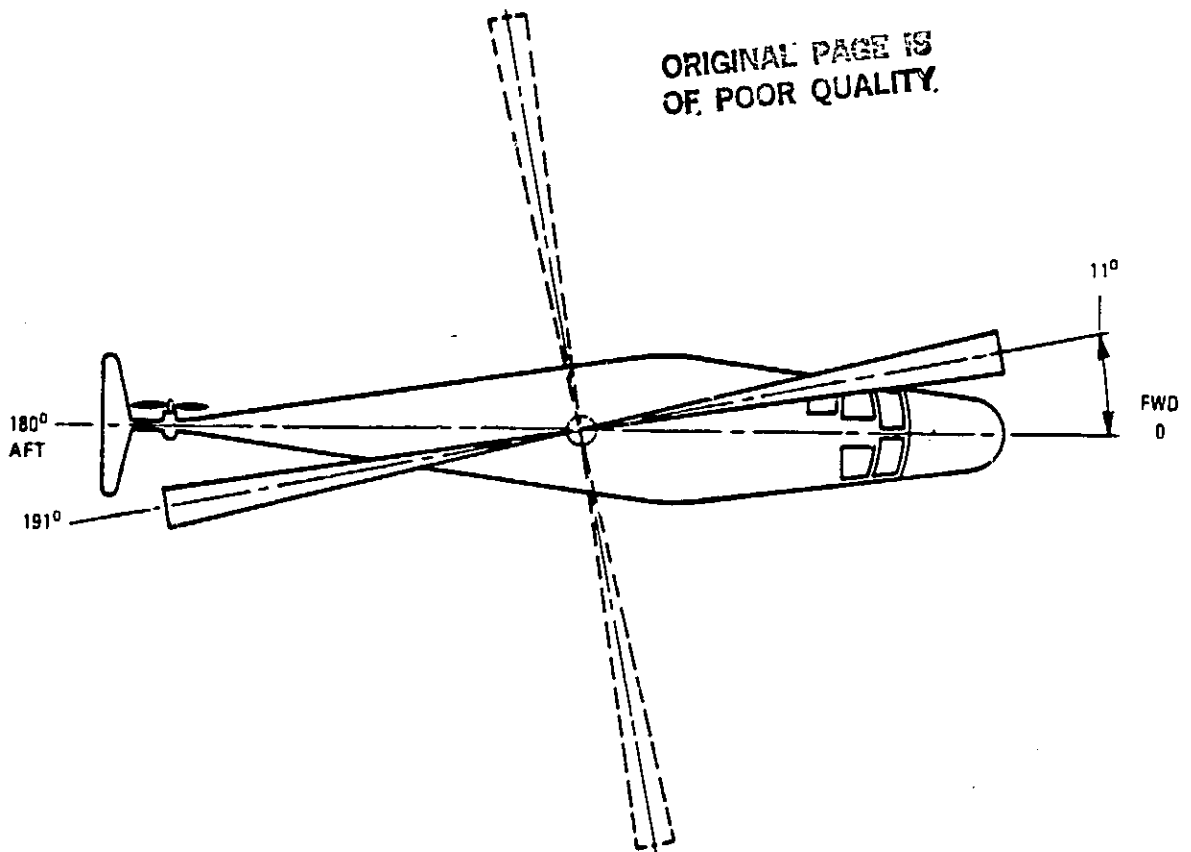


Figure 99. Current Blade Severance Position

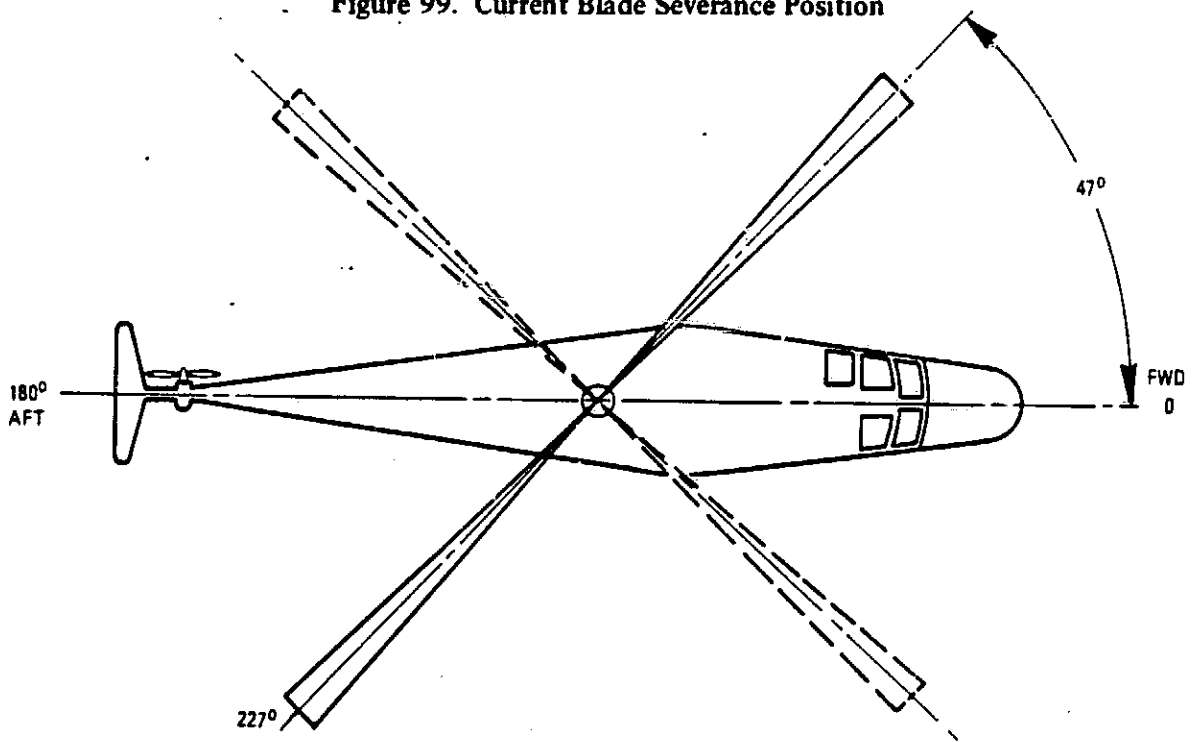


Figure 100. Alternate Plan for Blade Severance

therefore important to sever the forward blade with the maximum possible rotational clearance with respect to the flight crew. Figure 100 shows an alternate plan for blade severance. This plan presents a shortcoming in that the aft blade is severed with a trajectory generally corresponding with the aircraft flight path. Therefore the overall philosophy of blade severance angles must be studied in depth to achieve the optimum severance angles for the ITR/FRR systems.

### Blade Severance Assembly (BSA)

The major effort anticipated for this program will be the establishment of spanwise severance location and the optimum charge size for severance. It is important for aircrew safety to use the smallest possible explosive charge while ensuring maximum or total severance. TMC/S proposes to approach this by first testing various charge sizes against flat-plate specimens followed by partial to full functional tests of the severance assembly against actual ITR/FRR cross sections. These tests would be conducted in Phase III of this program:

Based on the severance of the CH-47D fiberglass blade under the referenced study program, the analysis of the blade design indicated that the severance point would be immediately adjacent to station 46.280. Adjusting for the centerline of the BSA, the actual severance point would be at station 46.780. The current RSRA severance point is at station 45.50, which means that the CH-47D design would protrude an additional 1.28 inches into the aircrew ejection path. This added intrusion into the aircrew ejection envelope did not appear to be significant. However, from a review of the ITR/FRR concepts it is indicated that this approach will result in more intrusion into the aircrew ejection envelope. This may dictate that this method of severance be accomplished inboard on the flexure and blade torque sleeve/cuff.

Experience has shown that two additional methods of blade severance are feasible. As described in Reference 15, tests were conducted simulating these methods during the HUP helicopter in-flight escape system development program by Boeing Vertol and Unidynamics under sponsorship of the Navy Bureau of Weapons. The two methods tested were the use of linear shaped charges placed along the rotor hub hinge and placing an explosive charge within the hinge bearing pin. Both methods worked equally well, but the linear shaped charge method was selected for use in the actual flight operations. In flight testing, the blade severance and severance of the crew-occupied section of a helicopter along with parachute recovery of the occupied section were successfully accomplished. A droned HUP helicopter was flown and each of the three-bladed rotors was severed in flight. Two blades were severed at the hinge and the third blade was jet-tisoned by severing the rotor shaft. This allowed the blade to carry away the rotor head, which was done to remove weight. The nose section was severed from the fuselage and the crew-occupied area was lowered by four parachutes propelled from the sides of the fuselage. The method of severance by explosive charge within the blade attachment pin will be considered for the ITR/FRR program, in addition to the shaped-charge flexure severance approach.

#### Rotating Transfer Unit (RTU)

When modified for this application this unit will consist of:

- a. New camshaft extension
- b. New rotating plate
- c. New stationary plate

15. Unidynamics Report, Contract N178-8519, Naval Weapons Laboratory, U.S. Navy Bureau of Weapons, Washington, DC, December 1964.

- d. Two sequencers
- e. Four cam thrusters
- f. Eight firing pin assemblies
- g. Necessary interconnect lines from the stationary side of the aircraft to the BSAs.

Qualification Testing

The FRR emergency escape system preliminary design effort will only define requalification requirements. Requalification will be necessary for only that portion of the system that is changed for the ITR/FRR systems. The principal area of testing will be the severance device. Table 16 defines the tentative test conditions and environments. Sled tests of the complete escape system or of the rotor severance system are not considered to be necessary. Sequence severance will be tested under condition E.

TABLE 16. SEVERANCE SYSTEM QUALIFICATION TESTS

Test No.	Condition	Environment	Test Specimen
1	A	Ambient	-
2	A	Ambient	-
3	B	-25°F	MIL-STD-810
4	C	-25°F	MIL-STD-810
5	D	+200°F	MIL-STD-810
6	D	Vibration	MIL-STD-810
7	D	15-g shock	MIL-STD-810
8	D	10-day humidity	MIL-STD-810
9	E	Ambient	-
10	E	-25°F	MIL-STD-810

TABLE 16 - Continued

<u>NOTES:</u>	1.	Condition A:	Severance system charge portion of system only (one blade)
	2.	Condition B:	Severance system (one blade) using only basic energy transfer lines
	3.	Condition C:	Severance system (one blade) using only redundant energy transfer lines
	4.	Condition D:	Severance system (one blade) using basic and redundant energy transfer lines
	5.	Condition E:	Severance system (four blades) using basic and redundant energy transfer lines.

#### Rotor Severance System Reliability

The rotor severance system should have demonstrated a minimum reliability of 90 percent at the 90-percent lower confidence limit after completion of testing. A minimum of 10 tests should be performed under various conditions and environments. These 10 tests must be consecutively successful, and the failure of any one test shall require necessary modifications and the rerun of the series from the beginning to demonstrate the reliability of the complete system. A failure of the instrumentation should not be construed as requiring rerun of the tests.

#### ANALYSIS OF CRITICAL COMPONENTS

Critical components of the test demonstration aircraft, as configured and modified to test the ITR rotor system, must be analyzed for structural integrity appropriate for airworthiness and flight demonstration testing. Assembly and layout drawings as needed to define the required modifications will be made.

The modifications to the RSRA for the demonstration and research testing of both the ITR and FRR must be analyzed in the critical structural areas. Drawings and layouts must be made to define the RSRA modifications.

## REFERENCES

1. Dixon, P. G. C., DESIGN, DEVELOPMENT, AND FLIGHT DEMONSTRATION OF THE LOADS AND STABILITY CHARACTERISTICS OF A BEARINGLESS MAIN ROTOR, USAAVRADCAM TR80-D-3, Applied Technology Laboratory, U.S. Army Research and Technology Laboratories (AVRADCAM), Fort Eustis, VA, 23604, June 1980.
2. McHugh, F. J., and McVeigh, M. A., RECENT ADVANCES IN ROTOR TECHNOLOGY AT BOEING VERTOL, 30th Annual Forum of the American Helicopter Society, Anaheim, California, May 1982.
3. Ormiston, R., TECHNIQUES FOR IMPROVING THE STABILITY OF SOFT INPLANE HINGELESS ROTORS, NASA TMX62-390, National Aeronautics and Space Administration, Washington, DC, 1962.
4. Huber, H. B., EFFECT OF TORSION-FLAP-LAG COUPLING ON HINGELESS ROTOR STABILITY, Preprint 731, 29th Annual Forum of the American Helicopter Society, Inc., 1325 18th Street, N.W., Suite 103, Washington, DC 20036, May 1973.
5. FLIGHT EVALUATION OF LOADS AND STABILITY CHARACTERISTICS OF A BEARINGLESS MAIN ROTOR, PRELIMINARY DESIGN, VOLUME A, Boeing Document D210-11129-1, Boeing Vertol Company, P. O. Box 16858, Philadelphia, Pennsylvania 19142, September 1976.
6. Chen, C., and Staley, J. A., FLIGHT EVALUATION OF LOADS AND STABILITY CHARACTERISTICS OF A BEARINGLESS MAIN ROTOR, 1/5.86 Froude Scale Model Test Results, Boeing Document D210-11245-1, Boeing Vertol Company, P. O. Box 16858, Philadelphia, Pennsylvania 19142, June 1977.
7. Gardner, B., and Sheffler, M., BMR-II WIND TUNNEL MODEL TEST: STABILITY DATA ANALYSIS, Boeing Document D210-11488-1, Boeing Vertol Company, P. O. Box 16858, Philadelphia, Pennsylvania 19142, November 1979.
8. Sheffler, M., Staley J., Hoover, J., Sovjak, C., and White, F., FULL SCALE AND TUNNEL INVESTIGATION OF A BEARINGLESS MAIN HELICOPTER ROTOR: FINAL REPORT, NASA CR152373, National Aeronautics and Space Administration, Washington, DC, October 1980.
9. Sheffler, M., Warmbrodt, W., and Staley, J., EVALUATION OF THE EFFECT OF ELASTOMERIC DAMPING MATERIAL ON THE STABILITY OF A BEARINGLESS MAIN ROTOR SYSTEM, Preprint I-2, National Specialists Meeting on Rotor System Design, American Helicopter Society, Inc., 1325 18th Street, N.W., Suite 103, Washington, DC, October 1980.
10. ADVANCED SYSTEM DESIGN STUDY OF A COMPOSITE STRUCTURES ROTOR, NASA Report No. NASA CR-145092, Boeing Vertol Document D210-11092-1.

11. Bishop, H. E., FINAL REPORT - PREDESIGN STUDY FOR A MODERN 4-BLADED ROTOR FOR THE NASA ROTOR SYSTEMS RESEARCH AIRCRAFT, NASA Report No. CR-166153, Boeing Vertol Document D210-11723-3.
12. Rorke, J., PERFORMANCE, STABILITY AND CONTROL REPORT, Sikorsky Report No. SER-72006, 21 June 1974.
13. Monteleone, R., SYSTEM REQUIREMENTS HANDBOOK FOR THE ROTOR SYSTEMS RESEARCH AIRCRAFT, Sikorsky Document No. SER-72039, 15 May 1977.
14. Bishop, H. E., et al, FINAL REPORT - PREDESIGN STUDY FOR A MODERN 4-BLADED ROTOR FOR THE NASA ROTOR SYSTEMS RESEARCH AIRCRAFT, NASA CR-166153, January 1981.
15. Unidynamics Report, Contract N178-8519, Naval Weapons Laboratory, U.S. Navy Bureau of Weapons, Washington, DC, December 1964.